NSP

Monticello Nuclear Generating Plant Reload Safety Evaluation Methods NSPNAD-8608, Rev. 1

August 1988

Nuclear Analysis Department
Northern States Power Company

RELOAD SAFETY EVALUATION METHODS

FOR

APPLICATION TO THE MONTICELLO NUCLEAR GENERATING PLANT

NSPNAD-8608

August 1988

Revision 1

Prepared By	C J Pitsch	Date 8/17/88
Reviewed By	Cliff Bonneau	Date 8/17/88
Approved By	Roger O. Anderson	Date 8/17/88

Reload Safety Evaluation Methods

for

Application to the Monticello Nuclear Generating Plant

NSPNAD-8608
August 1988
Revision 1

Principal Contributors

Northern States Power Company

Roger Anderson
Cliff Bonneau
Craig Gantner
Jon Kapitz
Scott Montgomery
Craig Nierode
Jeff Olson
Dave Rautmann
Pat Riedel
Paras Shah

Utility Associate International

Dr. Richard Kern

LEGAL NOTICE

This report was prepared by or on behalf of Northern States Power Company (NSP). Neither NSP, nor any person acting on behalf of NSP:

a. Makes any warranty or representation, express or implied, with respect to the accuracy, completeness, usefulness, or use of any information, apparatus, method or process disclosed or contained in this report, or that the use of any such information, apparatus, method, or process may not infringe privately owned rights; or

b. Assumes any liabilities with respect to the use of, or for damages resulting from the use of, any information, apparatus, method, or process disclosed in the report.

Table of Contents

Table of Contents (continued)

Table of Contents (continued)

Table of Contents (continued)

List of Figures

Figures (continued)

Figures (continued)

Figures (continued)

Figures (continued)

List of Tables

List of Tables (continued)

1.0 INTRODUCTION AND SUMMARY

This report addresses the methods developed by Northern States Power Co. Nuclear Analysis Department (NSPNAD) to perform reload safety evaluations and other licensing transient analyses for the Monticello Nuclear Generating Plant.

Section 2 of this report describes the DYNODE-B computer program. DYNODE-B is a transient simulator of the nuclear steam supply system (NSSS) of a boiling water reactor (BWR). This program simulates all the important features of a BWR design which significantly influence the response of the NSSS to transient conditions. The NSPNAD version of DYNODE-B includes a hot channel model which uses the General Electric GEXL correlation to calculate critical power ratio (CPR).

Section 3 describes the code qualification benchmark analysis done with DYNODE-B. This includes comparisons to other approved licensing codes (i.e., GE REDY and ODYN codes) as well as comparisons to data (i.e., Monticello startup tests and the Peach Bottom turbine trip tests). In all cases, DYNODE-B provides acceptable results.

Section 4 describes the methodology that will be used to perform licensing analyses. This includes a description of the models and input parameters used, the spectrum of events to which the methodology applies, a description of the application of uncertainties and conservatisms, a description of the applicable acceptance criteria, and an evaluation of margin.

The methodology described in this document used in conjunction with the DYNODE-B computer code provides a conservative evaluation of margins with respect to thermal limits (CPR), ASME overpressure limits, and system stability limits.

2.0 DYNODE-B CODE DESCRIPTION

2.1 GENERAL DESCRIPTION

The DYNODE-B computer program [6] is a transient simulator of the nuclear steam supply system (NSSS) of a boiling water reactor (BWR). This program represents all the important features of current types of BWR design which significantly influence the response of the NSSS to transient conditions. The major components of a BWR which are simulated are shown in Figure 2.1-1.

Each major component is represented by a set of time-dependent differential equations. A self-initialization procedure is carried out for each of the component models in DYNODE-B at the beginning of each initial case. This self-initialization procedure is consistent with specified initial conditions.

The major technical features of DYNODE-B are as follows:

- Provision for simulating a wide variety of transient conditions.
- Provisions for a representation of all current types of BWR design.
- Multinode radial fuel rod and multinode axial coolant channel representations in core.
- Point kinetics, one-dimensional (axial) space-time kinetics, or power-forced options for core power transients.
- Solution to conservation equations of mass, energy, volume, and momentum for the reactor vessel fluid and main steam system regions.

- Explicit representation of the main steam system relief, isolation, bypass, and turbine valves.

- Representation of the turbine.

- Representation of heat transfer with the structural metal components of NSSS.

- Representation of the reactor protective and safety injection systems.

- Representation of the major control systems.

- Complete self-initialization.

- Full range of water properties.

2.2 SPECIFIC MODEL DESCRIPTIONS

2.2.1 CORE MODEL

The core model consists of the neutronic and thermal-hydraulic analysis of the fuel and coolant. The average fuel rod is represented radially by a set of equal volume nodes in the uranium dioxide (maximum of 8) and two nodes in the cladding. The axial representation consists of a set of equal volume nodes with a maximum of 25. The heat conduction model allows temperature-dependent conductivity and heat capacity for the uranium dioxide. The gap is represented by an effective heat transfer coefficient which is a function of the average fuel temperature. The power distribution across the uranium dioxide is also modeled. The core heat generation in the moderator is dependent on the coolant void fraction. Heating of the bypass water region is also represented. The surface heat transfer coefficient is based on the Thom correlation.

The conservation of mass and energy equations are solved in the coolant channel for a set of equal volume axial nodes subject to the core flow, pressure, and inlet subcooling boundary conditions which are obtained from the reactor vessel model which is described later. The core pressure is assumed to be spatially uniform. Several void fraction models are available; the preferred model is a profile-fit model to compute the flow quality, which is then used to calculate the void fraction from a modified Zuber-Findlay drift-flux relationship.

The Critical Power Ratio (CPR) for a number of limiting bundles is obtained using the GEXL correlation to compute the critical quality.

The core power transient is optionally based on a point or a one-dimensional (axial) space-time kinetics model. The power transient can also be specified by the user. The kinetics models account for the important reactivity components which are void (density), fuel temperature (Doppler), and rod motion (scram). In addition, the user may specify a reactivity forcing function. The delayed neutrons are represented by a maximum of six precursors, and the decay heat is also explicitly modeled. The core may be initially subcritical. The one-dimensional kinetics model is based on the total fission source and a nodal representation for the average fuel and coolant channel. The nuclear parameters (K^{∞} and M^2) are obtained from a comparable three-dimensional model [1] in which a collapsing procedure is used to obtain the radially averaged values. Individual and groups of control rods (maximum of 10) may be represented. The collapsing procedure is used to obtain the initial condition parameters as well as the feedback parameters for the transient solution. Spatial variation of the total delayed neutron fraction and prompt neutron lifetime are represented. The initial power distribution is based on the solution of the neutron source equations with all time-derivatives set to zero.

2.2.2 REACTOR VESSEL FLUID MODEL

The reactor vessel (RV) excluding the core is represented by six fluid regions: upper downcomer, lower downcomer, lower plenum, bypass, riser (outlet plenum and separators), and steam dome. The conservation equations of mass and energy are solved for each region based on the boundary flows and enthalpies. Heat conduction with metal structural components can also be considered. The pressure distribution is assumed to be spatially uniform. The RV pressure is obtained from a consideration of the mass and energy balance in the steam dome which accounts for non-equilibrium effects. A separate model is provided to calculate the water level in the steam dome which accounts for steam carryunder in the recirculation water and area variations due to the steam separator geometry. Level sensing is also represented.

The RV flow is either user-specified or calculated from the conservation of momentum equations. In this latter case, the dynamics of the recirculation pumps (RP's) are also taken into consideration, and a wide variety of pump transients can be represented. The pump heat is included in the model. The hydraulic model for the RP's is based on homologous relationships. The hydraulic model represents the flow in the two individual recirculation loops and considers forward and reverse suction and drive line flows. Automatic RP trip on low RV level or high RV pressure can be specified. The initial suction and drive flows are specified, and the suction flow path loss coefficient is computed to provide momentum balance. This loss coefficient is assumed constant during the transient. Two-phase pressure drop and fluid inertial effects in the core, outlet plenum and steam separators are modeled. The transient core bypass flow fraction is computed based on the conservation of momentum equations. The initial pump status is user-specified as either on or off. The pump motor electrical torque is obtained from the output of the motor/generator (M/G) flow control system, which is described later.

It should be noted that, when the dynamic flow calculation is used, the temperature (enthalpy) distribution within the downcomer, recirculation lines, and jet pumps is represented in detail to provide an accurate model of the changes in core inlet subcooling due to changes in feedwater, high-pressure coolant injection system (HPCIS) and reactor core isolation cooling system (RCICS) flows and enthalpies.

The feedwater flow is assumed to enter the top of the downcomer. The feedwater flow can be specified by the user or controlled by a three-element control system which is described later. The feedwater enthalpy is user-specified.

The safety/relief valves (S/RV's) are represented as individual valves. Account is taken for accumulation and blowdown, valve opening/closing delays, and valve stroking.

2.2.3 MAIN STEAM SYSTEM MODEL

The main steam system consists of the main steam lines, main steam line isolation valves (MSIV's), bypass, turbine control and stop valves, and the turbine.

The main steam lines can be represented by either a lumped parameter model or a detailed model.

For the lumped parameter model, the steam line portion on the RV side of the MSIV's is included in the definition of the steam dome, and the remainder is represented by a single volume. The flow through the MSIV's is calculated from an orifice equation so that the steam inertial effects are neglected. The steam dome pressure is obtained from the RV model as described earlier, and the steam line pressure is based on conservation of mass assuming saturation conditions.

In the detailed model, the main steam system representation begins at the RV ex and consists of seven pipe segments per steam line. These seven segments consist of four in the main steam line (RV exit to S/RV location, S/RV to MSIV, MSIV to bypass valve location and bypass valve to turbine valve location), the relief valve line, the safety valve line, and the bypass valve line. Each pipe segment is subdivided into a finer mesh with a maximum of 11 mesh points per segment. The conservation equations for mass, energy and momentum are solved at each mesh point based on the Method of Characteristics (MOC). The MOC model provides for realistic modeling of the pressure waves within the main steam system resulting from rapid valve motion with minimal numerical dispersion. The solution of the MOC model is based on the appropriate boundary conditions which consist of the steam dome pressure and the S/R, bypass, and turbine valve flow rates.

Closure of the MSIV's is automatically initiated by any of the following three signals: low RV level, high steam flow, or low RV pressure. Appropriate time delays and valve closure rates are user specified.

The bypass valve flow is based on the bypass valve position (and hence area), which can be specified by the user or controlled by the Pressure Regulator Control System which is described later. Similar treatments are used for the turbine control and stop valves. Automatic bypass valve opening can be actuated on turbine stop valve closure.

The turbine model provides a representation of the turbine speed based on the angular momentum equation solution. The driving torque is related to the turbine inlet steam flow. The turbine speed can be used to simulate frequency changes for the M/G drive motor torque.

2.2.4 SAFETY SYSTEMS

The high pressure coolant injection system (HPCIS) model is based on a flow versus back pressure curve with a user-specified enthalpy. Automatic actuation with an appropriate time delay is provided based on either low RV water level or pressure.

The reactor core isolation cooling system (RCICS) is modeled in a similar manner to the HPCIS.

The reactor protective system represents five explicit automatic trip functions: high neutron power, high RV pressure, low RV level, high RV level, and MSIV closure fraction. A scram can also be initiated at a user-specified time. The flow dependence of the high neutron power trip is represented based on the sensed recirculation drive line flow. Each trip function has a unique time delay.

2.2.5 CONTROL SYSTEMS

The main feedwater controller is based on a three-element system with the sensed reactor vessel water level, sensed main steamline flow and the feedwater flow as the three input signals. The control system adjusts the feedwater valve position to attempt to obtain a zero error signal. RV back pressure effects on flow rate can be represented.

The M/G flow controller accepts the coupler scoop tube position and output signal from the turbine speed governor as input and adjusts the scoop tube position to maintain the appropriate setpoint. Control is provided for each loop independently. The M/G dynamic model is based on solving the conservation of angular momentum for the motor and generator separately. Idle loop recirculation pump startup can be modeled. Automatic drive motor trip on high RV pressure can be specified.

The pressure regulator control system accepts the sensed RV pressure and the turbine speed governor output signal as input. This system controls the turbine control and bypass valve positions to maintain the RV pressure at the appropriate setpoint. RV back pressure effects on steam flow can be represented.

2.2.6 INTEGRATION SCHEME

The reactor core model equations are integrated by using a fifth-order Runge-Kutta-Merson method in which the time step is automatically selected to achieve a user-specified accuracy limit. This same method is used to integrate the dynamic flow equations for the RV flow rates. Note that the core and RV time step sizes are usually different with the former being smaller. The MOC solution in the steam lines is carried out over a user-specified fraction of the RV time step using an explicit integration technique and linear variation of the boundary conditions over the RV time step.

2.3 COMPARISONS WITH OTHER APPROVED LICENSING CODES

This section provides a comparison with two other approved licensing codes: REDY [8] and ODYN [9].

In general, the development of DYNODE-B paralleled the evolution of these two codes from the standpoint of applications to licensing analyses. Early versions of DYNODE-B were patterned after REDY, based on the information provided in Reference 8, so that the models, assumptions, and approximations in these early versions are similar to those of REDY. The advanced versions incorporated more sophisticated models in the areas of the core kinetics (1-D axial) and steam line hydraulics, following the improvements of ODYN over REDY. The nature of the DYNODE-B enhancements are similar to those of ODYN, but slightly different in implementation, as discussed later.

The remainder of this section presents the major technical differences between ODYN and DYNODE-B.

2.3.1 CORE NEUTRONICS

ODYN is based on one-group diffusion theory, in which the cross sections are a function of coolant density, fuel temperature, and control state. DYNODE-B is based on the total fission source nodal formulation, in which neutron migration is represented by coupling coefficients between adjacent nodes. The coupling coefficients are functions of the migration area, M^2. Local neutron multiplication is given in terms of the infinite multiplication factor, K^∞. The forms of the equations for these two models are similiar in nature, and the DYNODE-B nodal formulation can be derived from the one-group equations. The treatment of the delayed neutrons is identical in the two codes. The DYNODE-B model treats decay heat precursors in conformance with the 1971 ANS Standard while ODYN uses a simple exponential decay heat model. The radial collapsing procedures used to develop the one-dimensional parameters are identical in nature.

2.3.2 STEAM LINES

ODYN is based on a single-phase, one-dimensional nodal representation of the steam line (8 nodes) in which the steam is assumed to behave isentropically. DYNODE-B is based on a Method of Characteristic (MOC) solution to the one-dimensional conservation equations for mass, energy, momentum, and state. The MOC methodology is more rigorous and does not assume a priori that the steam is isentropic. The MOC method was used as a reference in establishing the validity of the ODYN model.

2.3.3 REACTOR VESSEL PRESSURE DISTRIBUTION

ODYN explicitly calculates the pressure at the reactor inlet and the RV dome. DYNODE-B calculates the pressure in the RV dome. The reactor core pressure is obtained by simulating the appropriate transport delay between the dome and the core outlet based on the sonic velocity and the distance between these two points.

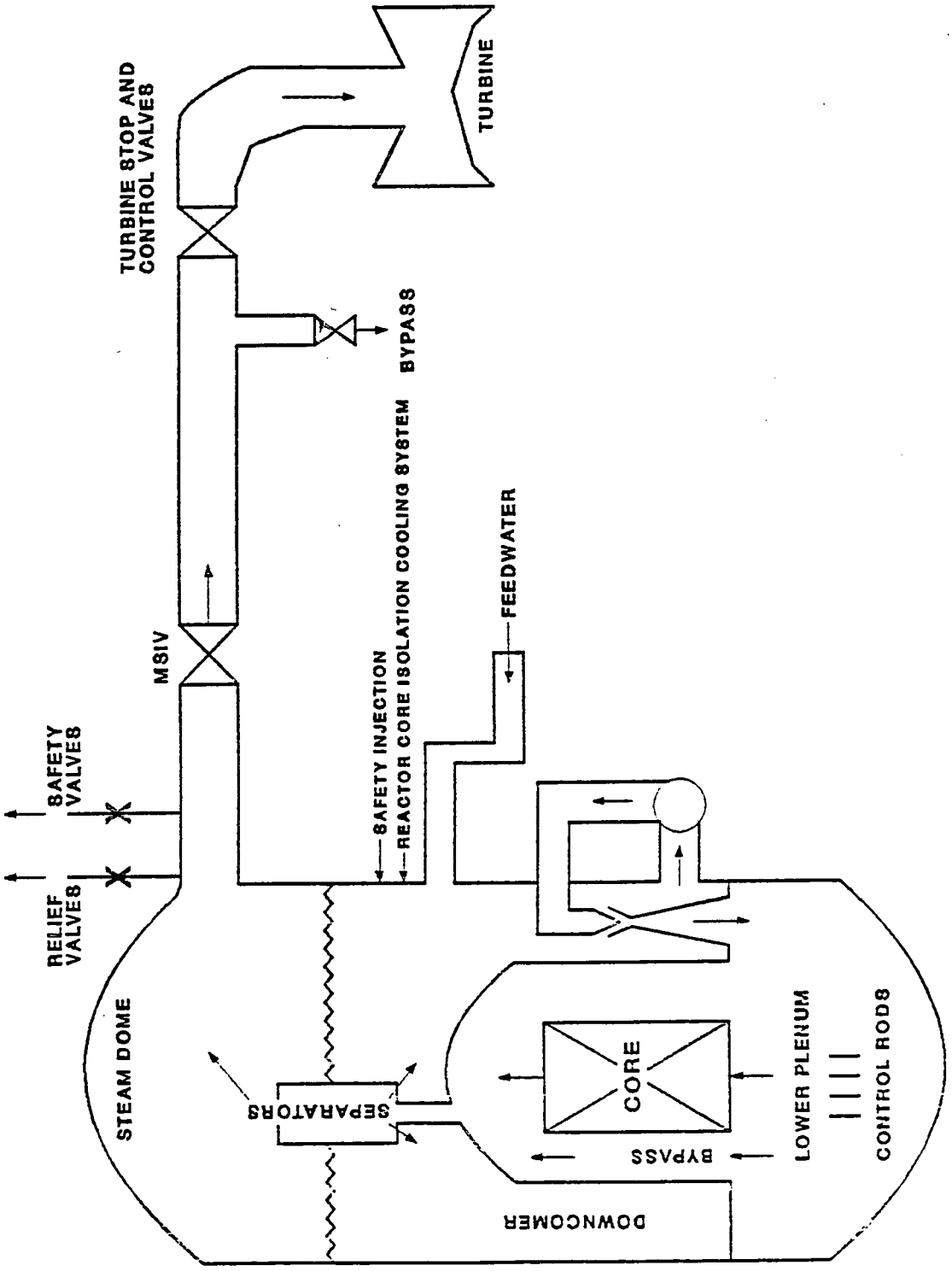

Figure 2.1-1
Schematic of BWR NSSS Representation

3.0 DYNODE-B CODE QUALIFICATION

This section discusses the benchmark analyses performed to qualify the DYNODE-B computer code for BWR analysis.

The nuclear models (1-D kinetics parameters) are compared to results from the 3-D simulator [1] in Section 3.1.

The thermal-hydraulic models are compared to other approved licensing codes, i.e., GE's REDY and ODYN codes, and to test data, i.e., Peach Bottom turbine trip tests, and Monticello startup tests. These results are shown in Section 3.2.

It is the intent of this section to determine the applicability of the DYNODE-B code models to BWR analysis only. The application of DYNODE-B to licensing analysis and an evaluation of margin is contained in Section 4.

3.1 NUCLEAR MODEL COMPARISONS

The 1-D kinetics parameters which are input to DYNODE-B are derived from a radial collapsing of the 3-D results from the corresponding NDH parameters (Reference 1). Since the NDH model has been qualified against plant measurements, the accuracy of the 3-D parameters is well founded, and thus the only other uncertainty associated with the 1-D parameters is that which is introduced by the collapsing process and the calculation of the feedback parameters. This additional uncertainty can be assessed by direct comparisons of reactivity changes between NDH and DYNODE-B results for comparable changes in the statepoints. This assessment has been made for the void, scram and Doppler reactivity components, since the dominant reactivity changes occur due to these three components during events analyzed with the 1-D model (overpressurization events). It should be noted that any uncertainty associated with these procedures will be included in the ΔCPR/ICPR uncertainty due to input parameter uncertainties as applied in section 4.4.1.

The results of specific comparisons for Monticello are presented in the following sections to demonstrate the nature of this process.

3.1.1 SCRAM REACTIVITY

The change in scram reactivities, calculated with NDH and DYNODE-B, for the case of all-rods-out (ARO) to all-rods-in (ARI) with the highest worth rod stuck out are shown in Figure 3.1-3. The percent difference between these two curves is presented in Figure 3.1-4. The DYNODE-B error is conservative when it is greater than zero. The vertical line on these curves shows the amount of control rod insertion when the minimum critical power ratio (MCPR) occurs for the turbine trip without bypass transient. For this case, no uncertainty need be applied for the scram reactivity component, since the control rod worth up to the time of MCPR is conservative relative to NDH. This is expected since the Δk^{∞} input into DYNODE-B for the scram reactivity is determined between a fully converged, static, ARO NDH case and a source converged, NDH case with all but the highest worth rod inserted. The rods in NDH case held the independent core parameters, such as core power, flow, and void distribution constant. This does not take into account the flux redistribution effects as the control rods are stepped in. The neglect of this effect results in an added conservatism.

3.1.2 VOID REACTIVITY

The calculated values for K-eff between NDH and DYNODE-B for a change in subcooling are shown in Table 3.1-1. The corresponding power distributions are shown on Figures 3.1-1 and 3.1-2. These results show that the DYNODE-B result for void reactivity feedback is slightly more conservative. For each DYNODE-B case shown in Table 3.1-1, the corresponding NDH collapsed 1-D parameters were used directly to determine the DYNODE-B K_{∞} and M^2 distributions. In section 7.24 of this report, the DYNODE-B cases used the feedback tables to determine the K-eff changes. The results of that analysis also confirm that no additional uncertainty needs to be applied due to the 3-D to 1-D collapsing process.

3.1.3 DOPPLER REACTIVITY

The comparison of the Doppler reactivity using the collapsed 1-D parameters directly from NDH is shown in section 7.3 of this report. The comparison using the transient tables is shown in section 7.24 of this report. The results of section 7.3 show that NDH and DYNODE-B reactivities are the same when the

collapsed 1-D parameters are input directly into DYNODE-B, and section 7.24 sh[redacted] that an additional uncertainty is needed when the transient tables are used.

3.2 THERMAL - HYDRAULIC COMPARISONS

This section is intended to benchmark the thermal-hydraulic models in the DYNODE-B code. This is accomplished by benchmarking to other approved licensing codes and to test data. The test data benchmarks provide the primary checkout. The code benchmarks provide a secondary check of the overall behavior; however, exact comparisons are not expected, due to modeling and input differences. Essentially, these benchmarks provide a full system checkout of the models in DYNODE-B, including the main models described in Section 2.

In order to provide an accurate comparison, an effort was made to duplicate the comparative conditions as closely as possible, i.e. models used in the case of benchmark codes and the measured test conditions for data comparisons.

These benchmarks are meant only to test the modeling of the DYNODE-B code. Th[redacted] methodology used for Reload Safety Evaluations is described in Section 4, and these results are referenced where applicable.

3.2.1 CODE-CODE COMPARISONS

In this section the DYNODE-B code is benchmarked to the General Electric REDY code [8] results in the FSAR analysis [2] and the ODYN code [9] results in the Cycle 11 reload safety analysis [4].

3.2.1.1 GENERAL ELECTRIC REDY CODE

The models described in Reference 8 were duplicated as closely as possible for these cases.

The major discrepancies in the code modeling are: REDY uses a second-order sweep model to calculate the dynamic void effects, whereas DYNODE-B uses a profile-fit non-equilibrium flow quality void model; REDY calculates decay heat from the Stehn-Clancey correlation [8], whereas DYNODE-B calculates decay heat as part of the kinetics equations; and REDY assumes a constant value of cladding surface heat transfer coefficient throughout the transient, whereas DYNODE-B assumes the heat transfer coefficient to behave according to the Thom correlation.

The input from Reference 13 was used wherever possible. In cases where the REDY input value was unknown, typical or actual plant values were used in the DYNODE-B models. In particular, the majority of the controller (flow, pressure, and level) model inputs to REDY were not known.

Fourteen transients from the FSAR [2] were benchmarked. The following sections describe each transient and document the benchmark analysis results.

3.2.1.1.1 TURBINE TRIP WITHOUT BYPASS

Description Of The Accident

This transient is a severe abnormal event which results directly in a primary system pressure increase. It represents the sequence of events that would follow an instantaneous loss of condenser vacuum with failure of the low condenser vacuum scram signal, so that scram occurs upon automatic closure of the turbine stop valves. For this event, the turbine bypass valves are assumed to be inoperable because of the loss of condensor vacuum. Reactor scram is initiated by position switches on the turbine stop valves.

Summary Of Accident Analysis

The reactor is assumed initially to be at rated power (1670 MWt). The turbine stop valves are taken to close in a conservatively short duration (0.1 second), and the insertion of scram reactivity is limited to the rate of insertion allowed by the Technical Specifications with the most reactive rod stuck out. The fuel temperature reactivity is assumed to correspond to its least negative time in life, while the void reactivity is taken as the most negative to maximize the power spike and pressure increases which result from the stop valve closure. The transient is mitigated by the action of the safety/relief valves, which are taken to open at the maximum pressure permitted by the Technical Specifications. Initial system pressure is conservatively placed 25 psi above the nominal operating pressure.

Figures 3.2-1 through 3.2-7 show the DYNODE-B versus GE REDY results for the Turbine Trip without Bypass transient.

The results show excellent comparison. DYNODE-B slightly overpredicts the peak power, and hence pressure, response (344% nominal versus 321% from REDY). Both codes predict the same initial water level response, though REDY predicts a stronger recovery of level. This is due to the differences in the transient void models.

DYNODE-B accurately reproduces the REDY results. The minor discrepancies that exist are due to code modeling differences. This case therefore provides an acceptable benchmark.

3.2.1.1.2 TURBINE TRIP WITH BYPASS

Description of the Accident

The sequence of events for the turbine trip with bypass malfunction are similar to that for the turbine trip without bypass (Section 3.2.1.1.1), except that the condenser heat sink is presumed to be available and hence the turbine bypass valves are operable. Following stop valve closure, the pressure regulator controls react to open the bypass valves and relieve steam to the condenser.

Summary of Accident Analysis

The reactor is assumed initially to be at rated power (1670 MWt). The turbine stop valves are taken to close in a conservatively short duration (0.1 second), and the insertion of scram reactivity is limited to the rate of insertion allowed by the Technical Specifications with the most reactive rod stuck out. The fuel temperature reactivity is taken to be at its least negative time in life while the void reactivity is at its most negative value. A rapid power spike and pressure increase follow the valve closure. The transient is terminated by the reactor scram, opening of the turbine bypass valves, and by the safety/relief valves whose opening setpoints are presumed at the maximum value permitted by the Technical Specifications. The initial system pressure is conservatively assumed to be 25 psi above the nominal setpoint.

Figures 3.2-8 through 3.2-14 show the DYNODE-B versus GE REDY results for the Turbine Trip with Bypass transient.

The results show excellent comparison. DYNODE-B slightly overpredicts the power, and hence pressure, response. Both codes predict the same initial water level response, though REDY predicts a stronger recovery of level. This is due to the differences in the transient void models. The increased level predicted by REDY in turn causes the feedwater controller to cut back on flow. This effect is not seen in DYNODE-B, since the level does not recover to the same degree.

DYNODE-B accurately reproduces the REDY results. The minor discrepancies that exist are due to code modeling differences. This case therefore provides an acceptable benchmark.

3.2.1.1.3 GENERATOR TRIP

Description of the Accident

The generator trip transient is a severe overpressurization transient which is similar in nature to the turbine trip. It represents the sequence of events which would follow rapid closing of the turbine control valves, which could follow a complete loss of electrical load. Reactor scram is initiated automatically by relays which sense the fast turbine control valve closure.

Summary of Accident Analysis

The reactor is assumed initially to be at rated power (1670 MWt). The turbine control valves are taken to close in a conservatively short duration (0.2 second), and the insertion of scram reactivity is limited to the rate of insertion allowed by the Technical Specifications with the most reactive rod stuck out. A rapid pressure increase follows the valve closure, the magnitude of which depends principally on the scram reactivity insertion rate and the void reactivity. The fuel temperature reactivity is conservatively taken at its least negative time in life, while the void reactivity is at its most negative to maximize the power excursion. The transient is mitigated by opening of the turbine bypass valves and the safety/relief valves.

Figures 3.2-15 through 3.2-21 show the DYNODE-B versus GE REDY results for the Generator Trip with Bypass transient.

The results show excellent comparison for all variables except water level and feedwater flow. Both codes predict the same initial water level response, though REDY predicts a stronger recovery of level. This is due to the differences in the transient void models. The increased level predicted by REDY in turn causes the feedwater controller to cut back on flow. This effect is not seen in DYNODE-B, since the level does not recover to the same degree.

DYNODE-B accurately reproduces the REDY results. The minor discrepancies that exist are due to code modeling differences. This case therefore provides an acceptable benchmark.

3.2.1.1.4 CLOSURE OF ALL MAIN STEAM ISOLATION VALVES

Description of the Accident

Closure of all the main steam isolation valves (MSIV) while the reactor is at power can result in a significant overpressure transient in the reactor vessel. The MSIV's can be closed directly by operator action while at power. Normally, as the valves close in all four steamlines, a reactor scram is initiated by position switches which sense the closure. As the system isolates, pressure rises in the vessel until the safety/relief valves open to mitigate the accident.

Summary of Accident Analysis

The reactor is assumed to be at rated power (1670 MWt). The MSIVs are taken to close in three seconds with a nonlinear valve flow characteristic. Fuel temperature reactivity is taken to be at its least negative time in life, while the void coefficient is at the most negative to maximize pressurization. Position switches on each MSIV will cause a reactor scram when valves in three of the four steamlines reach approximately 10% closed. This results in a scram before any significant steam flow interruption takes place. System pressure rises due to heat stored in the core. Insertion of scram reactivity is limited to the rate allowed by the Technical Specifications with the most reactive rod stuck out. The transient is mitigated by opening of the safety/relief valves, with lift setpoints assumed at the maximum Technical Specification limit. Initial system pressure is assumed 25 psi above the nominal value.

Figures 3.2-22 through 3.2-28 show the DYNODE-B versus GE REDY results for the MSIV Closure transient.

The DYNODE-B results show excellent comparison for all variables. The peak pressure predicted by REDY is approximately 10 psi greater than predicted by DYNODE-B. This difference can be caused by slight differences in the non-linear MSIV position versus area curve input.

DYNODE-B accurately reproduces the REDY results. The minor discrepancies that exist are due to code modeling and input differences. This case therefore provides an acceptable benchmark.

3.2.1.1.5 FEEDWATER CONTROLLER MALFUNCTION, MAXIMUM DEMAND

Description of the Accident

Failure of the feedwater controller in the direction of increased feedwater flow results in a moderator temperature and void decrease and a reactor power increase through the effect of the negative reactivity void coefficient. Water level increases during the initial part of the transient until the high water level turbine trip setpoint is reached. The turbine and feedwater pump trips, the reactor scrams, and an overpower and overpressure transient occurs.

Summary of Accident Analysis

The reactor is taken to be at 65% rated power (1085.5 MWt). The feedwater controller is assumed to fail in such a manner as to cause the feedwater flow to increase to its full run-out value. The water level and core inlet subcooling increase, causing reactor power to increase until the high water level turbine trip setpoint is reached, causing a turbine trip, feedwater pump trip, and a subsequent reactor scram due to turbine stop valve closure. Fuel temperature reactivity is taken at its least negative time in life, while the void reactivity is at its most negative to maximize the power and pressure transient. The insertion of scram reactivity is limited to the rate of insertion allowed by the Technical Specifications with the most reactive rod stuck out. The transient is mitigated by opening the turbine bypass valves and the safety/relief valves. The safety/relief valves are assumed to open at the maximum pressure permitted by the Technical Specifications.

Figures 3.2-29 through 3.2-35 show the DYNODE-B versus GE REDY results for the Feedwater Controller Failure - Maximum Demand transient.

The results show excellent comparison for all variables. The predicted scram time is slightly later in DYNODE-B. This is due to the fact that REDY assumes an instantaneous increase in feedwater flow whereas DYNODE-B assumes the feedwater control valve opens at the maximum rate. The peak pressure predicted by REDY is approximately 25 psi greater than predicted by DYNODE-B. This is due to the fact that the slight differences in the steam line models cause DYNODE-B to open the bypass valves, whereas REDY predicts they stay closed.

DYNODE-B accurately reproduces the REDY results. The minor discrepancies that exist are due to code modeling differences. This case therefore provides an acceptable benchmark.

3.2.1.1.6 LOSS OF FEEDWATER

Description of the Accident

A loss of feedwater flow results in a situation where the mass of steam leaving the reactor vessel exceeds the mass of water entering the vessel, resulting in a net decrease in the coolant inventory available to cool the core. Feedwater control system failures or feedwater pump trips can lead to partial or complete loss of feedwater flow. Feedwater flow would decay over a few seconds and the recirculation flow control system would ramp the recirculation pumps down to about 20% speed when the feedwater flow falls below 20% of rated. Water level declines rapidly and a reactor scram takes place when the low level trip setpoint is reached. The system subsequently closes the main steam isolation valves (MSIV's), and actuation of the high pressure coolant injection (HPCI) and reactor core isolation cooling (RCIC) systems on low level setpoints terminate the transient.

Summary of Accident Analysis

The reactor is taken to be at rated power (1670 MWt). The loss of feedwater is modeled as taking place over a three second period. When the feedwater flow reaches 20% of normal, the recirculation pump speed demand is set to 20%. The power level and system pressure decline in a fashion which depends principally on the void reactivity coefficient.

Figures 3.2-36 through 3.2-42 show the DYNODE-B versus GE REDY results for the Loss of Feedwater transient.

The DYNODE-B results show excellent comparison for all variables. The only minor discrepancy is that REDY predicts a reactor scram on low water level at approximately 13 seconds. DYNODE-B does not predict the scram throughout the 16 seconds simulated. This is due to the fact that the low water level scram input to REDY is 9 inches above that used in DYNODE-B.

DYNODE-B accurately reproduces the REDY results for this transient. The only discrepancy is caused by the input difference mentioned above. This case therefore provides an acceptable benchmark.

3.2.1.1.7 LOSS OF FEEDWATER HEATING

Description of the Accident

A loss of feedwater heating event can occur as the result of a loss of extraction steam to a feedwater heater. An alternative, but generally less severe, loss of heating can result from inadvertent actuation of high pressure coolant injection (HPCI), which delivers relatively cool water to the reactor through the feedwater sparger. Reduction in feedwater temperature follows, with a gradual rise in reactor power as the moderator temperature declines and reduces the core void fraction. If neutron power exceeds the reactor trip setpoint, a scram occurs; otherwise the system settles to a steady-state high-power condition until the operator intervenes.

Summary of Accident Analysis

The reactor is taken to be at rated power (1670 Mwt). The feedwater temperature change is modeled as a 100 °F decline with a 30-second exponential time constant. This is more severe than any loss of feedwater heating which can result from a single system malfunction. Fuel temperature reactivity is chosen at its least negative time in life, while void reactivity is at its most negative to maximize the power increase. Scram insertion, should it occur, is limited to the insertion rate permitted by the Technical Specifications.

Figures 3.2-43 through 3.2-49 show the DYNODE-B versus GE REDY results for the Loss of Feedwater Heating transient.

The DYNODE-B results show excellent comparison for all variables. DYNODE-B predicts a more conservative increase in power and average surface heat flux. This case therefore provides an acceptable benchmark of DYNODE-B's capabilities to reproduce the REDY code predictions.

3.2.1.1.8 PRESSURE REGULATOR FAILS OPEN

Description of the Accident

In the event that either the electrical or mechanical pressure regulator were to fail such that the turbine control and/or bypass valves were opened, steam flow from the reactor would increase. System pressure would drop, causing an increase in core voids and a consequent drop in reactor power. Depressurization would continue until the main steam isolation valve closure setpoint was reached, resulting in closure of the valves and a reactor scram. Decay heat then would cause the system to repressurize, limited by opening of the automatic safety relief valves until cooldown was initiated.

Summary of Accident Analysis

The reactor is taken to be at rated power (1670 MWt). The pressure regulator is taken to fail in such a way that the turbine control valves and/or bypass valves are opened to 110% steam demand (the maximum permitted by the control system). The excess demand depressurizes the system until the main steam isolation valves close and the reactor scrams. Thereafter, the pressure rises due to decay heat, and the automatic safety/relief valves lift intermittantly until cooldown is initiated.

Figures 3.2-50 through 3.2-56 show the DYNODE-B versus GE REDY results for the Pressure Regulator Fails Open transient.

DYNODE-B follows the REDY predicted steam dome pressure very closely with the exception that DYNODE-B predicts the MSIV closure on low turbine throttle pressure to occur approximately 2 seconds after REDY. This is due to differences in the steam line model. The same initial depressurization causes a greater void increase in REDY than in DYNODE-B due to the differences in the void models. This in turn causes the REDY predicted core power and core inlet flow to drop faster than DYNODE-B.

DYNODE-B accurately reproduces the REDY results for this transient. The discrepancies are caused by code modeling differences. This case therefore provides an acceptable benchmark.

3.2.1.1.9 RECIRCULATION PUMP SEIZURE

Description of the Accident

The recirculation pump seizure is a nearly instantaneous stoppage of a recirculation pump shaft and impeller. This stoppage results in a very rapid reduction in core flow and a subsequent decline in core power. Because the heat flux at the fuel pin surface declines more slowly than the core flow, there is a potential degradation of thermal margin. No reactor scram results, and the system settles to reduced power.

Summary of Accident Analysis

The reactor is taken to be at rated power (1670 MWt). The affected pump speed is instantaneously set to zero and the drive flow abruptly decays. Jet pump flow in the seized loop reverses in less than 1 second. As a result, core flow decreases, causing an increase in void fraction and a consequent reduction in reactor power. The degree of reduction in power depends principally on the void coefficient of reactivity, which is taken at its least negative time in life, while Doppler reactivity is at its most negative to maximize the heat flux to flow ratio during the transient. Heat flux from the fuel pins lags the core power decline, and the system relaxes to a reduced power steady state.

Figures 3.2-57 through 3.2-63 show the DYNODE-B versus GE REDY results for the Recirculation Pump Seizure transient.

The DYNODE-B results show excellent comparison for all variables. This case therefore provides an acceptable benchmark of DYNODE-B's capabilities to reproduce the REDY code predictions.

3.2.1.1.10 TWO RECIRCULATION PUMP DRIVE MOTOR TRIP

Description of the Accident

In the event that the power supply to both recirculation pump motor/generator (M/G) sets were lost, the pumps would coast down and coolant flow to the core would decline. Core voids would then increase and power would decline. The system settles to a natural circulation condition where core flow is provided through the jet pump suction path by the weight of subcooled water in the downcomer. Heat flux decline lags power and core flow, so there is a potential degradation of thermal margin limits.

Summary of Accident Analysis

The reactor is taken to be at rated power (1670 MWt). The transient is initiated by setting the recirculation pump drive motor torques to zero. The inertia of the M/G sets is included in the analysis because there is no single event which would result in simultaneously opening the pump generator breakers to both pumps. The void reactivity is taken at its least negative time in life, while fuel temperature reactivity is at its most negative to maximize the power to flow ratio during the event. The pumps, core flow, power, pressure, and steam flow all decline to steady-state, natural-circulation conditions.

Figures 3.2-64 through 3.2-70 show the DYNODE-B versus GE REDY results for the Two Recirculation Pump Drive Motor Trip transient.

DYNODE-B compares very well with the REDY-predicted core inlet flow during the initial flow coastdown. As the transient progresses, REDY predicts a slightly lower core inlet flow. This could be caused by differences in the pump model input. The lower core inlet flow predicted by REDY causes increased voiding and hence a greater power decrease and more level holdup. The lower power causes lower heat flux and lower pressure. The higher level causes a greater feedwater decrease in an attempt by the feedwater controller to compensate.

In general, DYNODE-B follows the same trends and reproduces the REDY result for this transient. The discrepancies are caused by code modeling difference. This case therefore provides an acceptance benchmark.

3.2.1.1.11 RECIRCULATION FLOW CONTROLLER FAILURE, INCREASE DEMAND

Description of the Accident

There are several possible failures which can result in an increase in core coolant flow. The most severe of these occurs when a motor/generator (M/G) set fluid coupler for one recirculation pump attempts to achieve full speed at maximum acceleration. The result is a surge of additional coolant through the core and a consequent power increase. If the neutron flux increases to the high power trip setpoint, the reactor scrams. The possibility of a large power increase allows for potential degradation of thermal margin.

Summary of Accident Analysis

The most severe initial condition for the increasing recirculation flow transient is near the low end of the automatic recirculation flow control range, where reactor power is approximately 65% of rated power and core flow is approximately 50% of rated flow. The pumps are operating at approximately 45% speed, and the relative M-G set fluid coupler scoop tube position is approximately 20%. The transient is modeled by moving the scoop tube position at its maximum rate to the maximum coupling position. Void reactivity is taken at its most negative time in life, while fuel temperature reactivity is at its least negative to maximize the power increase. As the pump speed increases, core flow and power increase and, if the power increase is sufficient, a scram occurs. The system then settles to a steady state until the operator intervenes.

Figures 3.2-71 through 3.2-77 show the DYNODE-B versus GE REDY results for the Recirculation Flow Controller Failure - Increased Demand transient.

The DYNODE-B results show excellent comparison for all variables. Minor discrepancies in the level response are caused by the transient void model differences.

DYNODE-B accurately reproduces the REDY results for this transient. The minor discrepancies are caused by code modeling differences. This case therefore provides an acceptance benchmark.

3.2.1.1.12 RECIRCULATION FLOW CONTROLLER FAILURE, DECREASE DEMAND

Description of the Accident

The failure of one recirculation pump motor/generator (M/G) set speed controller could cause the scoop tube position to move at its maximum speed in the direction of zero pump speed and flow. As a result, core flow, power, steam flow, and pressure all decrease. Because the decline in heat flux lags that of core flow and power, there is a potential degradation in thermal margin.

Summary of Accident Analysis

The reactor is taken to be at rated power (1670 MWt). The transient is initiated by forcing the scoop tube position of the affected loop M-G set from its initial value to zero at the maximum rate. Core flow, power, steam generation, and pressure all decline, and the system settles to a steady state at reduced power with reverse flow through the inactive jet pumps. Void reactivity is taken at the least negative time in life while fuel temperature reactivity is at the most negative to maximize the power to flow ratio during the transient.

Figures 3.2-78 through 3.2-84 show the DYNODE-B versus GE REDY results for the Recirculation Flow Controller Failure - Decreased Demand transient.

The DYNODE-B results show excellent comparison for all variables. The DYNODE-B predicted core inlet flow drops slightly lower than the REDY-predicted flow. This can be due to minor input differences in the coupler torque versus slip and coupling function. All of the other discrepancies are insignificant and attributable to the void model differences.

DYNODE-B accurately reproduces the REDY results for this transient. The slight discrepancies are caused by code modeling or input differences. This case therefore provides an acceptance benchmark.

3.2.1.1.13 IMPROPER START OF AN INACTIVE RECIRCULATION LOOP

Description of the Accident

Improper start of an inactive recirculation loop involves activating an improperly warmed idle recirculation pump while the reactor is at power. Depending on the initial reactor condition, this incident can cause a significant power increase and reduction of thermal margin. The system settles out to an increased power steady state or, in the event the high neutron power trip setpoint is reached, the reactor scrams.

Summary of Accident Analysis

The initial conditions of the system substantially affect the results of the transient. One recirculation pump is presumed operating at full speed while the second pump is stopped. The idle loop pump discharge valve is taken to be initially closed with the discharge bypass valve open. The inactive drive line is assumed to be filled with cold (100 °F) water. Reactor power and core flow are conservatively placed at midrange values with analyses performed to determine the most adverse conditions. The motor/generator (M/G) set fluid coupler for the idle pump is initially set for 50% speed demand.

The transient sequence of events is as follows:

A. At t = 0, the idle M/G set drive motor breaker is closed.

B. The drive motor reaches near-synchronous speed quickly, while the generator reaches approximately 80% speed in 5 seconds.

C. At 5 seconds the generator field breaker is closed, loading the generator and applying starting torque to the pump motor. Generator speed decreases, the pump breaks into rotation and builds up speed.

D. Generator speed demand is programmed back to 20% starting at 8 seconds.

E. The pump discharge valve/drive motor interlock is cleared, and the valve opens with a 60-second stroke time.

The transient system behavior depends, to a great degree, on initial system power. At relatively high power, the pressure drop across the core becomes large and the starting pump does not develop sufficient head to reverse the backflow through the idle loop diffusers. Consequently, the water injected out the idle drive lines is swept back into the downcomer, where it is heated before eventually returning to the lower plenum through the active loop. In contrast, at low power, the starting pump may cause the jet pump flow to become positive, sending the cold water directly into the immediate core flow path and resulting in a substantial core power increase and a possible reactor trip on high flux.

Following the pump start, core flow abruptly increases, causing a power increase. If the reactor does not trip, the power peaks and then settles to a new level. As the pump discharge valve opens, power will increase as the valve permits flow to increase. If the reactor does trip, the scram terminates the power increase and causes the system to settle to zero power conditions. In either case, heat flux will increase to a maximum value at which time thermal margin will reach a minimum, and then the heat flux will decline.

Figures 3.2-85 through 3.2-91 show the DYNODE-B versus GE REDY results for the Improper Start of an Inactive Recirculation Loop transient.

The DYNODE-B results show the same general trends for all parameters as those predicted by GE REDY, although the magnitudes of the responses are different. This is due primarily to an apparent discrepancy between GE's written description of this transient and the plotted results (Reference 2). In the description, it is stated that the active pump initially produces 115% of normal rated flow in its associated jet pumps; in the figure, a flow of 150% is indicated. In either case, the core receives 54% of its normal rated flow, and all remaining flow from the active loop appears as reverse flow through the inactive loop. Therefore, the reverse flow through the inactive loop is much higher in the case of 150% active pump flow. The DYNODE-B analysis uses 115% active loop flow, per the written description.

Because of the initially high reverse flow in the GE REDY case, the inactive pump is unable to establish positive flow during the transient. As a result, the cold water in the loop is swept up into the downcomer, where it mixes with the bulkwater before being pumped through the core by the active loop. This causes a relatively gradual reactivity insertion, so that the resulting power spike and rise in heat flux are mild.

In contrast, the reverse flow in the DYNODE-B case is low enough so that the idle pump does establish positive flow upon starting up. The cold water is therefore pumped directly into the lower plenum and through the core, causing a faster reactivity insertion than in the GE REDY case. At the same time, establishing positive flow through the idle loop means an additional power increase because of the higher core flow. As a result, the power spike and the rise in heat flux are higher in the DYNODE-B case. The responses of other parameters are correspondingly altered.

Despite this input difference which causes DYNODE-B to predict a more severe transient than REDY, both codes predict the same trends and show the same general results for this transient. This case therefore provides an acceptance benchmark.

3.2.1.2 GENERAL ELECTRIC ODYN CODE

The models described in Reference 9 were duplicated as closely as possible for these cases. Major differences in the code models are described in Section 2.3.

Wherever possible, the input from the Monticello Cycle 11 ODYN analysis [4] was used. The major input discrepancy in these cases is that the 1-D kinetics inputs used by the ODYN code were unknown and had to be estimated.

Three transients from the Cycle 11 Supplemental Reload Analysis [4] were benchmarked. The following sections describe each transient and document the benchmark analysis results.

3.2.1.2.1 LOAD REJECTION WITHOUT BYPASS

Description of the Accident

Fast closure of the turbine control valves is initiated whenever electrical grid disturbances occur which result in significant loss of load on the generator. The turbine control valves are required to close as rapidly as possible to prevent overspeed of the turbine generator rotor. The closing causes a sudden reduction of steam flow which results in a nuclear system pressure increase. The reactor is scrammed by the fast closure of the turbine control valves.

Summary of Accident Analysis

The reactor and turbine/generator are initially operating at full power when the load rejection occurs. The power/load unbalance device steps the load reference signal to zero and closes the turbine control valves at the earliest possible time. The turbine accelerates at a maximum rate until the valves start to close. The turbine control valves close in 0.25 sec.

Reactor scram is initiated upon sensing control valve fast closure. The insertion of scram reactivity is limited to the rate of insertion allowed by the Technical Specifications with the most reactive rod stuck out. A rapid pressure increase follows the valve closure, the magnitude of which principally depends on the scram reactivity insertion rate and the void reactivity. If the pressure rises to the pressure relief set point, some or all of the relief valves open, discharging steam to the suppression pool. If the pressure rises to ≥ 1150 psig, trip of the M/G set breaker occurs, causing both recirculation pumps to coast down.

Figures 3.2-92 through 3.2-98 show the DYNODE-B calculated results versus the General Electric ODYN results.

DYNODE-B underpredicts the ODYN power and hence heat flux, increase. This is due to differences in the void and scram reactivity functions. It is impossible to accurately reproduce the 1-D reactivity inputs used by General Electric based on the limited information available. A better response can be achieved by

performing sensitivity studies for the kinetics parameters. However, since the purpose of these benchmarks is only to perform a general check on the models used in DYNODE-B (the data comparisons in Section 3.2.2 perform the primary check), the benchmarks were left as is. It is sufficient to understand discrepancies due to input differences in this case.

Most of the remaining differences are attributable to the difference in the heat flux response. The larger heat flux predicted by ODYN causes the pressure to hang up for a longer time and the water level to recover more quickly due to a larger core resistance. Note that GE plots actual water level and DYNODE-B sensed water level which is the source of the difference in the initial values. Faster recovery of the water level causes the feedwater controller to ramp down the feedwater sooner.

The differences in core inlet flow response are partially attributable to the heat flux differences and partially due to code modeling differences. In DYNODE-B, the pressure difference between the core outlet plenum and the steam dome is not explicitly calculated. Thus, for the recirculation flow rate calculation, this pressure-difference is computed from the momentum equation in which the steam separator flow acceleration term is obtained by assuming that the separator flow is replaced by the total core flow. This assumption is equivalent to assuming that the core fluid is incompressible. Thus, in cases of rapid void collapse in the core, this acceleration term does not play a significant role. The effect of this assumption is expected to be small, since the core void fraction is primarily responding to changes in pressure which are being taken into account properly. For this transient, this assumption results in DYNODE-B underpredicting the core inlet flow increase during the initial pressurization. The impact of this effect on ΔCPR is insignificant.

This benchmark represents a positive check of DYNODE-B's capabilities to perform BWR transient calculations. The differences between the DYNODE-B and ODYN results are well understood and do not reflect deficiencies in the DYNODE-B code.

3.2.1.2.2 FEEDWATER CONTROLLER FAILURE - MAXIMUM DEMAND

Description of the Accident

This event is postulated on the basis of a single failure of a control device, specifically one which can directly cause an increase in coolant inventory by increasing the feedwater flow. The most severe applicable event is a feedwater controller failure resulting in maximum flow demand, which causes an increase of feedwater flow to the reactor vessel. This excess flow results in an increase in core subcooling, which results in a core power rise, and a rise in the reactor vessel water level.

The rise in the reactor vessel water level eventually leads to high water level trip of the feedwater pumps and turbine, in turn causing a reactor scram.

Summary of Accident Analysis

The reactor is taken to be initially at 98% rated power (1634 MWt) and 100% flow. This point was found to be more conservative than the 100% power/100% flow point for the cycle 11 core (Ref. 4).

The reactor is operating in a manual flow control mode which provides for the most severe transient. The feedwater controller is assumed to fail during the maximum flow demand. Maximum feedwater pump run out is assumed. The influx of excess feedwater flow results in an increase in core subcooling which reduces the void fraction and thus induces an increase in reactor power. The excess feedwater flow also results in a rise in the reactor vessel water level which eventually leads to high water level; main turbine and feedwater trip and turbine bypass valves are actuated. Reactor scram trip is actuated from main turbine stop valve position switches. Relief valves open as steamline pressures reach relief valve setpoints. If the pressure rises to ≥1150 psig, trip of the M/G set breakers occurs, causing the recirculation pumps to coast down.

Figures 3.2-99 through 3.2-105 show the DYNODE-B calculated results versus the General Electric ODYN results.

The DYNODE-B results compare very well to the ODYN results. The same input and modeling differences exist as in the previous benchmark (Section 3.2.1.2.1 Load Rejection without Bypass). The Feedwater Controller Failure transient is not as sensitive to void reactivity as is the Load Rejection transient and hence provides a much better code comparison.

The DYNODE-B results are slightly time shifted (approximately 0.5 sec). This is due to the fact that General Electric assumes instantaneous feedwater runout flow, whereas DYNODE-B opens the feedwater control valves at the maximum rate to runout flow. Time to runout in DYNODE-B is 1.1 sec.

This case provides an excellent check of DYNODE-B's capabilities to perform BWR transient analysis. The differences between the ODYN and DYNODE-B results, for this transient, are insignificant.

3.2.1.2.3 MSIV CLOSURE (FLUX SCRAM)

Description of the Accident

This event is performed to show compliance with the ASME Vessel Pressure Code. The MSIV's can be closed directly by operator action while at power. Closure of all main steam isolation valves (MSIV) while at power can result in a significant overpressure transient in the reactor vessel. Normally, as the MSIV's close, a reactor scram is initiated by position switches which sense closure. In addition, a secondary reactor scram will be initiated on high neutron flux. As the system isolates, pressure rises in the vessel until the safety/relief valves open to mitigate the accident.

Summary of Accident Analysis

The reactor is assumed initially to be at rated power (1670 MWt). The MSIV's are taken to close in three seconds with a non-linear valve flow characteristic. A reactor scram on MSIV position is conservatively ignored. Reactor scram is initiated on high neutron flux. The insertion of scram reactivity is limited to the rate of insertion allowed by the Technical Specifications with the most reactive rod stuck out. A rapid pressure increase follows closure of the MSIV's. If the pressure rises to the pressure relief set point, some or all of the relief valves open, discharging steam to the suppression pool. If the pressure rises to $\geq$ 1150 psig, trip of the M/G set breakers occurs.

Figures 3.2-106 through 3.2-112 show the DYNODE-B calculated results versus the General Electric ODYN results.

The DYNODE-B results compare favorably to the ODYN results. The same input and modeling differences exist as in the Load Rejection without Bypass benchmark (Section 3.2.1.2.1) since the two transients are very similar in response. The MSIV closure transient pressurizes more slowly and therefore is less sensitive to void reactivity and hence the DYNODE-B and ODYN results compare more closely. The maximum increase in the reactor vessel pressures are within 10 psi. The differences between the DYNODE-B and ODYN responses to this transient are insignificant.

3.2.2 CODE-DATA COMPARISONS

In this section the DYNODE-B code is benchmarked to three Peach Bottom turbine trip tests [16] and six Monticello start-up tests [14]. The purpose of these benchmarks is to qualify the models used in DYNODE-B and to quantify the conservatism in the DYNODE-B code. Section 4 discusses the quantification of the code conservatisms.

3.2.2.1 PEACH BOTTOM 2 EOC 2 TURBINE TRIP TESTS

Three instrumented turbine trips were carried out at the Peach Bottom-2 reactor during April 1977. These tests were conducted with the direct scram on stop valve position bypassed so that a trip on high flux was obtained. This departure from the normal reactor condition was required to obtain a sufficiently large flux response to allow a more complete model-test comparison. A detailed description of the test conditions and measurement process can be found in Reference 16.

3.2.2.1.1 TEST SUMMARY

The initial power and flow conditions for each test are shown in Table 3.2-1. These test conditions were selected in order of increasing power along a line of constant reactor flow. Prior to the second turbine trip test, it was necessary to reduce core flow to obtain the power to within 1% of planned test power level due to the xenon level in the core at the time of the test. In each of the three tests, the turbine stop valve position scram was disabled and the flux scram setpoint was reduced. The scram setpoints are also listed in Table 3.2-1.

A total of 153 signals were recorded by a digital data acquistion system. The comparisons presented here will concentrate on those parameters which affect the transient ΔCPR.

3.2.2.1.2 MODEL INPUTS

The DYNODE-B program has been used to model the three Peach Bottom 2 End of Cycle 2 (PB2EOC2) turbine trip tests (TT1, TT2, and TT3) for the purpose of benchmarking against overpressure transients which result in a rapid power increase. This benchmark effort began with an early version of DYNODE-B which did not have a one-dimensional kinetics or a detailed steam line model, so that these results were based on point kinetics and the lumped steam line models. This same model was used in pre-test predictions which validated the corresponding REDY results. Subsequently, the latest version of DYNODE-B was used to incorporate spatial kinetics and steam line momentum effects. The development process is described below.

The initial modeling of PB2 EOC2 was accomplished by utilizing design data and operational characteristics published in Reference 11 for the Reactor Coolant System (RCS). The point kinetics parameters were generated with a full 3-D nodal model of the core, similiar to the models for Monticello described in Reference 1, using the actual initial test conditions. This work was performed by UAI (formerly NAI) and documented in Reference 10. This Best Estimate model utilized the MOC solution for the steam line momentum effects as well as actual APRM trip setpoints, actual turbine and bypass valve positions, scram velocities, and recorded initial test conditions (RV pressure and flow, core power, steam flow, and core inlet subcooling) from Reference 16.

The results of these comparisons provided satisfactory agreement with the measured core power and pressure transient data.

Later on, after the one-dimensional kinetics model had been implemented in DYNODE-B, the benchmarks were repeated. However, for these analyses, the one-dimensional kinetics could not be obtained directly from the 3-D model, since the model is no longer available. Thus, an approximate approach was taken in which the reactivity dependencies on void, fuel temperature, and control state were established to give results which were comparable with the point kinetics data. The void dependency was then adjusted until the peak power matched the test data, and the scram worth was adjusted until the integrated power matched the test data. This procedure effectively eliminates the uncertainty due to the kinetics parameters. The test data comparisons thus represent differences due to the DYNODE-B computer code uncertainties only. Therefore, these tests therefore represent a way to quantify these uncertainties (See Section 4.4).

3.2.2.1.3 DATA COMPARISONS

This section describes the calculated to measured comparisons for the most important transient parameters; neutron flux, steam dome pressure, turbine throttle pressure, and critical power ratio. Table 3.2-1 summarizes the comparisons. A detailed description of each of the above four parameters follows.

Neutron Flux Comparisons

The neutron flux transient is initiated by the main steam line pressure rise due to turbine stop valve (TSV) closure. Normally a reactor scram on TSV position would occur at 10% closure of three out of four valves. This scram signal was bypassed for these tests. A pressure wave, due to TCV closure, travels down the steamline and into the core, causing void collapse and a flux increase. The largest flux rise occurs near the top of the core, which has the largest void fraction and the largest void coefficient. The flux increase causes a reactor scram on high neutron flux. The power peaks and turns around due to the insertion of scram reactivity as well as a decrease in the void reactivity and an increase in the negative Doppler reactivity. For the Peach Bottom Test conditions, the scram reactivity is the dominant contributor to the flux transient turn-around. This is due to the fact that many control rods are inserted in the core, initially giving rise to a strong scram reactivity.

Figures 3.2-114, 3.2-117 and 3.2-120 show the calculated versus measured responses of the relative neutron flux (APRM Channel A from Reference 16) for tests TT1, TT2, and TT3, respectively. The uncertainties in void reactivity and scram reactivity have been factored out as discussed previously. Therefore, as would be expected, the DYNODE-B results show excellent comparison in the peak flux, flux slopes, and widths of the flux peak.

Transient Pressure Comparisons

Dynamic pressure measurements were recorded at the turbine inlet, in the steamline 90 ft downstream from the vessel, the vessel dome, and near the core exit plenum. In all of the pressure comparisons listed in this section, the data shown are the unfiltered data as recorded by the pressure sensors. The sensors are connected to the appropriate measurement locations by water-filled sensor lines. These sensor lines have their own second-order response which can often give rise to oscillations in the recorded data. Further discussion of the sensor line effects is contained in Reference 16.

Figures 3.2-115, 3.2-118 and 3.2-121 show the calculated versus measured response of the turbine throttle pressure for TT1, TT2, and TT3, respectively. DYNODE-B accurately predicts the initial pressure oscillation in both timing and magnitude, indicating that the initial time effects; i.e. delays, rise times, and frequencies; are well modeled. As the transient progresses, the calculated wave frequencies are accurately predicted, though the wave amplitudes are greater. The increased amplitude does not appreciably affect the transient results with respect to CPR. The overall magnitude of the turbine throttle pressure is conservatively overpredicted for the latter part of the transients.

Figures 3.2-113, 3.2-116 and 3.2-119 show the calculated and measured steam dome pressures follow the same trends as the turbine throttle pressures; the initial pressure rise and wave frequency are well predicted, the wave amplitudes are slightly over predicted, and the overall magnitude is conservatively overpredicted.

Critical Power Ratio

Critical Power Ratio is defined as the ratio of the bundle power which would produce onset of transition boiling to the actual bundle power. A good measure of the relative severity of a particular reactor transient is the maximum change of CPR, divided by the initial or steady-state CPR (ICPR). The "measured" CPR is taken from Reference 9 and is determined as follows:

"For the Peach Bottom turbine trips, the CPR comparisons have been made by driving a hot channel transient thermal-hydraulic calculation with experimentally determined inlet flow, pressure, and fuel heat generation rate. The pressure input was taken from the core pressure signal, which was filtered with a 5 Hz low pass filter. The transient fuel heat generation rate was taken to be proportional to the total APRM response. Core flow was obtained from pressure drop measurements taken across four of the jet pumps throughout the three turbine trips. Changes in core flow can be detected by assuming the jet pump pressure drop to be proportional to the square of the flow. In practice, however, this is not an accurate measure of core flow because of the large amount of noise in the jet pump pressure drop signal. In this case, a 5 Hz filter was applied to the four jet pump signals to reduce the noise component and then averaged to obtain a pressure drop. The steady-state flow was normalized to the recorded flow at the beginning of each transient."

"For the transient CPR calculations driven by the experimental data, uncertainties in the input quantities will contribute to an uncertainty in the ratio CPR/ICPR. [Reference 16] quotes a ±2 psi uncertainty in core pressure. This pressure uncertainty, coupled with a ±3% uncertainty in flow, results in a ±0.01 uncertainty in the ratio ΔCPR/ICPR. This CPR uncertainty is obtained from sensitivity calculations carried out on pressurization type transients."

The calculated CPR is determined from a hot-channel model in DYNODE-B using the GEXL correlation. The hot-channel dimensions are taken from Reference 11. The initial hot-channel bundle power was forced to give the correct ICPR.

In both cases, the initial conditions, channel properties, and the CPR correlation are identical. Only the transient forcing functions, i.e., power, pressure, flow, and inlet enthalpy are different, so that a good measure of the CPR uncertainty due to code model uncertainty is obtained.

The calculated versus measured CPR results are shown in Table 3.2-3. For each transient, the calculated ΔCPR/ICPR is approximately 10% greater than the measured value. This indicates that the DYNODE-B code model uncertainties provide a conservative 10% bias on transient ΔCPR/ICPR.

3.2.2.2 MONTICELLO START UP TESTS

The DYNODE-B code has been used to model six Monticello Start-Up Tests. These tests are described and documented in Reference 14.

The modeling of these tests was done using best-estimate input parameters. A 1-D kinetics model was used for the MSIV closure and Turbine Trip transients. Point kinetics were used for the remaining four cases. This is in accordance with the guidelines in Section 4.1.

The results for each transient are discussed in the following sections.

3.2.2.2.1 TURBINE TRIP WITH BYPASS AT 100% POWER (STP 16)

Description of the Test

The purpose of this test was to determine the response of the reactor system to a turbine trip.

The turbine was tripped with the Turbine Emergency Trip Switch at 1656 MWt. Reactor pressure peaked at 1115 psig, an increase of 105 psi. The M/G set breakers were tripped on turbine trip causing a flow coastdown. All four relief valves opened to terminate the pressure transient. A power increase was not observed on the APRMs.

Summary of the Test Analysis

Figures 3.2-122 through 3.2-127 show the calculated versus measured results for the Turbine Trip Start Up Test.

DYNODE-B overpredicts the core power response with a peak relative power of approximately 300 percent. The data does not show a power increase during the initial pressurization. This is probably due to a faster/stronger scram than was assumed in the analysis. Since DYNODE-B overpredicts the integrated power, it also overpredicts the vessel pressure response. Both the calculated and measured results show that all four relief valves open, but DYNODE-B predicts a peak vessel pressure of 1154 psia compared to the measured value of 1130 psia.

DYNODE-B conservatively predicts the vessel flow coastdown and does a good job of tracking level.

A "measured" Critical Power Ratio was calculated by forcing the DYNODE-B hot channel model with the measured data. This resulted in a "measured" ΔCPR/ICPR of 0.003. The DYNODE-B calculated results give a ΔCPR/ICPR of 0.156. This is due mainly to the difference in the power response.

This transient provides a good benchmark of DYNODE-B's capability to conservatively predict reactor vessel pressure and transient ΔCPR. It also provides an excellent benchmark of DYNODE-B's capability to model transient vessel flow response.

3.2.2.2.2 CLOSURE OF 4/4 MAIN STEAM ISOLATION VALVES AT 75% POWER (STP 11)

Description of the Test

The purpose of this test was to functionally check the main steam line isolation valves for proper operation, demonstrate the capability to perform isolation valve test closures without threatening reactor safety or causing a reactor scram, determine reactor transient behavior following simultaneous full closure of all MSIV's, and determine isolation valve closure times.

The full isolation test was done at 75% power by tripping the relays in the RCICS circuit with a special test switch to give a full isolation and subsequent scram. Following the full isolation at 75% power, reactor pressure increased 69 psi to 1069 psig two seconds after the MSIV's had closed.

Summary of the Test Analysis

Figures 3.2-128 through 3.2-132 show the calculated versus measured results for the MSIV Closure Start Up Test.

The measured feedwater flow did not behave as would be expected from automatic controller action. Therefore it was presumed that the feedwater was controlled manually during the test and the measured feedwater flow was forced onto the DYNODE-B solution. The measured steam flow shows unexplainable behavior and was assumed to be bad data. The two most important input parameters, MSIV closure time and scram time, are unknown and were assumed to match the nominal values in the DYNODE-B calculation.

Both the measured and calculated results show a rapid increase in pressure due to the MSIV closure. DYNODE-B predicts a faster initial rise than the data (50 psi/sec versus 30 psi/sec). The data shows that the pressure peaks at about 1080 psia (15 psi below the relief valve setpoint) and then slowly decays. DYNODE-B predicts that the pressure rises to the relief valve setpoint, cycling the relief valves to control pressure. The differences in pressure response could be attributable to several different factors; the test may have a slower MSIV closure than assumed, a faster scram than assumed, the MSIV valves may not have closed completely, or there may be a steam condensation effect due to uncovery of the feedwater sparger. In any case, there is insufficient data available to determine a cause and effect.

This test does not provide a very good benchmark due to the poor quality of the data. It does show that DYNODE-B tracks the water level very well during the initial pressurization and that DYNODE-B conservatively overpredicts the peak transient pressure.

3.2.2.2.3 2/2 RECIRCULATION PUMP TRIP (STP 14)

Description of the Test

The purposes of this test were to evaluate the recirculation flow and core power transients following trips of both of the recirculation pumps, calibrate the reactor core flow measurement system, and measure the reactor core flow by performing mass and energy balances on the reactor downcomer.

Both individual and dual pump trip transients were recorded. For the purposes of this analysis, only the two-pump trip case was examined, since this represents a more severe transient than the single pump trip. Prior to tripping the pumps, core performance data were taken to enable the peak heat flux and MCHFR to be evaluated. A recording was taken which included a trace of the core flow and the simulated heat flux.

Summary of the Test Analysis

Figures 3.2-133 and 3.2-134 show the calculated versus measured results for 2/2 Pump Trip Start Up Test.

DYNODE-B conservatively overpredicts the vessel flow coastdown, i.e., DYNODE-B predicts lower flow than the data. Also, DYNODE-B conservatively overpredicts the core average heat flux. Since these are the only variables available for comparison, it is concluded that DYNODE-B provides a conservative prediction of Critical Power Ratio for this transient.

3.2.2.2.4 AUTOMATIC FLOW DECREASE AT 100% POWER (STP 15)

Description of the Test

The purpose of this test was to determine the plant response to changes in the recirculation flow and to demonstrate the plant load-following capability.

To determine the plant response to changes in the recirculation flow, the master flow controller setpoint was stepped a nominal ± 10% of full scale. At each test condition, the test was repeated with several controller settings to aid in optimizing the response of the system. Initial individual loop control settings were at 500% proportional band and 15 repeats per minute reset. The optimized controller settings were arrived at during testing at 50% power, where the proportional band of both loops were set to 450%, loop A reset was set at 40 repeats per minute, and loop B reset was set at 20 repeats per minute. The initial master controller settings were 400% proportional band and 8 repeats per minute based on results obtained during 50% power testing. Instabilities which ocurred during flow ramp testing between 75 and 100% power on the 100% power-flow line were corrected by reducing the resets to 2 repeats per minute.

The upper and lower speed demand limits were set to 93% and 58% speed, respectively. This placed the limits of automatic and master manual flow control to a range from 75% to 100% power in the 100% power rod pattern.

The automatic flow control flow ramp tests were performed with the Electrical Pressure Regulator (EPR) setpoint adjuster gain (POT150P) at 3.0 psi/% and a time constant (POT162P) of 20 seconds.

To demonstrate plant load-following capability, the fast flow changes were made with the final control system settings described above. The load changes were made first in the Master Manual mode and then in the Automatic Flow Control mode. In the Automatic mode, the load changes were caused by ramping the turbine speed/load changer. Turbine load could be dropped very rapidly by the automatic opening of the bypass valves.

For the purposes of this analysis only the Pump Flow Decrease in Automatic Manual from 100% to 75% power was examined since this represents the most severe transient in the series.

As the flow controller responds to the setpoint step, the vessel flow ramps down and core power decreases due to the increased void feedback. The entire system decays to a new steady state. An APRM decay ratio of 0.25 was calculated based on the measured data.

Summary of the Test Analysis

Figures 3.2-135 through 3.2-140 show the calculated versus measured results for the Auto Flow Decrease Start Up Test.

The DYNODE-B predicted results show excellent comparison during the first 20 sec of the transient, tracking all variables very closely. Beyond this point, the DYNODE-B results deviate slightly. The data settles out to a new steady state condition very quickly, with a decay ratio of 0.25 calculated from the APRM response. DYNODE-B conservatively predicts a decay ratio of 0.89 and a longer frequency (approximately 30 sec versus 10 sec from the data).

This transient provides an excellent benchmark of DYNODE-B's capability to conservatively predict decay ratio.

3.2.2.2.5 PRESSURE REGULATOR SETPOINT STEP AT 100% POWER (STP 18)

Description of the Test

The purpose of this test was to determine the reactor and pressure control system responses to pressure regulator setpoint changes, to demonstrate the stability of the reactivity void feedback loop to pressure perturbations, and to optimize the pressure regulator setpoints.

Pressure setpoint changes were made with both the Electrical Pressure Regulator (EPR) and the Mechanical Pressure Regulator (MPR) to determine reactor and turbine system responses and to demonstrate the stability of the reactivity void feedback loop to pressure perturbations.

The pressure disturbances were obtained by changing the regulator setpoint downward and then upward as fast as possible to produce a nominal 10 psi change in reactor pressure. This was done with the load limits out of the way (load limiter set well above the reactor power level) and repeated with the load limits incipient (load limiter set at the reactor power level).

The changes in the EPR setpoint were made from a special test circuit located in the cable spreading room, which initiated a step change in the setpoint.

For the purposes of this analysis, only the -10 psi step of the EPR setpoint at 100% power was examined, since this represents the most severe transient in the series.

The pressure controller responds to -10 psi step by opening the turbine control valves to drop the turbine throttle pressure by 10 psi. As the pressure drops the core power drops due to increased voiding. The entire system decays to a new steady state with a period of approximately 8 seconds.

The stability of the reactivity void feedback loop was clearly demonstrated at this test condition.

Summary of the Test Analysis

Figures 3.2-141 through 3.2-145 show the calculated versus measured results for the Pressure Setpoint Step Start Up Test.

The DYNODE-B predicted results show excellent comparison to the test results. The predicted results exhibit approximately the same period with a slightly greater amplitude. The reported APRM decay ratio is zero, based on the measured data. DYNODE-B calculates a decay ratio of 0.21 for relative power.

This transient provides an excellent benchmark of DYNODE-B's capability to conservatively predit decay ratio.

3.2.2.2.6 FEEDWATER CONTROLLER LEVEL SETPOINT STEP AT 100% POWER (STP 20)

Description of the Test

The purposes of this test were to determine the effect of changes in subcooling on reactor power and steam pressure and to demonstrate that reactor responses to changes in subcooling are stable at all power levels.

The changes in subcooling were introduced by varying the vessel water level setpoint (3 and 6-inch changes), and the resulting transients were recorded.

Testing at all power levels, in three-element and one-element level control and automatic and manual recirculation flow control, yielded stable plant responses to changes in subcooling. Decay ratios of primary variables were less than 0.25 for all of these tests.

For the purposes of this analysis, only the 6 inch level step at 100% power in three-element control and automatic flow control was examined, since this represents the most severe transient in this series.

The feedwater controller responds to the 6-inch setpoint drop by cutting back the feedwater flow to attempt to balance the level error. As the feedwater flow drops, the core power and vessel pressure drop slightly due to the decreased inlet subcooling. As the level drops, the controller error goes to zero and the feedwater flow and all other core parameters return to their original level.

The stability of the reactor in response to subcooling changes was clearly demonstrated at this test condition.

Summary of the Test Analysis

Figures 3.2-146 through 3.2-149 show the calculated versus measured results for the Feedwater Controller Level Setpoint Step Start Up Test.

The DYNODE-B predicted results show excellent comparison to the test results. The predicted level response and feedwater flow track very closely. Both DYNODE-B and the data show a decay ratio of zero for the core power. There are no significant deviations between the predicted and measured results.

This transient provides an excellent benchmark of DYNODE-B's capability to predict decay ratio and to track water level.

Table 3.1-1

NDH - DYNODE-B VOID REACTIVITY COMPARISON

Dome Pressure (psia)	Subcooling (Btu/lbm)	K_{eff} NDH	K_{eff} DYNODE-B
1038	24.42	0.99833	0.99811
1238	53.20	1.01991	1.02003
	Reactivity Change =	0.0212	0.0215

$$\Delta\rho = (K_1 - K_2) / K_1 K_2$$

Table 3.2-1

PEACH BOTTOM-2 TURBINE TRIP TRANSIENT
TEST ACTUAL CONDITIONS

Test Number	Reactor Power (MWt)	Reactor Power (% Rated)	Core Flow Rate (10^6 lb/h)	Core Flow Rate (% Rated)	Core Pressure (psia)
TT1	1562	47.4	101.3	98.8	1005
TT2	2030	61.6	82.9	80.9	995
TT3	2275	69.1	101.9	99.4	1005

Test Number	Core Inlet Enthalpy (Btu/lb)	APRM Trip Set Point (% Rated)
TT1	528.4	85
TT2	519.8	95
TT3	523.6	77

Table 3.2-2

PEACH BOTTOM-2
TURBINE TRIP TRANSIENT TEST
PEAK MEASURED AND CALCULATED RESPONSES

Variable	TT1		TT2		TT3	
	Data	DYNODE-B	Data	DYNODE-B	Data	DYNODE-B
Average Nuetron Flux (% Rated)	239	239	280	281	339	342
Core Exit Pressure (psia)	1036	1053	1034	1066	1072	1088
Reactor Vessel Pressure (psia)	1031	1047	1038	1062	1061	1082

Data from Reference 16

Table 3.2-3

PEACH BOTTOM-2
TURBINE TRIP TRANSIENT TEST
CRITICAL POWER RATIO RESPONSE

Variable	TT1		TT2		TT3	
	Data	DYNODE-B	Data	DYNODE-B	Data	DYNODE-B
ICPR	2.536	2.536	2.115	2.115	2.048	2.048
ΔCPR	0.431	0.474	0.288	0.315	0.270	0.305
ΔCPR/ICPR	0.170	0.187	0.136	0.149	0.132	0.149

Data from Reference 9

Monticello Cycle 10
NDH - DNB Comparison

Figure 3.1-1
Relative Power

DNB053/86
NDH 85-536

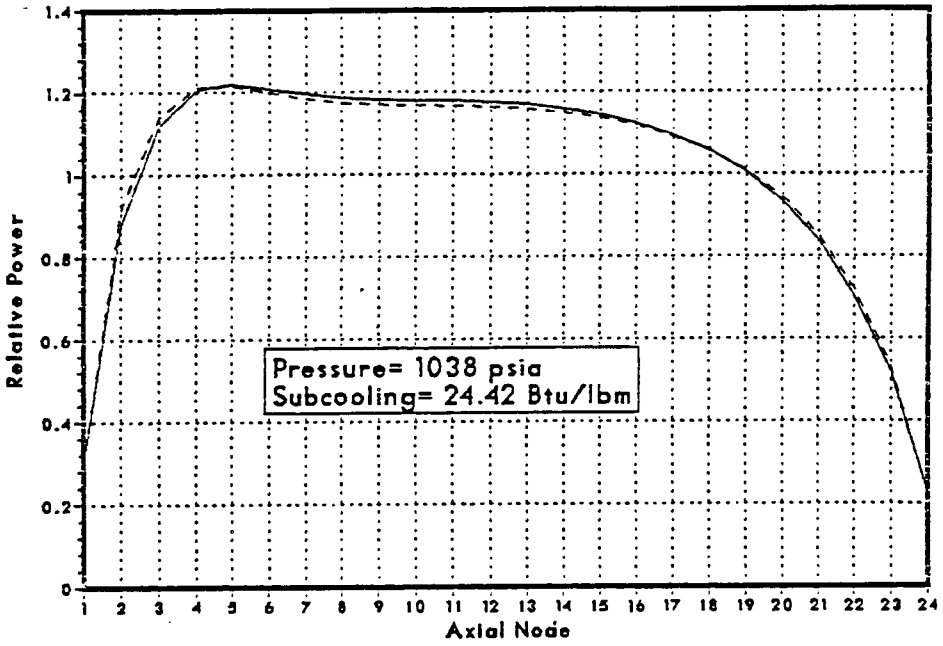

Figure 3.1-2
Relative Power

DNB054/86
NDH 85-589

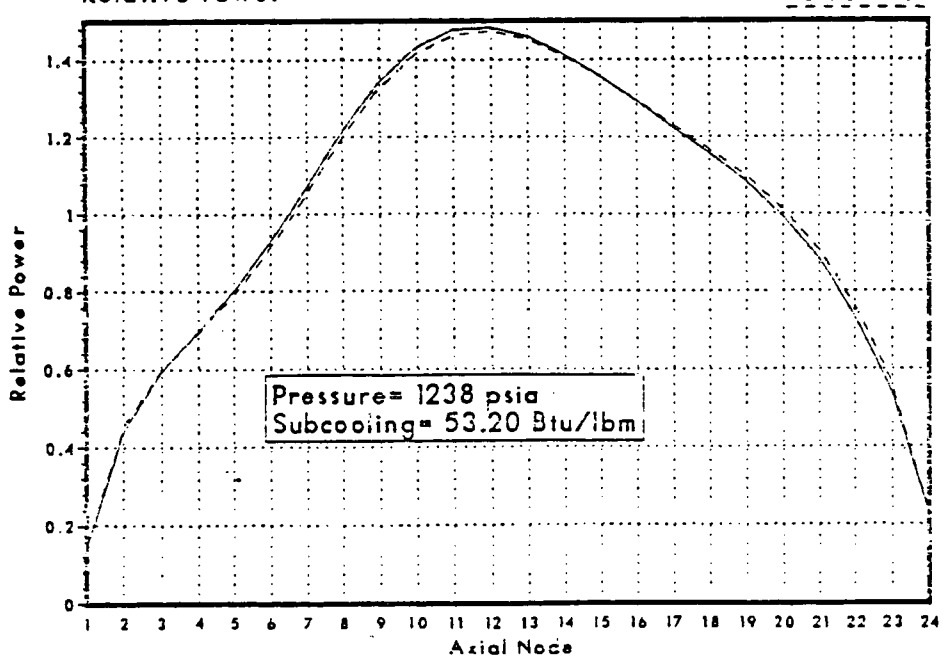

Monticello Cycle 13
NDH - DNB Comparison

Figure 3.1-3
Delta Rho

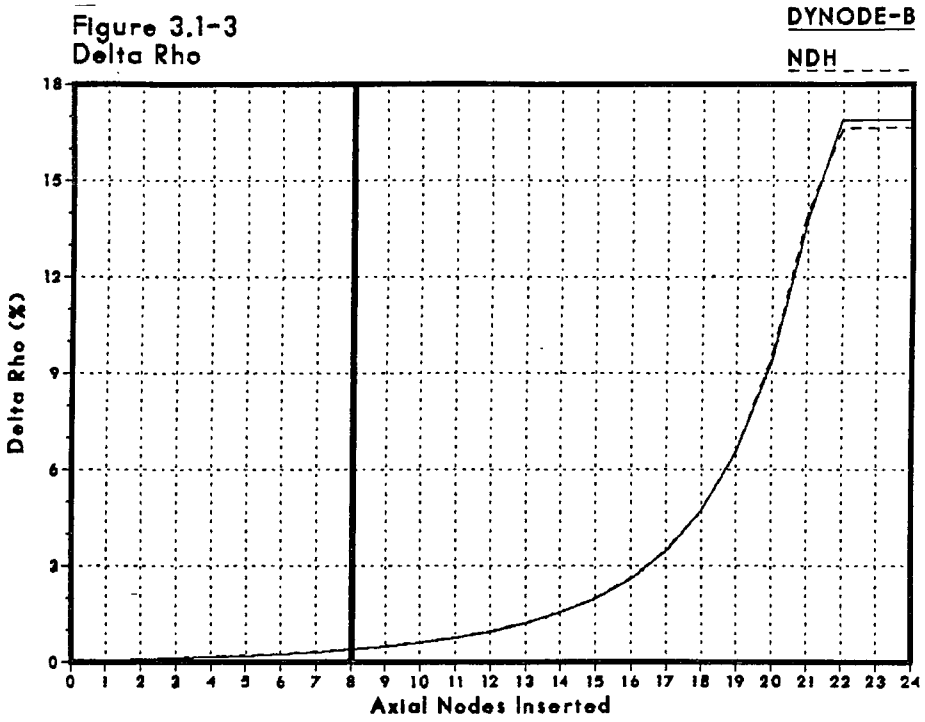

$$\text{Delta Rho} = \text{Rho}_{Base} - \text{Rho}_{i}$$

Figure 3.1-4
Delta Rho Error

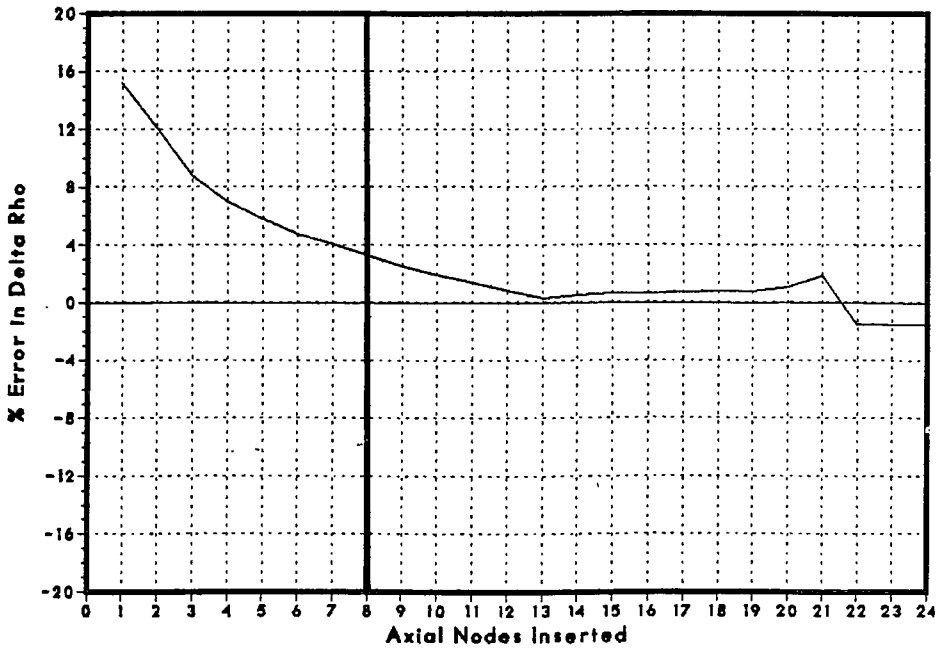

$$\%\ \text{Error} = (\text{Delta Rho}_{NDH} - \text{Delta Rho}_{DYNODE\text{-}B}) \ / \ \text{Delta Rho}_{NDH} \times 100\%$$

Monticello FSAR Benchmark
Turbine Trip w/o Bypass

Figure 3.2-1
Steam Dome Pressure

DNB063/86
FSAR

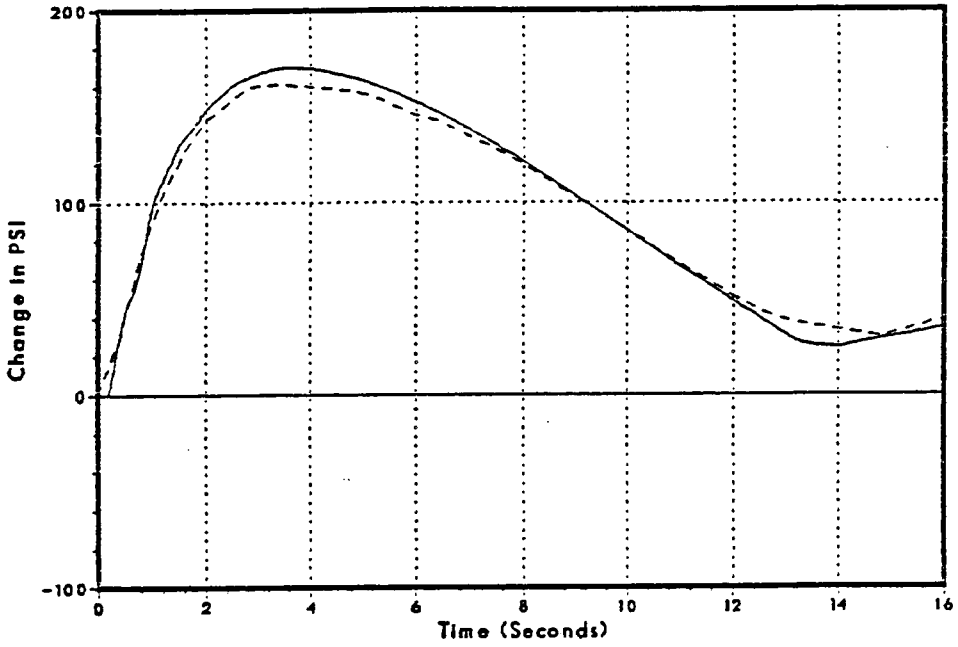

Figure 3.2-2
Relative Power

DNB063/86
FSAR

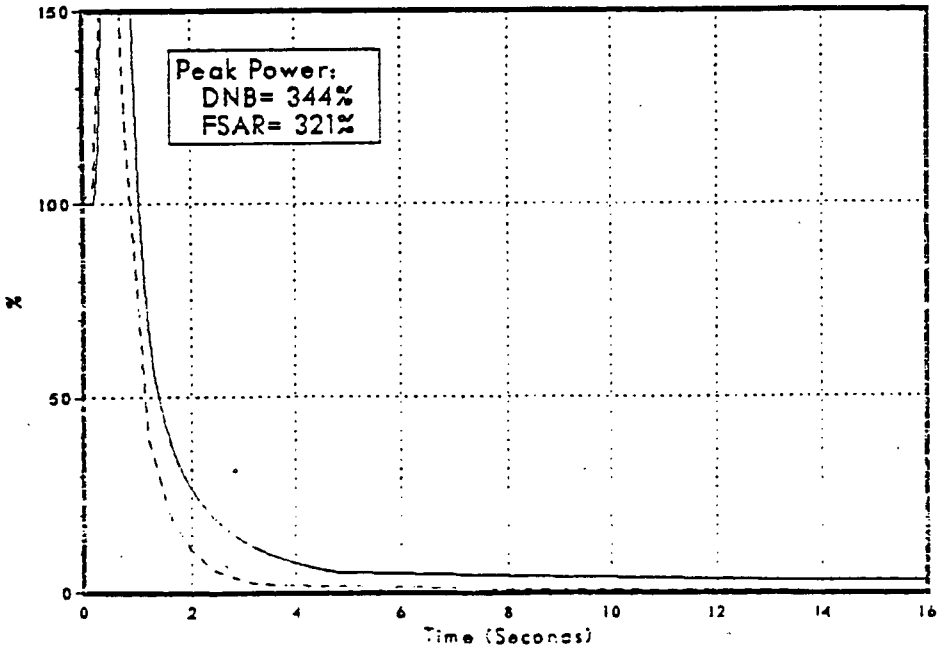

NSP

Monticello FSAR Benchmark
Turbine Trip w/o Bypass

Figure 3.2-3
Core Average Heat Flux

DNB063/86
FSAR

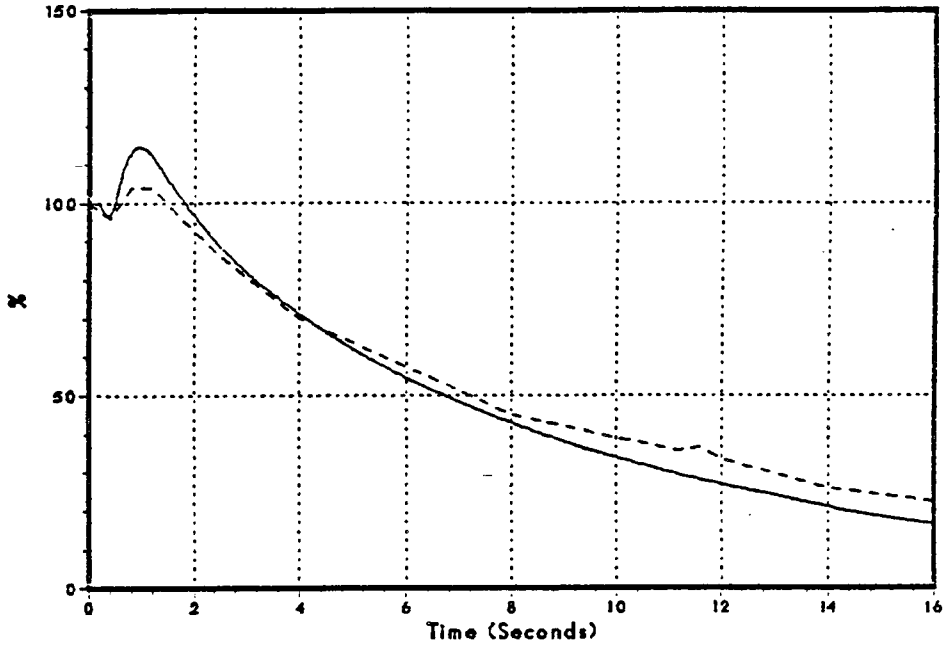

Figure 3.2-4
Core Inlet Flow

DNB063/86
FSAR

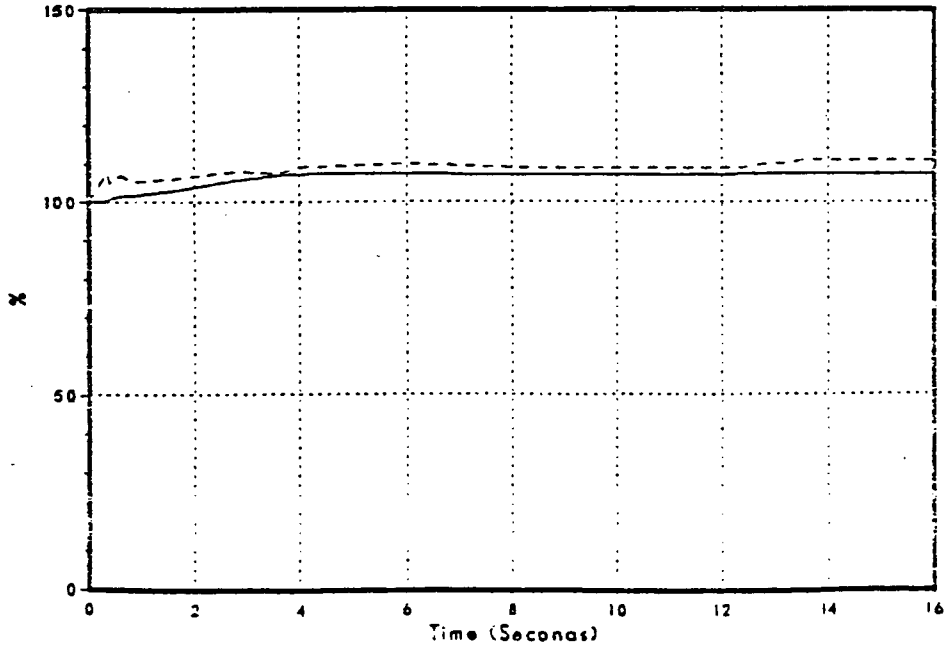

NSP

PREPARED BY NSP SAFETY ANALYSIS, 6/27/86

Monticello FSAR Benchmark
Turbine Trip w/o Bypass

Figure 3.2-5
Main Steam Line Flow

DNB063/86
FSAR

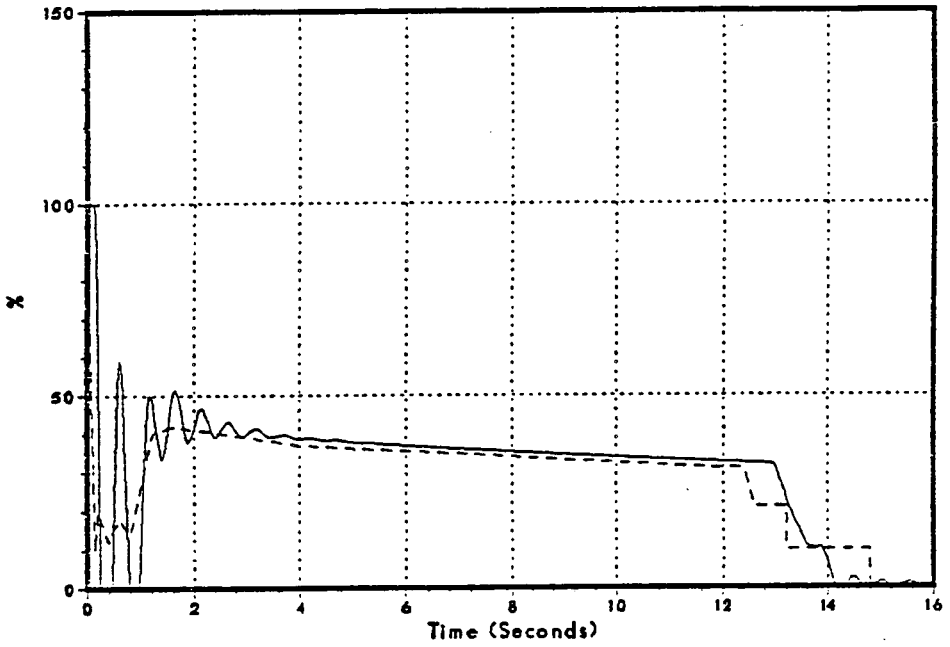

Figure 3.2-6
Feedwater Flow

DNB063/86
FSAR

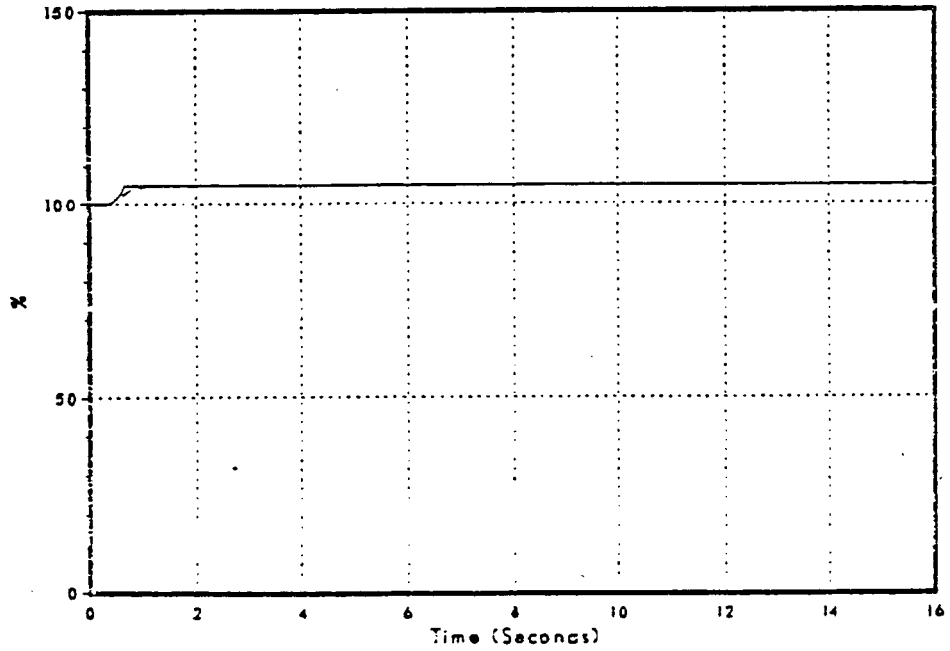

NSP

Monticello FSAR Benchmark
Turbine Trip w/o Bypass

Figure 3.2-7
Sensed Level

DNB063/86

FSAR _ _ _ _

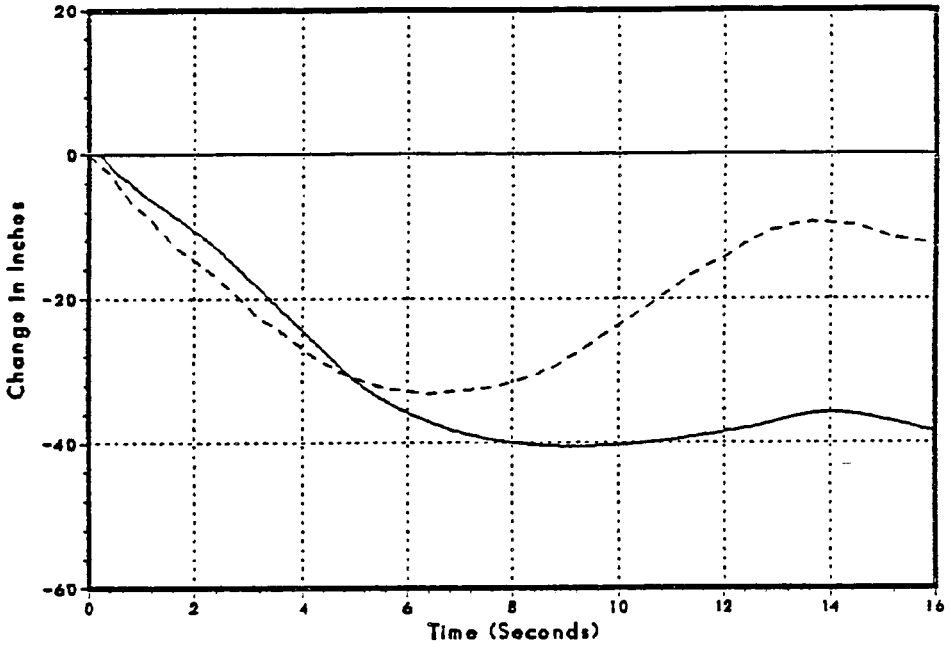

NSP

PREPARED BY NSP SAFETY ANALYSIS, 6/27/86

Monticello FSAR Benchmark
Turbine Trip w/ Bypass

Figure 3.2-8
Steam Dome Pressure

DNB070/86
FSAR

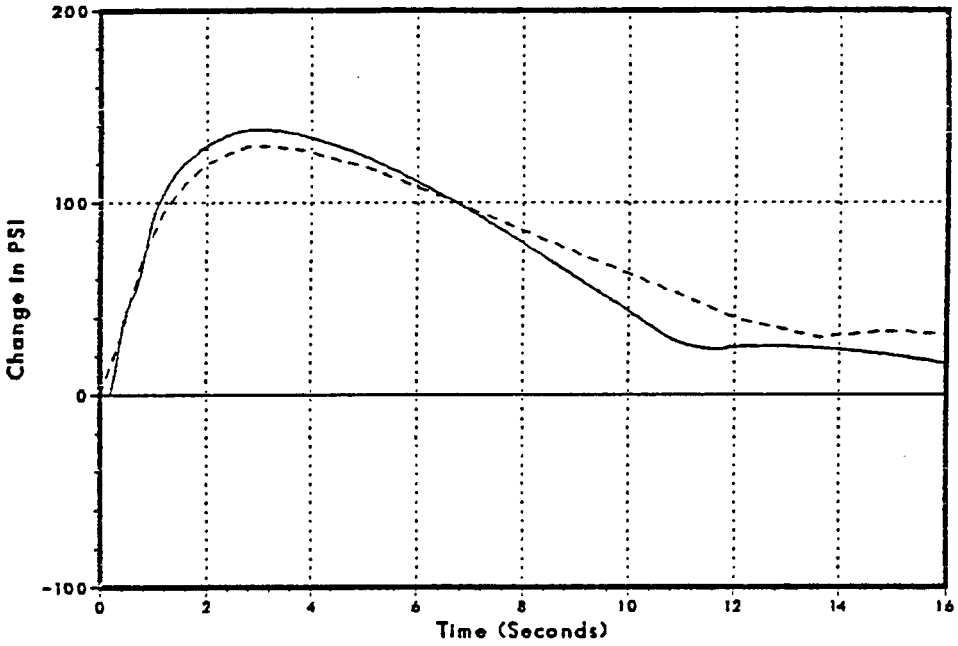

Figure 3.2-9
Relative Power

DNB070/86
FSAR

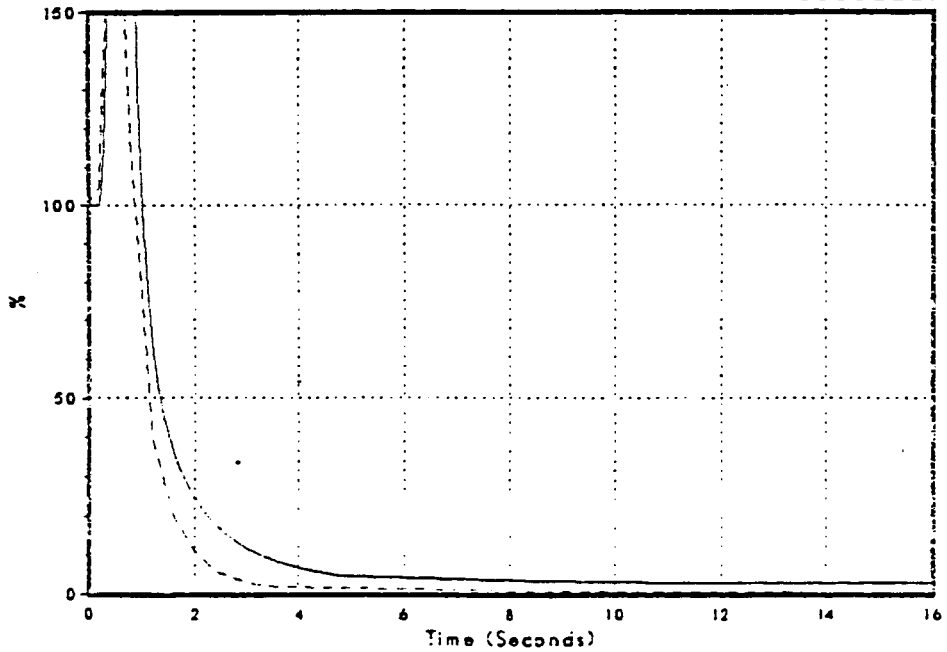

NSP

PREPARED BY NSP SAFETY ANALYSIS, 6/27/86

Monticello FSAR Benchmark
Turbine Trip w/ Bypass

Figure 3.2-10
Core Average Heat Flux

DNB070/86
FSAR

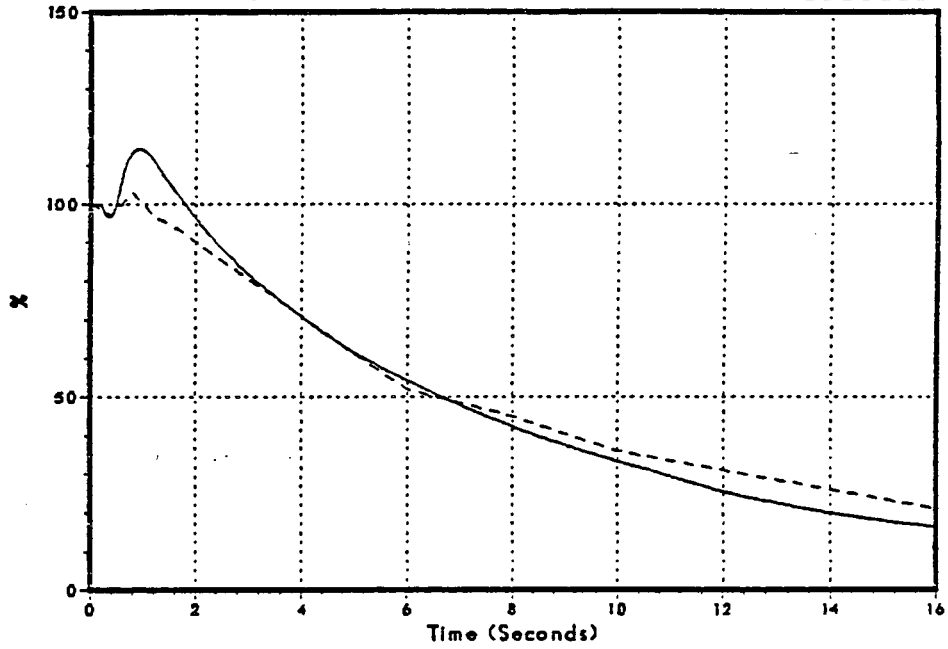

Figure 3.2-11
Core Inlet Flow

DNB070/86
FSAR

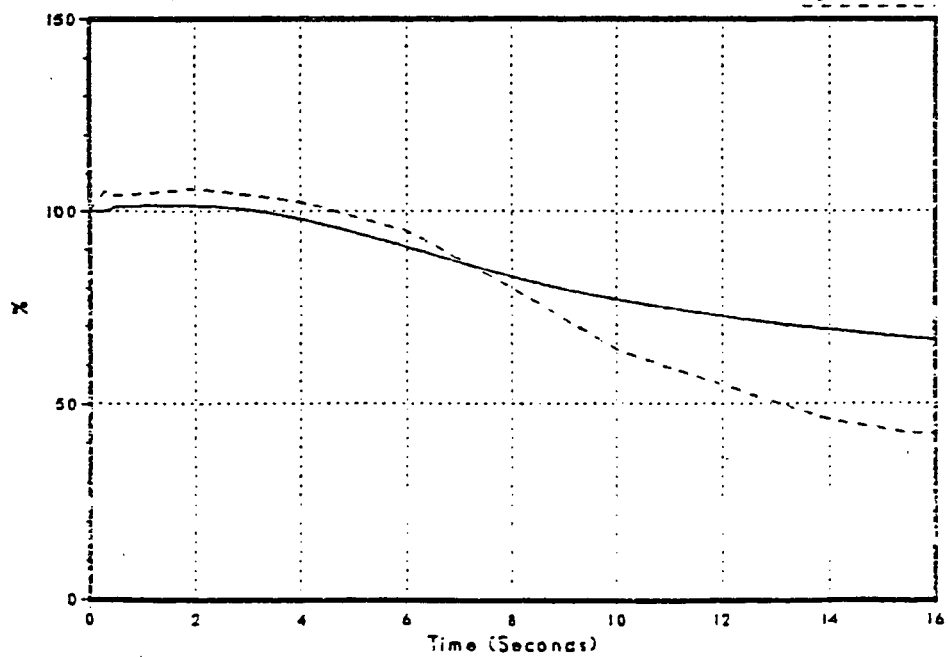

NSP

Monticello FSAR Benchmark
Turbine Trip w/ Bypass

Figure 3.2-12
Main Steam Line Flow

DNB070/86
FSAR

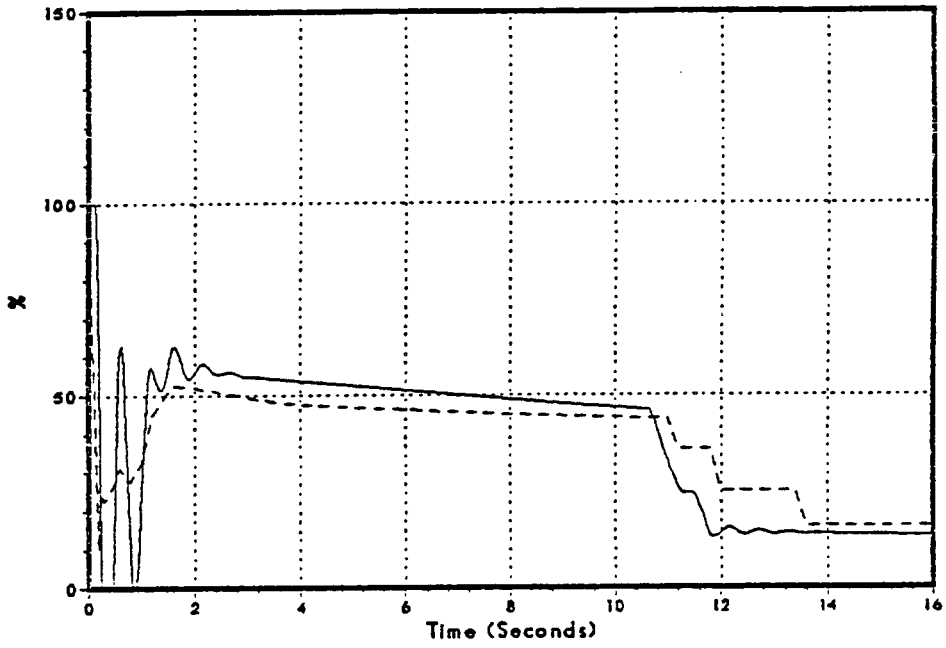

Figure 3.2-13
Feedwater Flow

DNB070/86
FSAR

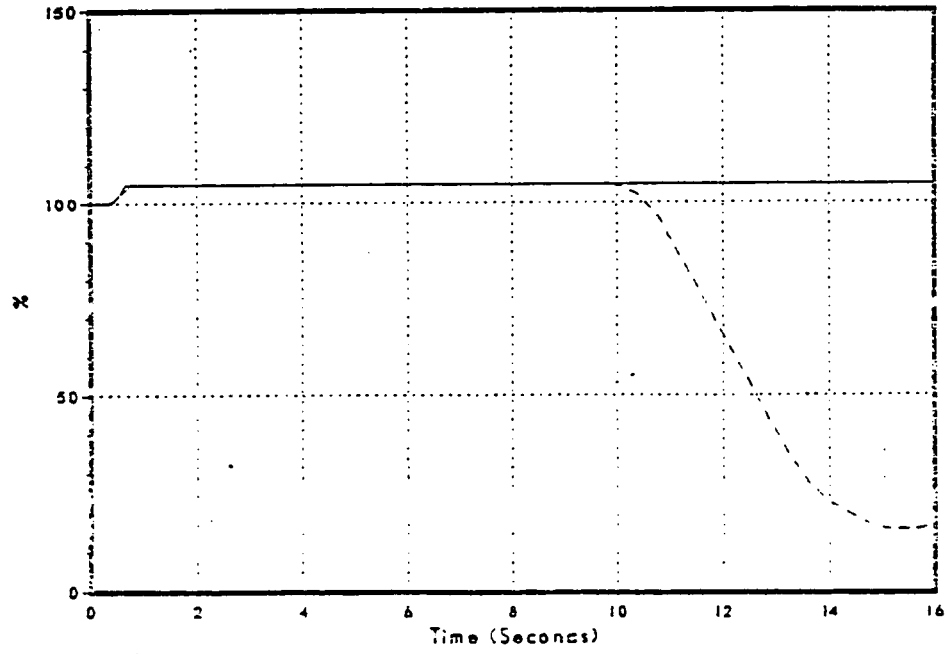

NSP

PREPARED BY NSP SAFETY ANALYSIS, 6/27/86

Monticello FSAR Benchmark
Turbine Trip w/ Bypass

Figure 3.2-14
Sensed Level

DNB070/86

FSAR

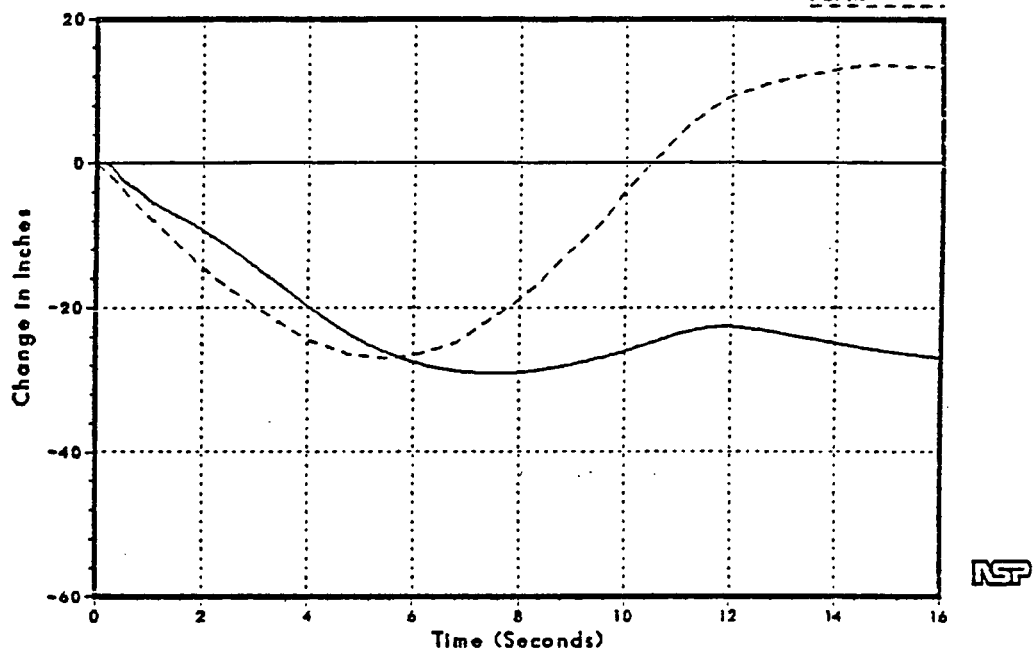

PREPARED BY NSP SAFETY ANALYSIS, 6/27/86

Monticello FSAR Benchmark
Generator Trip w/ Bypass

Figure 3.2-15
Sensed Level

DNB069/86
FSAR

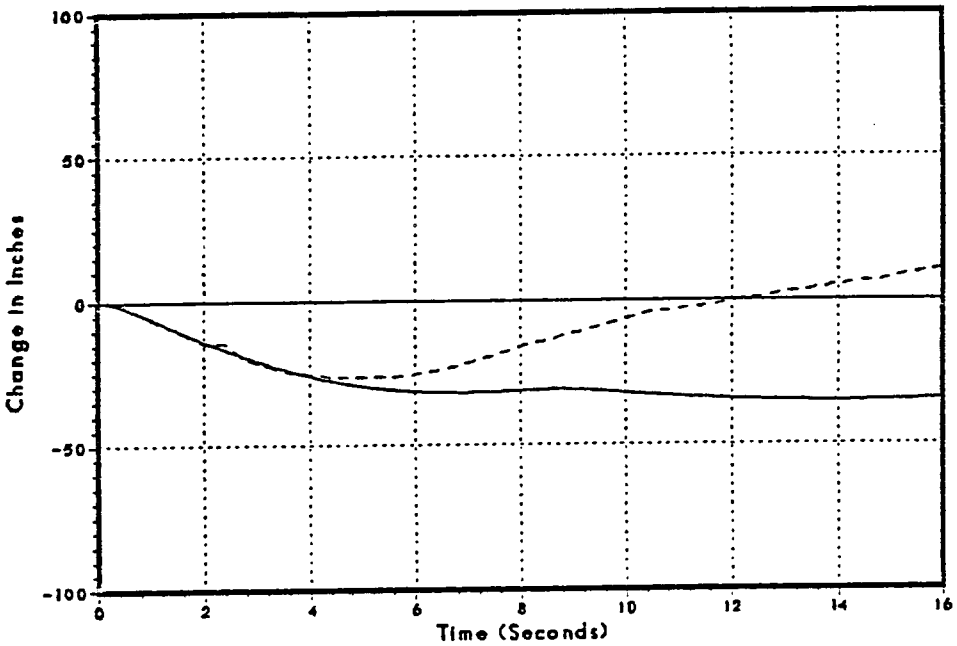

FIGURE 3.2-16
STEAM DOME PRESSURE

DNB069/86
FSAR

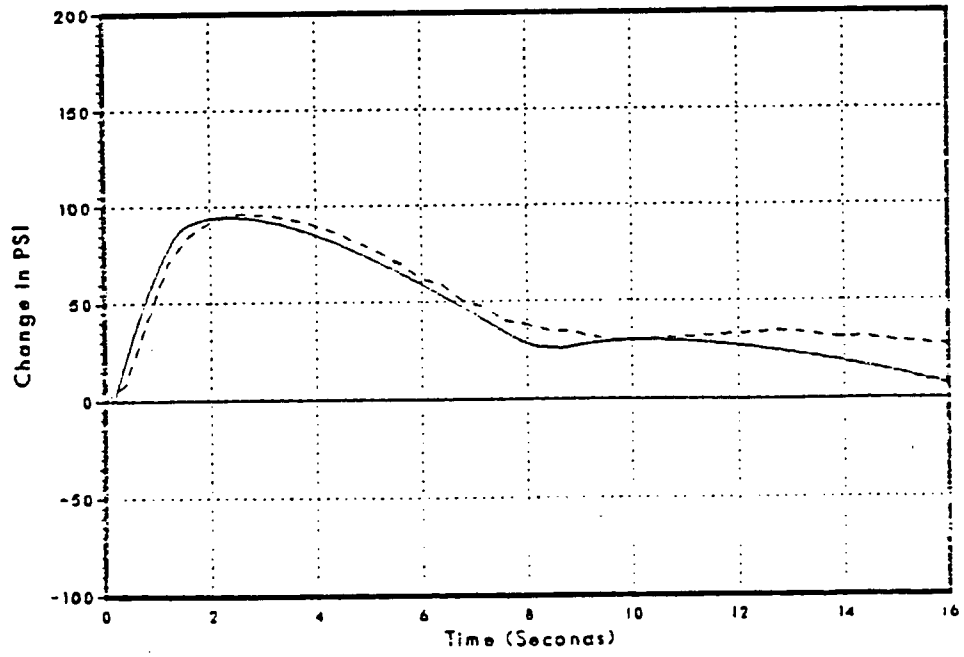

NSP

REPARED BY NSP SAFETY ANALYSIS, 5/12/86

Monticello FSAR Benchmark
Generator Trip w/ Bypass

Figure 3.2-17
Core Inlet Flow

DNB069/86
FSAR

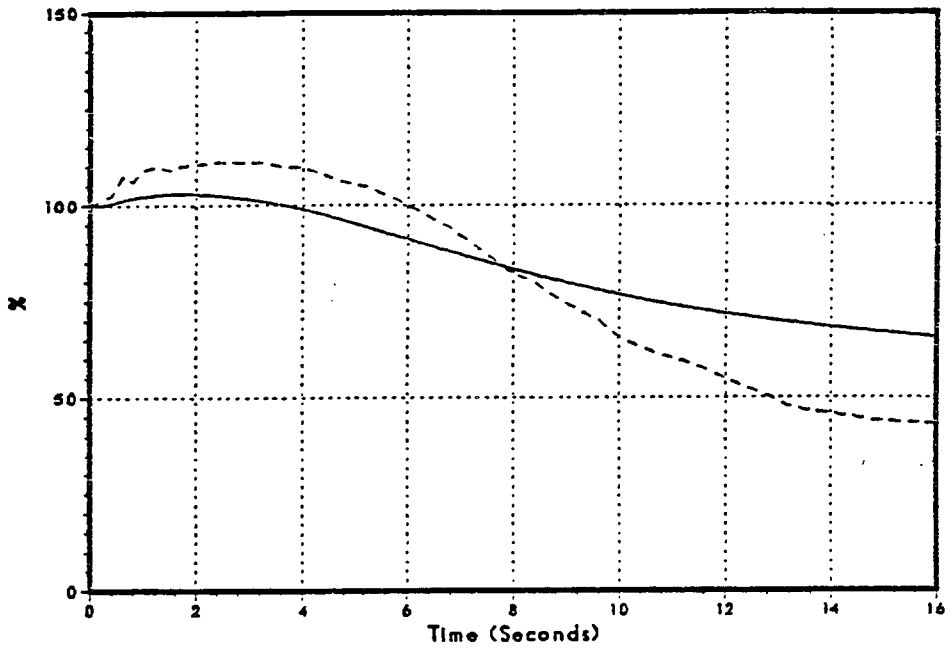

Figure 3.2-18
Average Surface Heat Flux

DNB069/86
FSAR

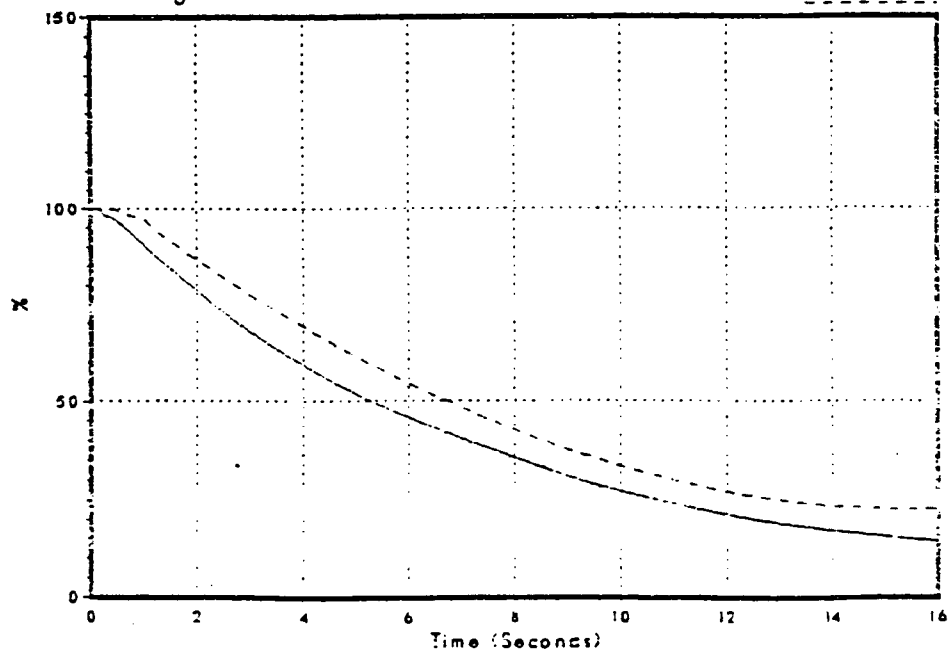

NSP

Monticello FSAR Benchmark
Generator Trip w/ Bypass

Figure 3.2-19
Relative Power

DNB069/86
FSAR

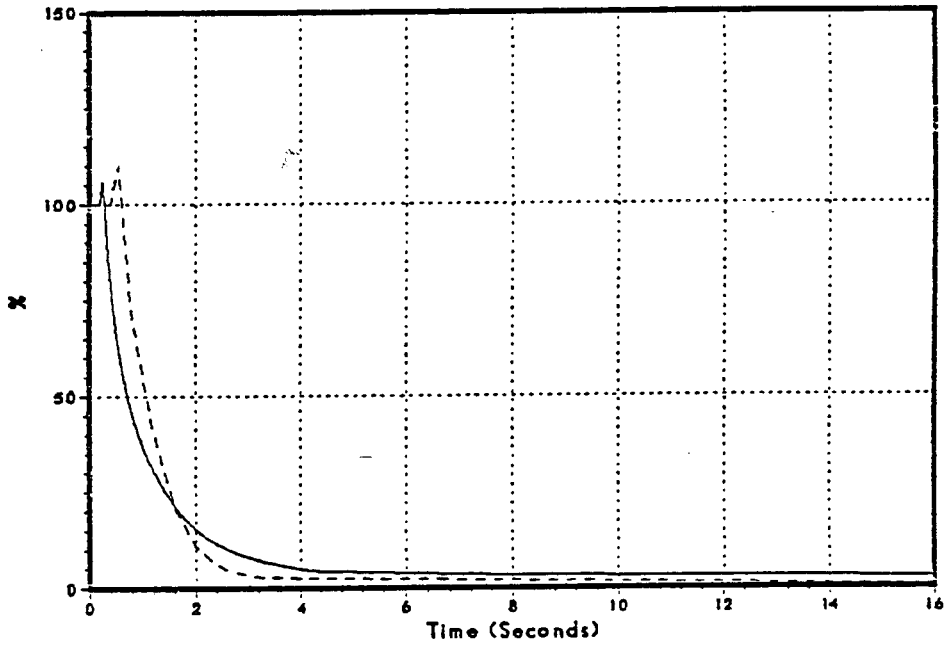

Figure 3.2-20
Feedwater Flow

DNB069/86
FSAR

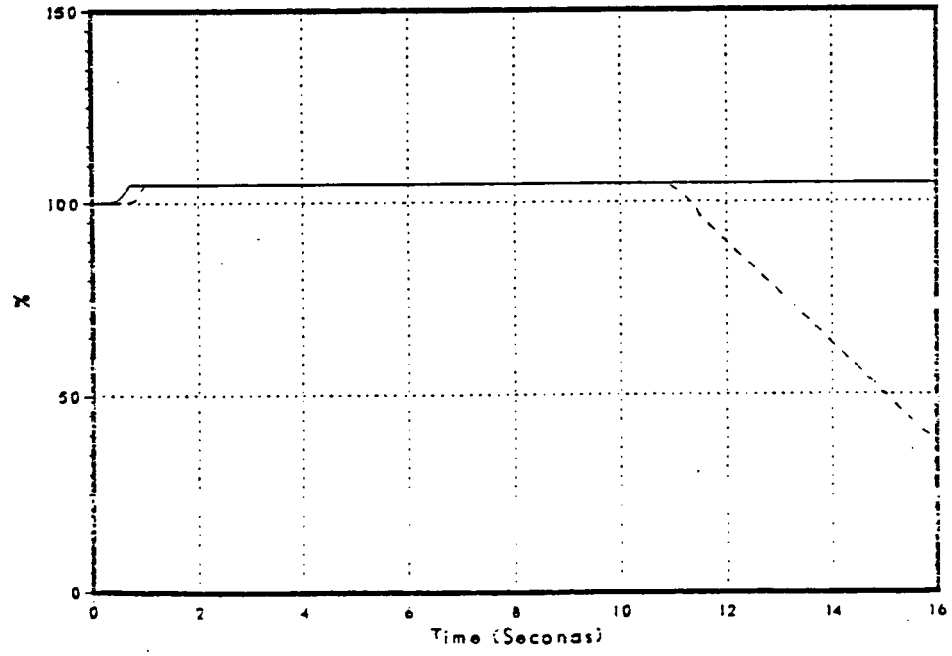

NSP

Prepared by NSP Safety Analysis, 5/12/86

Monticello FSAR Benchmark
Generator Trip w/ Bypass

Figure 3.2-21
Vessel Steam Flow

DNB069/86
FSAR

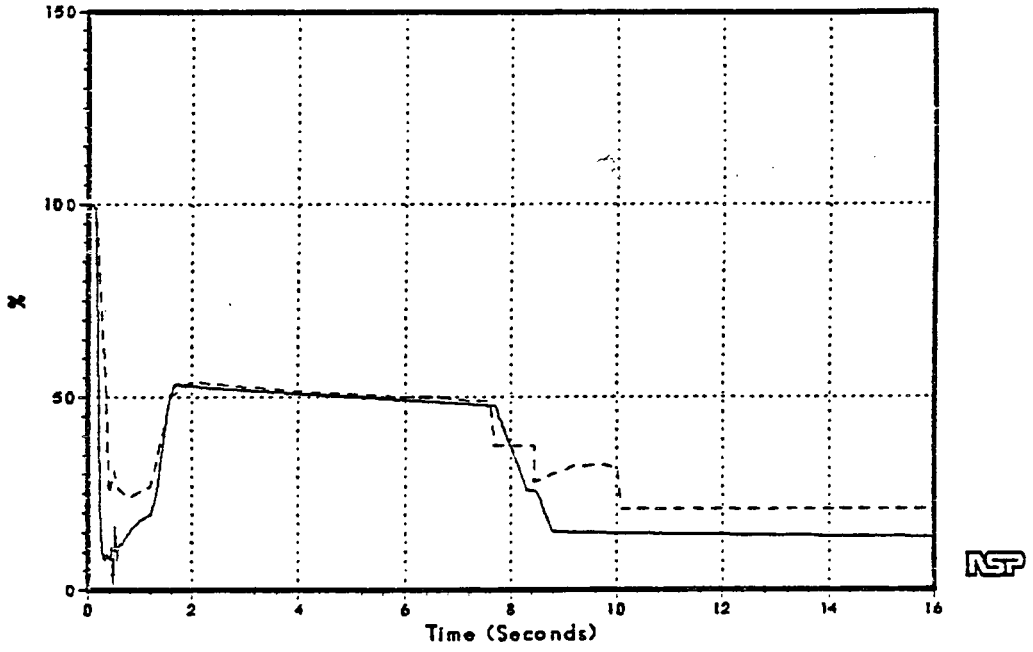

Prepared by NSP Safety Analysis, 5/12/86

Monticello FSAR Benchmark
100% MSIV Closure

Figure 3.2-22
Steam Dome Pressure

DNB064/86
FSAR

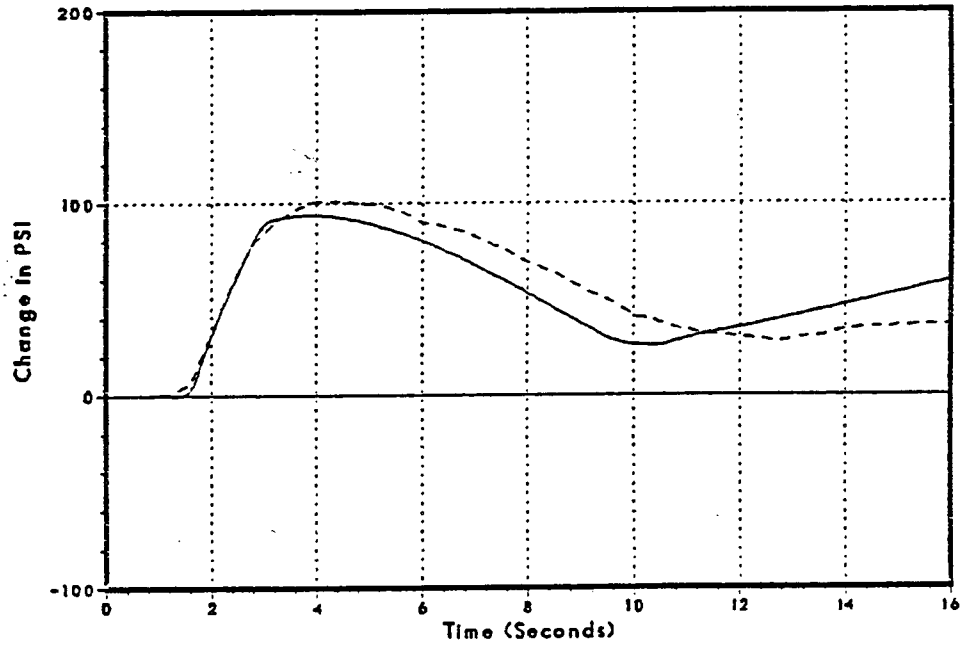

Figure 3.2-23
Relative Power

DNB064/86
FSAR

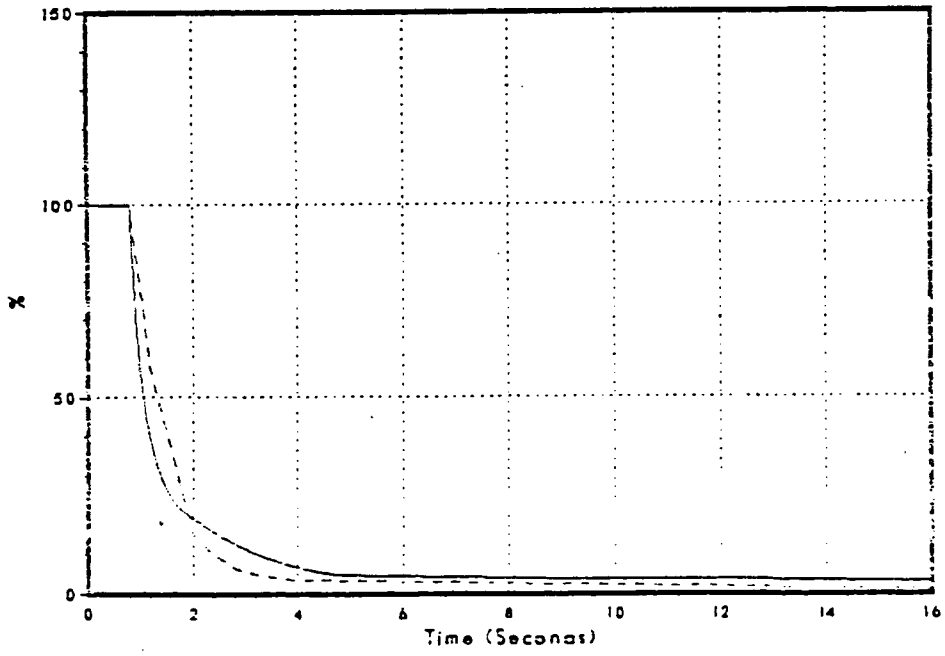

NSP

PREPARED BY NSP SAFETY ANALYSIS, 6/27/86

Monticello FSAR Benchmark
100% MSIV Closure

Figure 3.2-24
Core Average Heat Flux

DNB064/86
FSAR

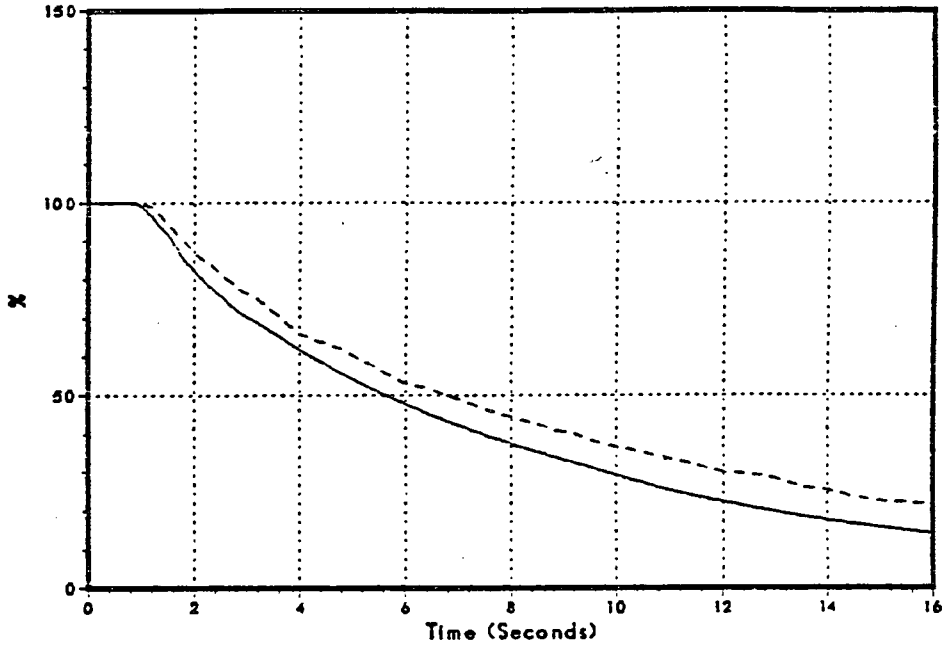

Figure 3.2-25
Core Inlet Flow

DNB064/86
FSAR

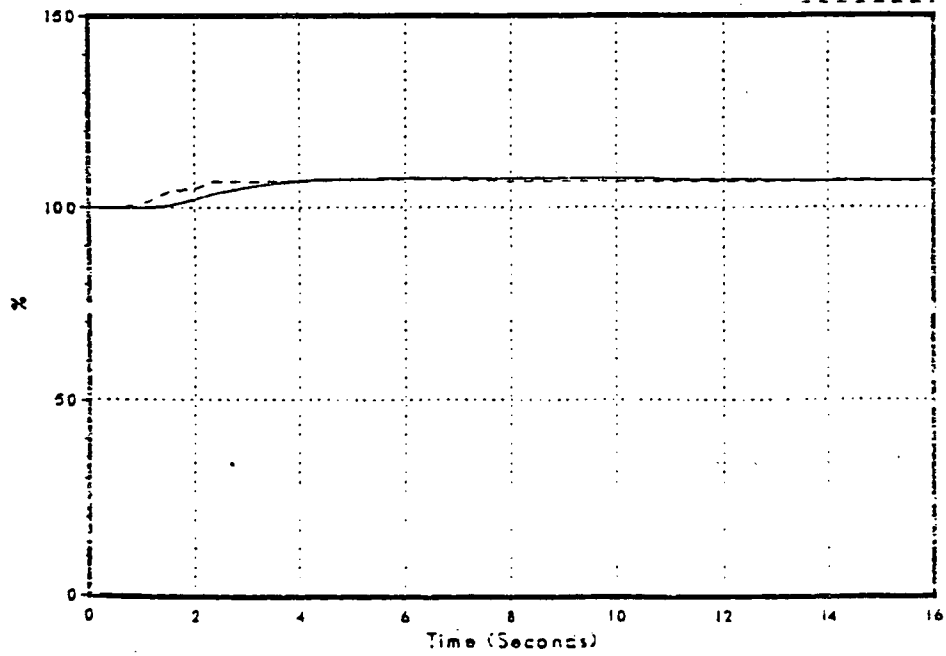

NSP

PREPARED BY NSP SAFETY ANALYSIS, 6/27/86

Monticello FSAR Benchmark
100% MSIV Closure

Figure 3.2-26
Main Steam Line Flow

DNB064/86
FSAR

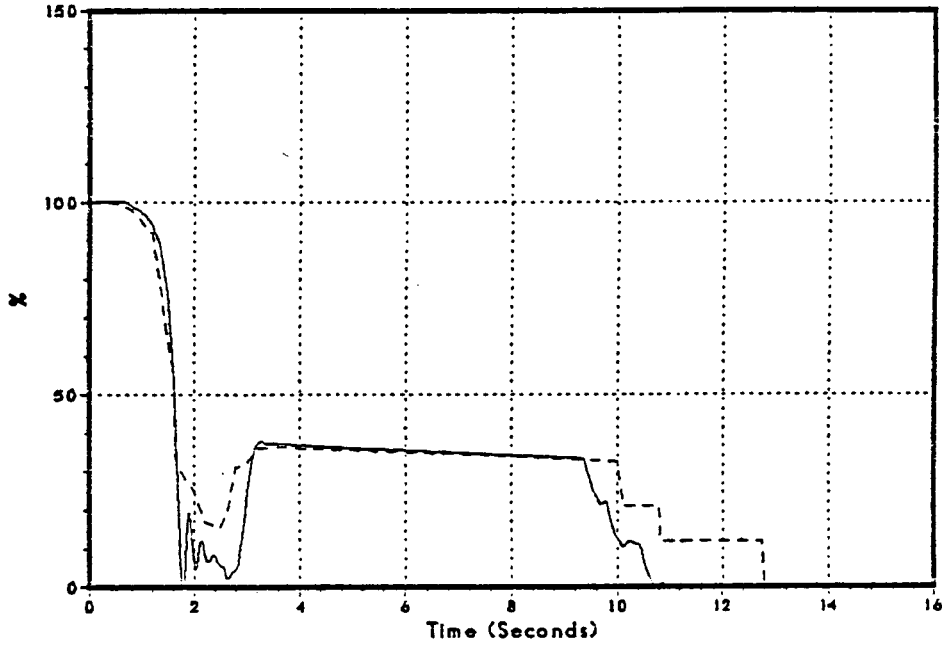

Figure 3.2-27
Feedwater Flow

DNB064/86
FSAR

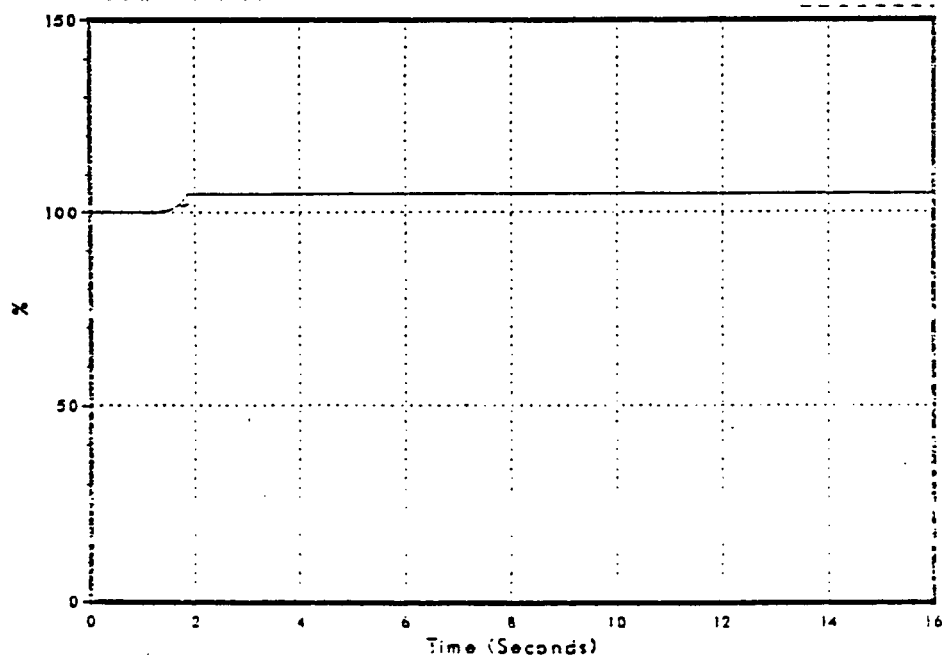

NSP

PREPARED BY NSP SAFETY ANALYSIS, 6/27/86

Monticello FSAR Benchmark
100% MSIV Closure

Figure 3.2-28
Sensed Level

DNB064/86

FSAR _ _ _ _ _

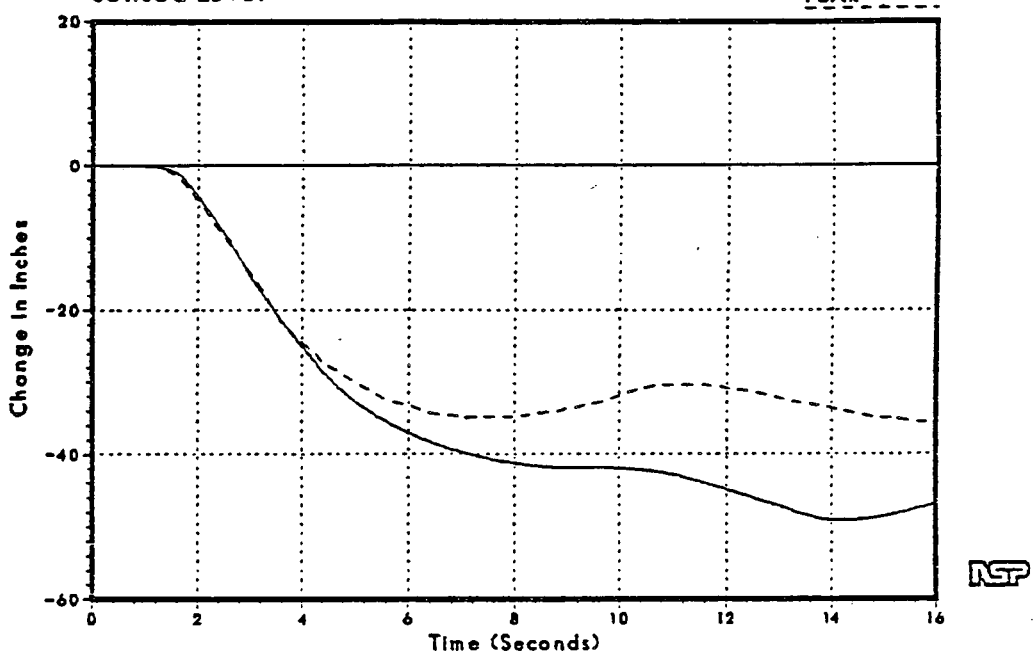

Monticello FSAR Benchmark
Feedwater Control Malfunction (Max Demand)

Figure 3.2-29
Sensed Level

DNB065/86
FSAR _ _ _ _

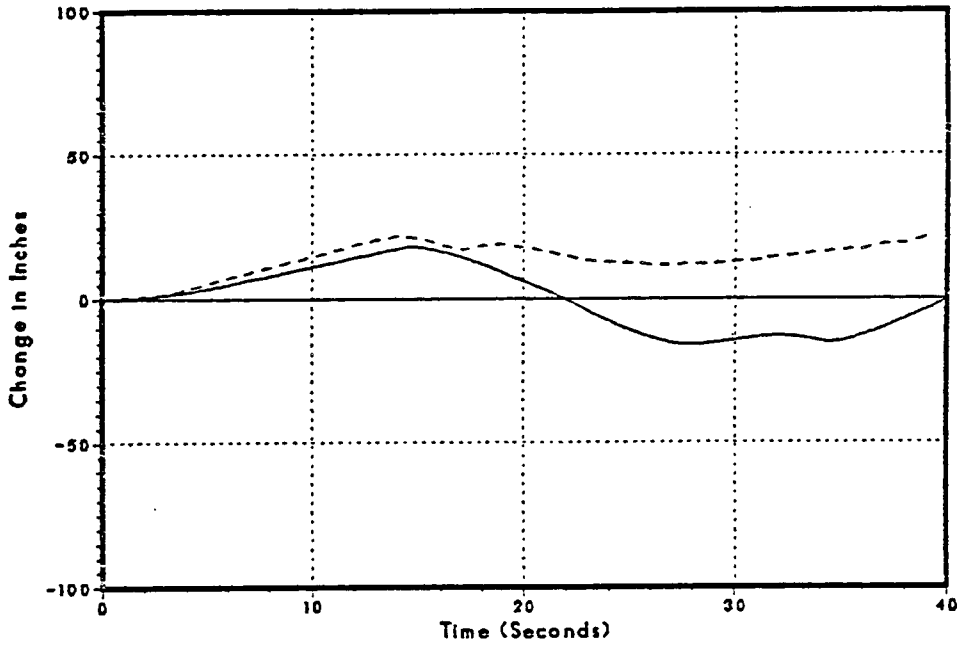

Figure 3.2-30
Steam Dome Pressure

DNB065/86
FSAR _ _ _ _

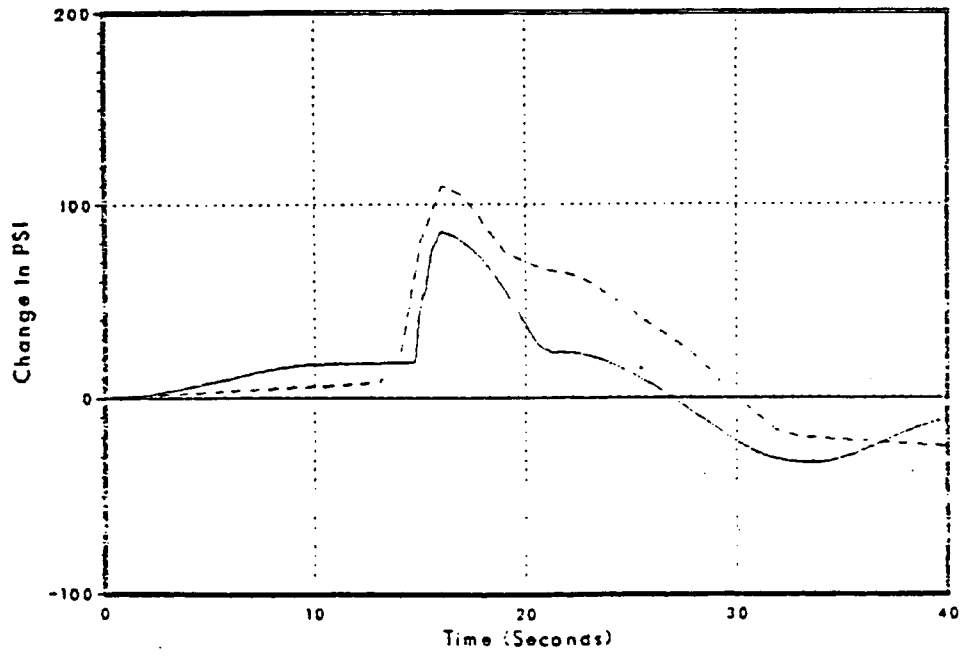

NSP

Prepared by NSP Safety Analysis, 5/14/86

Monticello FSAR Benchmark
Feedwater Control Failure (Max Demand)

Figure 3.2-31
Core Inlet Flow

DNB065/86
FSAR

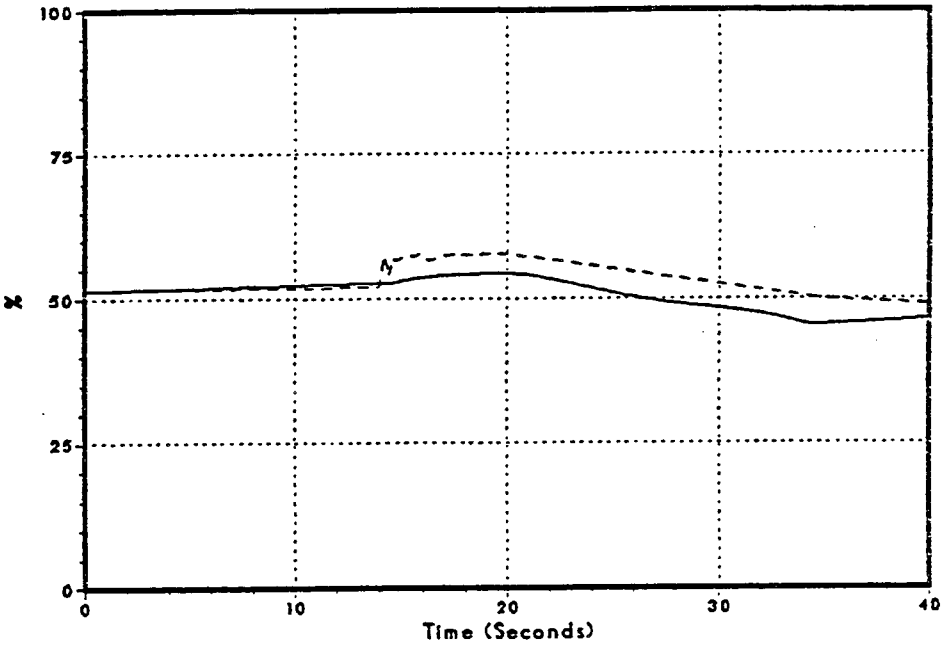

Figure 3.2-32
Average Surface Heat Flux

DNB065/86
FSAR

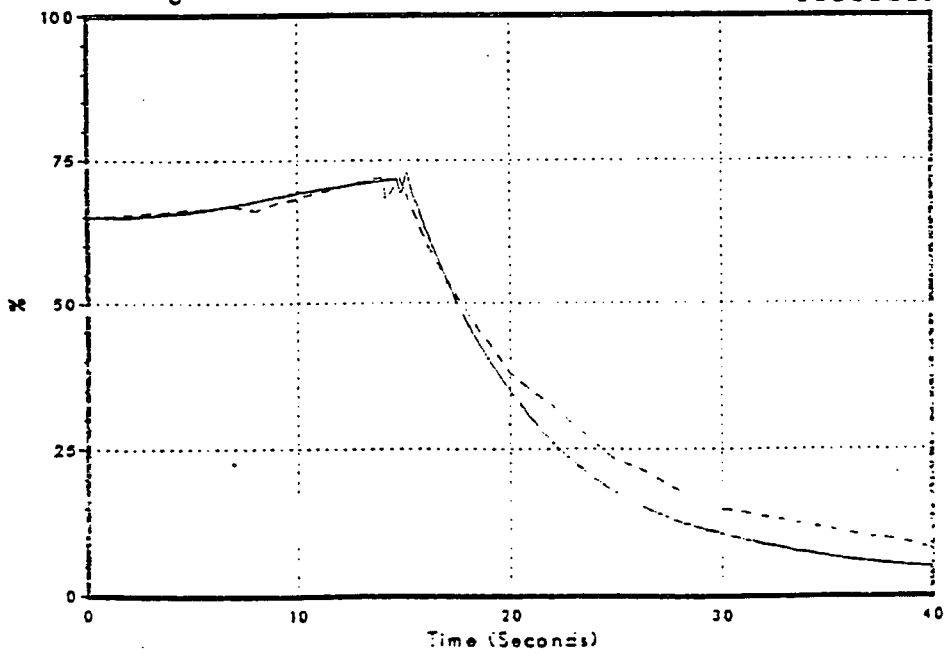

NSP

Monticello FSAR Benchmark
Feedwater Control Failure (Max Demand)

Figure 3.2-33
Relative Power

DNB065/86
FSAR

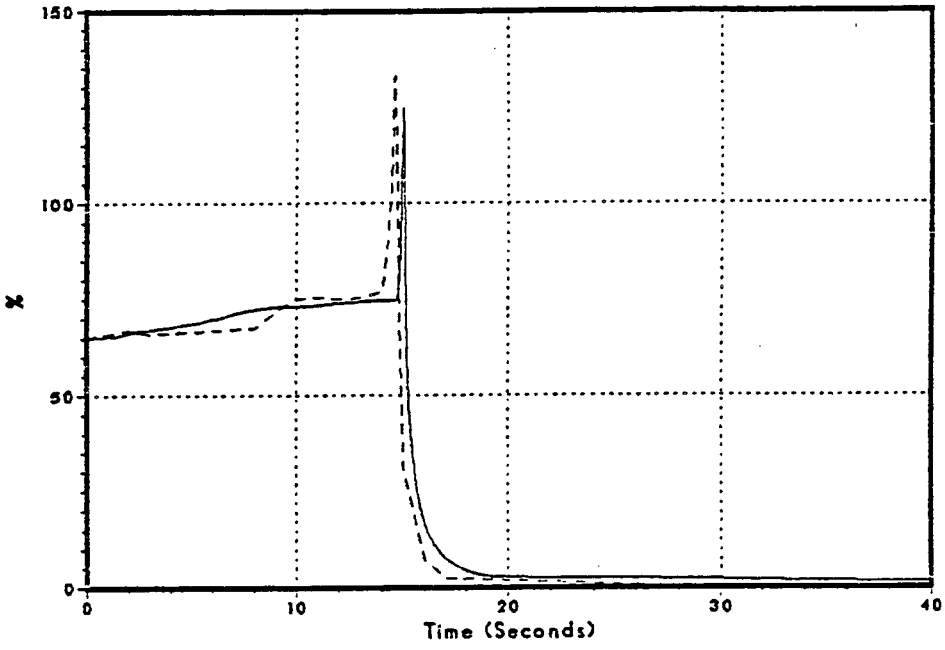

Figure 3.2-34
Feedwater Flow

DNB065/86
FSAR

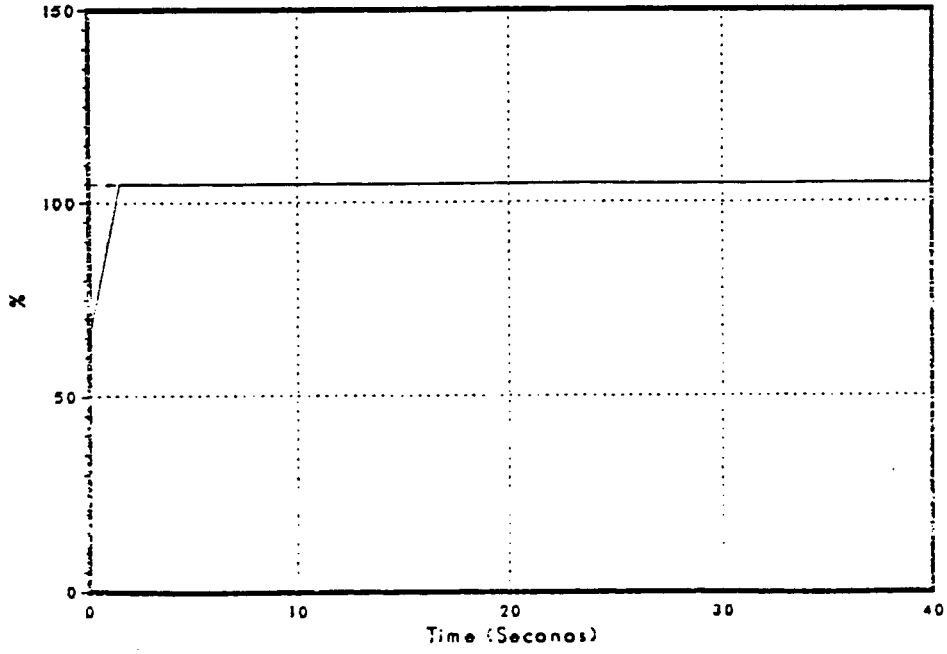

NSP

Prepared by NSP Safety Analysis, 5/14/86

Monticello FSAR Benchmark
Feedwater Control Failure (Max Demand)

Figure 3.2-35
Vessel Steam Flow

DNB065/86
FSAR

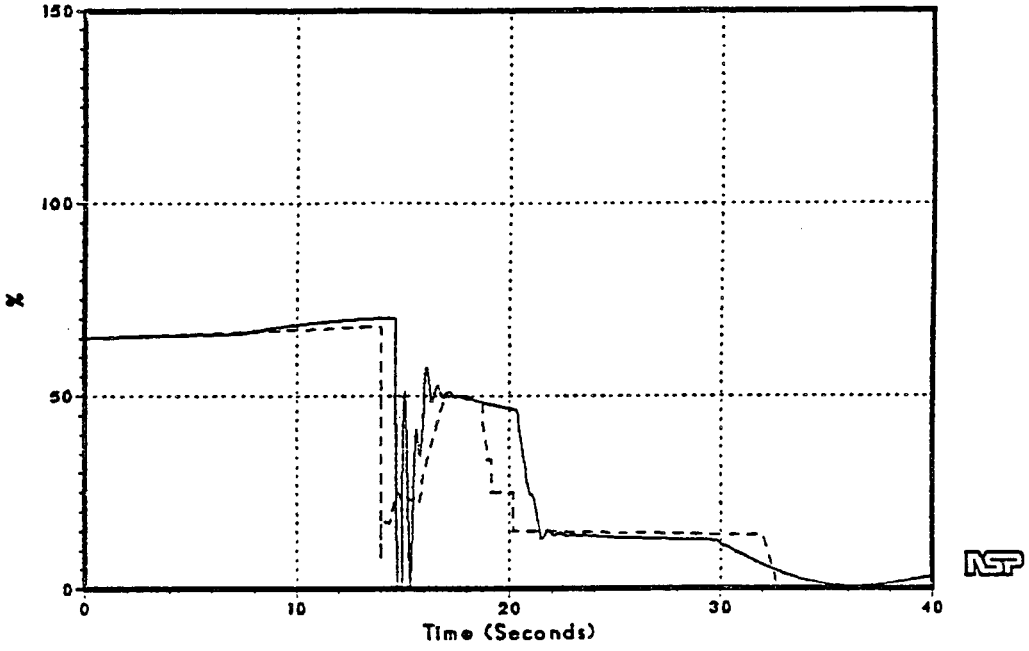

Monticello FSAR Benchmark
Loss of Feedwater

Figure 3.2-36
Sensed Level

DNB066/86

FSAR

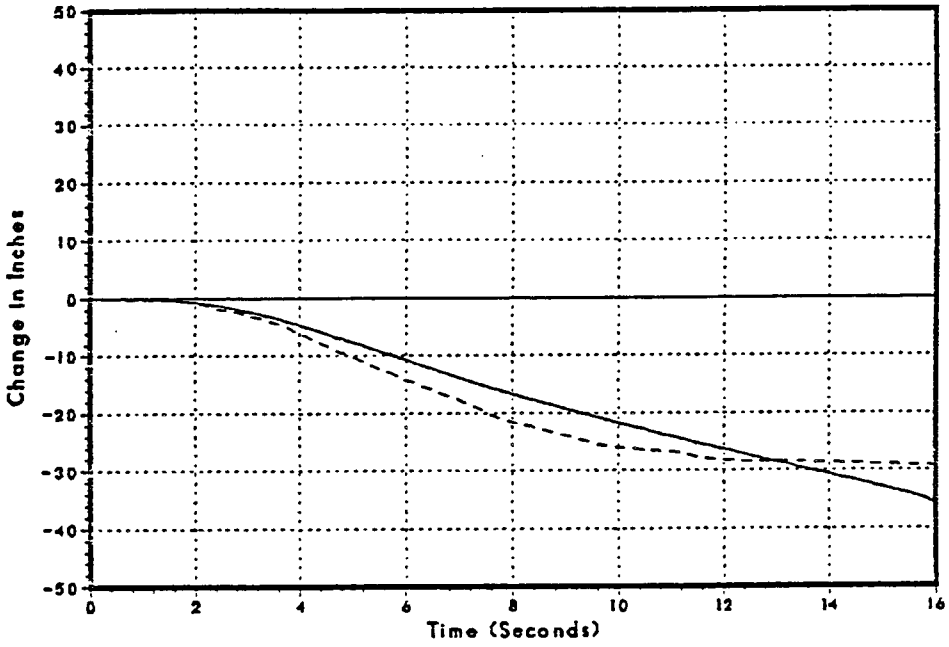

Figure 3.2-37
Steam Dome Pressure

DNB066/86

FSAR

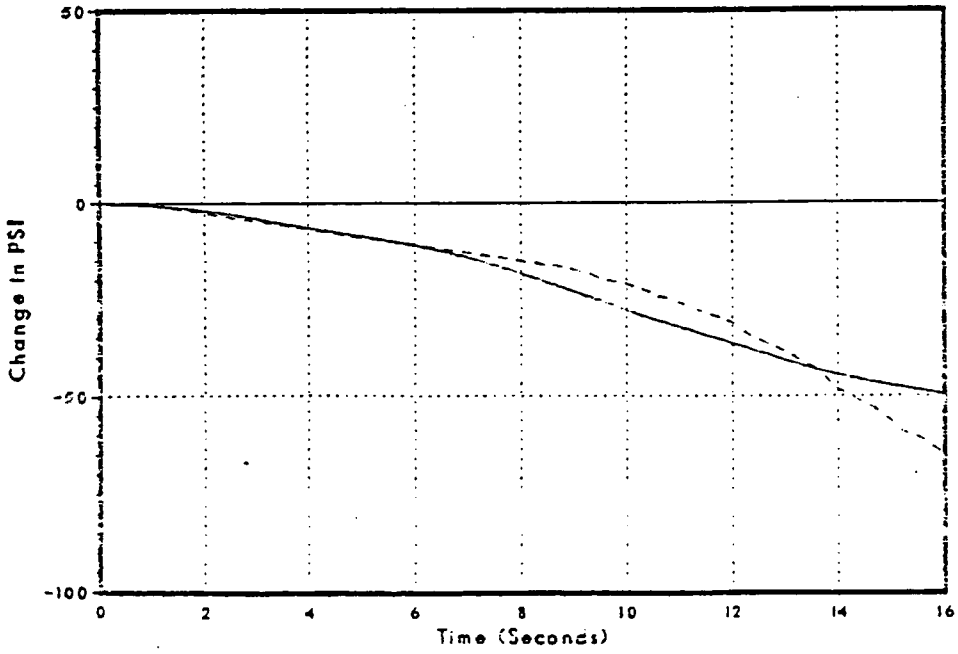

NSP

Prepared by NSP Safety Analysis, 5/06/86

Monticello FSAR Benchmark
Loss of Feedwater

Figure 3.2-38
Core Inlet Flow

DNB066/86
FSAR

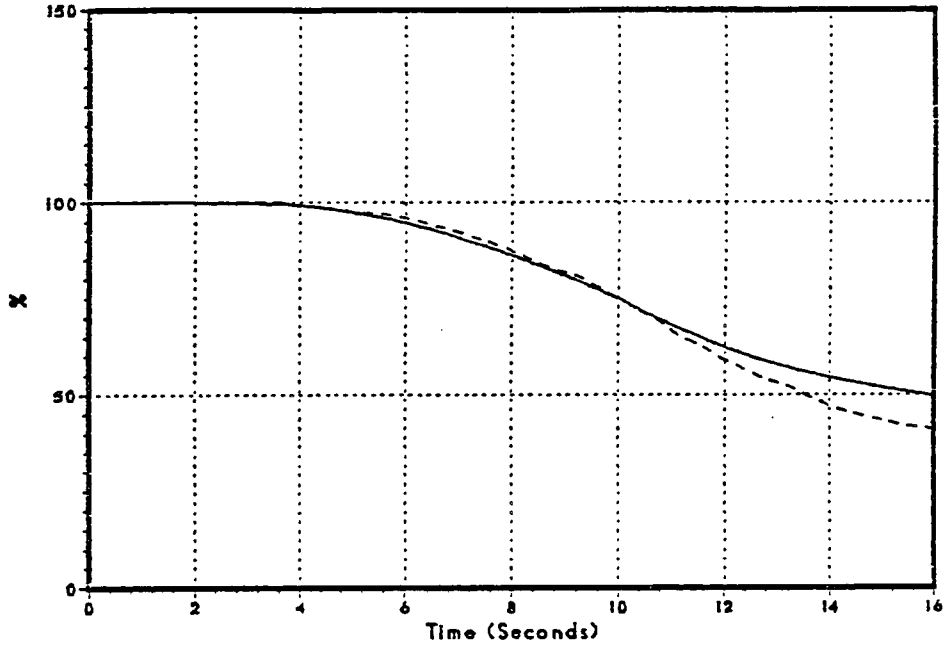

Figure 3.2-39
Average Surface Heat Flux

DNB066/86
FSAR

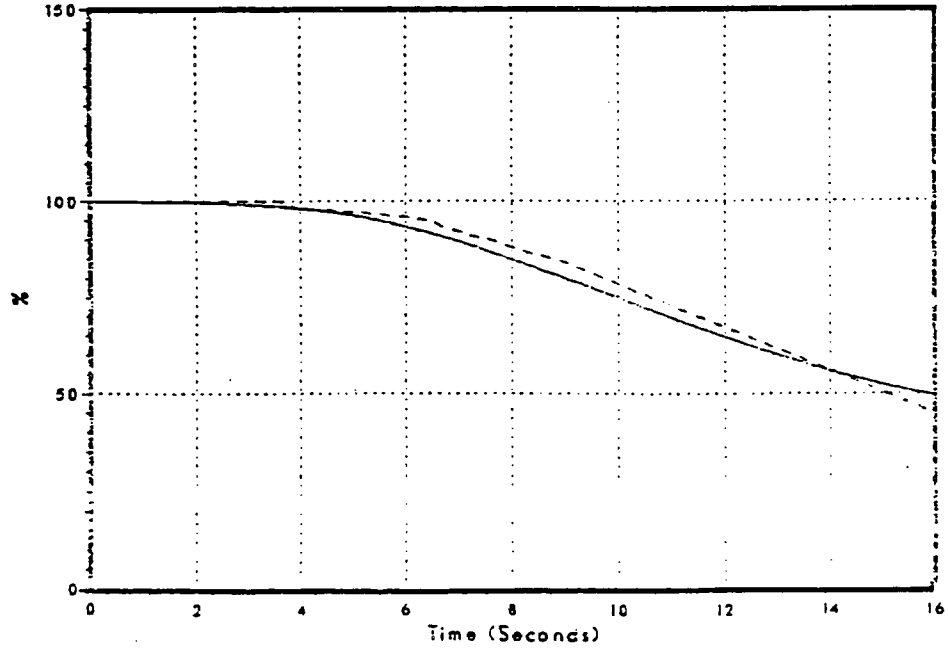

NSP

Prepared by NSP Safety Analysis, 5/06/86

Monticello FSAR Benchmark
Loss of Feedwater

Figure 3.2-40
Relative Power

DNB066/86
FSAR _ _ _ _

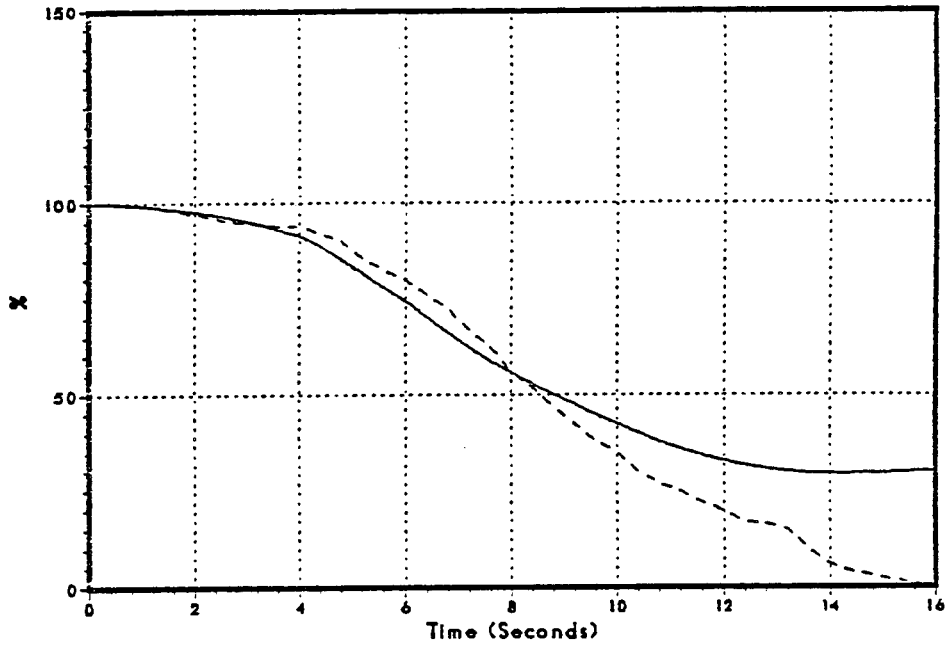

Figure 3.2-41
Feedwater Flow

DNB066/86
FSAR _ _ _ _

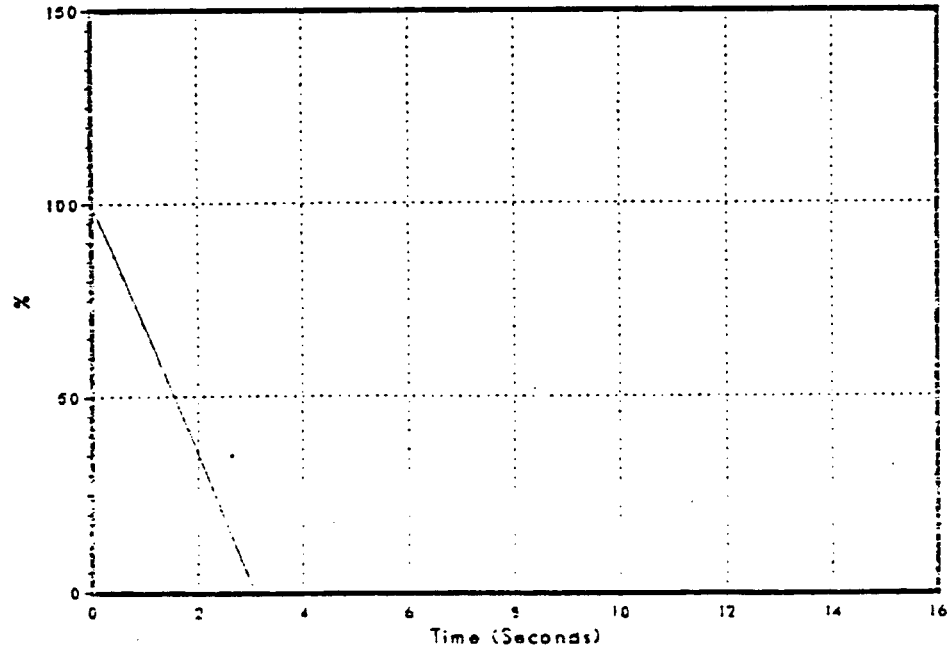

NSP

PREPARED BY NSP SAFETY ANALYSIS, 5/06/86

Monticello FSAR Benchmark
Loss of Feedwater

Figure 3.2-42
Vessel Steam Flow

DNB066/86
FSAR

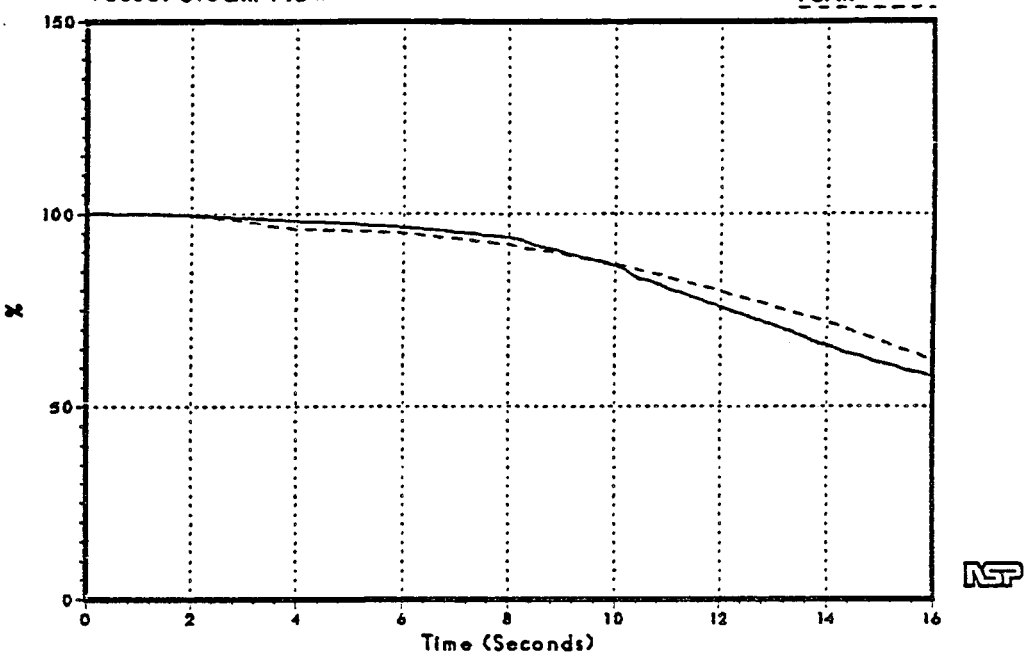

Prepared by NSP Safety Analysis, 5/06/86

Monticello FSAR Benchmark
Loss of Feedwater Heating

Figure 3.2-43
Sensed Level

DNB052/86
FSAR

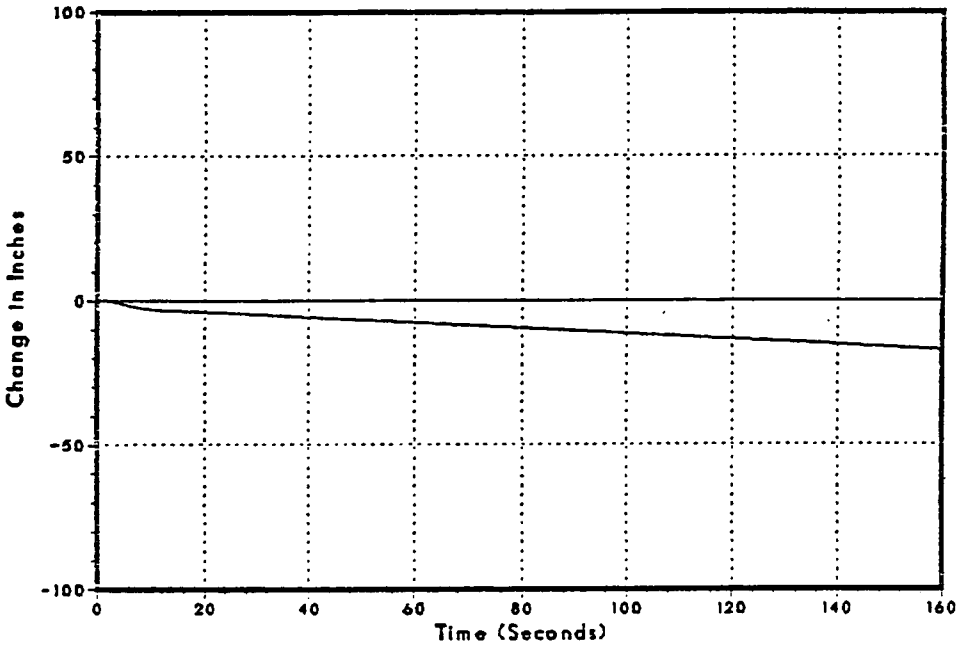

Figure 3.2-44
Steam Dome Pressure

DNB052/86
FSAR

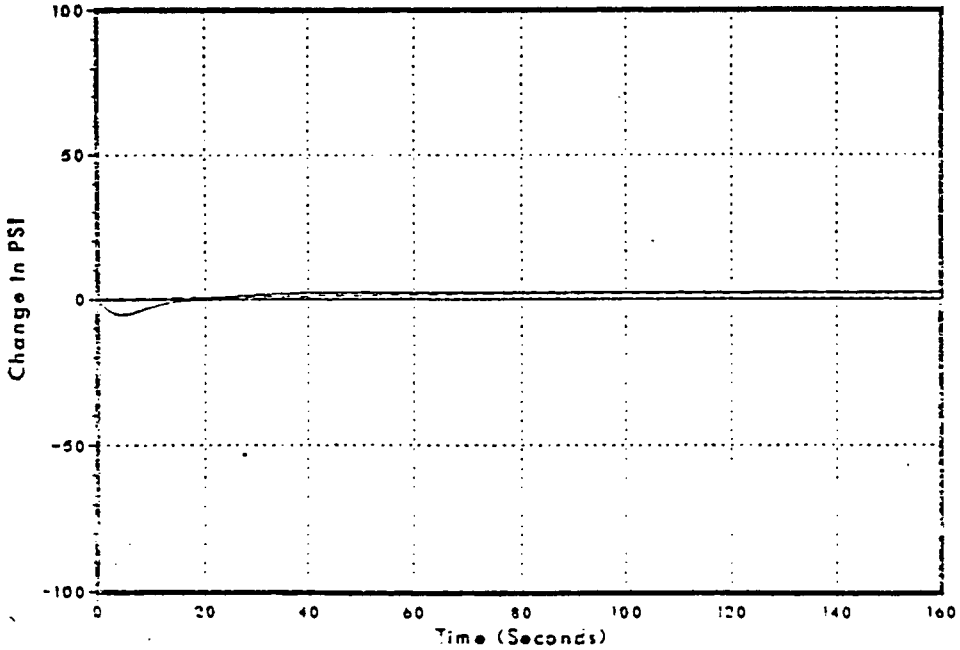

NSP

Monticello FSAR Benchmark
Loss of Feedwater Heating

Figure 3.2-45
Core Inlet Flow

DNB052/86
FSAR

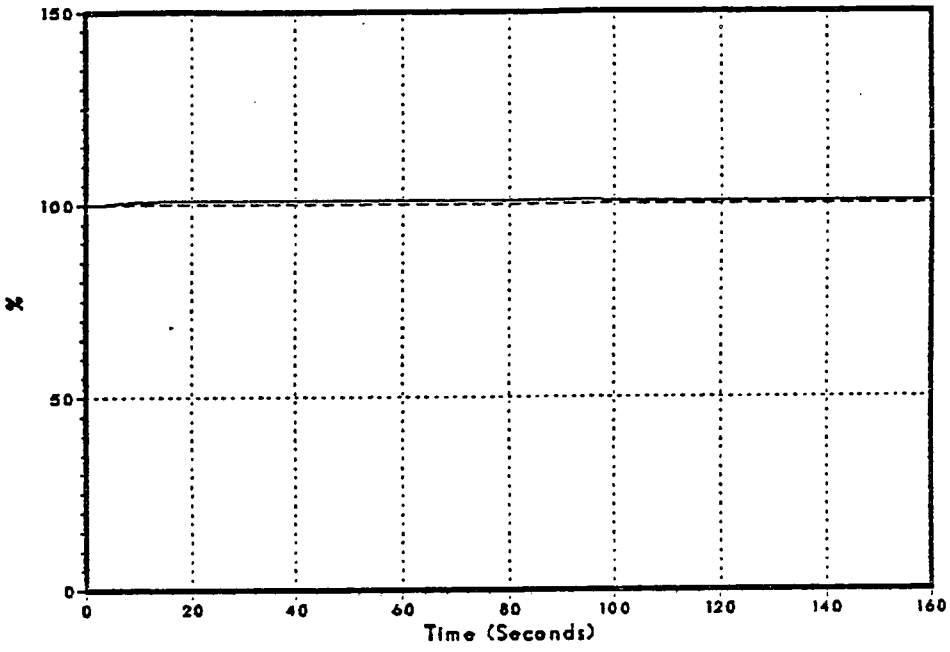

Figure 3.2-46
Average Surface Heat Flux

DNB052/86
FSAR

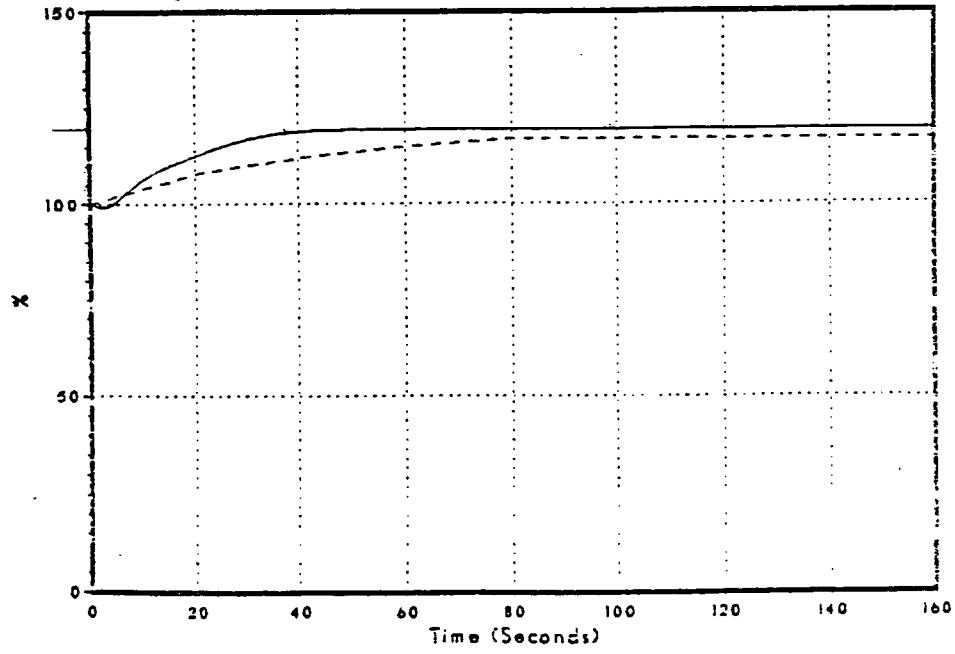

NSP

Monticello FSAR Benchmark
Loss of Feedwater Heating

Figure 3.2-47
Relative Power

DNB052/86
FSAR

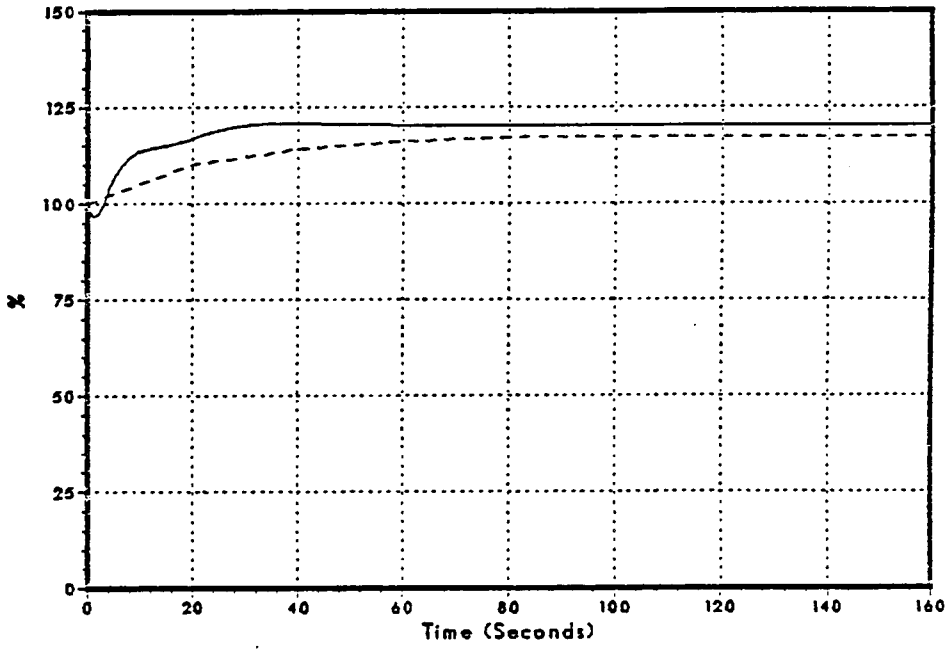

Figure 3.2-48
Feedwater Flow

DNB052/86
FSAR

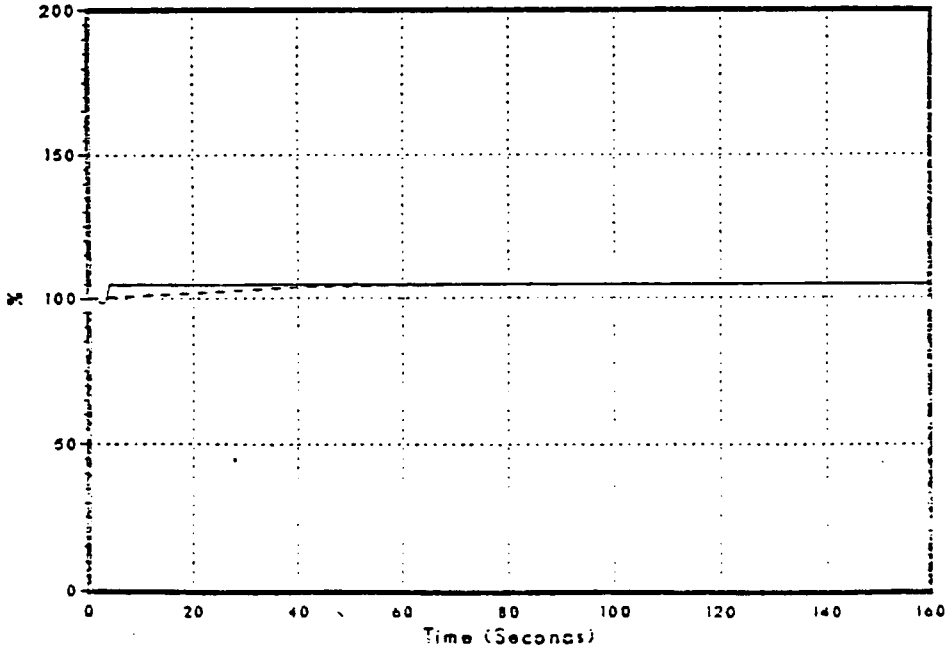

NSP

Monticello FSAR Benchmark
Loss of Feedwater Heating

Figure 3.2-49
Vessel Steam Flow

DNB052/86
FSAR _ _ _ _

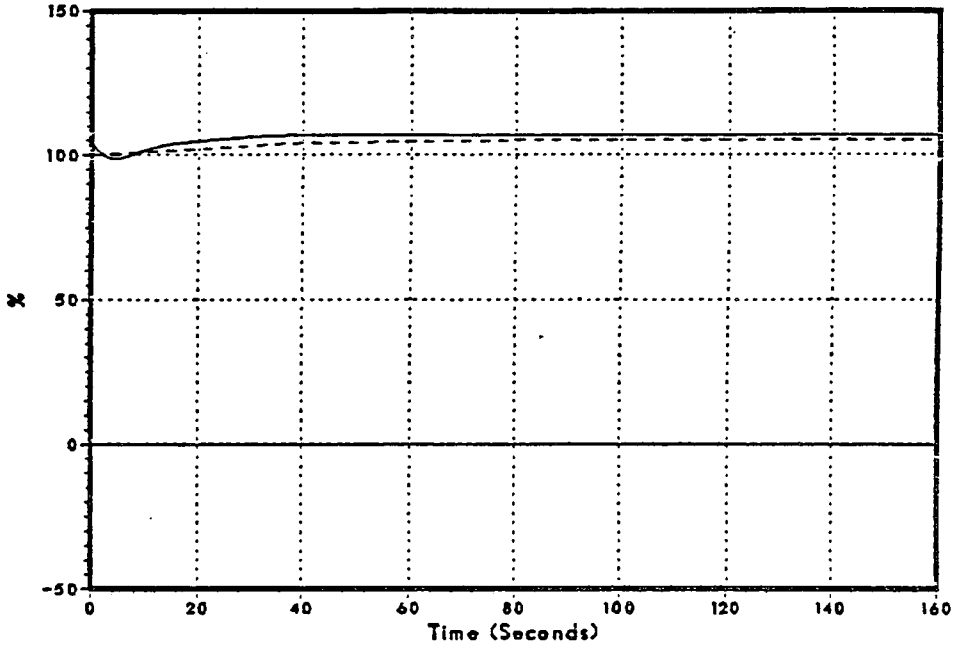

NSP

Prepared by NSP Safety Analysis, 4/25/86

Monticello FSAR Benchmark
Pressure Regulator Fails Open

Figure 3.2-50
Steam Dome Pressure

DNB071/86
FSAR _ _ _

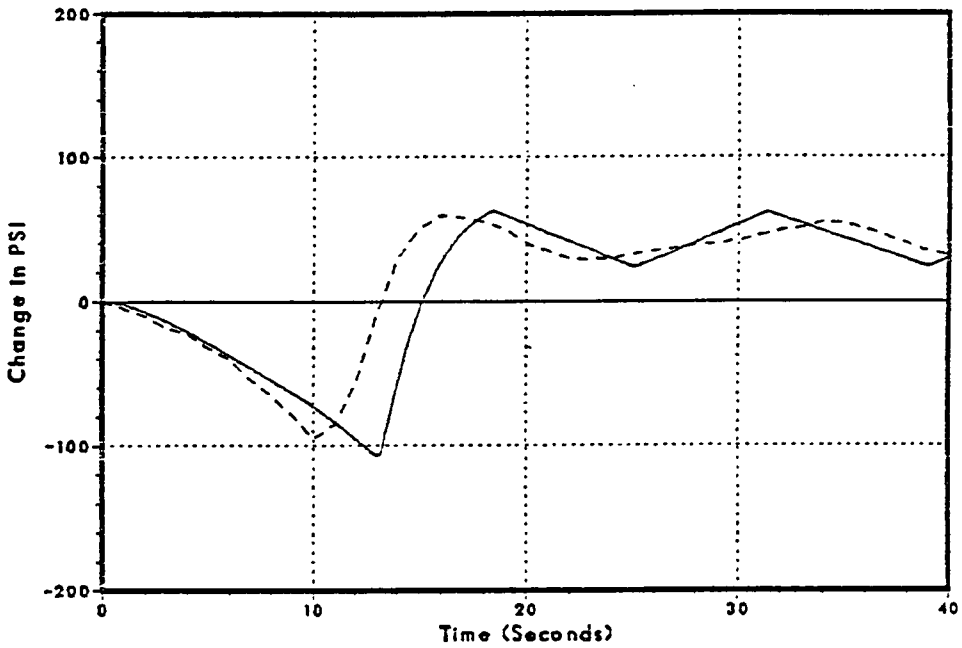

Figure 3.2-51
Relative Power

DNB071/86
FSAR _ _ _

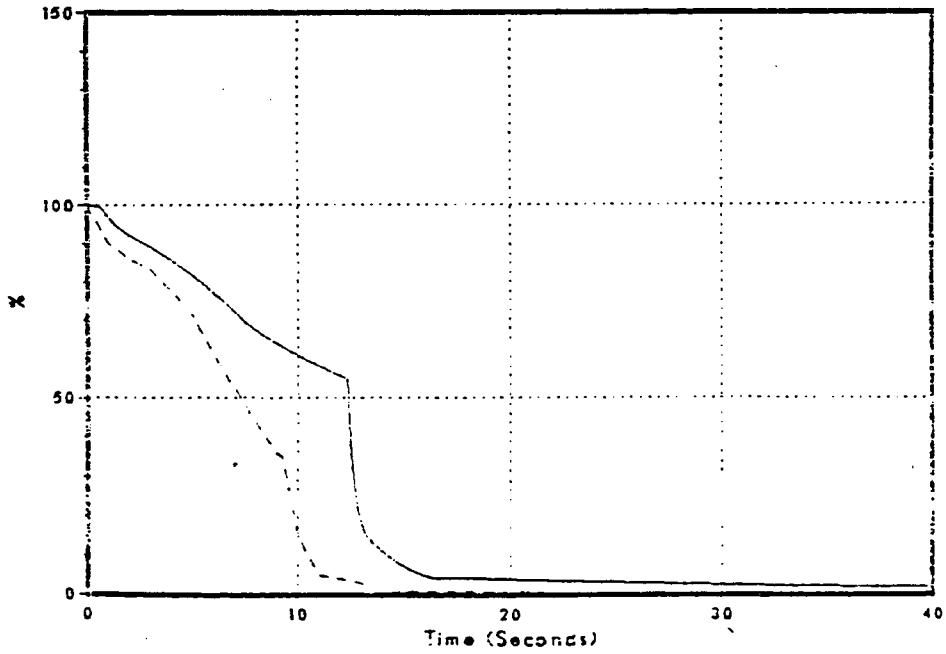

NSP

PREPARED BY NS[illegible]ETY ANALYSIS, 4/27/86

Monticello FSAR Benchmark
Pressure Regulator Fails Open

DNB071/86

Figure 3.2-52
Core Average Heat Flux

FSAR _ _ _ _

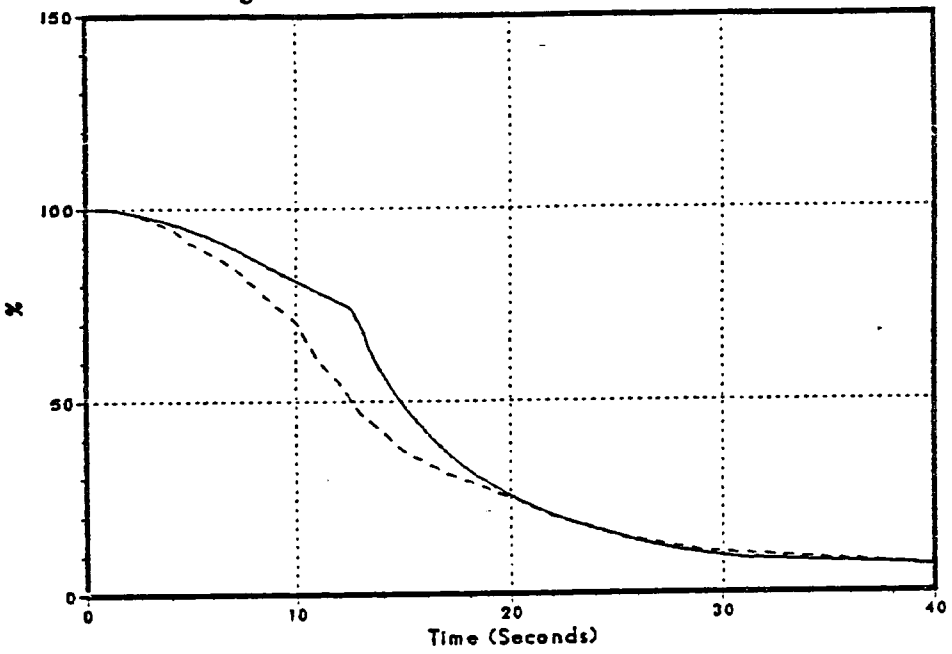

DNB071/86

Figure 3.2-53
Core Inlet Flow

FSAR _ _ _ _

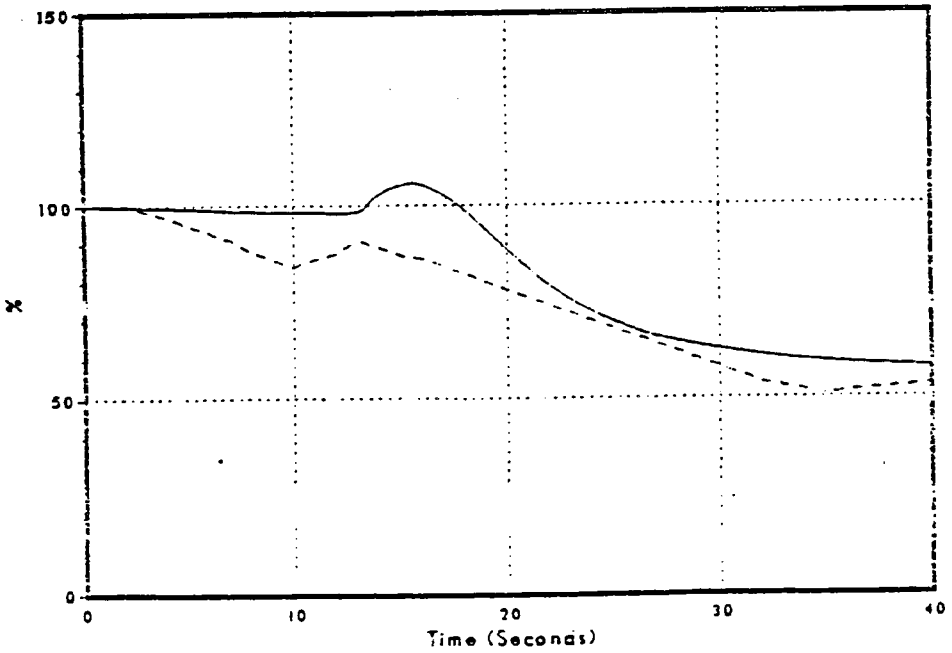

NSP

PREPARED BY NSP SAFETY ANALYSIS, 4/27/86

Monticello FSAR Benchmark
Pressure Regulator Fails Open

DNB071/86

Figure 3.2-54
Main Steam Line Flow

FSAR _ _ _

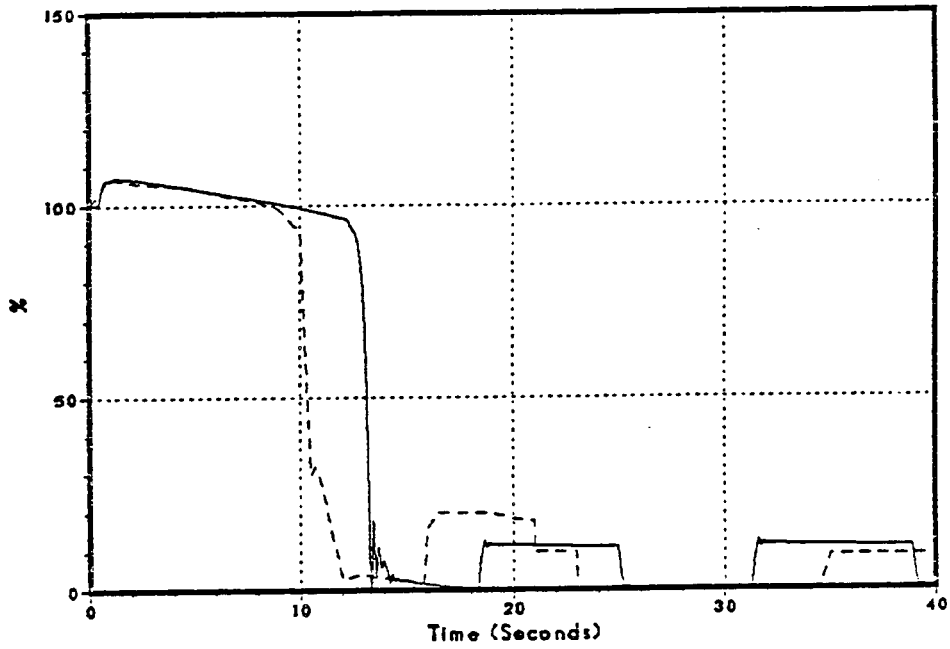

DNB071/86

Figure 3.2-55
Feedwater Flow

FSAR _ _ _

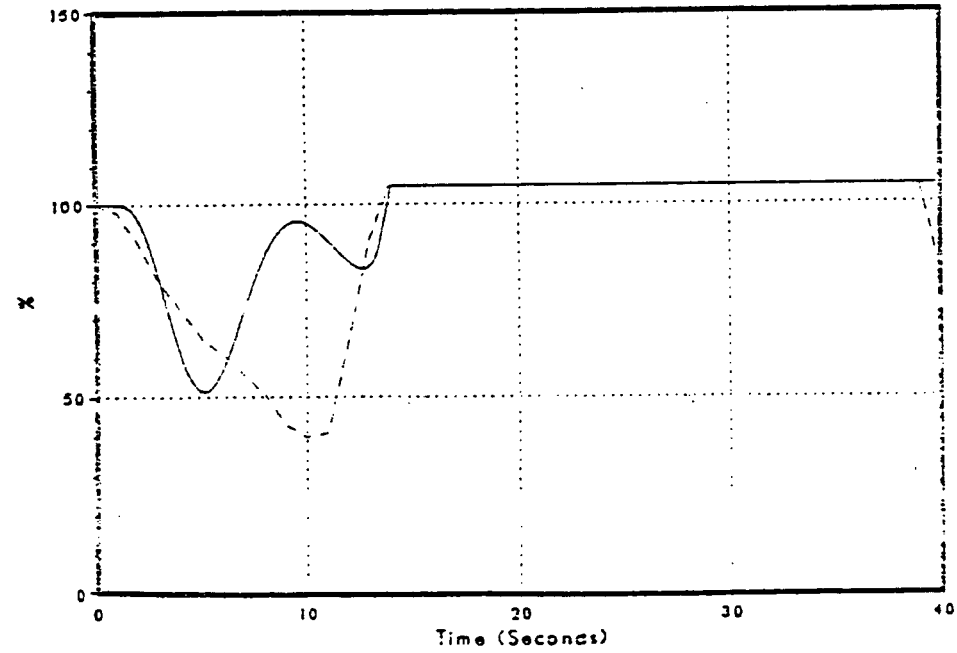

PREPARED BY NSP SAFETY ANALYSIS, 4/27/86

Monticello FSAR Benchmark
Pressure Regulator Fails Open

Figure 3.2-56
Sensed Level

DNB071/86
FSAR

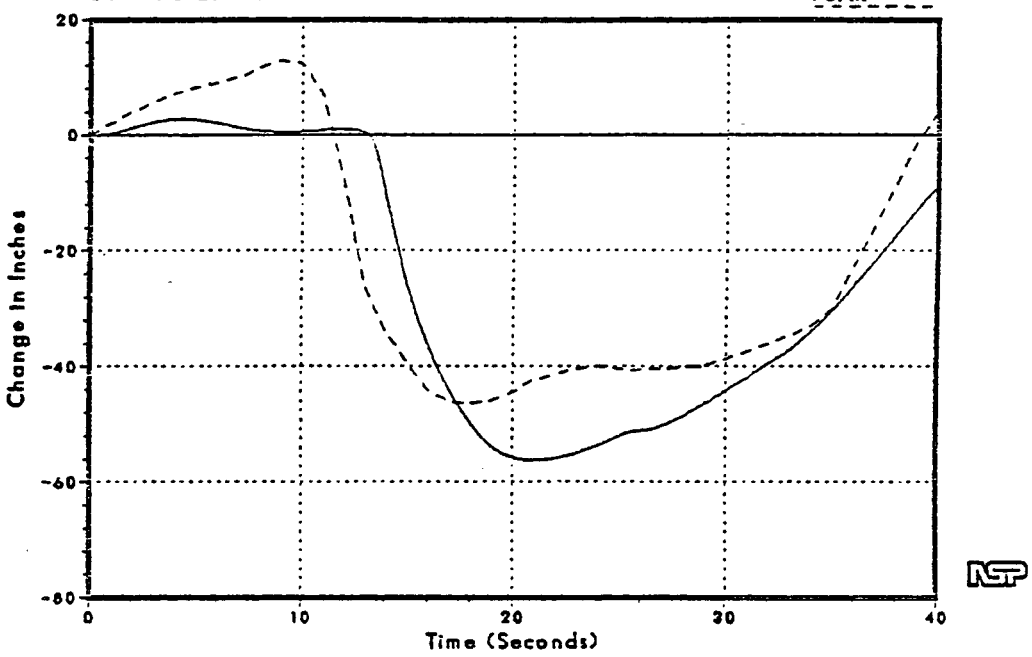

Monticello FSAR Benchmark
Recirculation Pump Seizure

Figure 3.2-57
Sensed Level

DNB067/86
FSAR

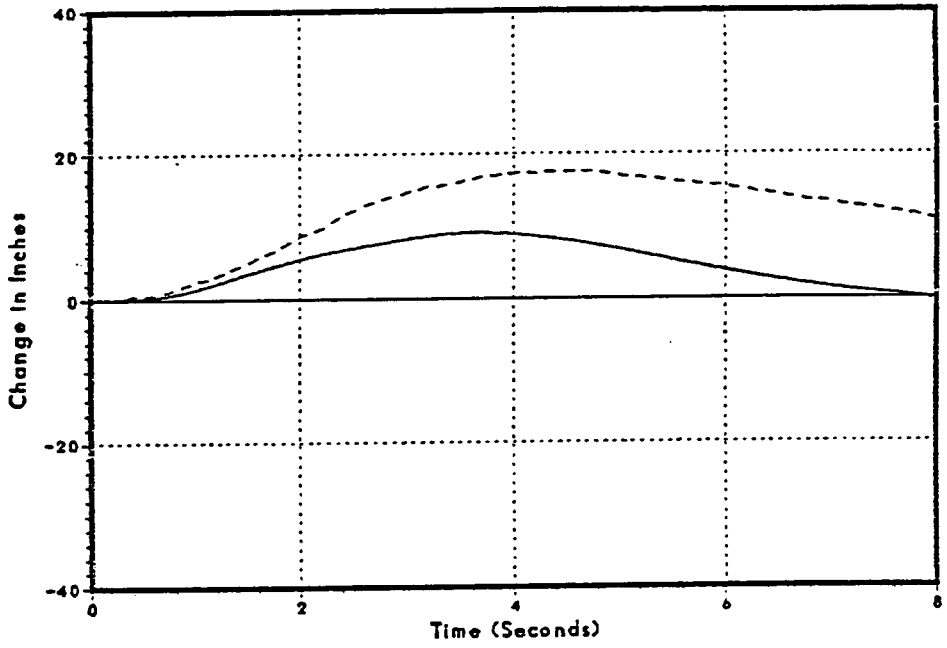

Figure 3.2-58
Steam Dome Pressure

DNB067/86
FSAR

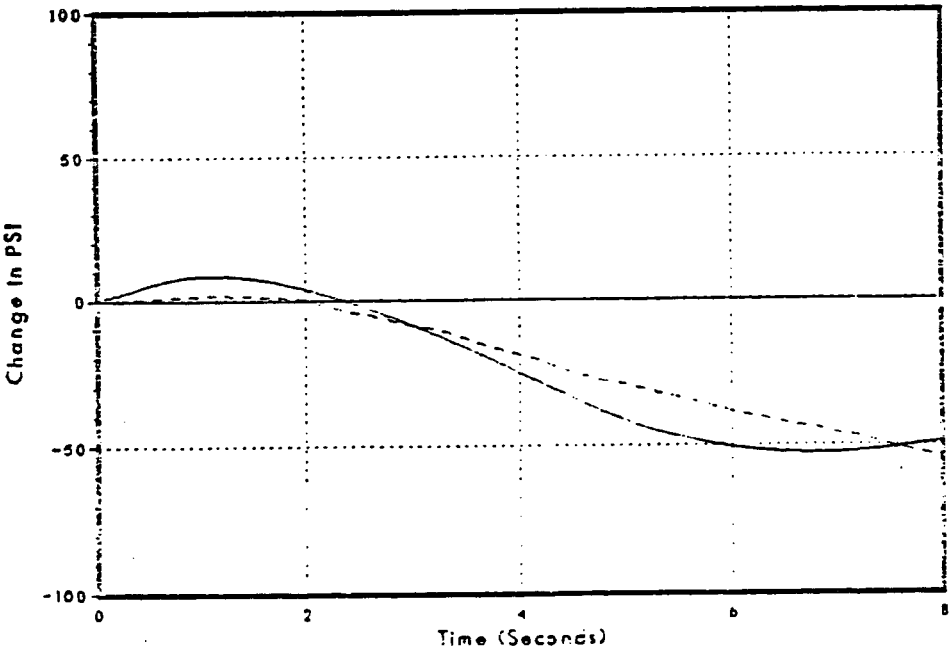

NSP

Monticello FSAR Benchmark
Recirculation Pump Seizure

Figure 3.2-59
Core Inlet Flow

DNB067/86
FSAR

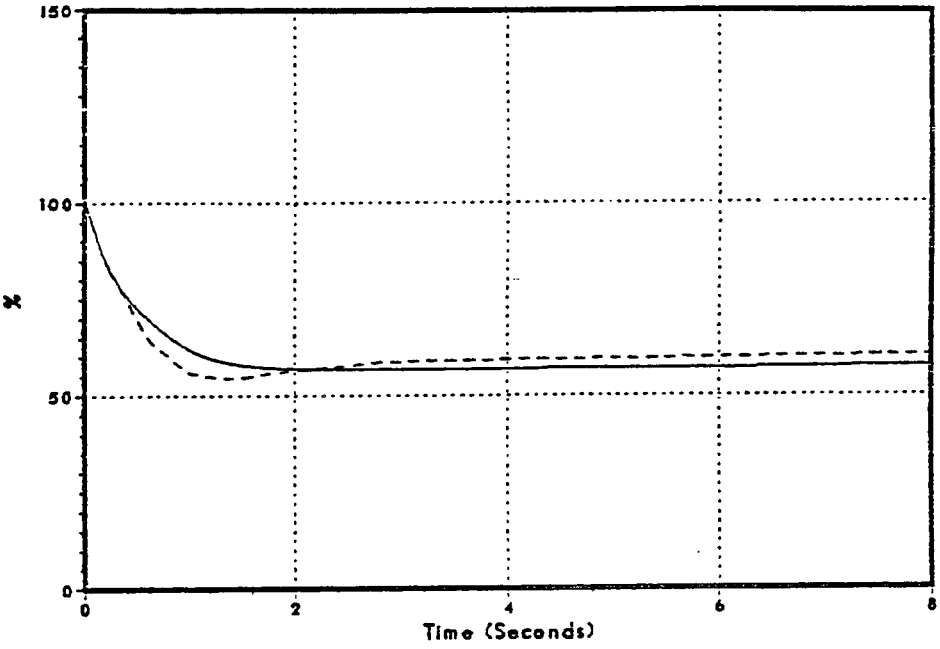

Figure 3.2-60
Average Surface Heat Flux

DNB067/86
FSAR

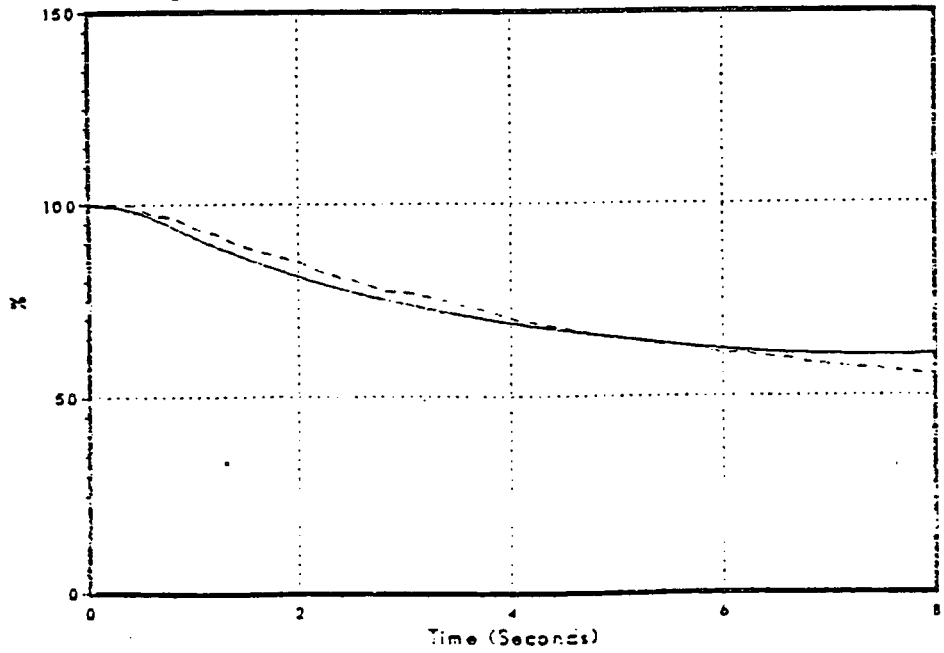

NSP

Prepared by NSP Safety Analysis, 5/01/86

Monticello FSAR Benchmark
Recirculation Pump Seizure

Figure 3.2-61
Relative Power

DNB067/86
FSAR

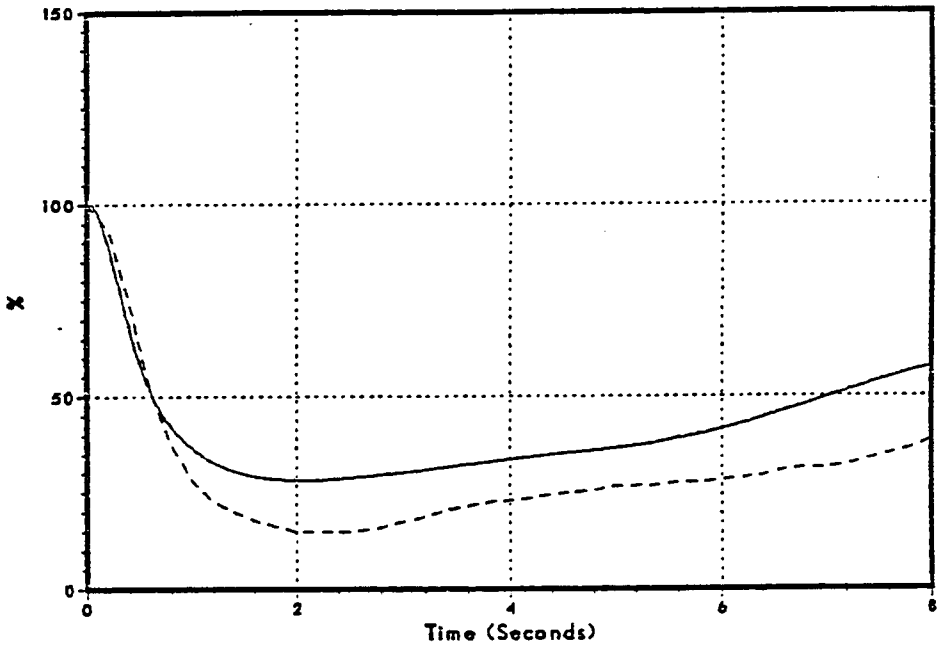

Figure 3.2-62
Feedwater Flow

DNB067/86
FSAR

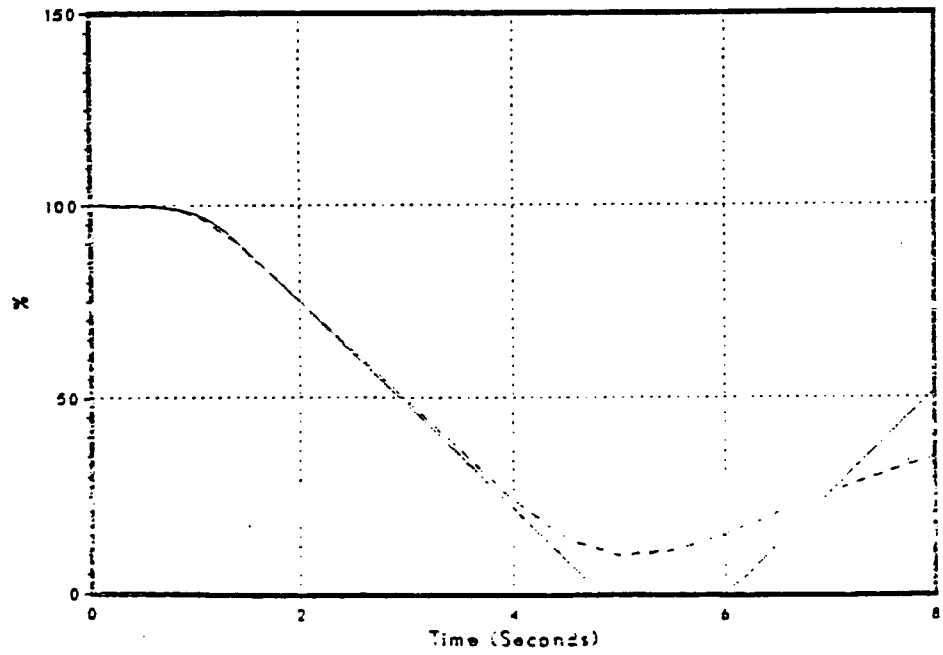

NSP

Prepared by NSP Safety Analysis, 5/01/86

Monticello FSAR Benchmark
Recirculation Pump Seizure

Figure 3.2-63
Vessel Steam Flow

DNB067/86
FSAR

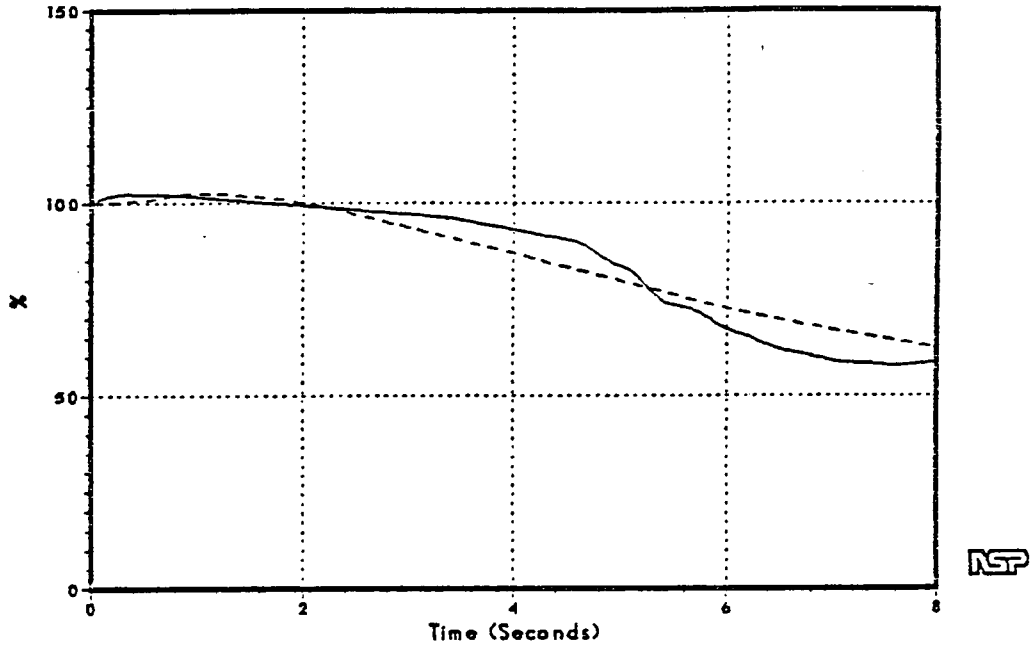

NSP

Prepared by NSP Safety Analysis, 5/01/86

Monticello FSAR Benchmark
2/2 Recirculation Pump Trip

Figure 3.2-64
Sensed Level

DNB073/86
FSAR

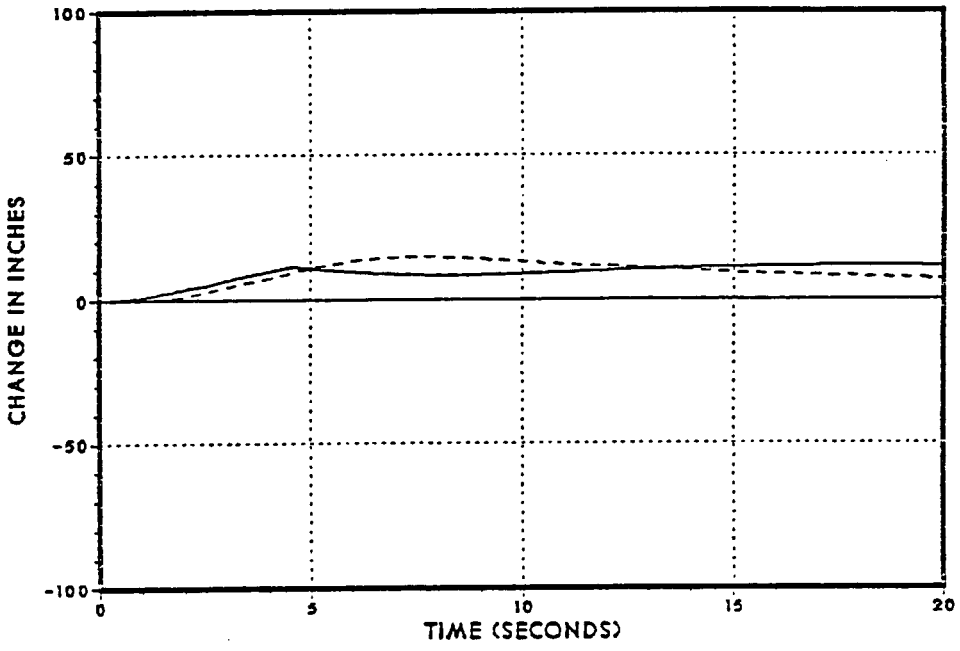

Figure 3.2-65
Steam Dome Pressure

DNB073/86
FSAR

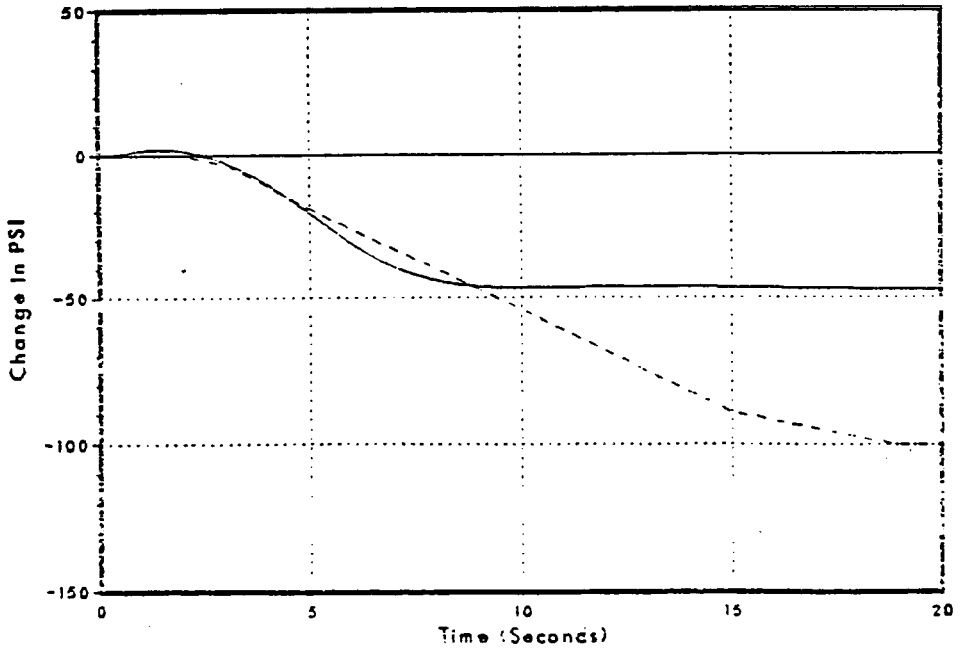

NSP

Monticello FSAR Benchmark
2/2 Recirculation Pump Trip

Figure 3.2-66
Core Inlet Flow

DNB073/86
FSAR

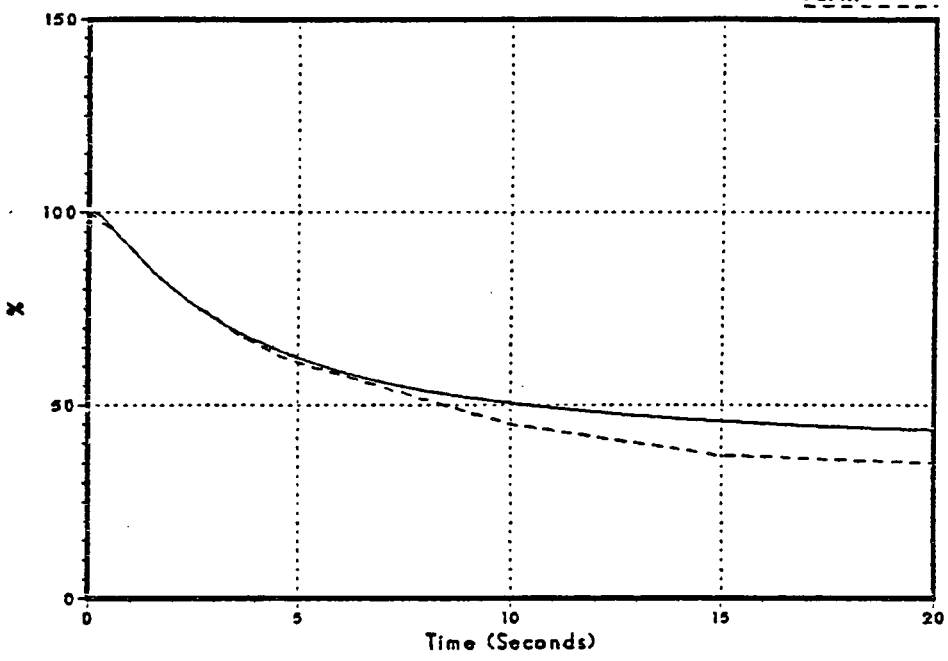

Figure 3.2-67
Average Surface Heat Flux

DNB073/86
FSAR

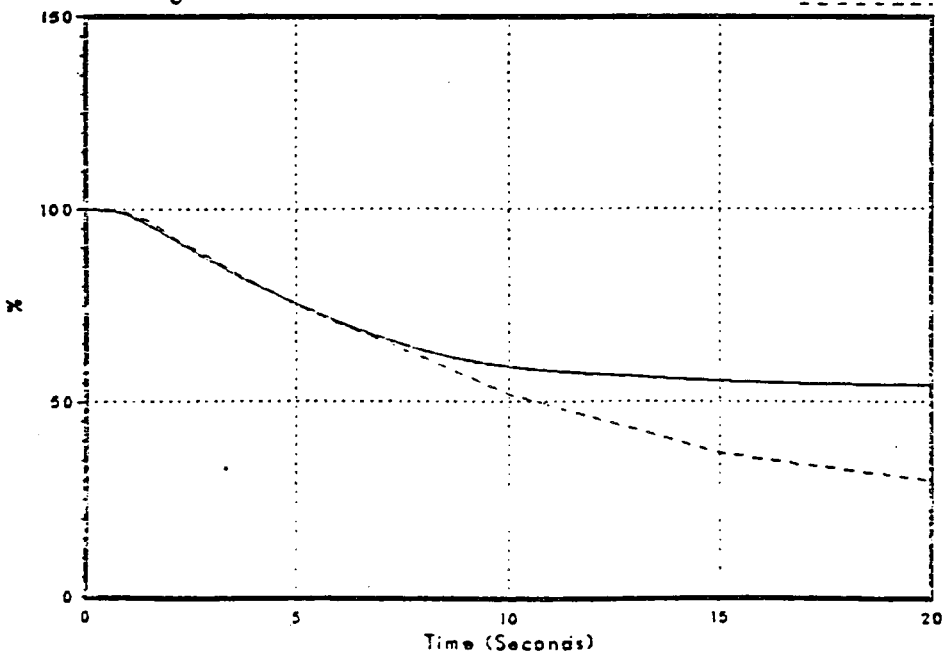

NSP

PREPARED BY NSP SAFETY ANALYSIS, 6/26/86

Monticello FSAR Benchmark
2/2 Recirculation Pump Trip

Figure 3.2-68
Relative Power

DNB073/86
FSAR

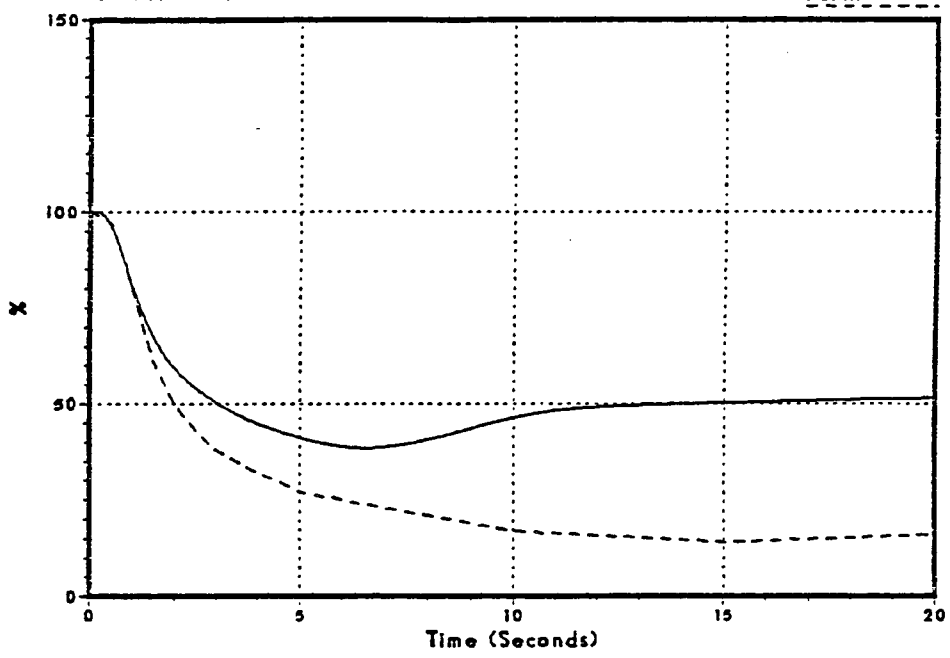

Figure 3.2-69
Feedwater Flow

DNB073/86
FSAR

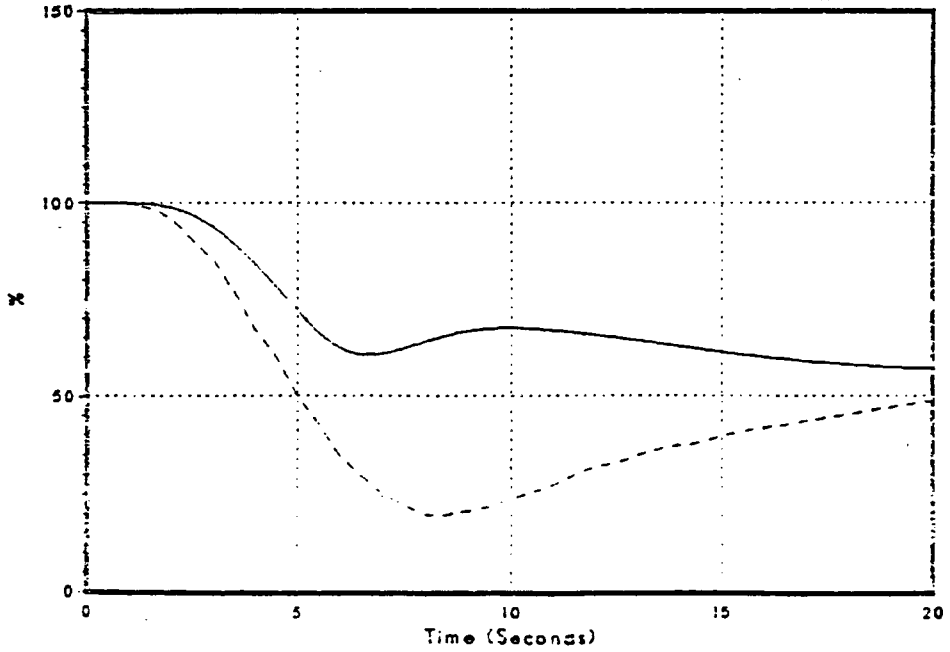

NSP

Prepared by NSP Safety Analysis, 6/26/86

Monticello FSAR Benchmark
2/2 Recirculation Pump Trip

Figure 3.2-70
Vessel Steam Flow

DNB073/86
FSAR _ _ _ _

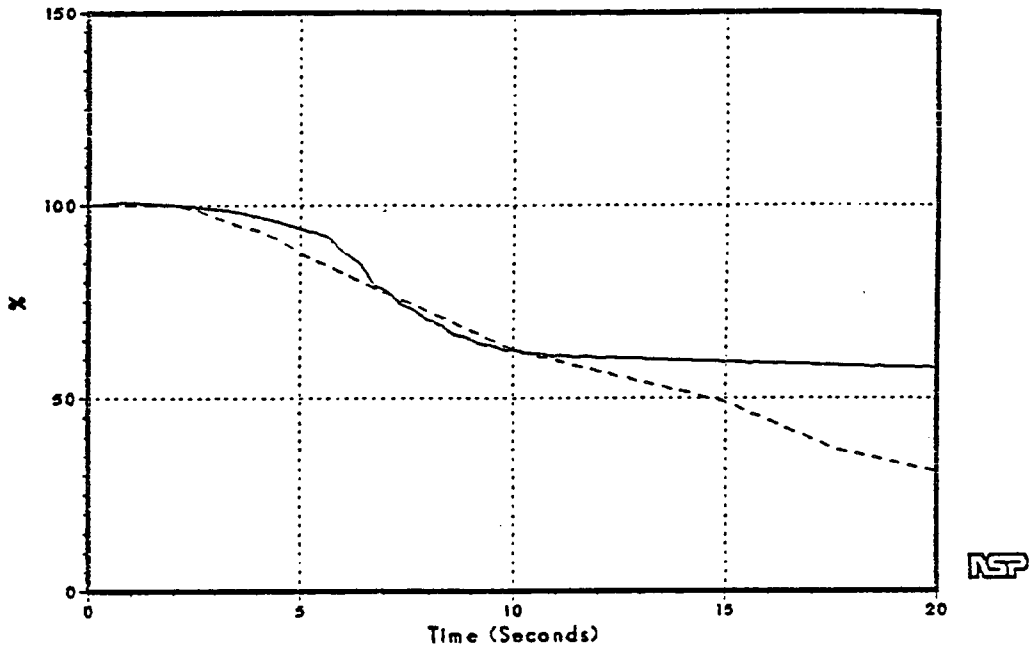

Monticello FSAR Benchmark
Recirculation Controller Fails (Increase)

Figure 3.2-71
Sensed Level

DNB072/86
FSAR

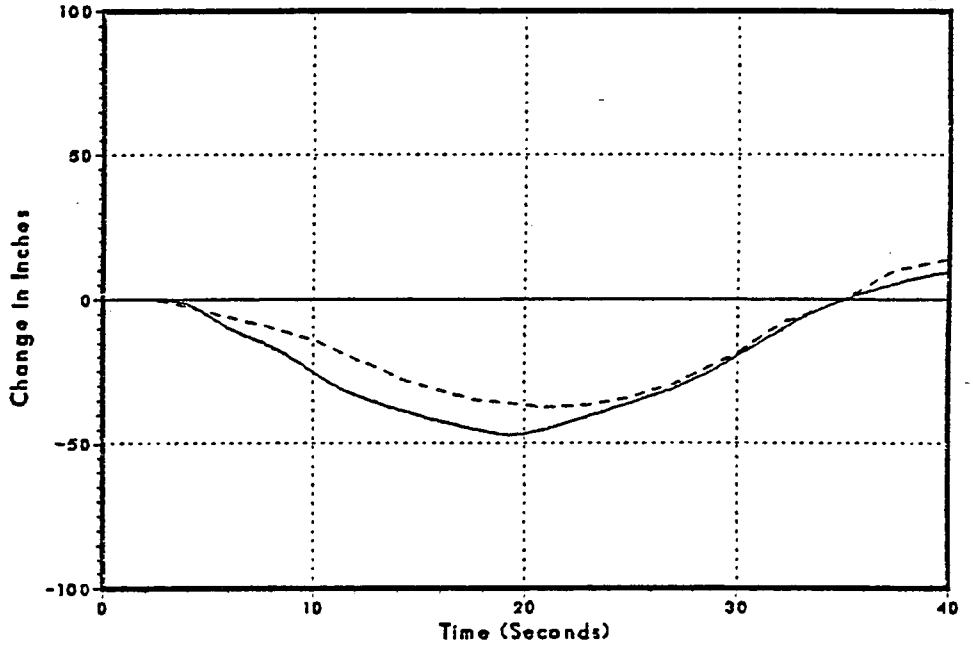

Figure 3.2-72
Steam Dome Pressure

DNB072/86
FSAR

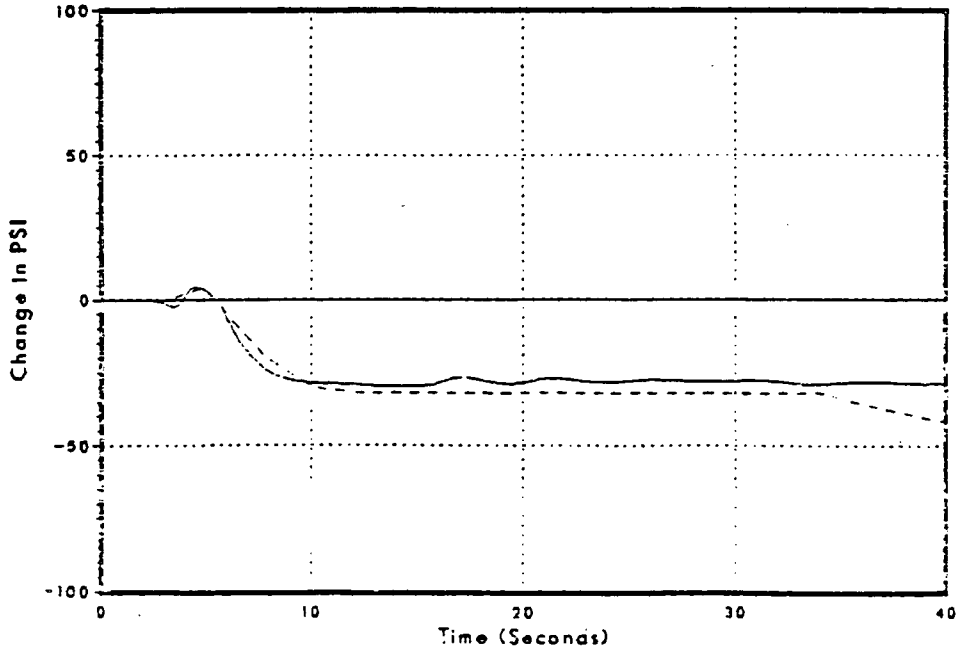

NSP

Monticello FSAR Benchmark
Recirculation Controller Fails (Increase)

Figure 3.2-73
Core Inlet Flow

DNB072/86
FSAR

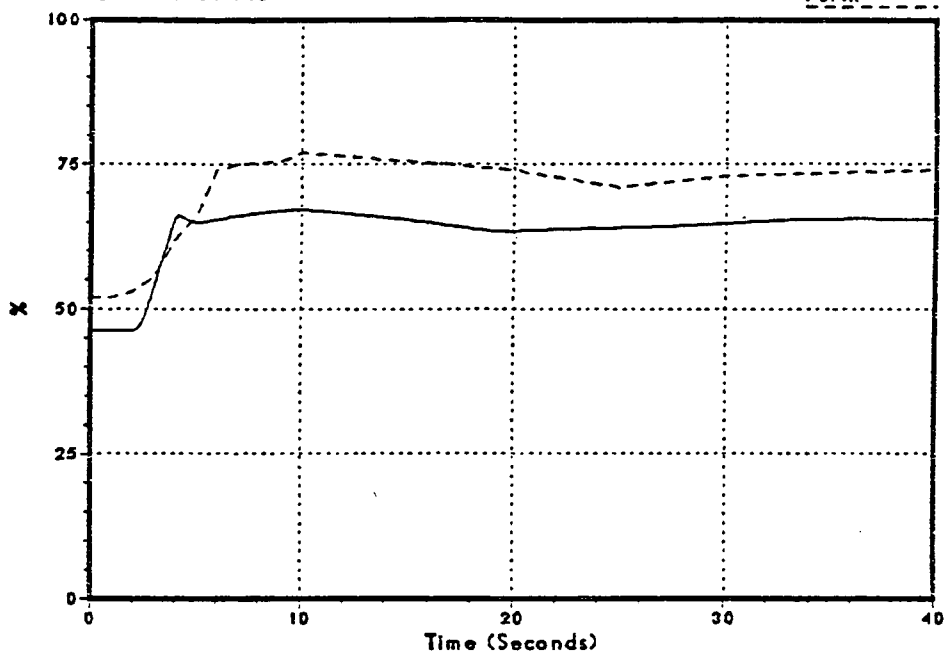

Figure 3.2-74
Average Surface Heat Flux

DNB072/86
FSAR

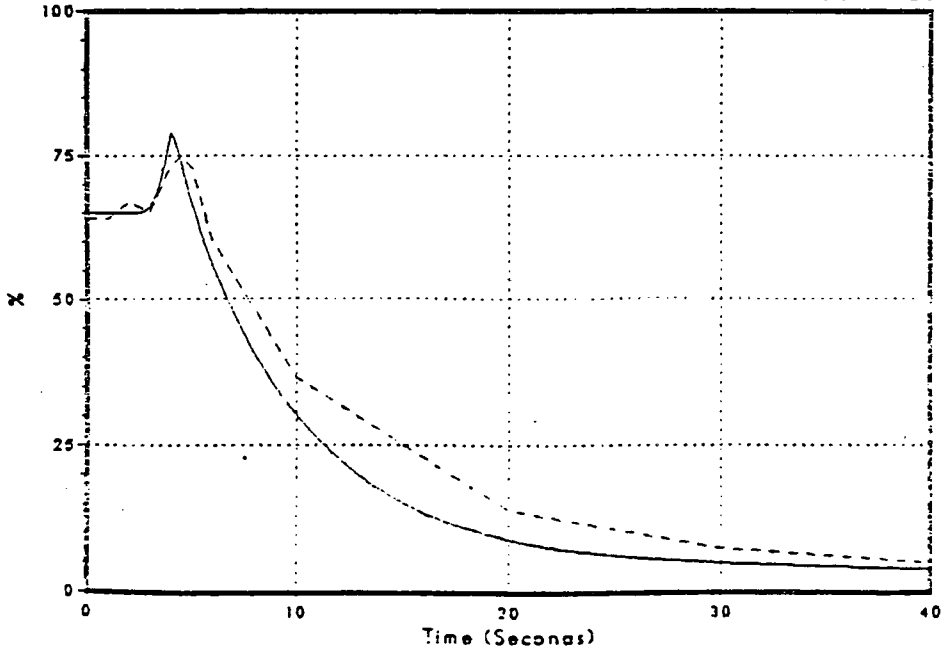

NSP

Monticello FSAR Benchmark
Recirculation Controller Fails (Increase)

Figure 3.2-75
Relative Power

DN8072/86
FSAR

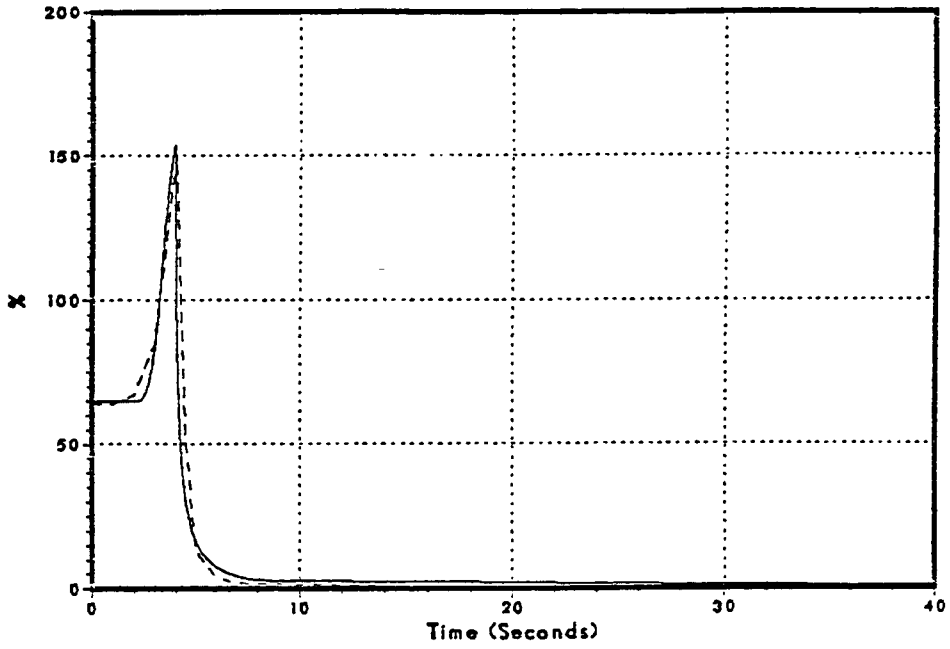

Figure 3.2-76
Feedwater Flow

DN8072/86
FSAR

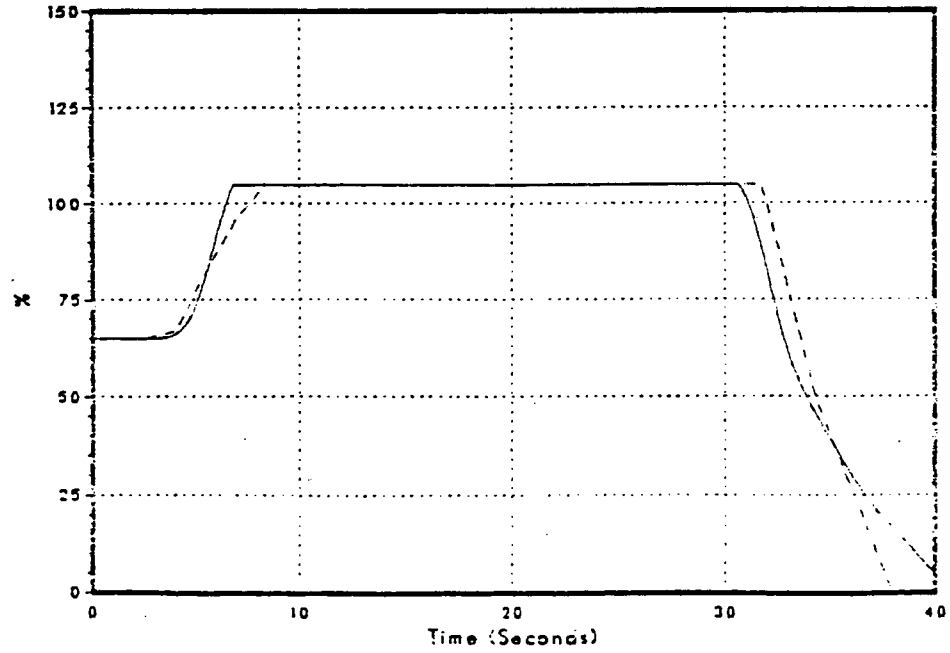

NSP

Prepared by NSP Safety Analysis, 5/18/86

Monticello FSAR Benchmark
Recirculation Controller Fails (Increase)

Figure 3.2-77
Vessel Steam Flow

DNB072/86
FSAR

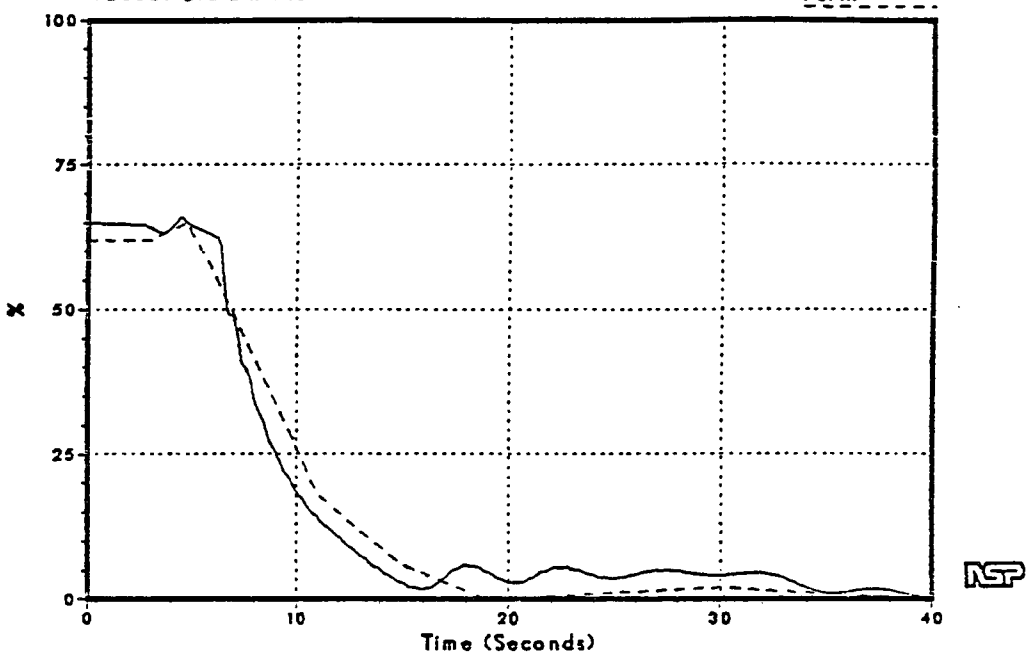

Monticello FSAR Benchmark
Recirculation Controller Fails (Decrease)

Figure 3.2-78
Sensed Level

No FSAR Data Available
DNB074/86

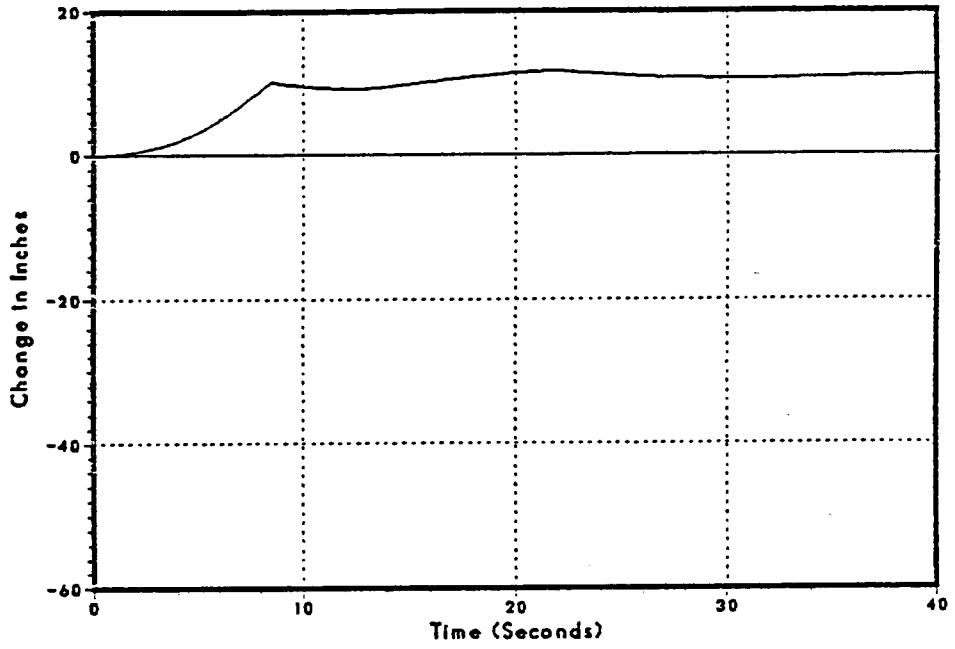

Figure 3.2-79
Steam Dome Pressure

DNB074/86
FSAR

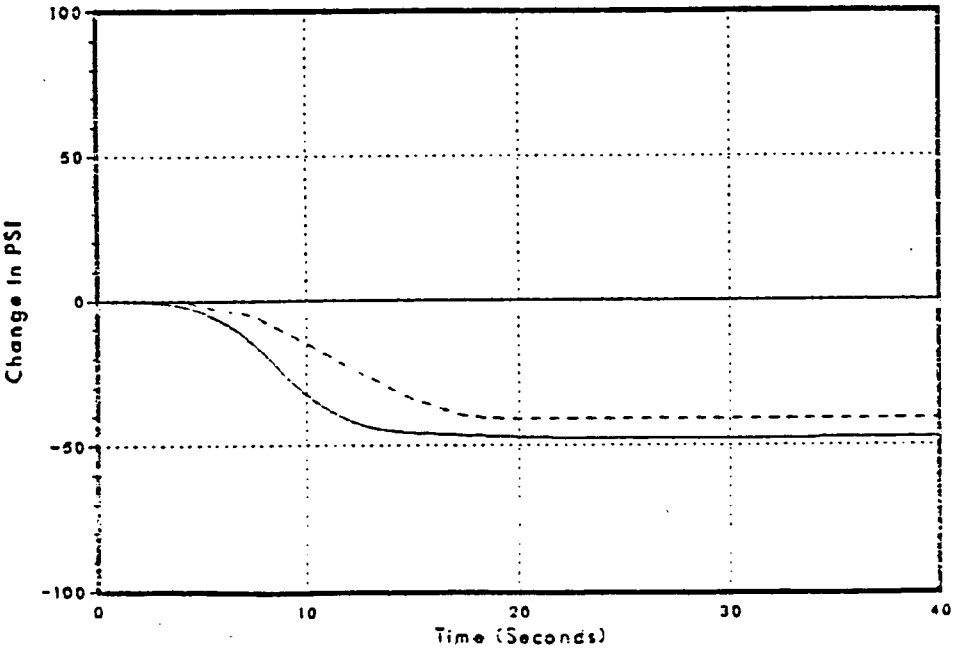

NSP

Monticello FSAR Benchmark
Recirculation Controller Fails (Decrease)

Figure 3.2-80
Core Inlet Flow

DNB074/86
FSAR

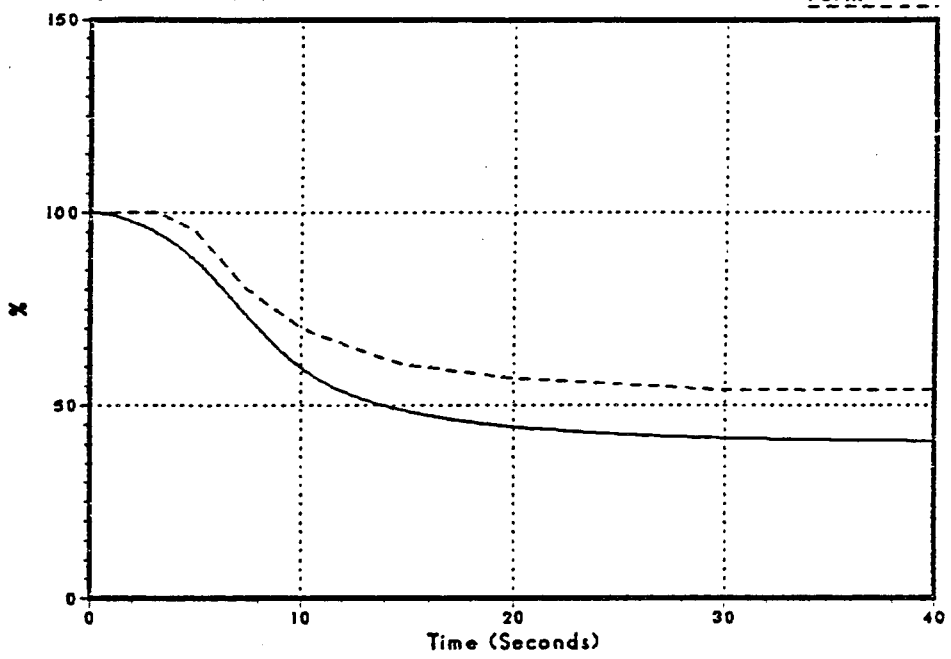

Figure 3.2-81
Average Surface Heat Flux

DNB074/86
FSAR

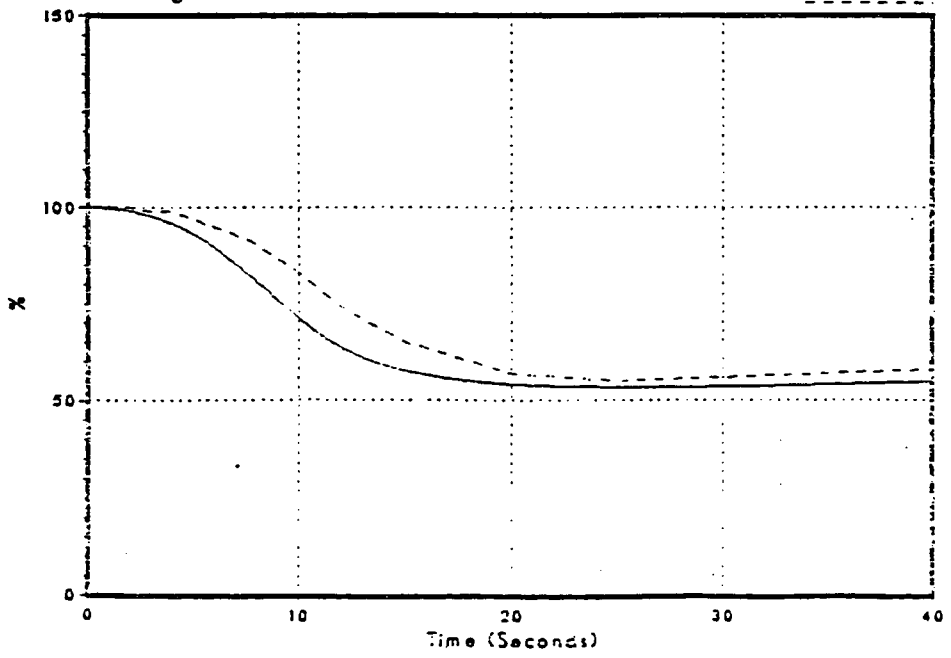

NSP

Prepared by NSP Safety Analysis, 6/26/86

Monticello FSAR Benchmark
Recirculation Controller Fails (Decrease)

Figure 3.2-82
Relative Power

DNB074/86
FSAR

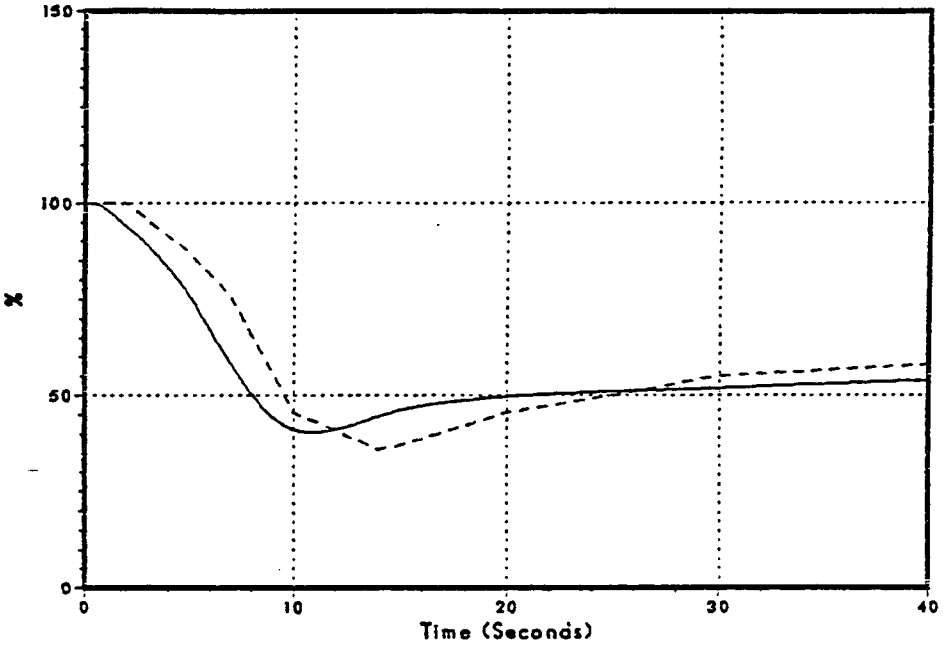

Figure 3.2-83
Feedwater Flow

DNB074/86
FSAR

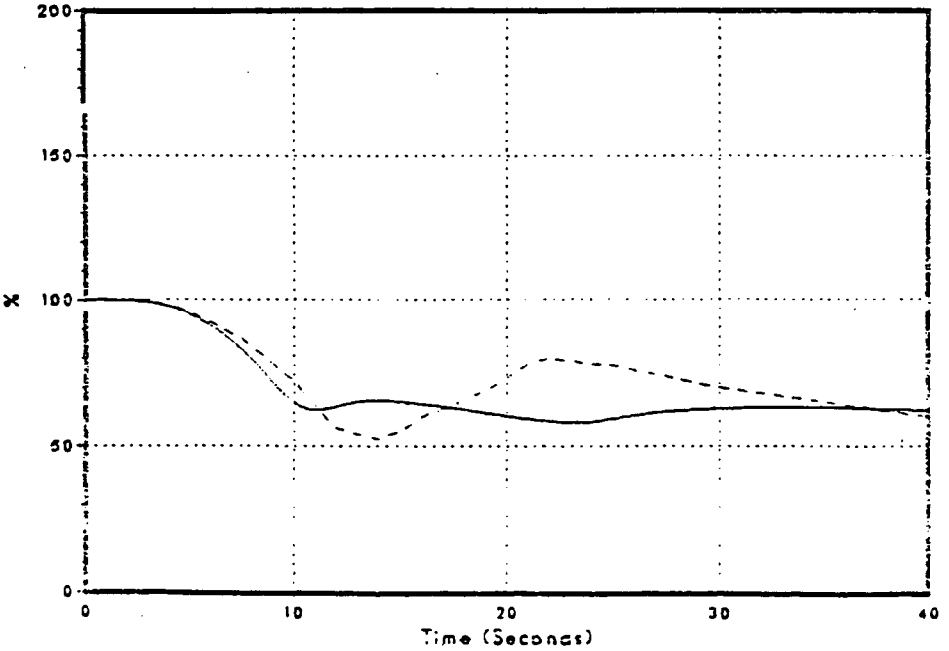

NSP

Prepared by NSP Safety Analysis, 6/26/86

Monticello FSAR Benchmark
Recirculation Controller Fails (Decrease)

Figure 3.2-84
Vessel Steam Flow

DNB074/86
FSAR

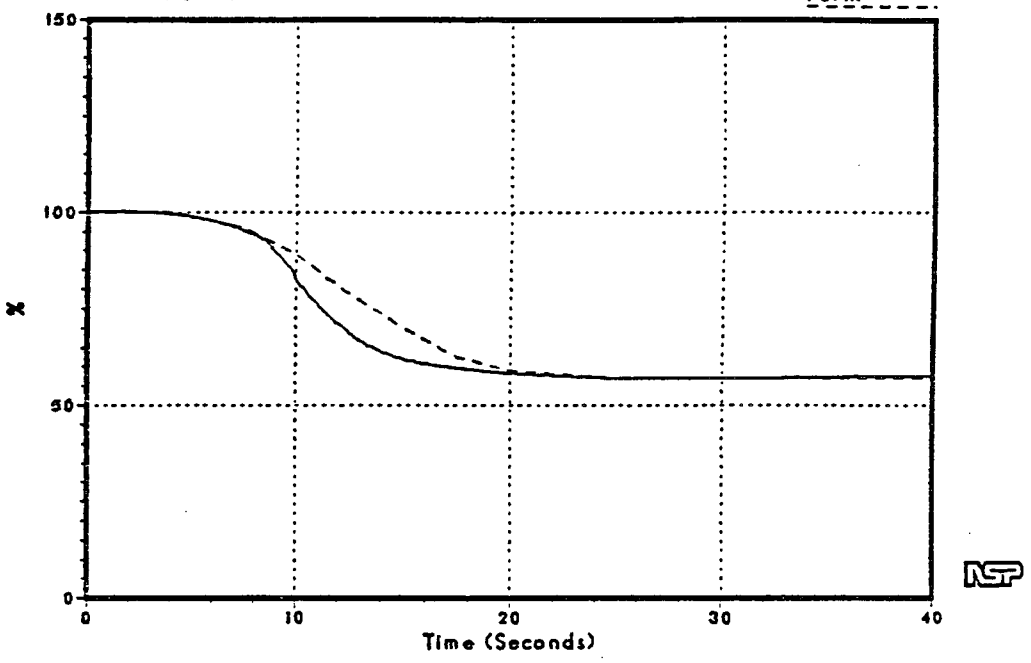

Monticello FSAR Benchmark
Idle Loop Startup

Figure 3.2-85
Sensed Level

DNB068/86
FSAR

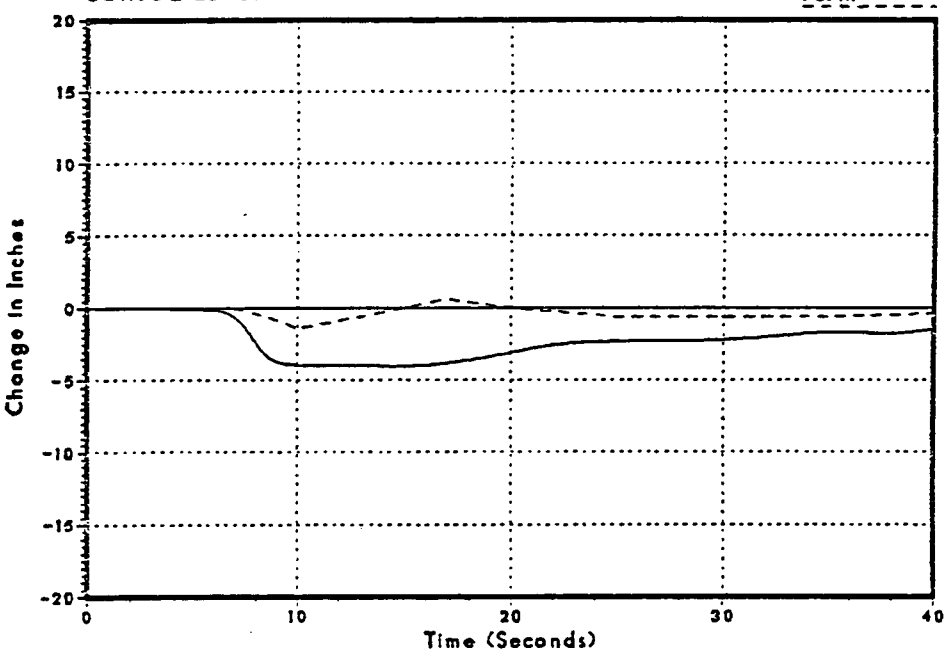

Figure 3.2-86
Steam Dome Pressure

DNB068/86
FSAR

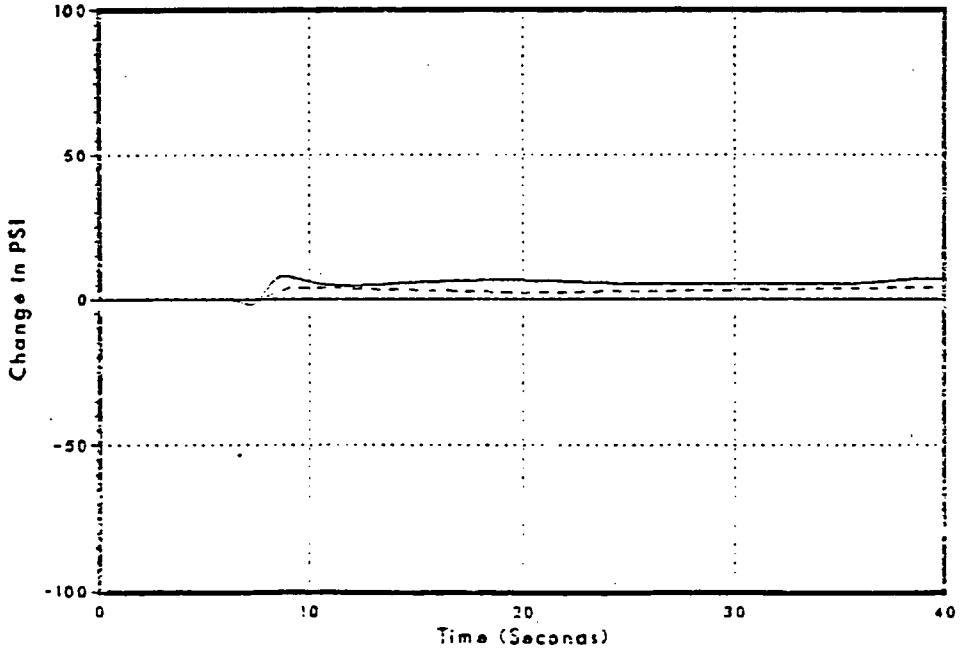

NSP

Monticello FSAR Benchmark
Idle Loop Startup

Figure 3.2-87
Core Inlet Flow

DNB068/86
FSAR

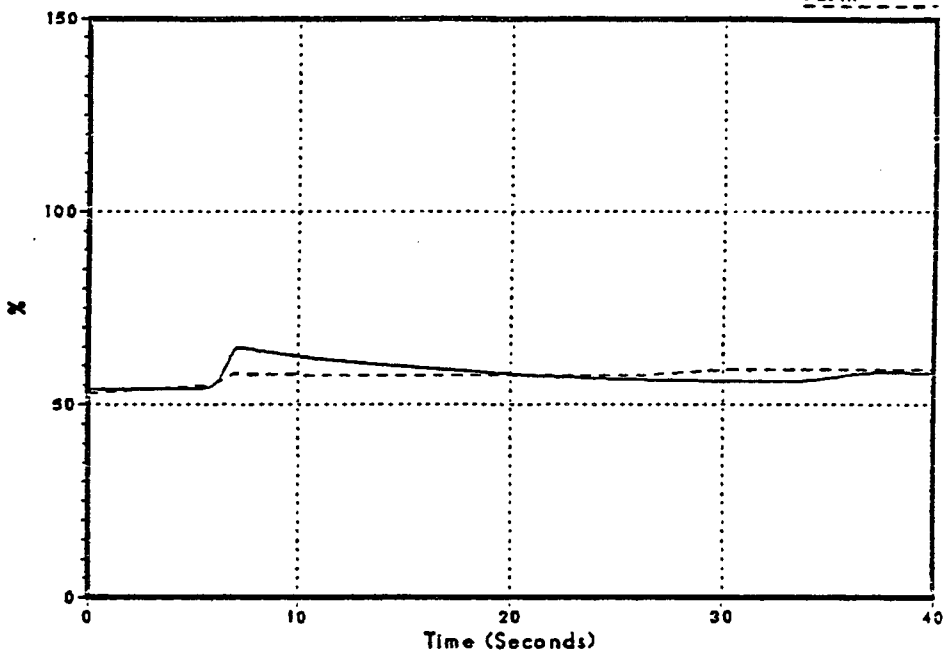

Figure 3.2-88
Average Surface Heat Flux

DNB068/86
FSAR

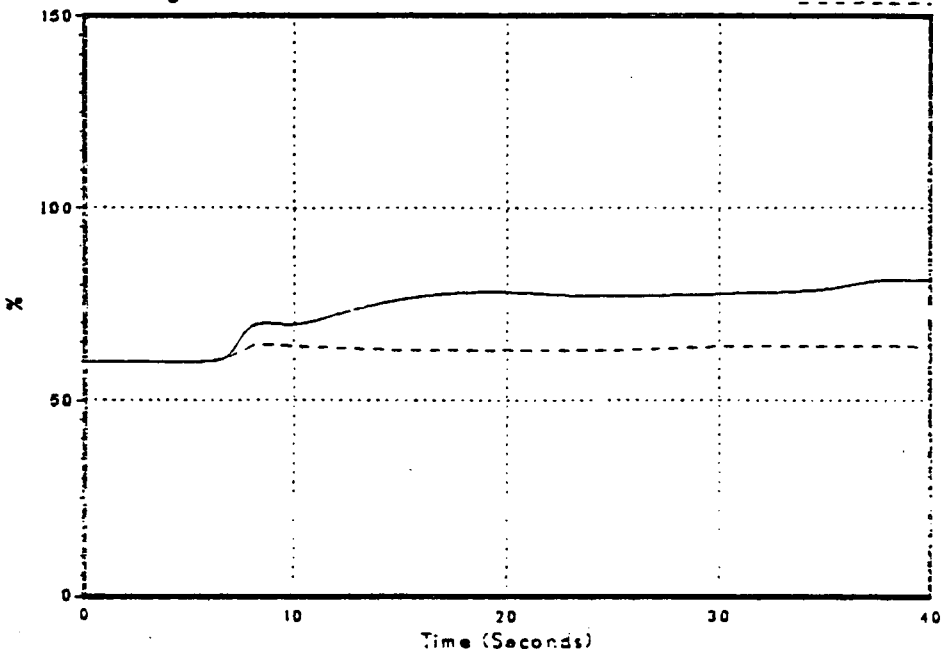

NSP

Monticello FSAR Benchmark
Idle Loop Startup

Figure 3.2-89
Relative Power

DNB068/86
FSAR

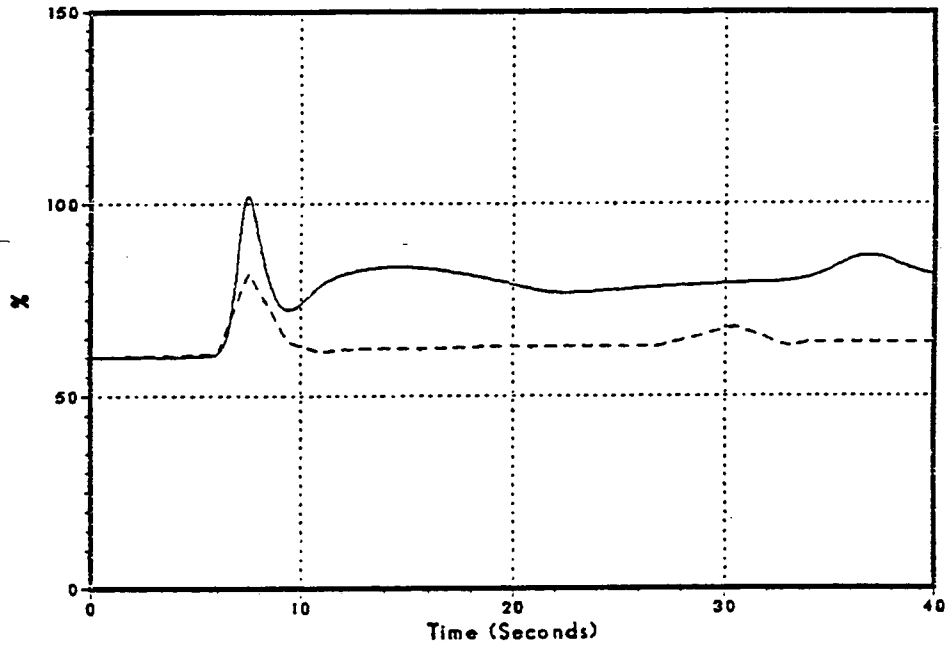

Figure 3.2-90
Feedwater Flow

DNB068/86
FSAR

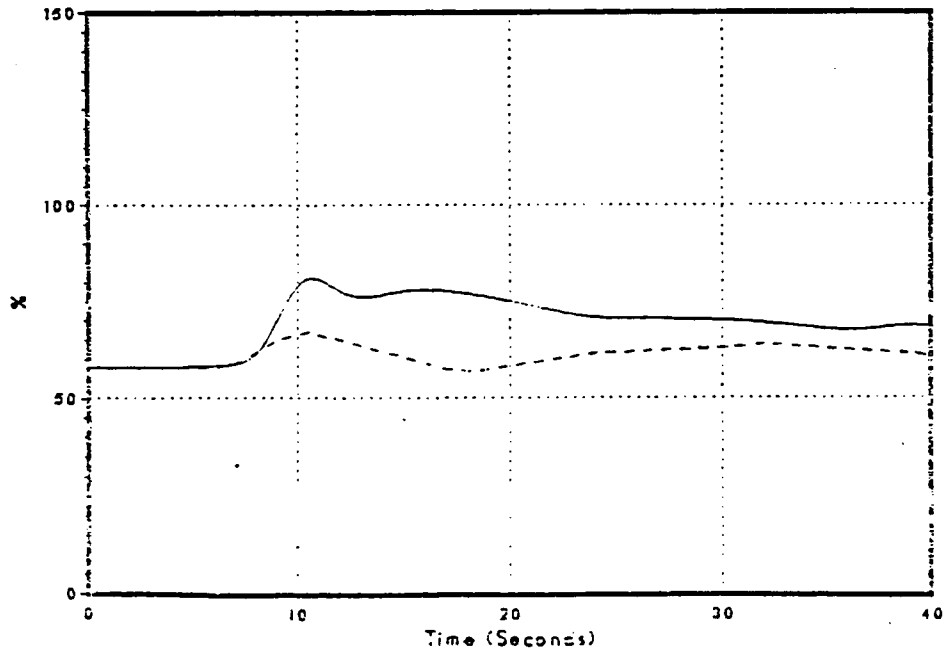

NSP

Monticello FSAR Benchmark
Idle Loop Startup

Figure 3.2-91
Vessel Steam Flow

DNB068/86
FSAR ____

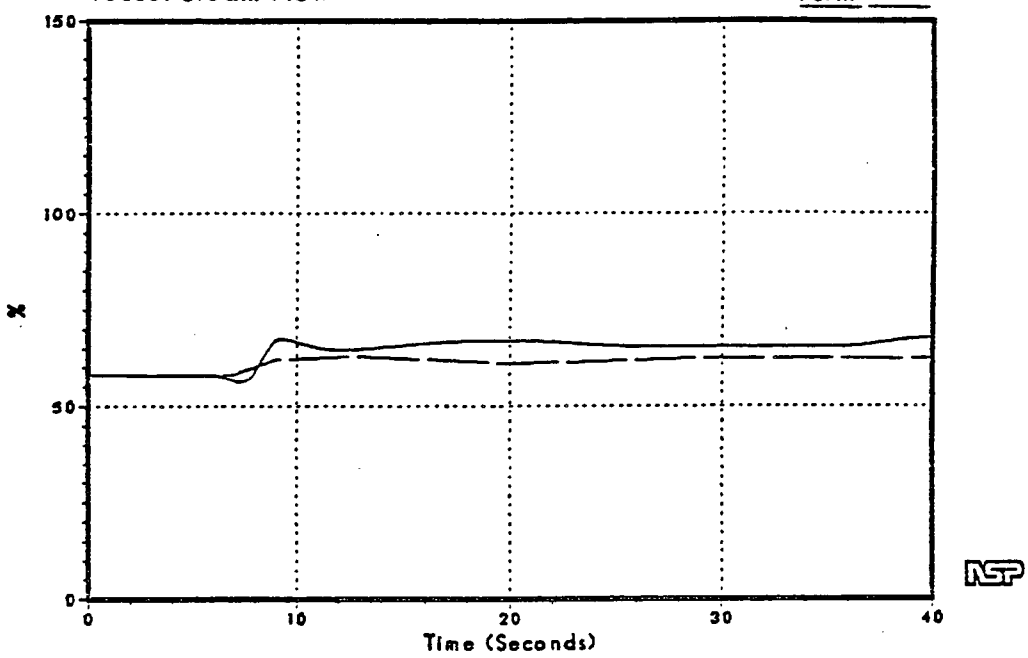

Monticello Cycle 11
Load Rejection without Bypass

Figure 3.2-92
Vessel Pressure Rise

DYNODE-B
GE Analysis

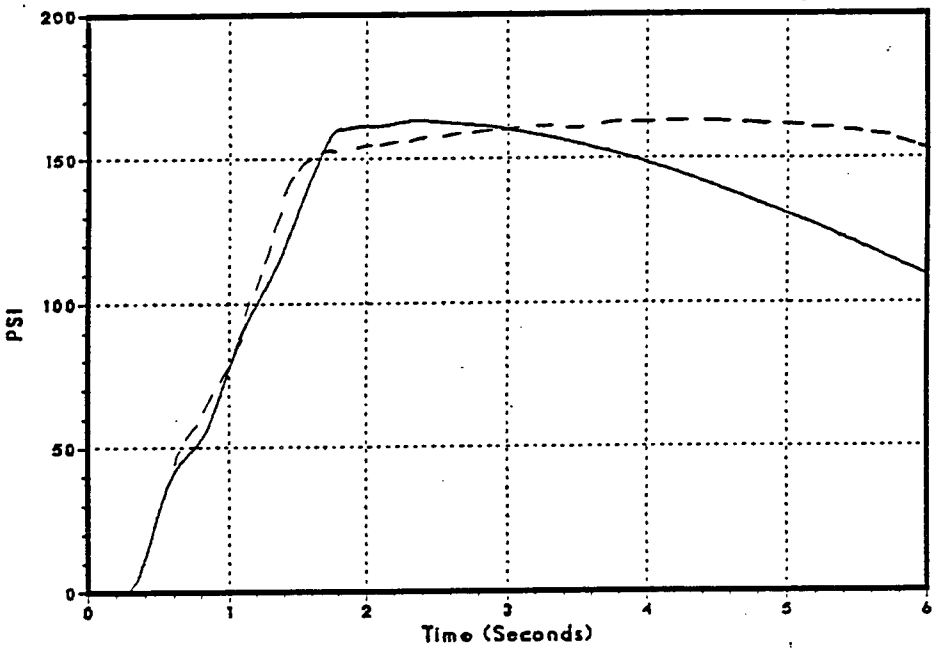

Figure 3.2-93
Relative Power

DYNODE-B
GE Analysis

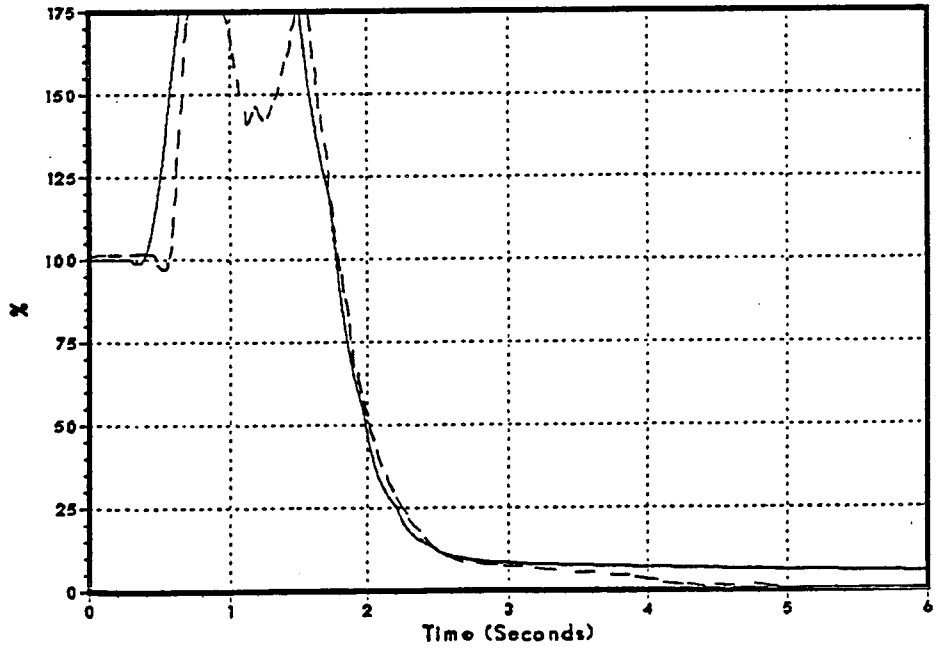

Monticello Cycle 11
Load Rejection without Bypass

Figure 3.2-94
Core Average Heat Flux

DYNODE-B
GE Analysis

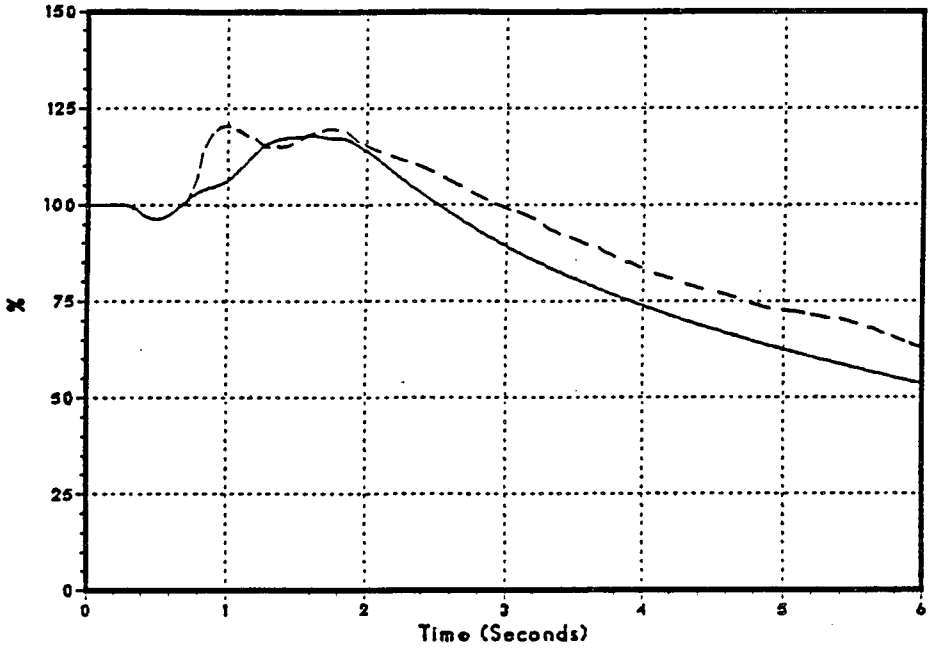

Figure 3.2-95
Core Inlet Flow

DYNODE-B
GE Analysis

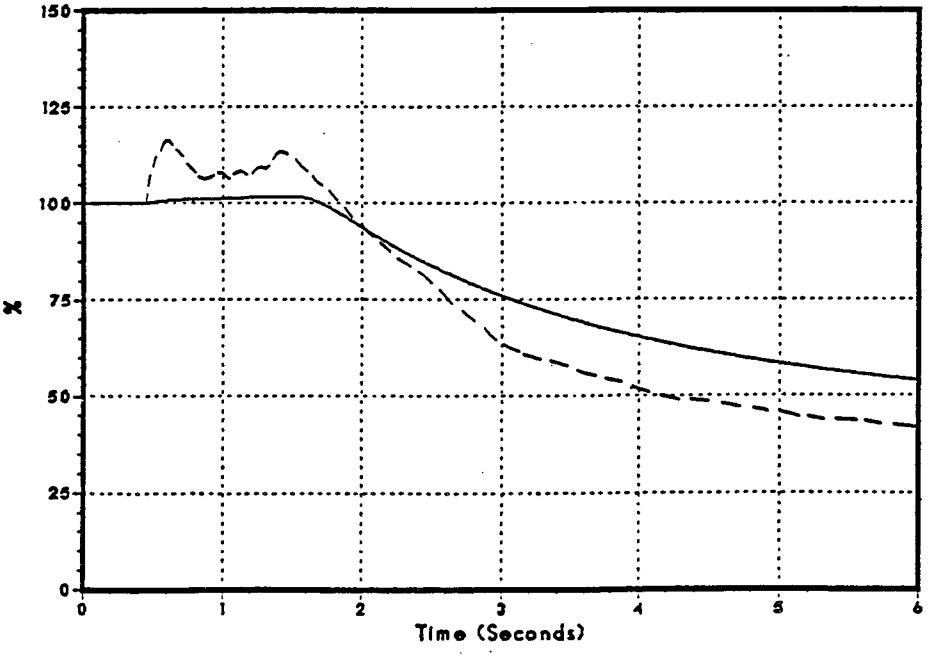

Monticello Cycle 11
Load Rejection without Bypass

Figure 3.2-96
Main Steam Line Flow

DYNODE-B
GE Analysis

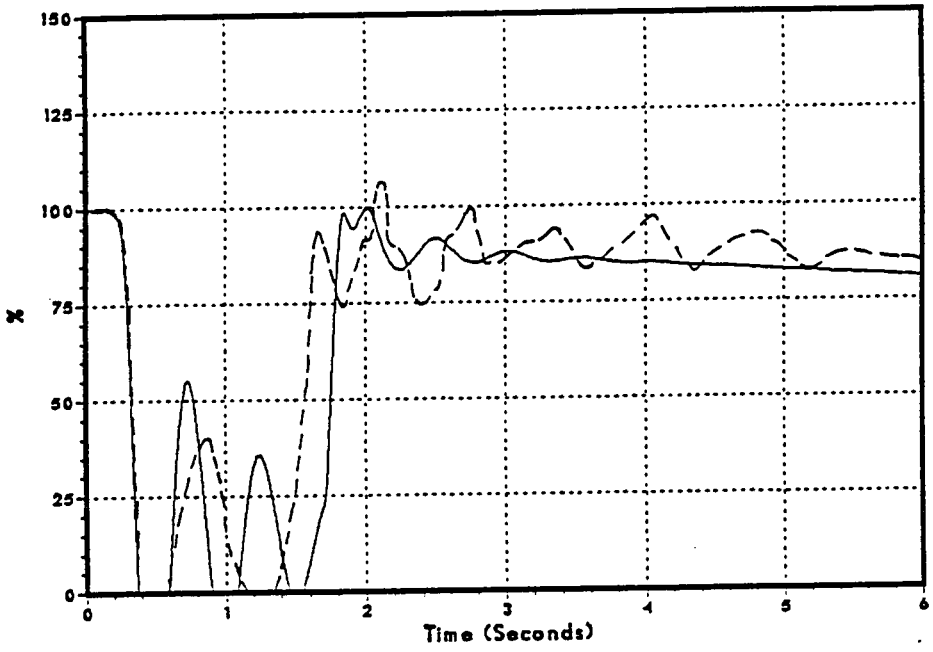

Figure 3.2-97
Feedwater Flow

DYNODE-B
GE Analysis

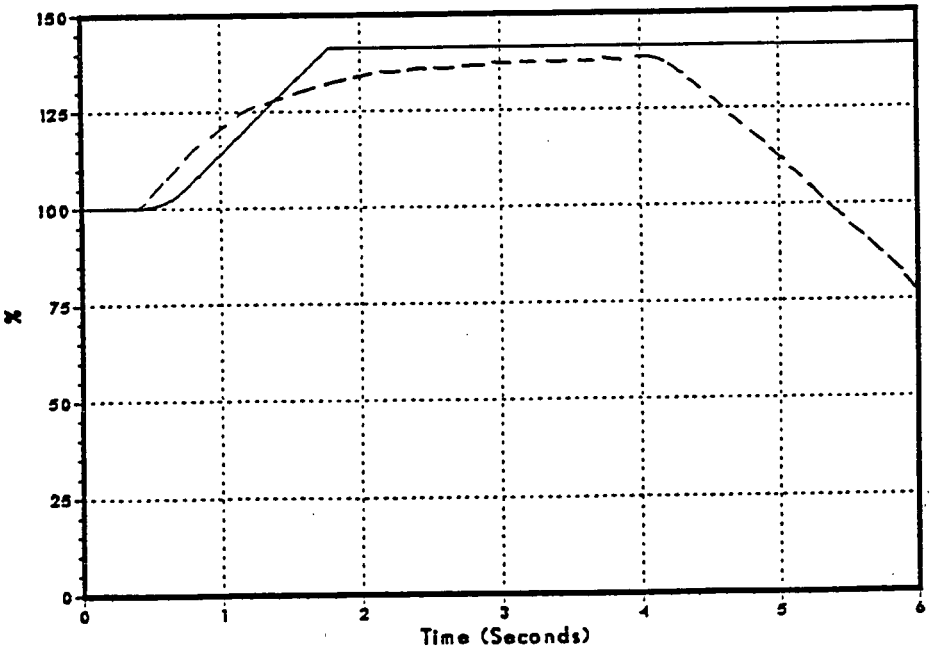

Monticello Cycle 11
Load Rejection without Bypass

Figure 3.2-98
Sensed Reactor Water Level

DYNODE-B
GE Analysis

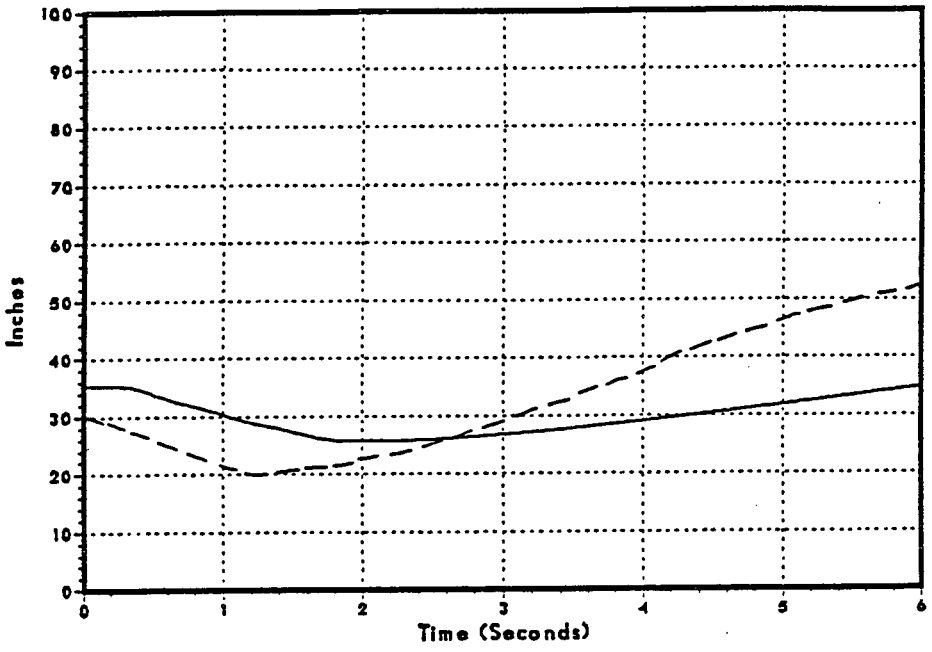

Monticello Cycle 11
Feedwater Controller Failure

Figure 3.2-99
Vessel Pressure Rise

DYNODE-B
GE Analysis

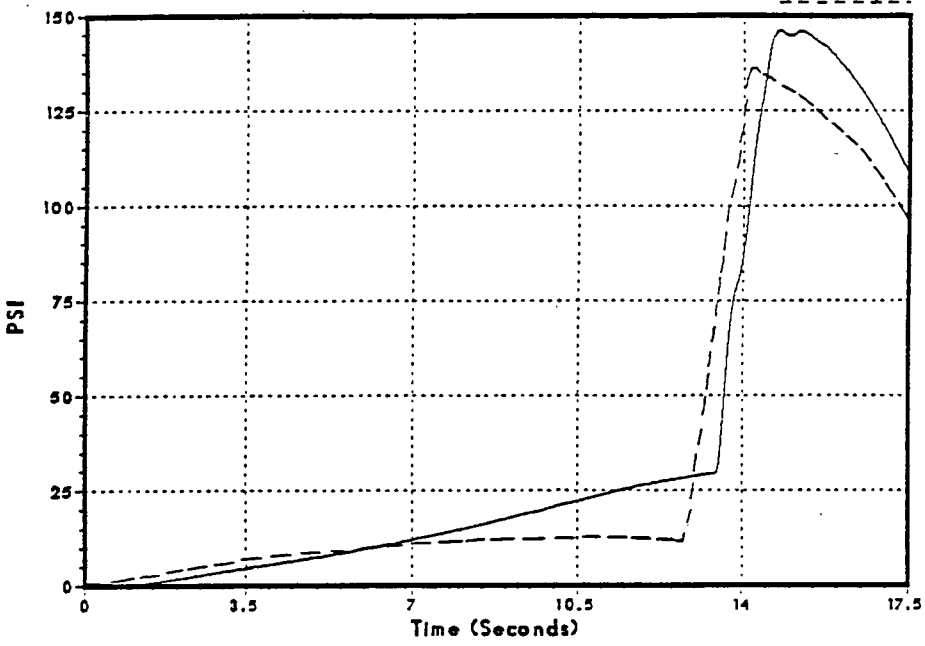

Figure 3.2-100
Relative Power

DYNODE-B
GE Analysis

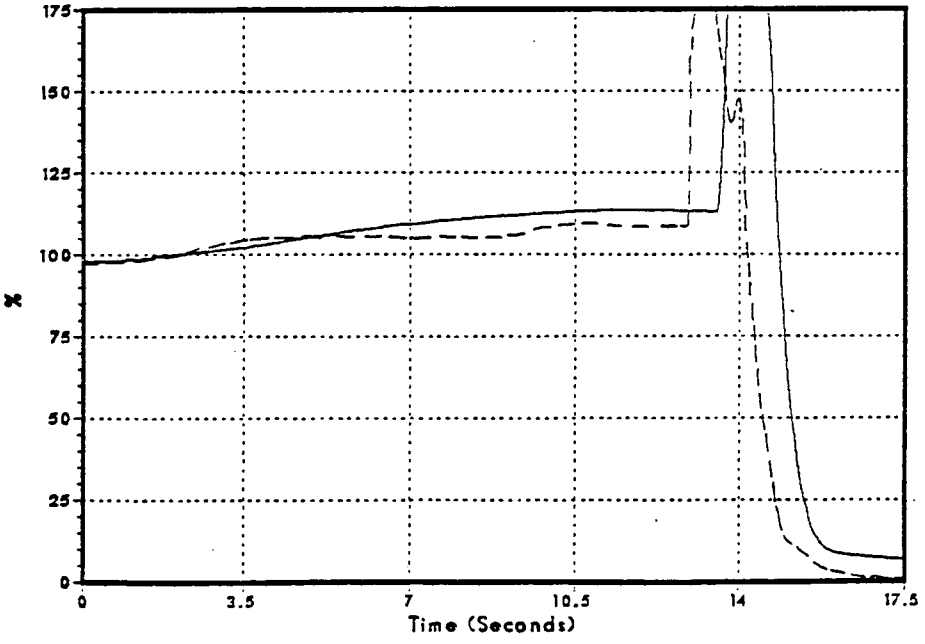

Monticello Cycle 11
Feedwater Controller Failure

Figure 3.2-101
Core Average Heat Flux

DYNODE-B
GE Analysis

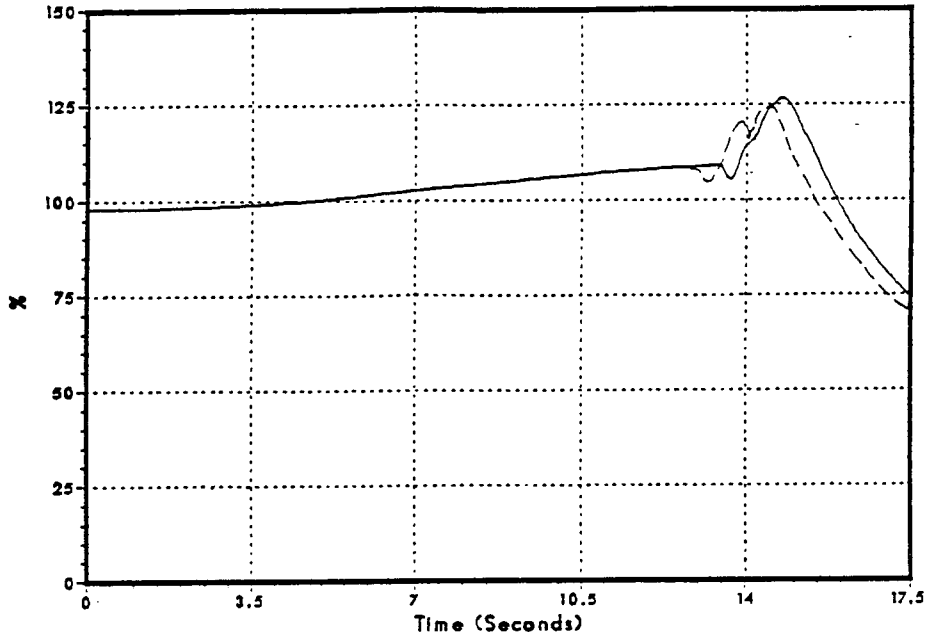

Figure 3.2-102
Core Inlet Flow

DYNODE-B
GE Analysis

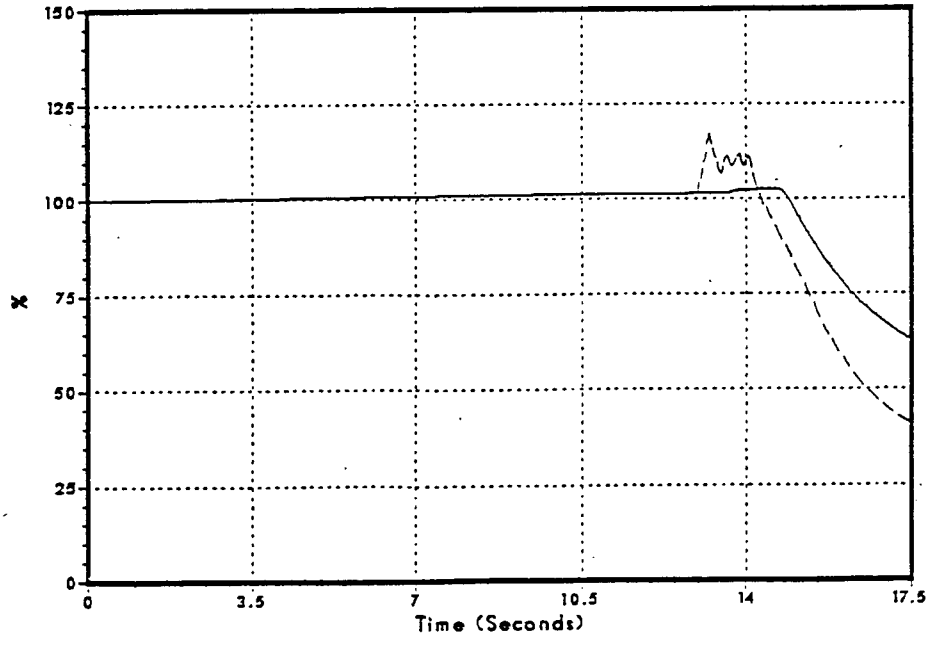

Monticello Cycle 11
Feedwater Controller Failure

Figure 3.2-103
Core Inlet Subcooling

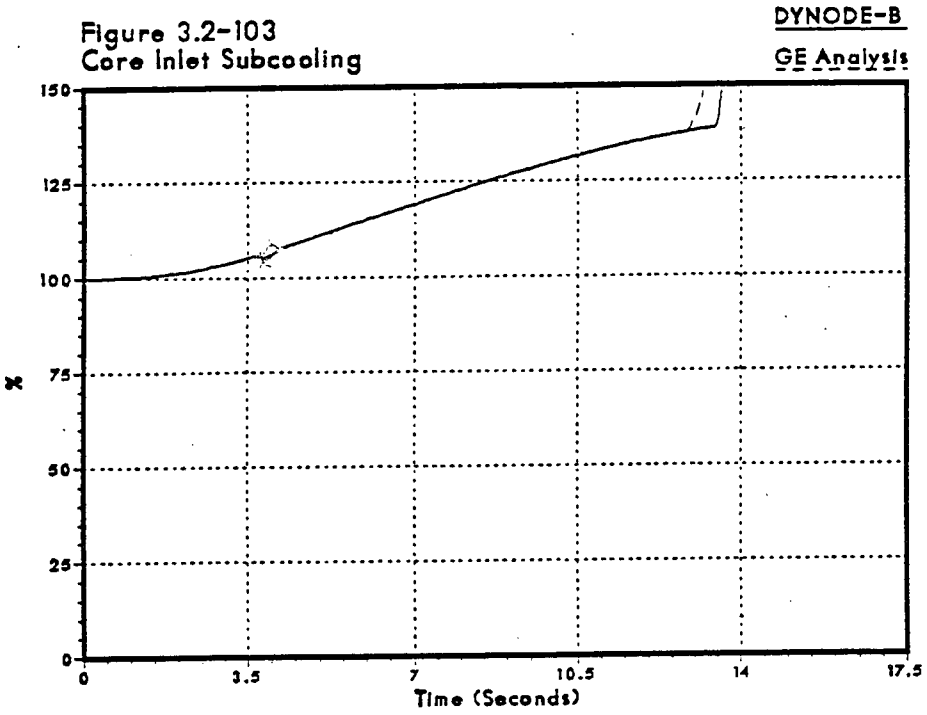

Figure 3.2-104
Main Steam Line Flow

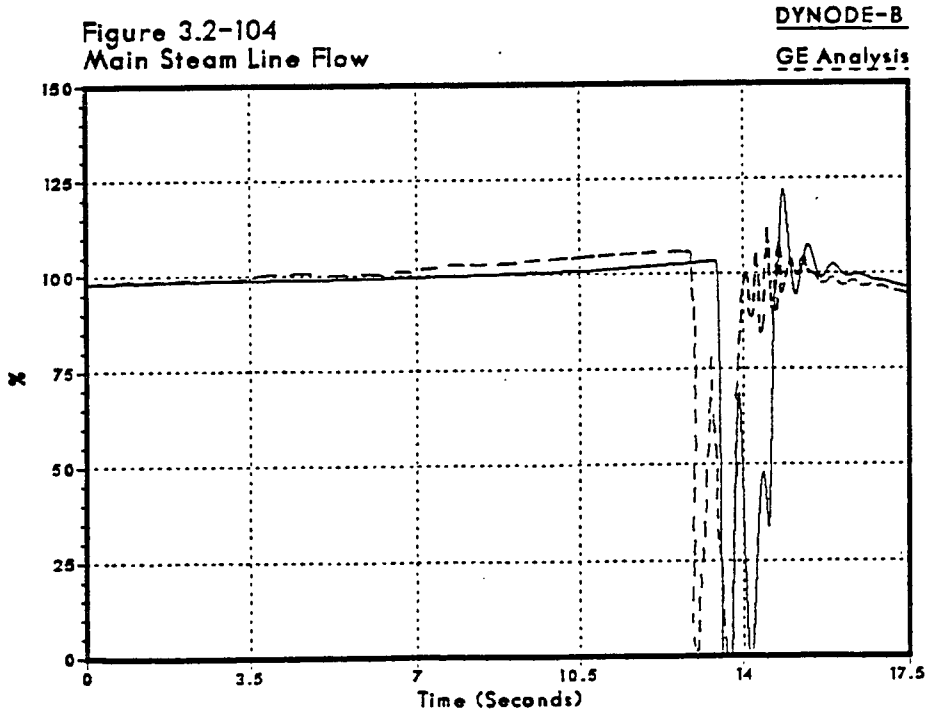

Monticello Cycle 11
Feedwater Controller Failure

Figure 3.2-105
Sensed Reactor Water Level

DYNODE-B
GE Analysis

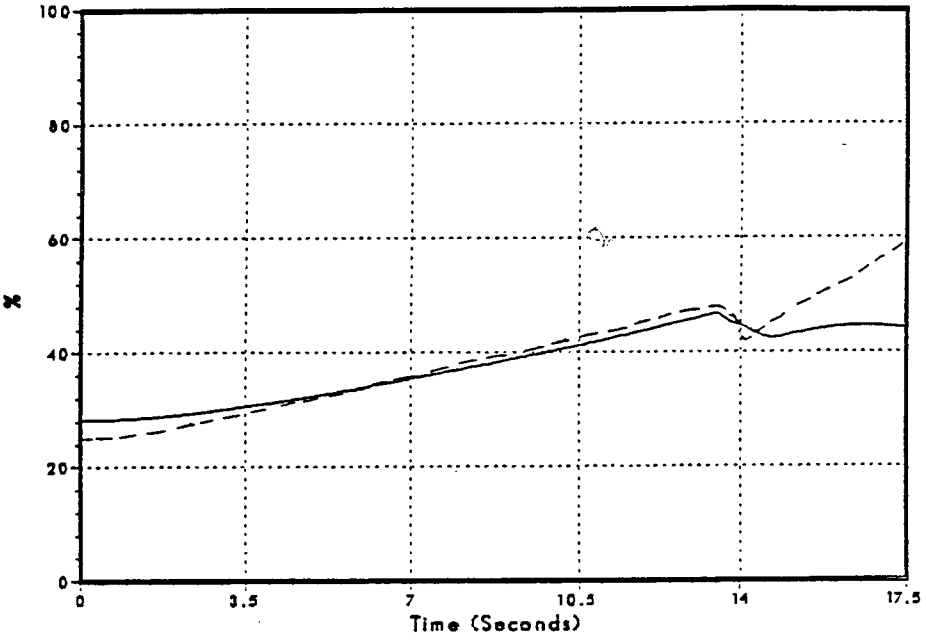

Monticello Cycle 11
100% MSIV Closure

Figure 3.2-106
Vessel Pressure Rise

DYNODE-B
GE ANALYSIS

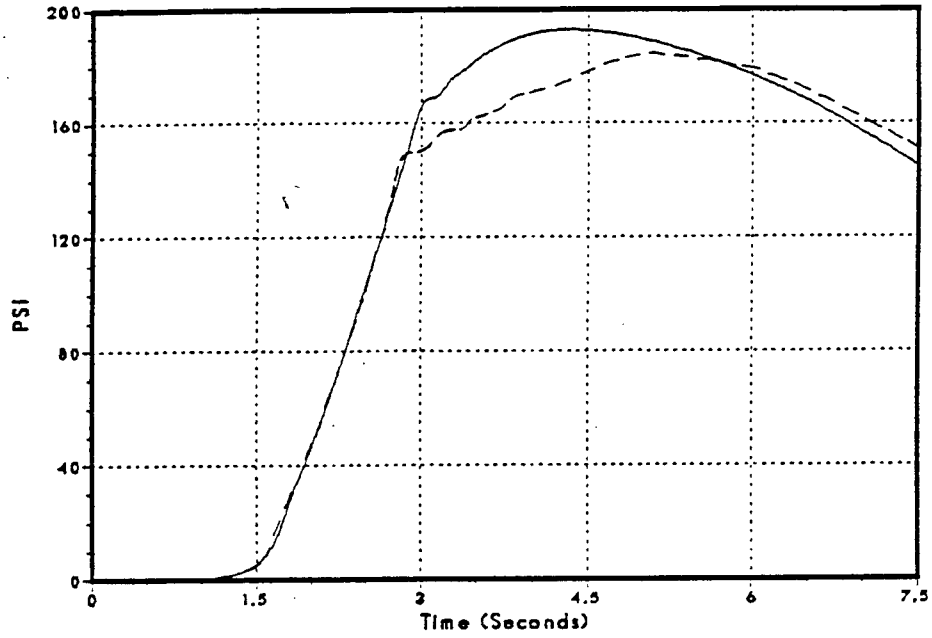

Figure 3.2-107
Relative Power

DYNODE-B
GE ANALYSIS

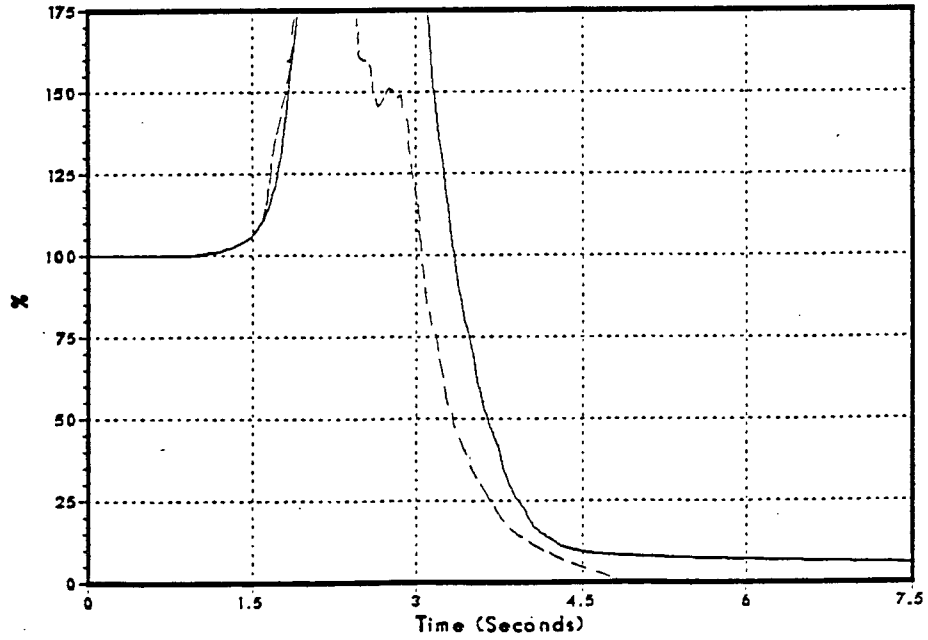

Monticello Cycle 11
100% MSIV Closure

Figure 3.2-108
Core Average Heat Flux

DYNODE-B
GE ANALYSIS

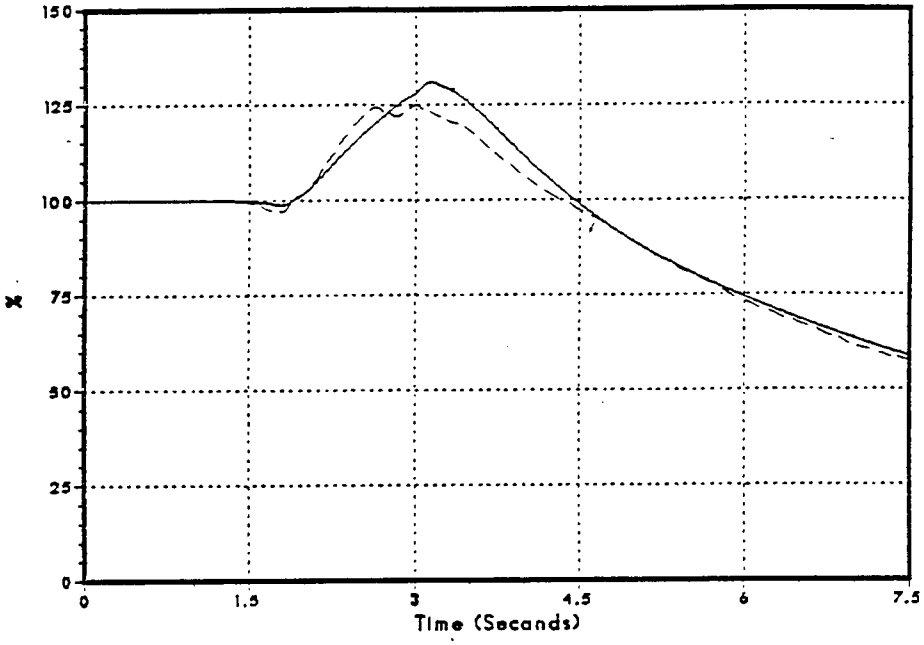

Figure 3.2-109
Core Inlet Flow

DYNODE-B
GE ANALYSIS

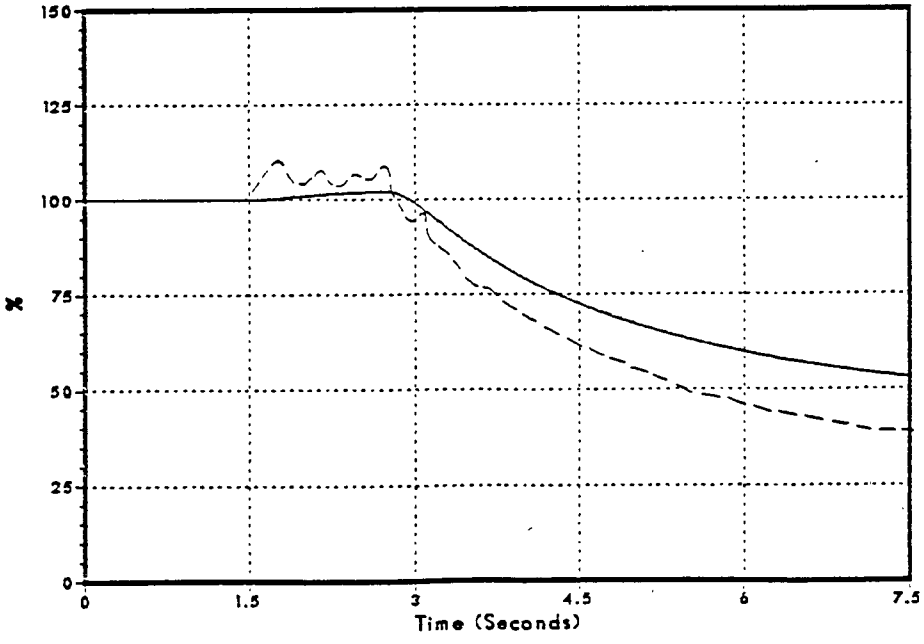

Monticello Cycle 11
100% MSIV Closure

Figure 3.2-110
Main Steam Line Flow

DYNODE-B
GE ANALYSIS

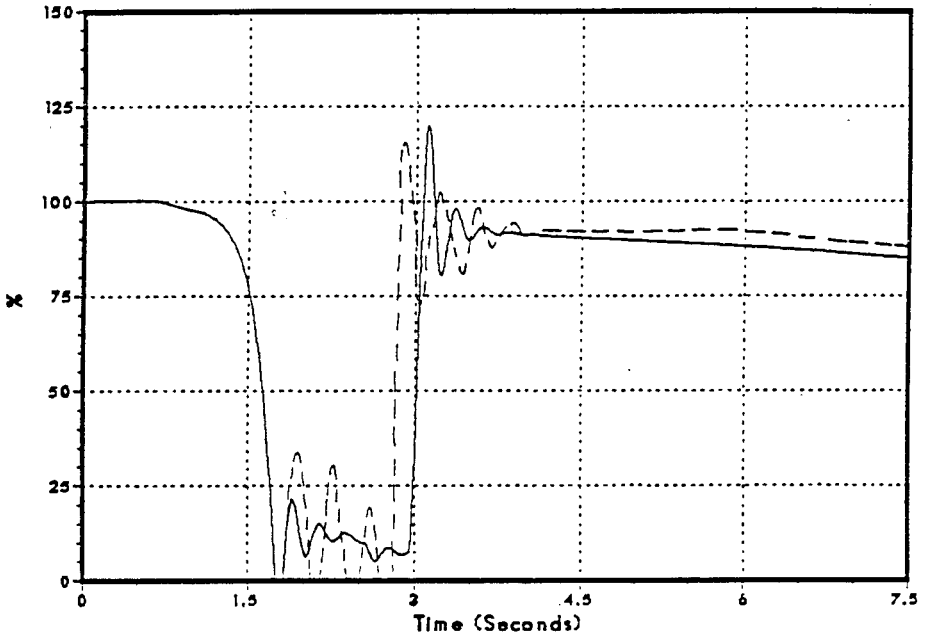

Figure 3.2-111
Feedwater Flow

DYNODE-B
GE ANALYSIS

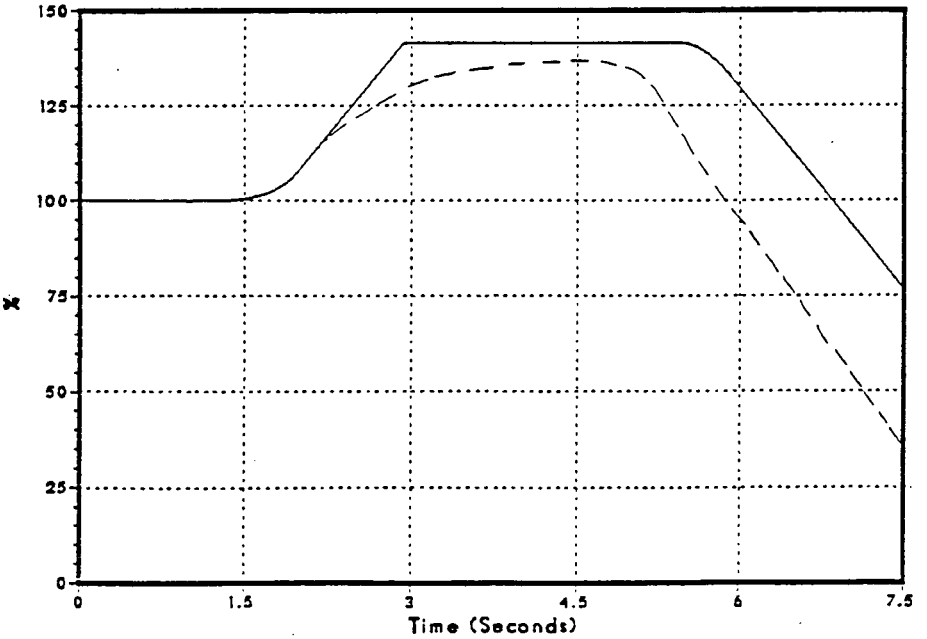

Monticello Cycle 11
100% MSIV Closure

Figure 3.2-112
Sensed Reactor Water Level

DYNODE-B
GE ANALYSIS

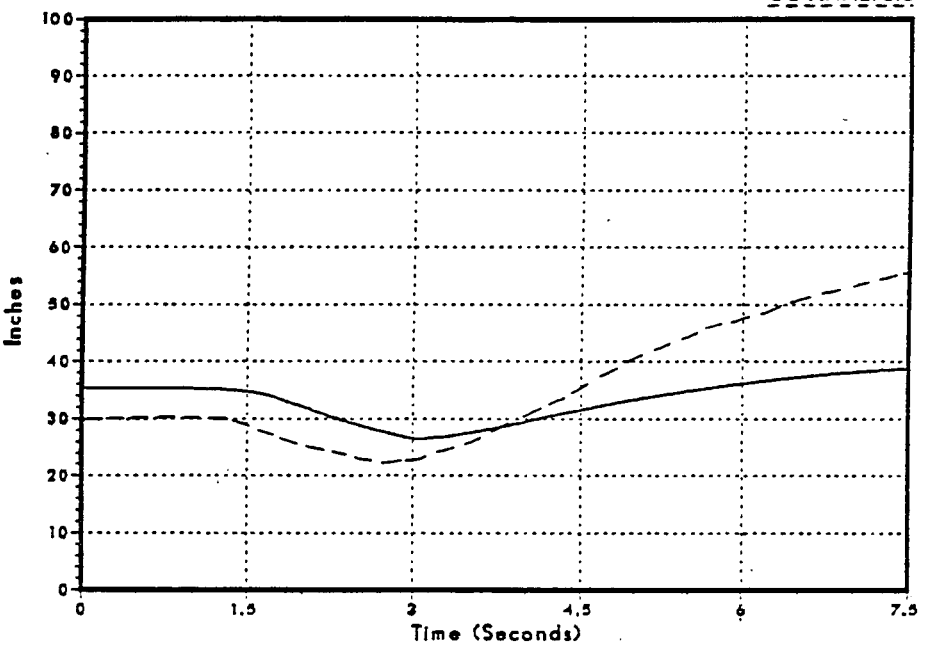

Peach Bottom Turbine Trip
Test TT1

Figure 3.2-113
Steam Dome Pressure

DNB001/86

Test Data

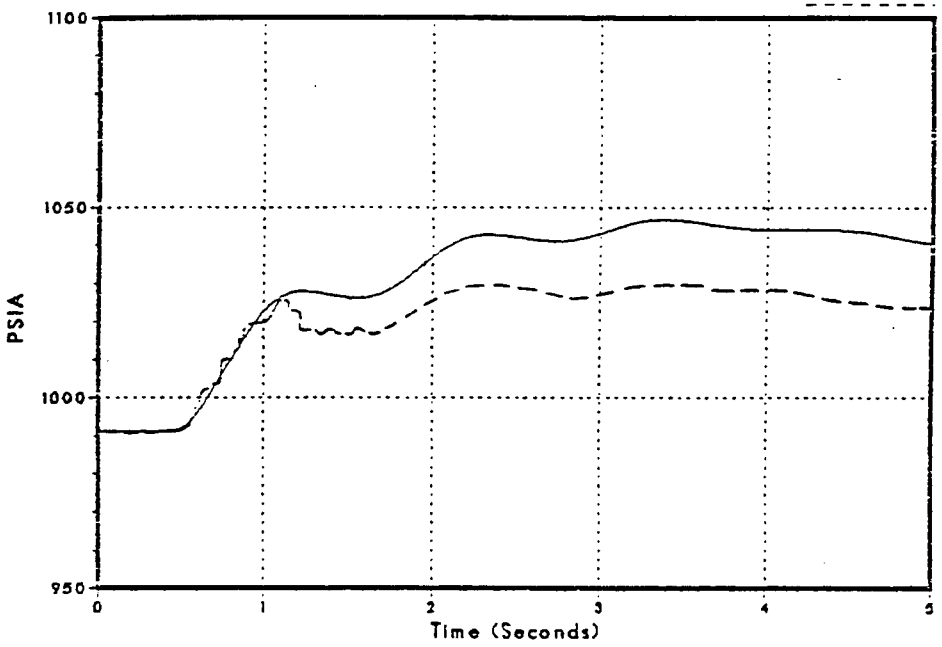

Figure 3.2-114
Relative Power

DNB001/86

Test Data

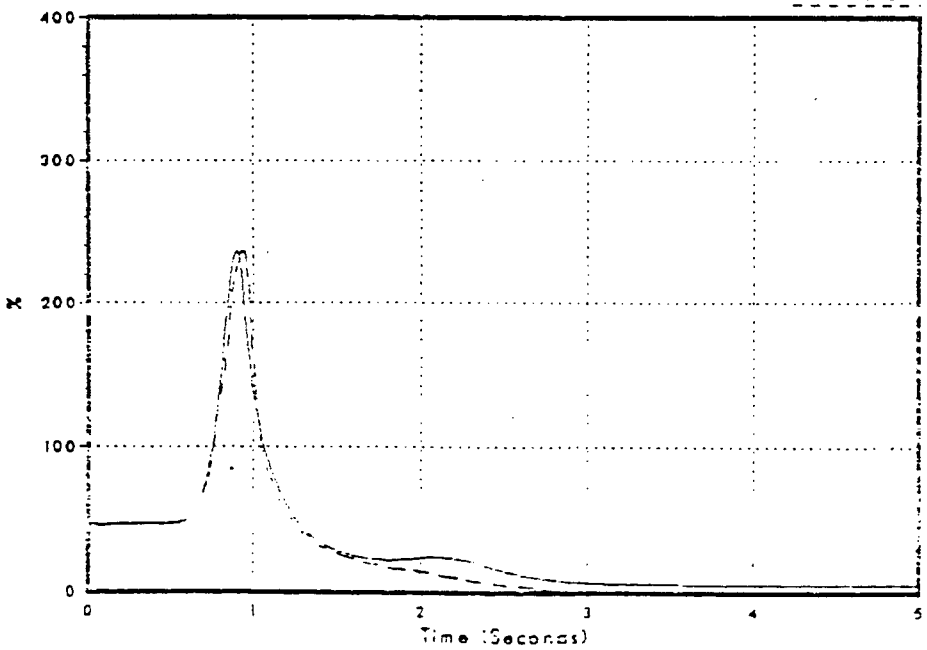

NSP

Prepared by NSP Safety Analysis, 5/20/86

Peach Bottom Turbine Trip
Test TT1

Figure 3.2-115
Turbine Throttle Pressure

DNB001/86

Test Data

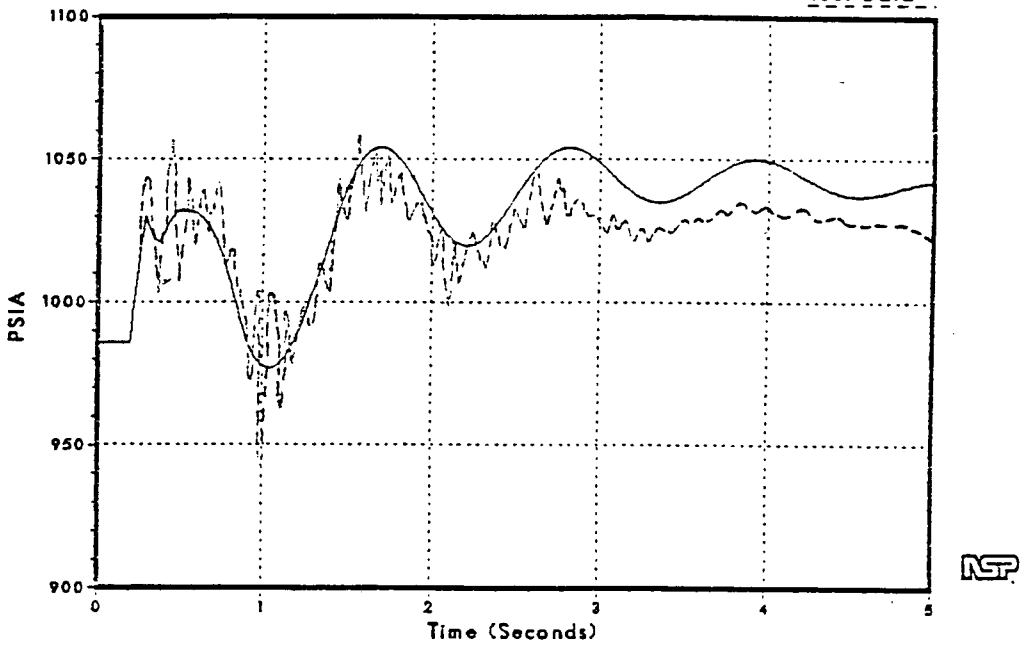

Prepared by NSP Safety Analysis, 5/20/86

Peach Bottom Turbine Trip
Test TT2

Figure 3.2-116
Steam Dome Pressure

DNB002/86
Test Data

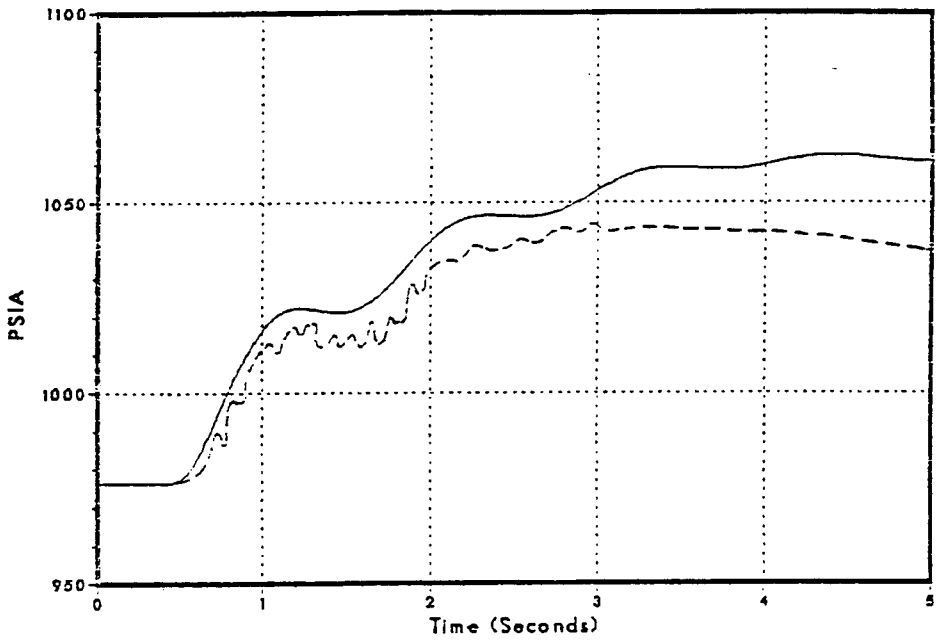

Figure 3.2-117
Relative Power

DNB002/86
Test Data

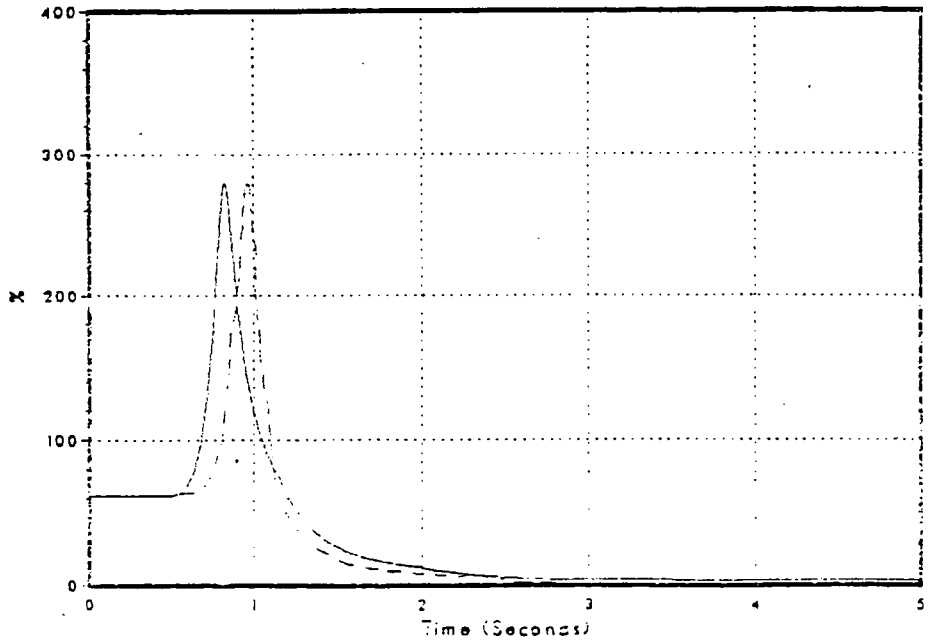

NSP

Prepared by NSP Safety Analysis, 5/15/86

Peach Bottom Turbine Trip
Test TT2

Figure 3.2-118
Turbine Throttle Pressure

DNB002/86

Test Data

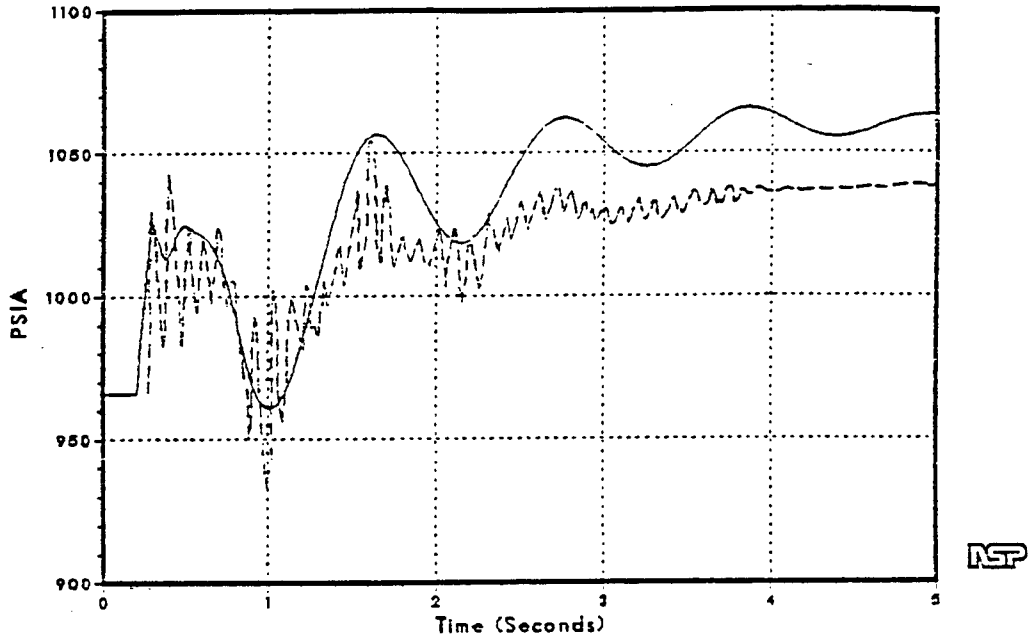

Prepared by NSP Safety Analysis, 5/15/86

Peach Bottom Turbine Trip
Test TT3

Figure 3.2-119
Steam Dome Pressure

DNB003/86

Test Data

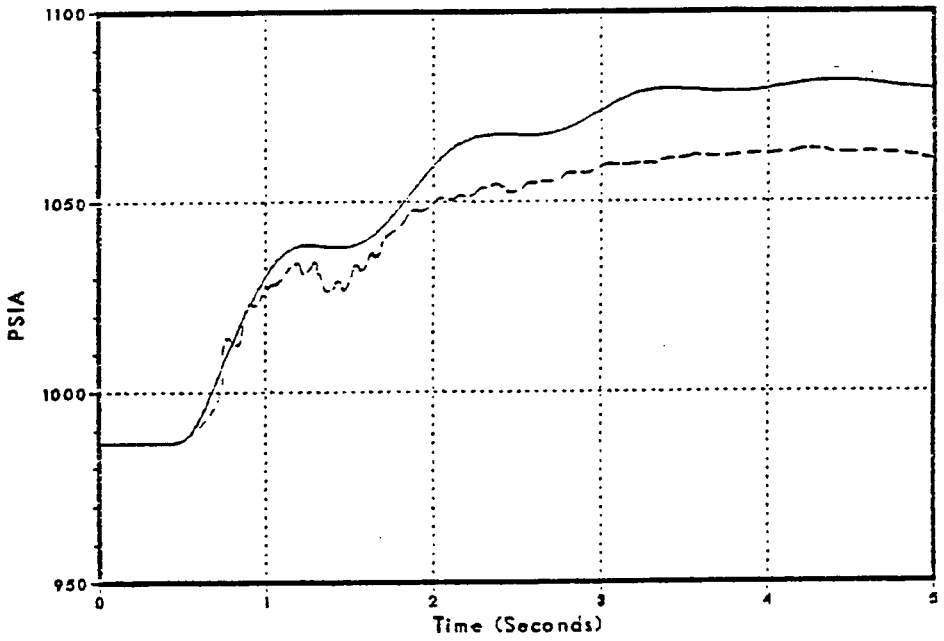

Figure 3.2-120
Relative Power

DNB003/86

Test Data

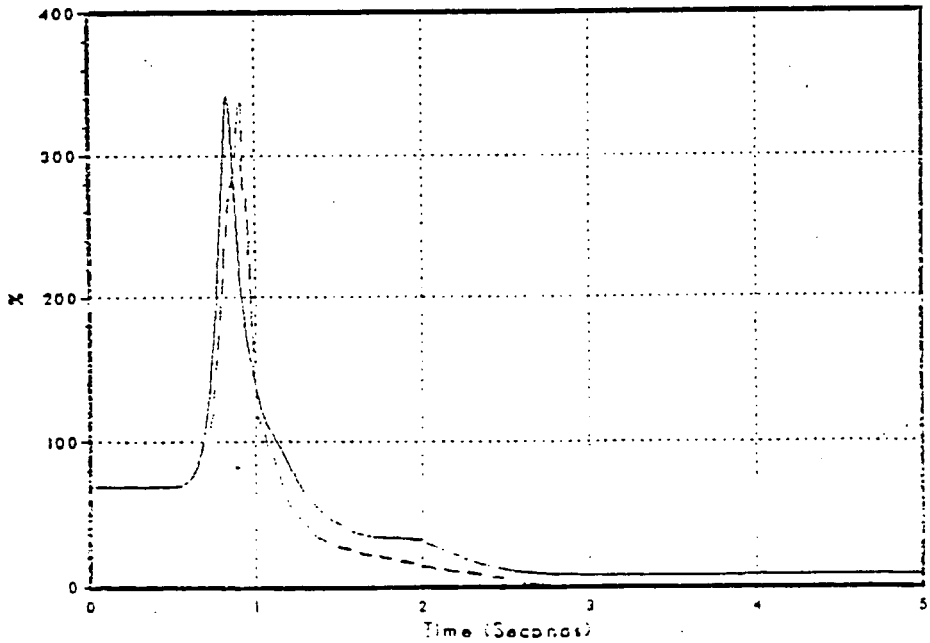

NSP

Prepared by NSP Safety Analysis, 5/20/86

Peach Bottom Turbine Trip
Test TT3

Figure 3.2-121
Turbine Throttle Pressure

DNB003/86

Test Data

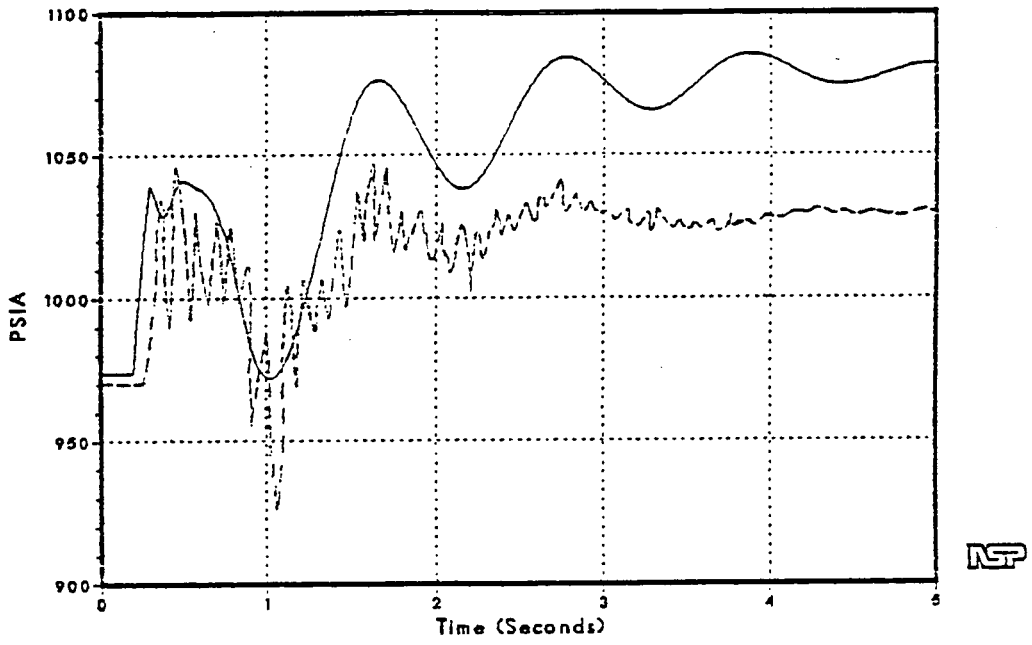

NSP

Prepared by NSP Safety Analysis, 5/20/86

Monticello Cycle 1
Turbine Trip Startup Test

Figure 3.2-122
Steam Dome Pressure

DNB038/86
Test Data

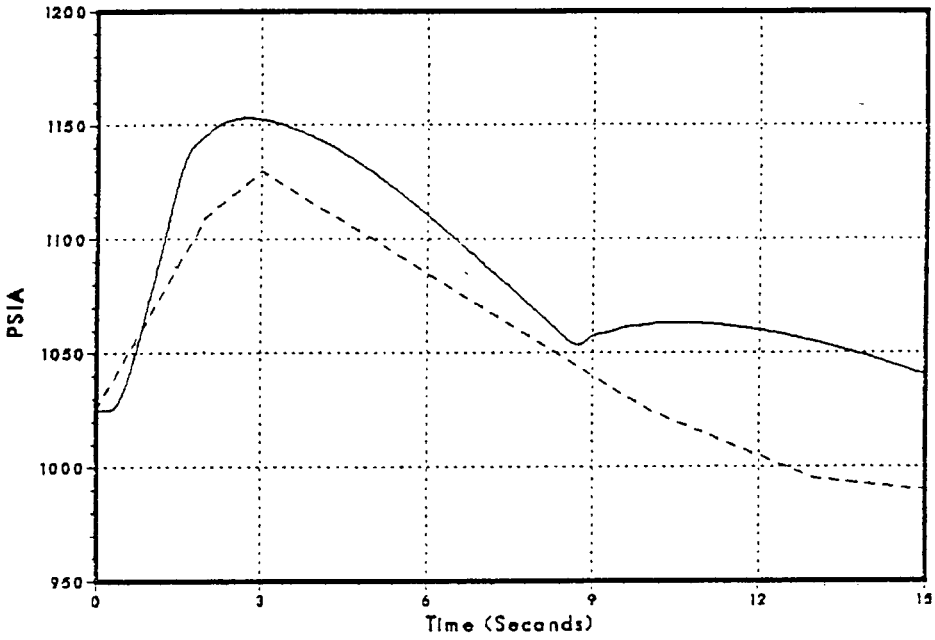

Figure 3.2-123
Total Vessel Flow Rate

DNB038/86
Test Data

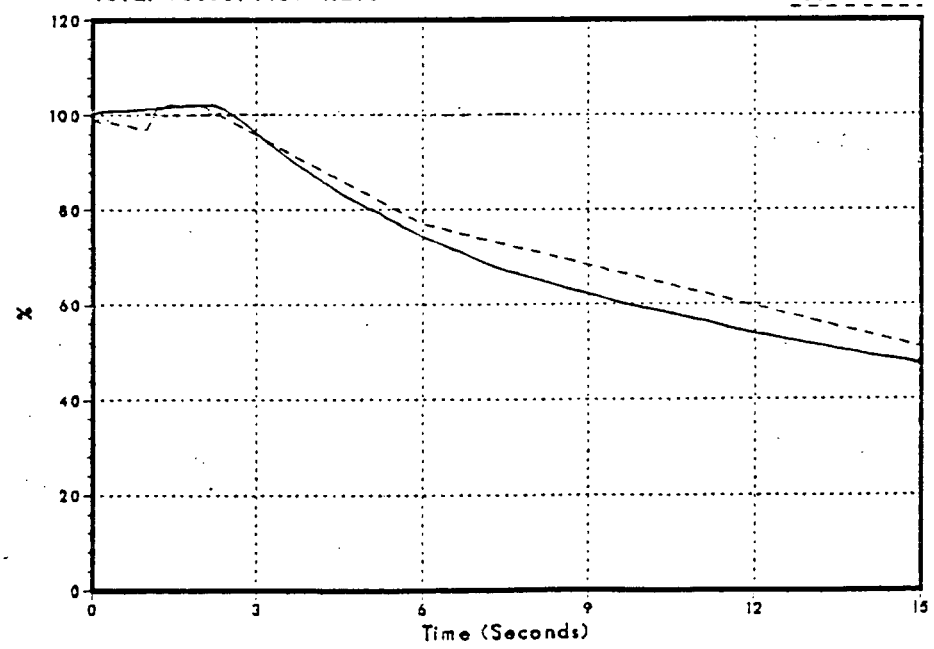

NSP

Prepared by NSP Safety Analysis, 4/25/86

Monticello Cycle 1
Turbine Trip Startup Test

Figure 3.2-124
Relative Power

DNB038/86
Test Data

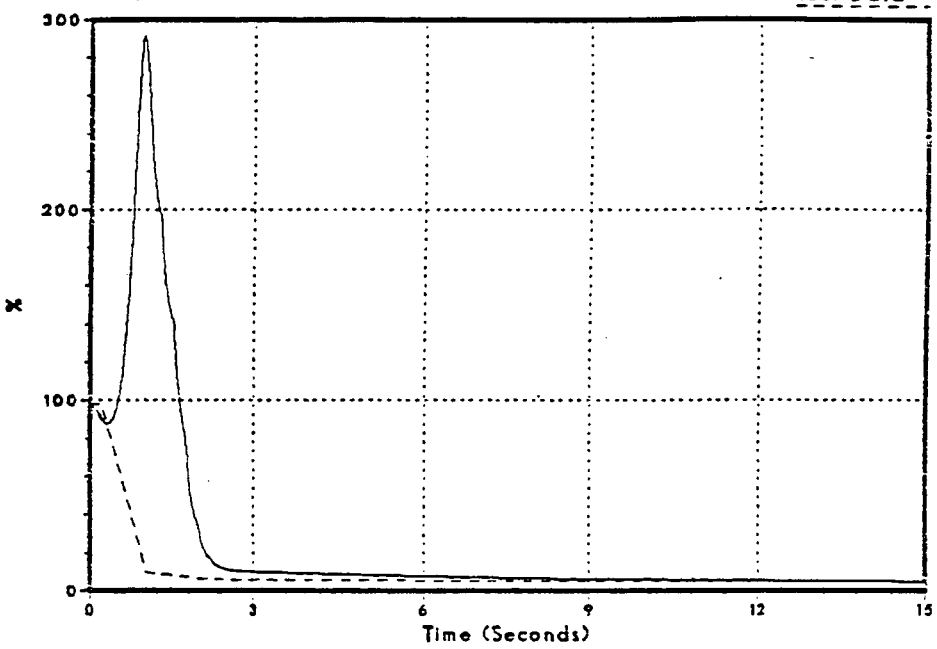

Figure 3.2-125
Main Steam Line Flow

DNB038/86
Test Data

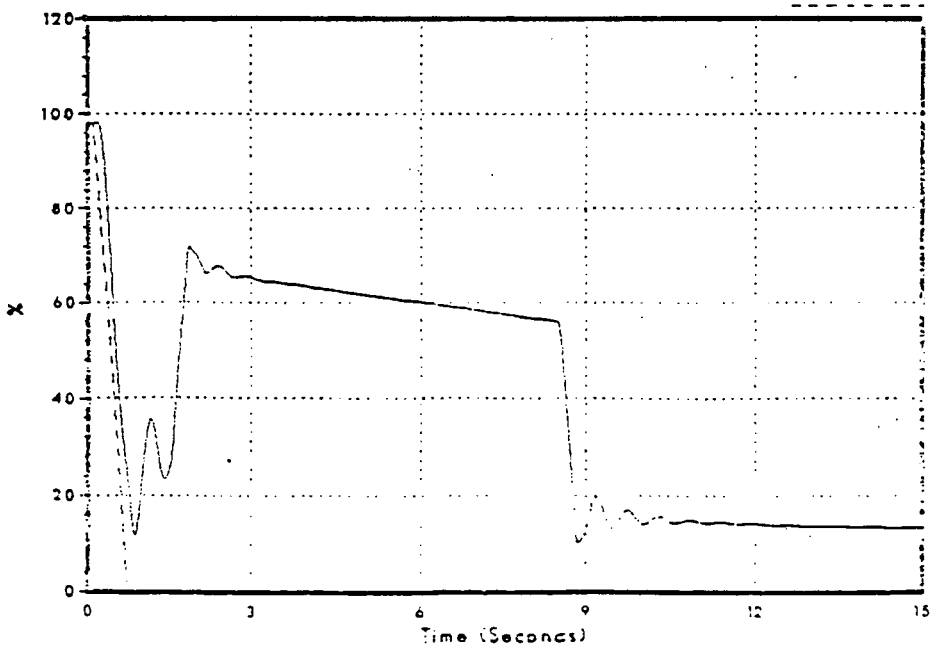

NSP

Monticello Cycle 1
Turbine Trip Startup Test

Figure 3.2-126
Feedwater Flow

DNB038/86
Test Data

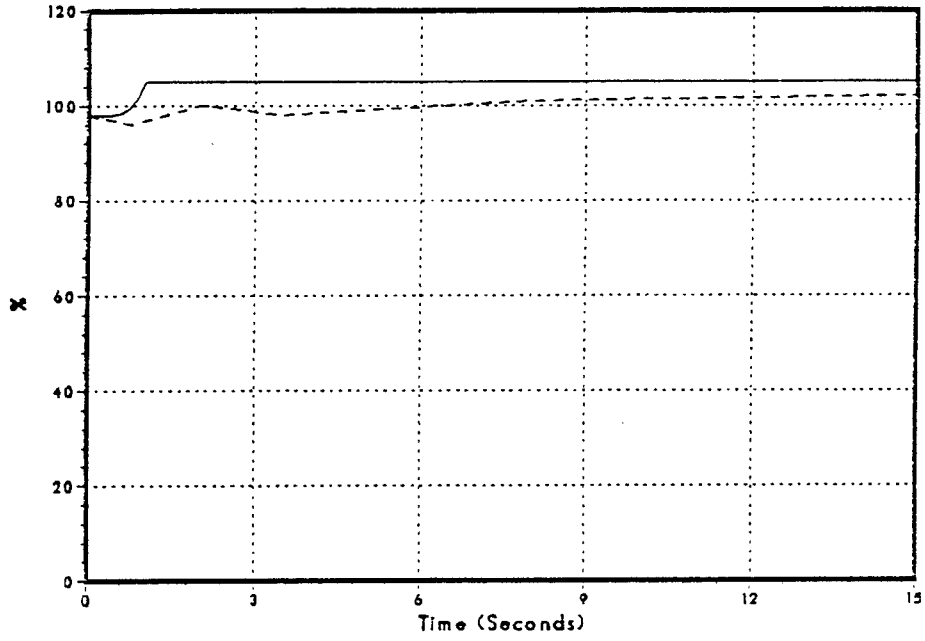

Figure 3.2-127
Sensed Reactor Water Level

DNB038/86
Test Data

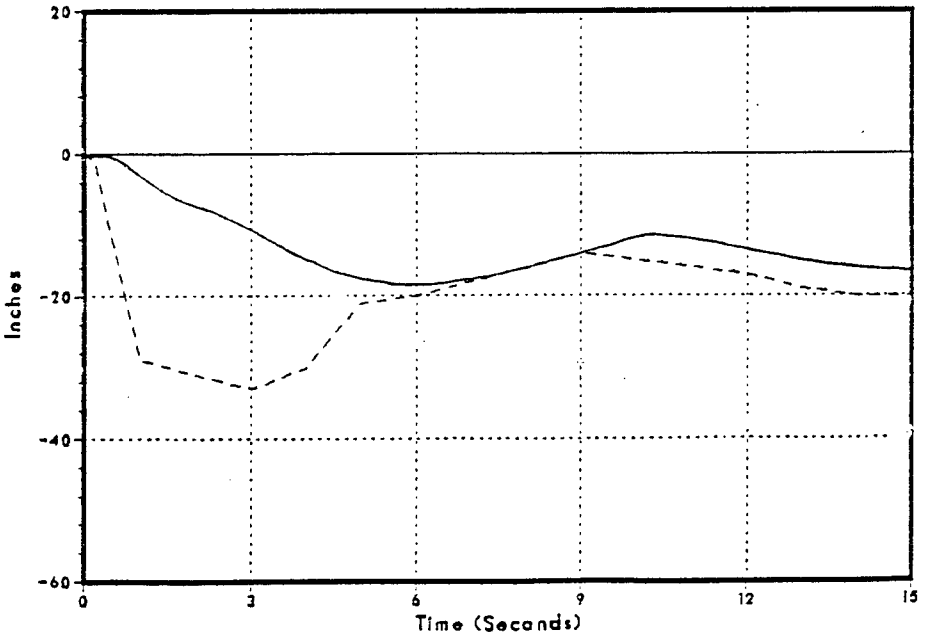

NSP

Prepared by N[illegible]ly Analysis, 4/25/86

Monticello Cycle 1
4/4 MSIV Closure Startup Test

Figure 3.2-128
Steam Dome Pressure

DNB035/86
Test Data

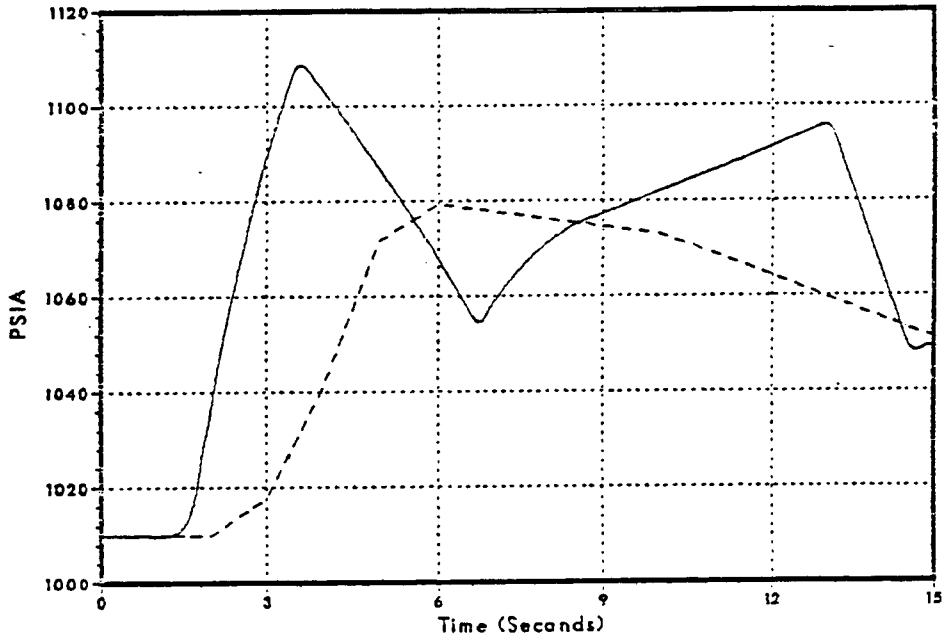

Figure 3.2-129
Relative Power

DNB035/86
Test Data

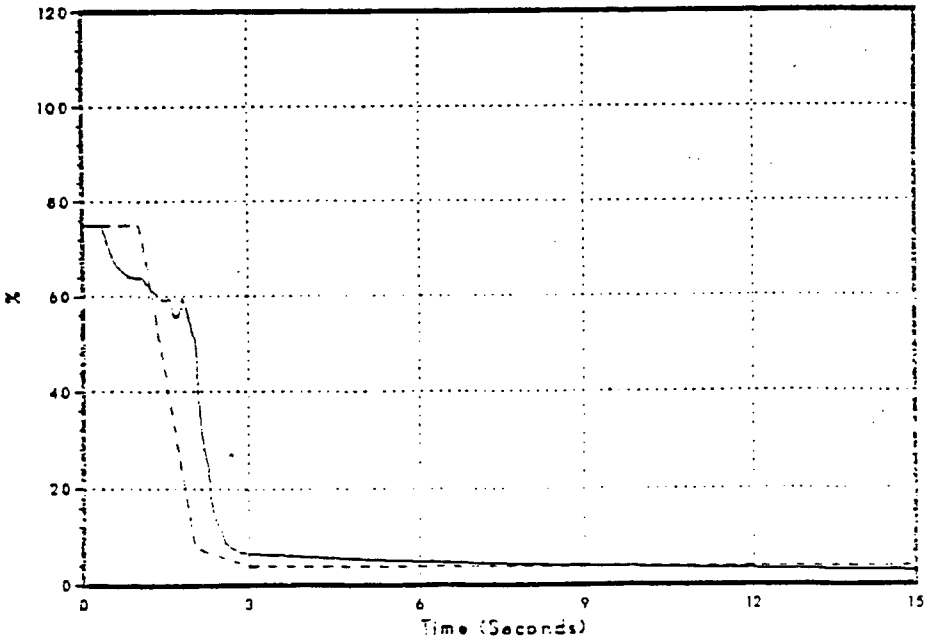

NSP

Prepared by NSP Safety Analysis, 5/14/86

Monticello Cycle 1
4/4 MSIV Closure Startup Test

Figure 3.2-130
Steam Dome Water Level

DNB035/86
Test Data

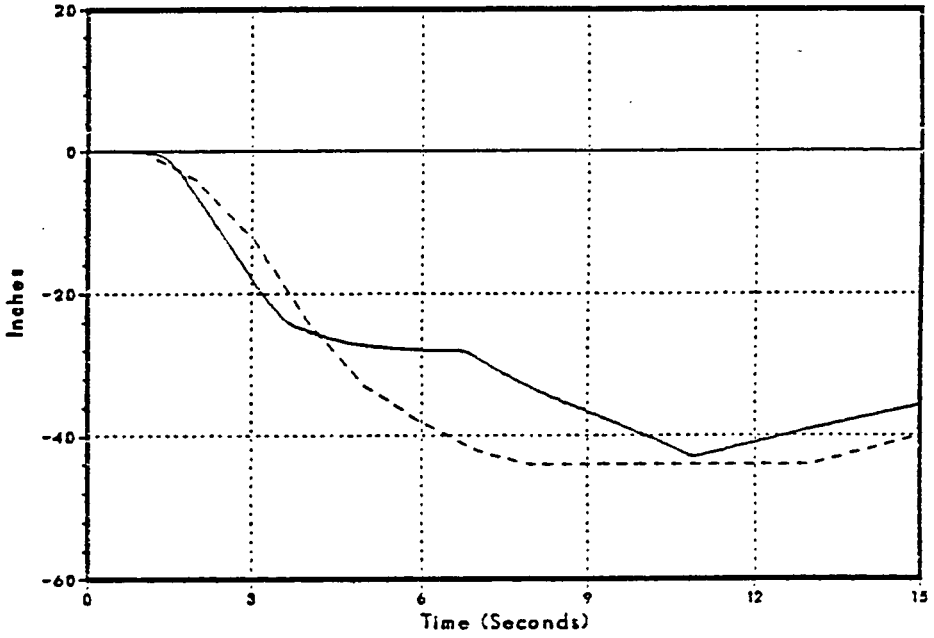

Figure 3.2-131
Main Steam Line Flow

DNB035/86
Test Data

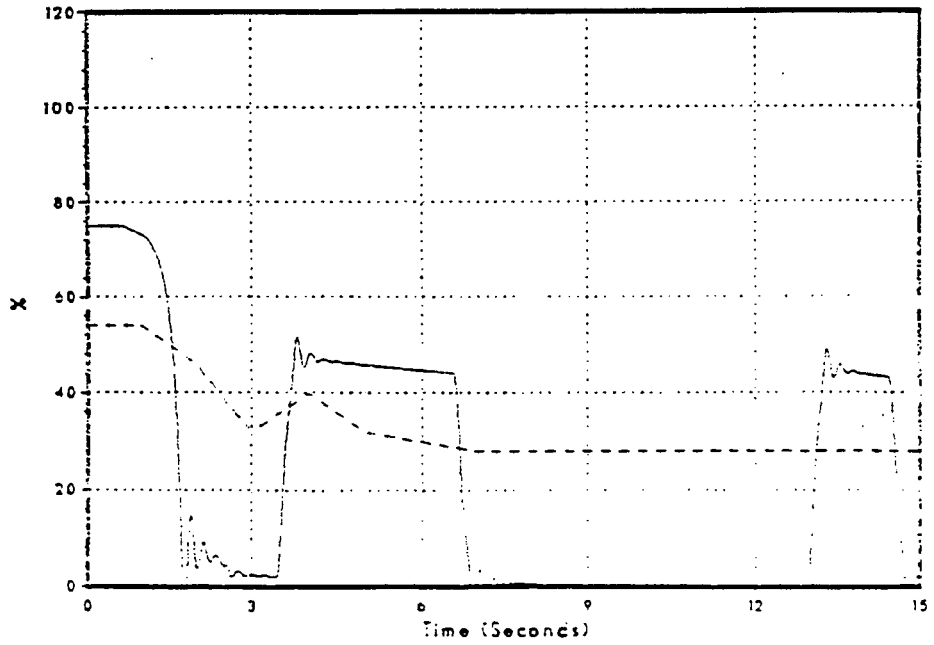

NSP

Prepared by NSP Safety Analysis, 5/14/86

Monticello Cycle 1
4/4 MSIV Closure Startup Test

DNB035/86

Figure 3.2-132
Feedwater Flow

Test Data

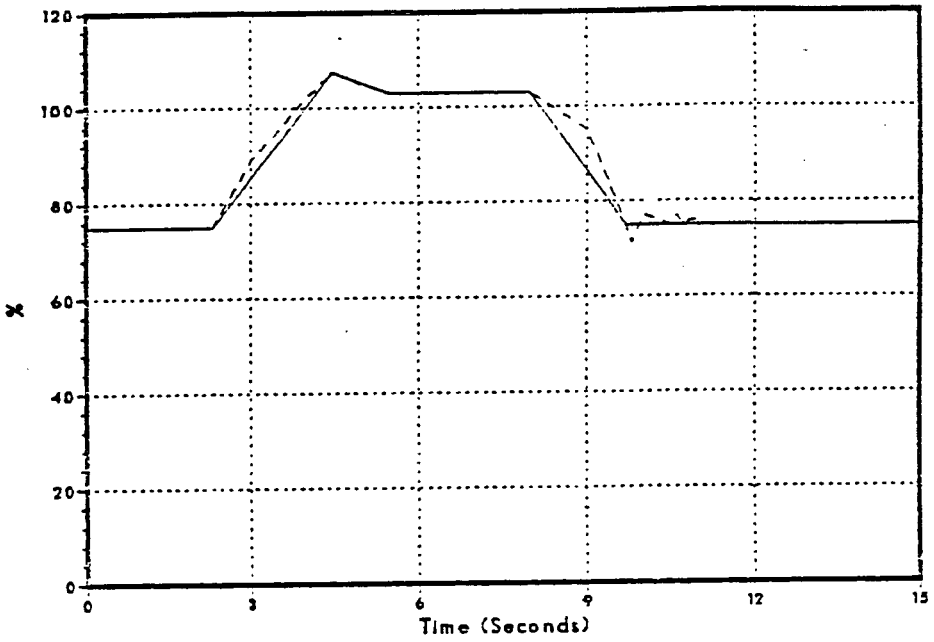

Prepared by NSP Safety Analysis, 5/14/86

Monticello Cycle 1
2/2 Pump Trip Startup Test

Figure 3.2-133
Total Vessel Flow Rate

DNB036/86
Test Data

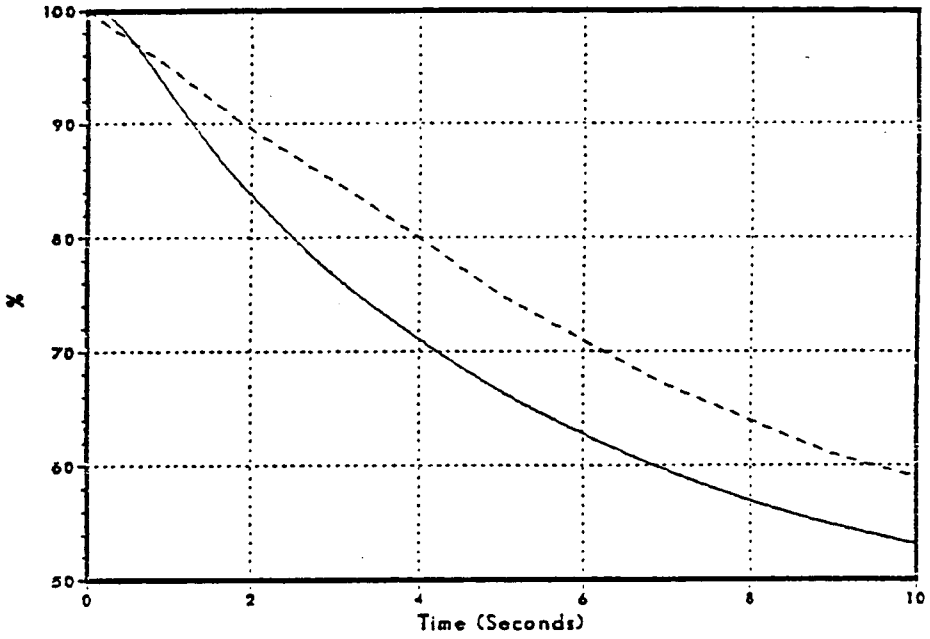

Figure 3.2-134
Core Average Heat Flux

DNB036/86
Test Data

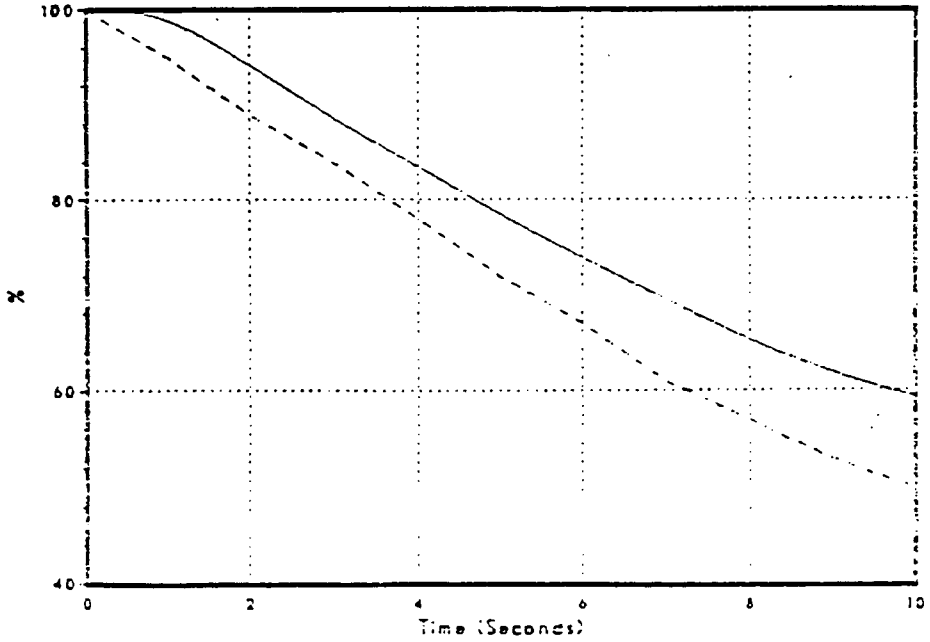

Prepared by NSP Safety Analysis, 4/25/86

Monticello Cycle 1
Auto Flow Decrease Startup Test

Figure 3.2-135
Steam Dome Pressure

DNB037/86
Test Data

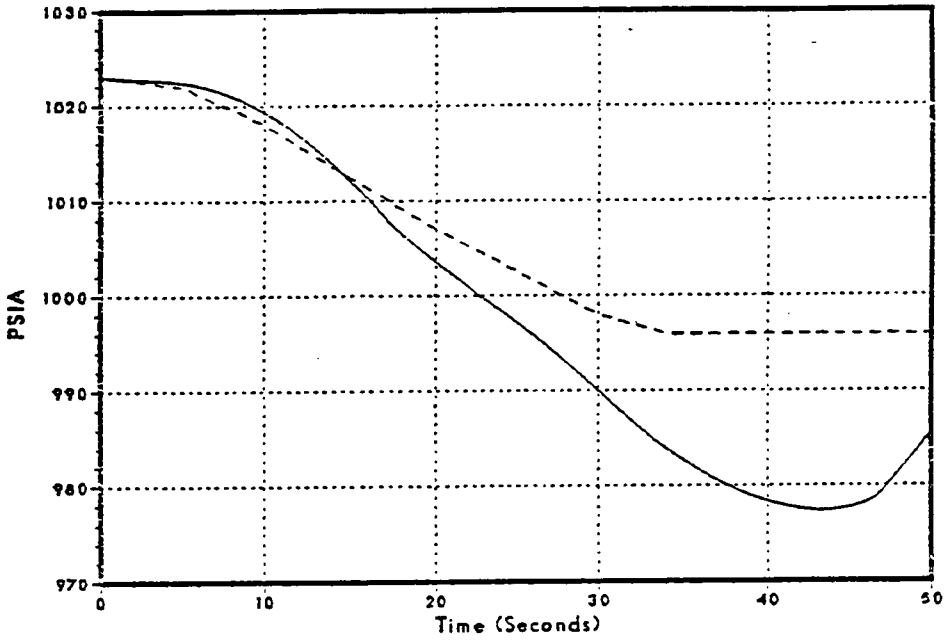

Figure 3.2-136
Relative Power

DNB037/86
Test Data

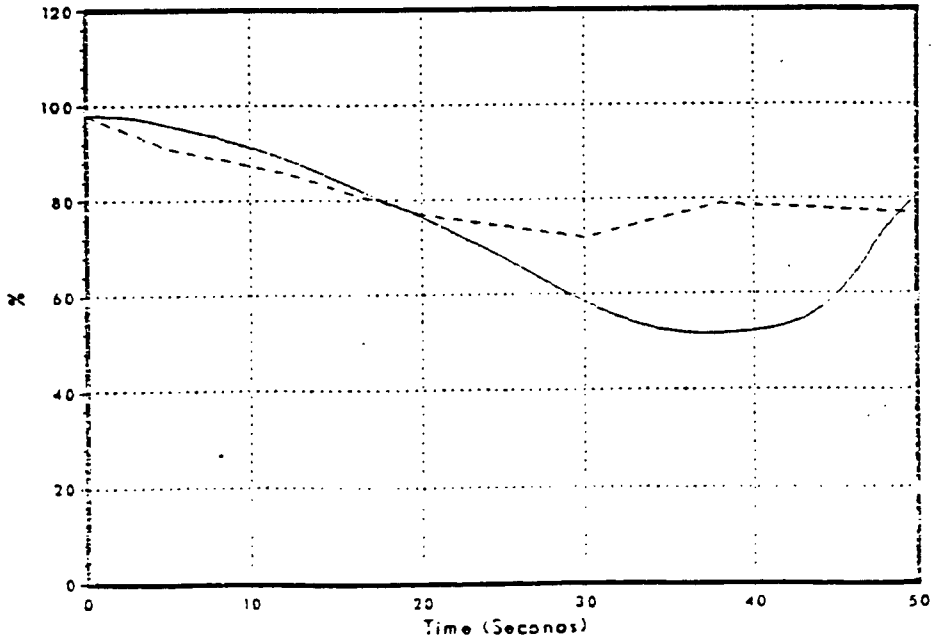

NSP

Prepared by NSP Safety Analysis, 5/01/86

Monticello Cycle 1
Auto Flow Decrease Startup Test

Figure 3.2-137
Main Steam Line Flow

DNB037/86
Test Data

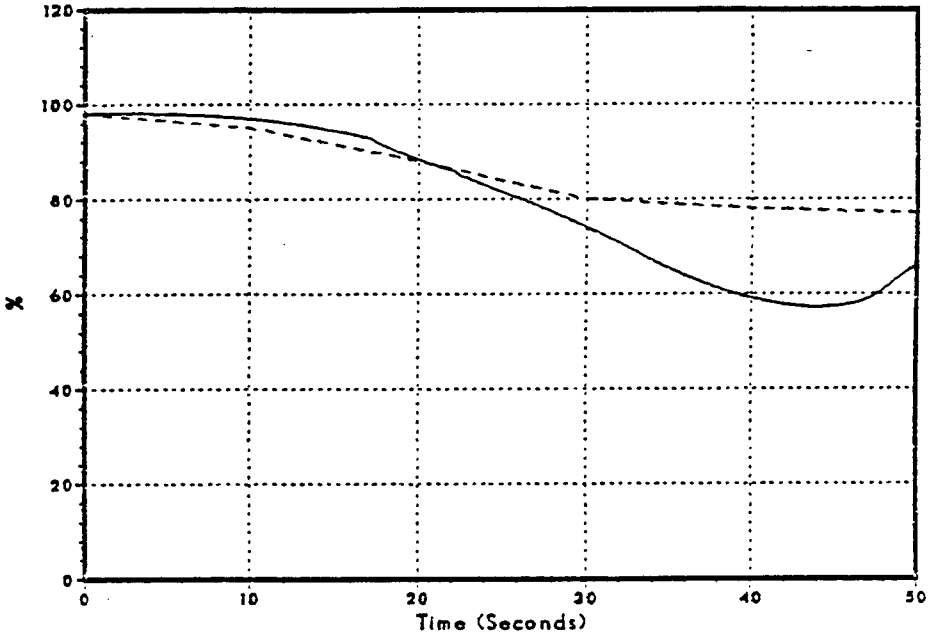

Figure 3.2-138
Feedwater Flow

DNB037/86
Test Data

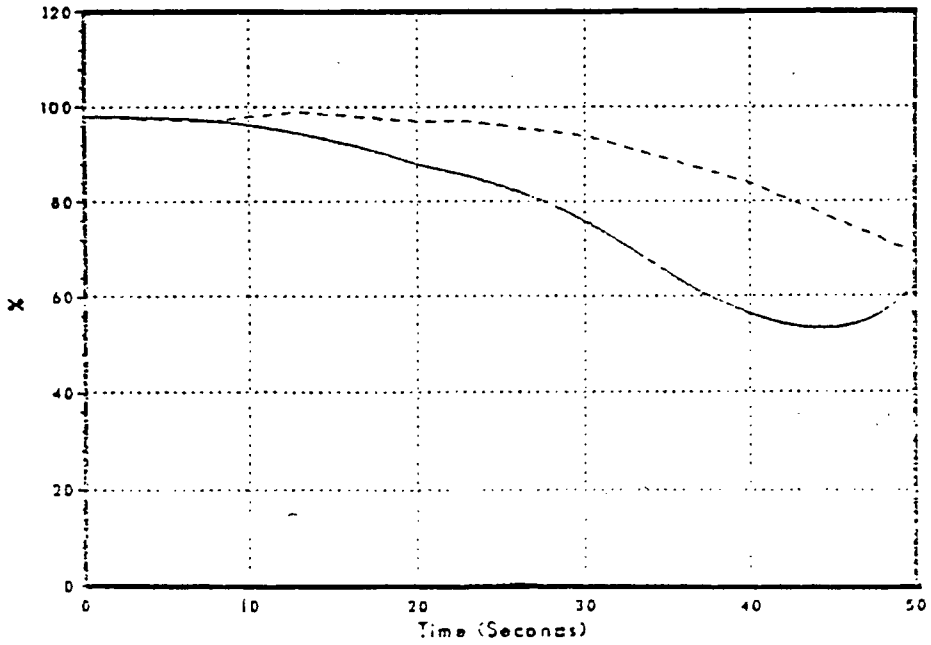

NSP

Prepared by NSP Safety Analysis, 5/01/86

Monticello Cycle 1
Auto Flow Decrease Startup Test

Figure 3.2-139
Sensed Reactor Water Level

DNB037/86

Test Data

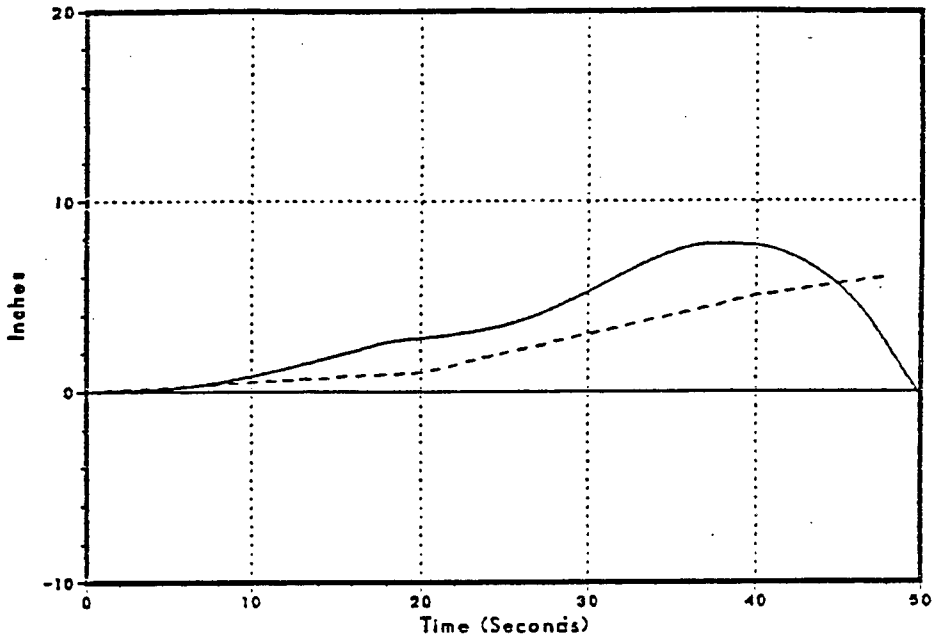

Figure 3.2-140
Total Vessel Flow Rate

DNB037/86

Test Data

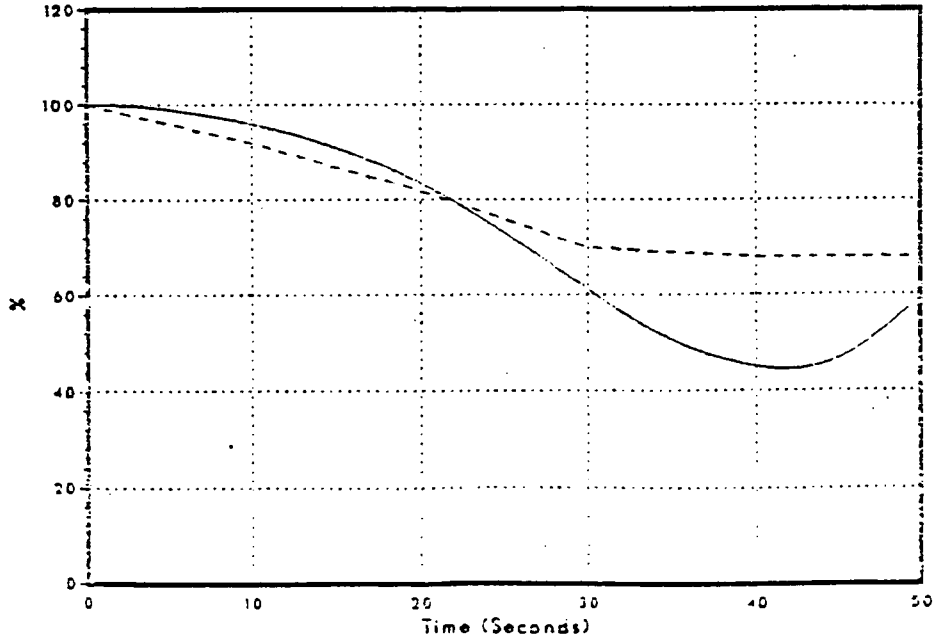

NSP

Prepared by NSP Safety Analysis, 5/15/86

Monticello Cycle 1
Pressure Step Startup Test

Figure 3.2-141
Steam Dome Pressure

DNB039/86

Test Data

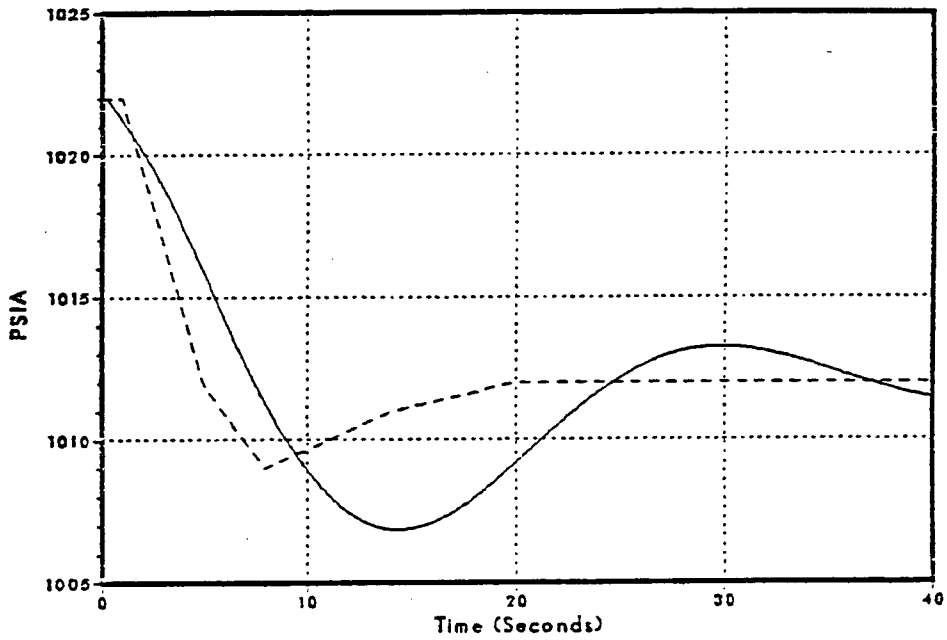

Figure 3.2-142
Relative Power

DNB039/86

Test Data

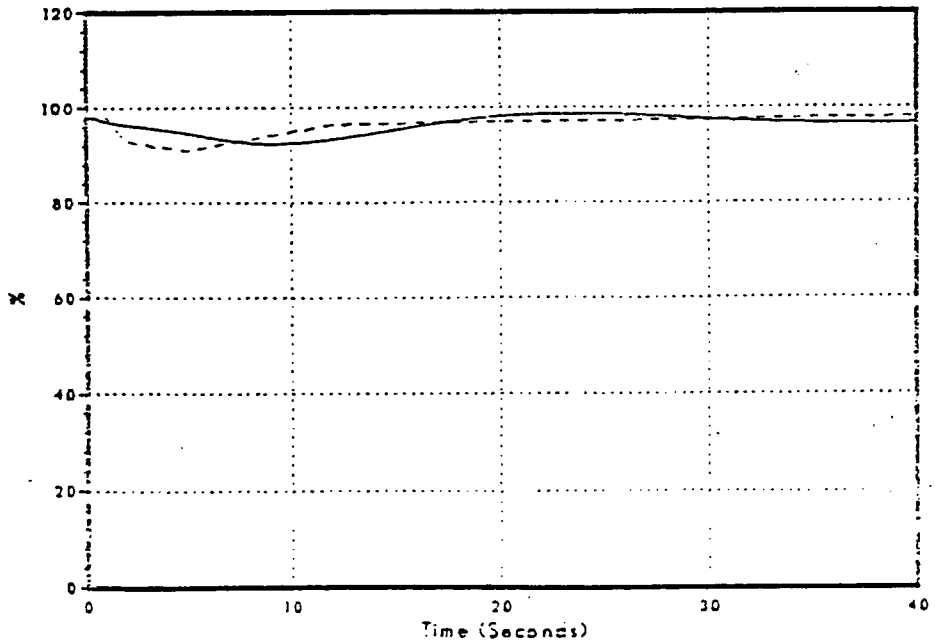

NSP

Monticello Cycle 1
Pressure Step Startup Test

Figure 3.2-143
Main Steam Line Flow

DNB039/86
Test Data

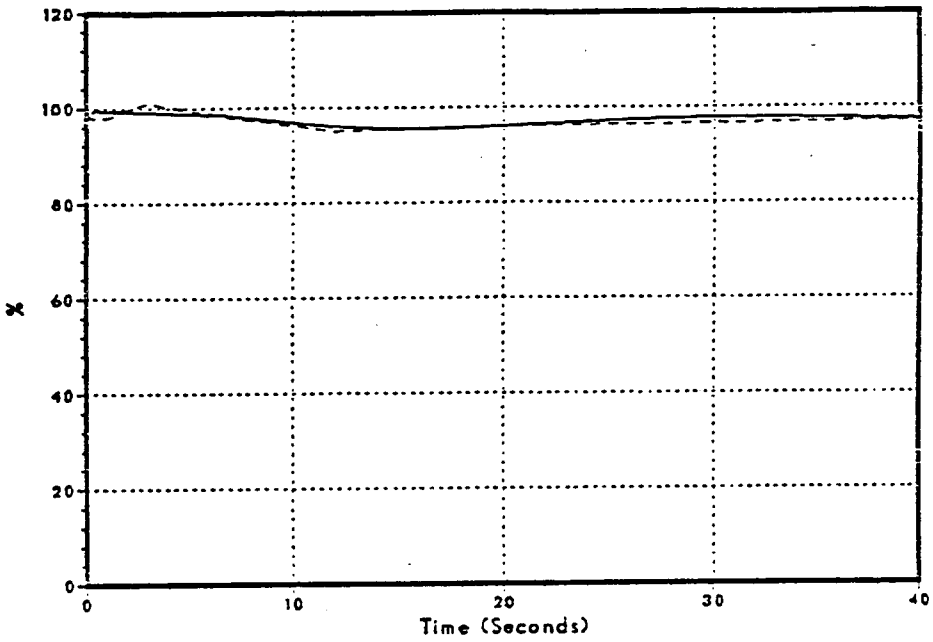

Figure 3.2-144
Feedwater Flow

DNB039/86
Test Data

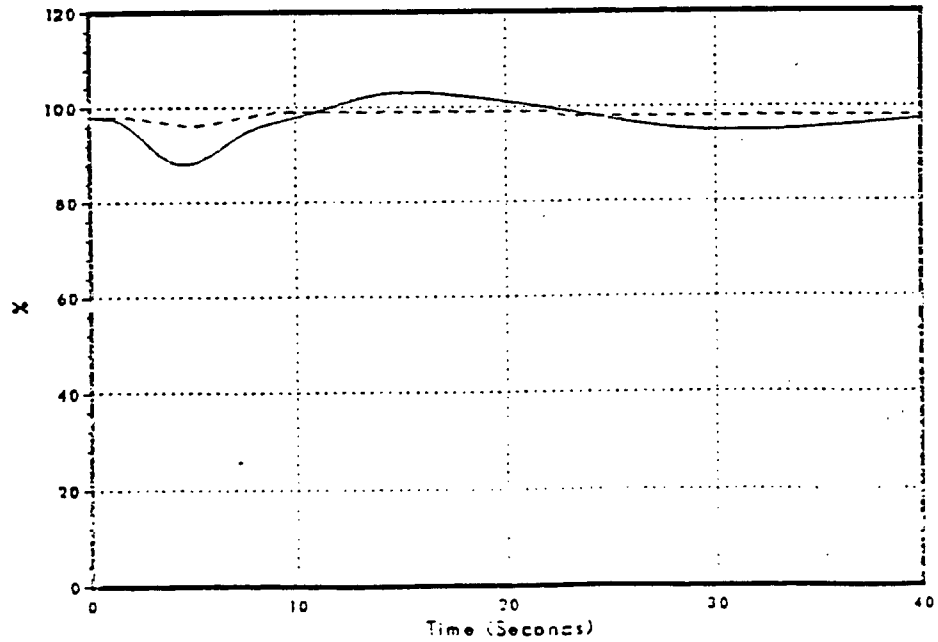

NSP

Prepared by NSP Safety Analysis, 5/14/86

Monticello Cycle 1
Pressure Step Startup Test

Figure 3.2-145
Sensed Reactor Water Level

DNB039/86

Test Data

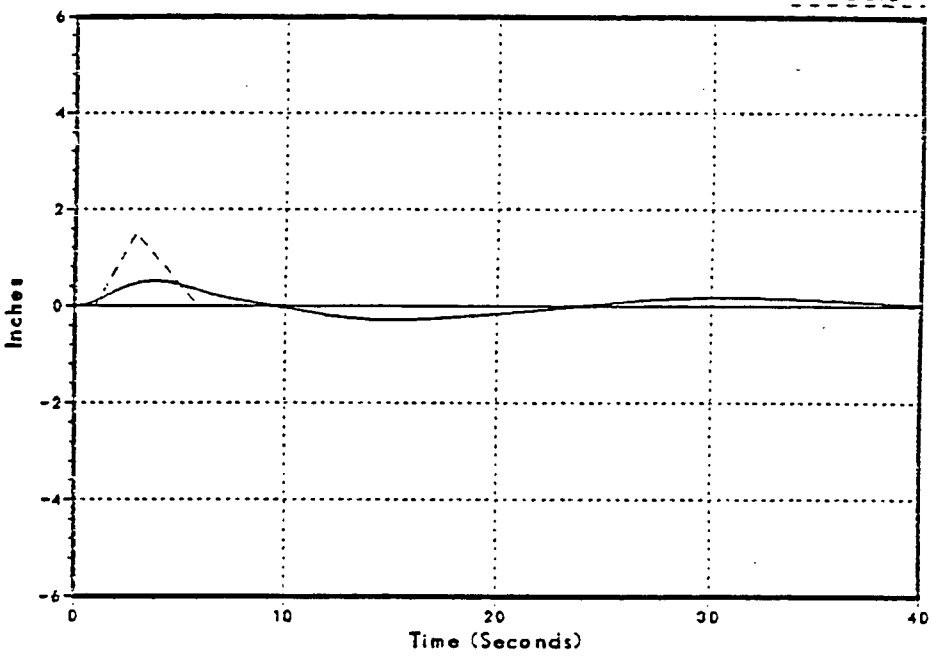

Monticello Cycle 1
FW Level Setpoint Step Startup Test

Figure 3.2-146
Steam Dome Pressure

DNB040/86
Test Data

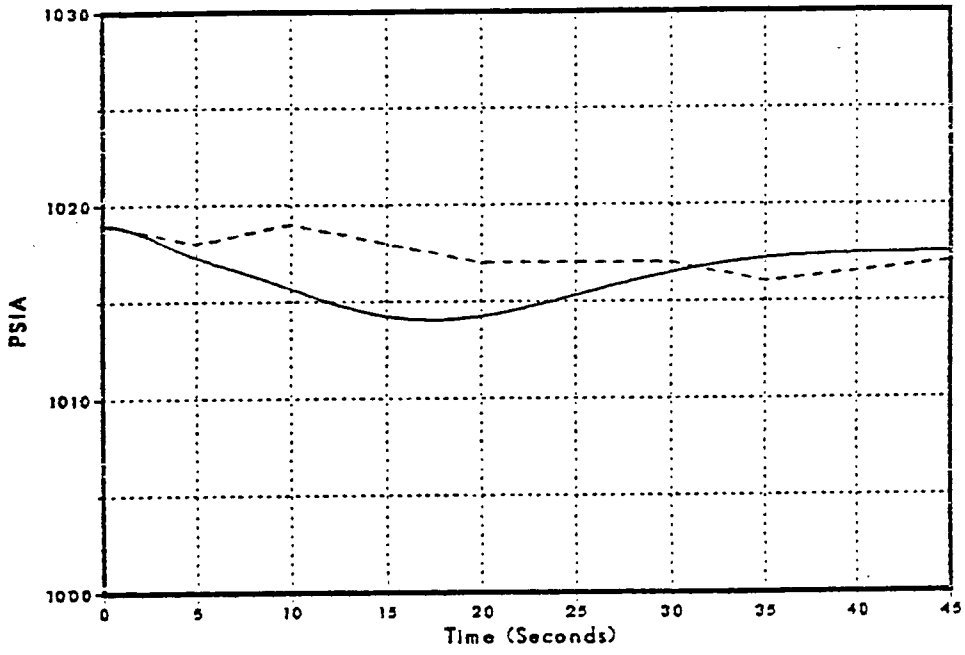

Figure 3.2-147
Relative Power

DNB040/86
Test Data

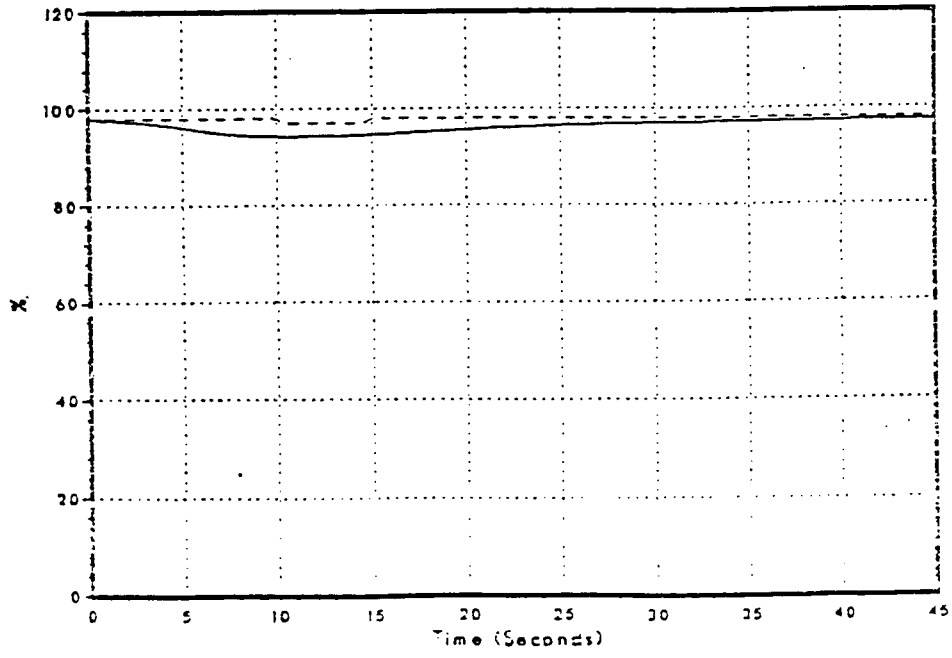

NSP

Prepared by NSP Safety Analysis, 5/15/86

Monticello Cycle 1
FW Level Setpoint Step Startup Test

DNB040/86

Figure 3.2-148
Feedwater Flow

Test Data

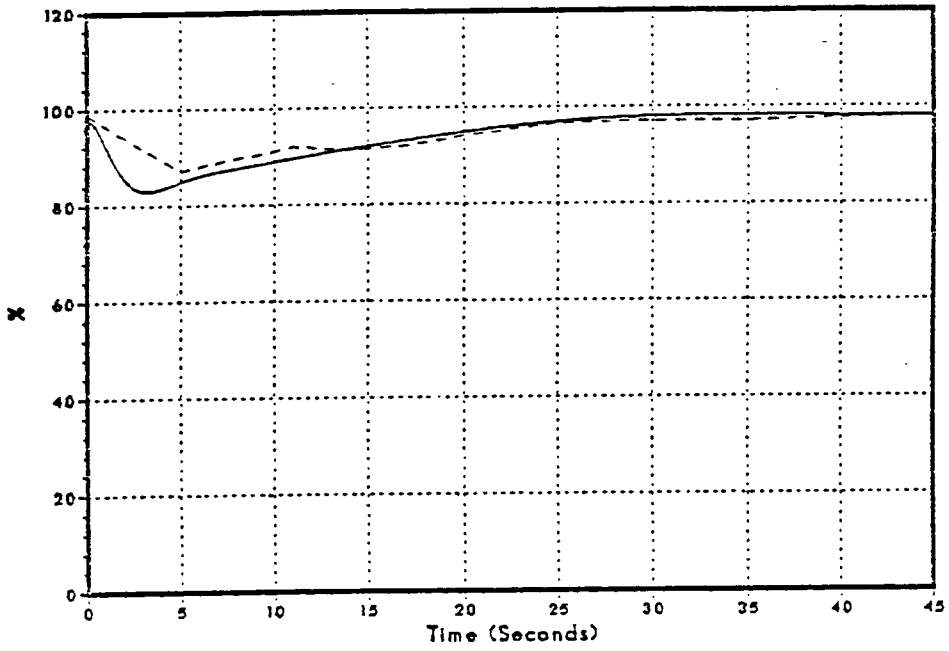

DNB040/86

Figure 3.2-149
Sensed Reactor Water Level

Test Data

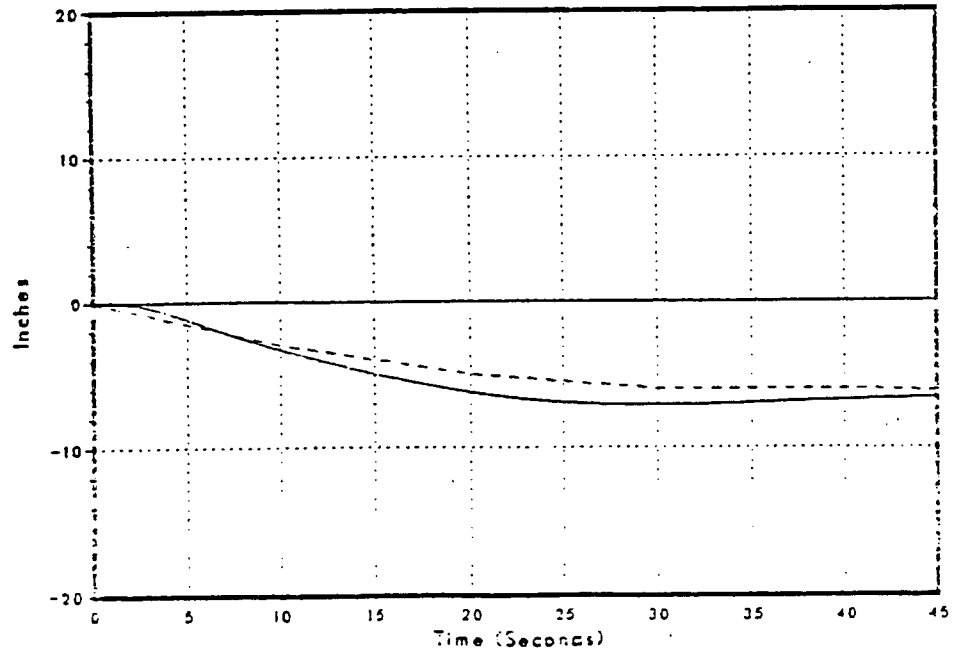

NSP

Prepared by NSP Safety Analysis, 5/15/86

4.0 RELOAD SAFETY EVALUATION METHODS

This section provides a description of the methodology used by the Northern States Power Company Nuclear Analysis Department (NSPNAD) to perform licensing analyses. These analyses will be used, in conjunction with analyses performed by the fuel vendor, to establish reactor operating limits and to demonstrate acceptable margin to established safety limits.

The NSPNAD BWR methodology is similar to GE's option A methodology [7]. The major components which describe these methods are:

- The spectrum of events covered by this submittal and the models used to simulate those events.
- The input parameters used.
- The applicable limiting acceptance criteria.
- Evaluation and application of uncertainties

These elements are discussed in detail in the following sections.

4.1 MODEL/EVENT APPLICATION

Tables 4.1-1, 4.1-2, and 4.1-3 summarize the standard spectrum of events covered by abnormal transient evaluations and the intended application of this document.

Included in Tables 4.1-1, 4.1-2, and 4.1-3 is a determination of the kinetics model used for each type of transient; i.e., point or 1-D (space-time). The kinetics model is the only code model which is dependent on event application. Table 4.1-4 summarizes the models used for licensing calculations.

The selection of a particular model for application to licensing analysis was based on the benchmark analyses presented in Section 3, as well as consultation with the primary code author, Dr. Richard Kern (Utility Associates International). If the power shape changes significantly during a transient, the point kinetics model may be run in conjunction with the 1-D model to verify the current selected model.

The philosophy used in selecting events for which the 1-D kinetics model will be applied, as opposed to the point kinetics model, was to evaluate the event phenomena with respect to the core axial behavior. Those transients which display a high degree of axial significance, e.g., overpressure transients, require a 1-D kinetics model in order to properly account for the event phenomena. The remaining transients, for which a point kinetics model will be used, do not require the more complex one-dimensional solution. Experience shows that the point kinetics model can accurately predict these remaining events.

Table 4.1-1 includes a determination of those events which are typically thermally limiting. In order to determine the limiting transient events, with respect to CPR, the relative dependency of CPR upon various thermal-hydraulic parameters was examined using the GEXL correlation. A sensitivity study was performed to determine the effect, over a range of nominal ±10%, of changes in bundle power, bundle flow, core inlet subcooling, core pressure, and R-factor. The results of this study are presented in Table 4.1-5 for 8x8 fuel. Included in this table are the General Electric generic results from Reference 7 for the same fuel type.

As can be seen from this study, the DYNODE-B results compare favorably with the GE results, indicating the correct application of the GEXL correlation. CPR is seen to be most sensitive to changes in the R-factor and bundle power. A slight sensitivity to core pressure and core flow is also shown, as well as relative independence to core inlet subcooling.

The R-factor is a function of bundle geometry and local pin power distribution and is assumed to remain constant throughout each transient. Therefore, transients which are thermally limiting are those that produce significant increases in power. These are identified in Table 4.1-1. Previous Monticello Reload analyses, performed by GE, verify this list.

4.2 INPUT PARAMETERS

This section describes the selection of input parameters for application to licensing analyses.

Table 4.2-1 summarizes typical input parameters for Monticello which were used for the REDY and ODYN benchmarks of section 3. Note that some transients are initiated at an operating point other than the 100% flow/100% power point indicated by Table 4.2-1. The initial operating point is selected to maximize the transient response. Measurement uncertainties are discussed in Section 4.4.

Equipment responses (e.g. scram setpoints and delays, relief valve setpoints and delays, and valve closure stroke times) are set at the most conservative values specified in the Technical Specifications [12].

The kinetics parameters, CRD scram time, and CPR model inputs are discussed in the following sections.

4.2.1 KINETICS PARAMETERS

This section describes the methods used in applying biases to the input kinetics parameters. Reference 1 describes the procedures used for determination of the biases. It is not the intent of this section to redefine the procedures used in Reference 1. However, some aspects of these procedures are presented here in order to clarify the approach taken in applying the biases.

The magnitude and application of the bias is independent of the kinetics model used in the transient analysis, i.e., point or 1-D. However, in the case of the 1-D kinetics model, an additional uncertainty is introduced due to the collapsing procedure used in going from 3-D to 1-D. This "collapsing" uncertainty is applied to the input parameter uncertainty $\Delta CPR/ICPR$ for the void, Doppler and scram reactivities, since these represent the major reactivity feedback mechanisms for a BWR.

4.2.1.1 BUNDLE POWER

Bundle powers are used in the DYNODE-B hot channel model to calculate Critical Power Ratio. The bundle powers are calculated using the three-dimensional nodal model [1].

The model bias is applied as follows:

$$P(I,J) = P(I,J)(MODEL) * (1+Bias) ;$$

where

P(I,J)(MODEL) = Absolute bundle power in assembly (I,J) as calculated by the 3-D nodal model.

Bias = 0.0 (Ref. 1).

The model bias is updated every cycle and the results documented in the Reload Safety Evaluation for that cycle.

4.2.1.2 CONTROL ROD WORTHS

Rod worths are calculated using the three-dimensional nodal model [1]. Worths are determined by varying the rod position, while the independent core parameters, such as core power, flow, and void distribution, are held constant.

The model bias is applied as follows:

$$\Delta K_{ROD} = \Delta K_{ROD}\ (MODEL) * (1 + Bias)\ ;$$

where

$\Delta K_{ROD}(MODEL)$ = Rod Worth

Bias = 0.0 (Ref. 1)

The model bias is updated every cycle and the results documented in the Reload Safety Evaluation for that cycle.

The rod worth scram reactivity is input to the transient model as a function of the total rod worth, ΔK_{ROD}, as follows:

$$\Delta K_{SCRAM_K} = \Sigma_I\ (\Delta K_{ROD_I} * CF_{I,K} * RWD_K)$$

where

ΔK_{SCRAM_K} = Rod worth scram reactivity in axial node K.

$CF_{I,K}$ = Source weighted control fraction of bank I in axial node K.

RWD_K = Relative rod worth in axial node K.

4.2.1.3 VOID REACTIVITY

For 1-D kinetics application, void reactivity effects are modeled in DYNODE-B via changes in K^{∞} and M^2 relative to an initial transient condition.

The initial transient condition is run with the CASMO/NDH model [1]. Thus the source, power, K^{∞}, and M^2 distributions are known throughout the core. The CASMO/NDH initial case is then perturbed. The differences in the values of the effective 1-D K^{∞} and M^2 distributions between the perturbed and initial cases are computed. In a similiar manner, DYNODE-B is run for the initial and perturbed conditions. From the results, $\Delta K^{\infty}/\Delta U$ and $\Delta M^2/\Delta U$ are constructed as a function of U, where U is the relative water density obtained from DYNODE-B. These curves are integrated to obtain K^{∞} vs U and M^2 vs U curves which are input to DYNODE-B.

The model bias is applied to the $\Delta K^{\infty}/\Delta U$ function prior to integration, as follows:

$$\Delta K^{\infty}/\Delta U = \Delta K^{\infty}/\Delta U \text{ (MODEL)} * (1 + \text{Bias})$$

where

$\Delta K^{\infty}/\Delta U$(MODEL) = ΔK^{∞} from NDH and ΔU from DYNODE-B as described above

Bias = 0.0 (Ref. 1).

For point kinetics application, the bias is applied as follows:

$$\alpha_V = \alpha_V \text{ (MODEL)} * (1 + \text{Bias}) \ ;$$

where

α_V (MODEL) = Void reactivity coefficient

and α_v is based on the K^{eff} changes calculated by CASMO/NDH and the corresponding DYNODE-B core average void fraction changes. The model bias is updated every cycle and the results documented in the Reload Safety Evaluation for that cycle.

4.2.1.4 DOPPLER COEFFICIENT

The Doppler coefficient is a measure of the change in core multiplication associated with a change in fuel temperature. Core reactivity is changed mainly due to Doppler broadening of the U-238 and U-240 parasitic resonance absorption cross sections due to increases in fuel temperature. For 1-D kinetics application, this effect is calculated by running CASMO/NDH cases [1] and DYNODE-B cases to develop a $\Delta K^{\infty}/\Delta\ (t_f^{\frac{1}{2}})$ versus $t_f^{\frac{1}{2}}$ curve, where t_f is the fuel temperature obtained from DYNODE-B.

The model reliability factor and bias are applied at each point as follows:

$$\Delta K^{\infty}/\Delta(t^{\frac{1}{2}}) = \Delta K^{\infty}/\Delta\ (t_f^{\frac{1}{2}})(\text{MODEL}) * (1 + \text{Bias})\ ;$$

where

$\Delta K^{\infty}/\Delta(t_f^{\frac{1}{2}})(\text{MODEL}) = \Delta K^{\infty}$ from NDH and $\Delta(t_f^{\frac{1}{2}})$ from DYNODE-B as discussed above

Bias = 0.0 (Ref. 1).

This distribution is then integrated to obtain the K^{∞} vs $t_f^{\frac{1}{2}}$ curve that is input to the transient code.

For point kinetics application, the bias is applied as follows:

$$\alpha_D = \alpha_D(\text{MODEL}) * (1 + \text{Bias})\ ;$$

where

α_D (MODEL) = Doppler reactivity coefficient

and α_D is based on the CASMO/NDH K^{eff} changes and the corresponding DYNODE-B core average fuel temperature changes. The model bias is updated every cycle and the results documented in the Reload Safety Evaluation for that cycle.

4.2.1.5 DELAYED NEUTRONS

For 1-D kinetics application, the delayed neutron group dependent constants, β_i and λ_i, are assumed to be uniform throughout the core and constant in time in DYNODE-B. The total delayed neutron fraction, β, is assumed to be spatially distributed and constant in time in DYNODE-B. The use of constant delay neutron constants corresponding to the initial conditions is justified by the results in Reference 22, which show that β_{eff} does not change significantly during a transient until the scram is over. Radial source weighting is used to obtain these constants to be consistent with the transient source solution used in DYNODE-B. The local values of β_i to be used in the weighting are the values taken directly from the infinite lattice calculations (CASMO) [1] without any spectral importance weighting.

Spectral importance weighting is unnecessary because the DYNODE-B source equations relate to the integral of the source over the entire energy spectrum so that the importance of the delayed neutrons does not depend on the energy at which they are born with respect to total source.

The axial-dependent total β's which are entered into DYNODE-B are obtained by source weighting of the $\Sigma\beta_i$ over the radial direction at each axial level so that:

$$\beta_K(\text{MODEL}) = \sum_R S_\ell \sum_i \beta^\ell{}_i \Big/ \sum_R S_\ell \ .$$

For point kinetics application the βeff is calculated by NDH and directly input into DYNODE-B.

4.2.1.6 NEUTRON SOURCE LIFETIME

In the transient model for 1-D kinetics applications, the neutron source lifetime is assumed to be spatially distributed and constant in time and is defined as:

$$\ell^*_K = (1/V\nu\Sigma_f)_K$$

where V is the velocity of the source neutrons (cm/s) and source averaging over the radial plane is used for consistency with the transient source solution used in DYNODE-B.

The neutron source lifetime is calculated in the CASMO/NDH model (Reference 1) in each node ℓ from a curve fit of $(V\nu\Sigma_f)$ as a function of exposure, moderator density, and control fraction for each fuel type. ℓ^*_K is then source weighted as follows:

$$\ell^*_k(\text{MODEL}) = \left(\sum_R S_\ell / (V\nu\Sigma_f)_\ell\right) / \left(\sum_R S_\ell\right)$$

where

ℓ^*_k(MODEL) = Neutron source lifetime at axial level K.

For point kinetics applications the ℓ^* is calculated by NDH and directly input into DYNODE-B.

4.2.2 CRD SCRAM TIME

The mean scram time assumed in the analysis must be greater than the measured weighted cycle average scram time at a 95% confidence level for all points in the cycle. This determination is made at the 20% insertion position (~ notch 38).

That is :

$$\tau_{AVE} \leq \tau_D \ ;$$

where

τ_{AVE} = weighted cycle average scram time at a 95% confidence level.

τ_D = mean scram time assumed in the DYNODE-B analysis.

and

$$\tau_{AVE} = \left[\left(\sum_{i=1}^{n} N_i \, \tau_i\right) / \sum_{i=1}^{n} N_i\right] + \left[0.0875 \left(N_1 / \sum_{i=1}^{n} N_i\right)^{\frac{1}{2}}\right]$$

n = the number of surveillance tests performed to date in this cycle.

N_i = number of control rods measured in the ith test.

τ_i = average scram time to the 20% insertion position of all rods measured in the i th test.

N_1 = total number of active rods measured in the first test following core alterations.

0.0875 = 1.65 * 0.053; where 1.65 is the appropriate statistical number to provide a 95% confidence level, and 0.053 is the standard deviation of the distribution 20% position. This latter factor is based on extensive plant measurements by General Electric and is documented in Reference 21.

The transient analyses will be performed with either a single bounding scram time or with a spectrum of scram times, allowing the plant to take full credit for the measured scram times. The spectrum of analysis scram times will be performed at small enough intervals to allow an interpolation of results.

4.2.3 CRITICAL POWER RATIO

Critical Power Ratio is calculated using the General Electric BWR Thermal Analysis Basis (GETAB) [18, 19, 20]. The GEXL correlation was obtained from General Electric for use by Northern States Power as a part of the current fuel contract.

The GEXL correlation has been incorporated into the DYNODE-B hot channel model. Input to this model consists of the bundle average radial peaking factor, the relative bundle inlet flow, the bundle initial pressure and inlet enthalpy, the bundle R-factor, and the axial power distribution. The axial power distribution used in the analysis is given in Table 4.2-2, which is taken from Reference 7. The R-factors are supplied by General Electric.

The bundle average radial peaking factor and the relative bundle inlet flow factor are assumed constant throughout the transient and are calculated from the three-dimensional simulator [1] with the appropriate uncertainties included (see section 4.2.1.1). The GEXL correlation safety limit (see section 4.3.1) includes an 8.7% (one standard deviation) uncertainty on TIP readings. As long as the NSPNAD determined bundle power model reliability factor (see section 4.2.1.1) is less than 8.7%, no additional uncertainty need be applied.

Proper programming and use of the GEXL correlation was tested by comparing steady state CPR values for the fuel types of interest. Small differences will exist between the GE and DYNODE-B values due to a slight difference in the water property tables used. These comparisons are shown in Table 4.2-3. Further comparisons are also shown in Table 4.1-5.

These comparisons show that NSPNAD has properly implemented the GEXL correlation and that it can be used, along with the associated safety limit (see section 4.3.1), in licensing calculations.

4.3 LIMITING ACCEPTANCE CRITERIA

Limits on plant operation are established to assure that the plant can be safely operated and does not pose any undue risk to the health and safety of the public.

There are three limiting acceptance criteria which must be met for the spectrum of events being analyzed.

4.3.1 THERMAL LIMITS

Reference 5, Section 4.4, "Thermal and Hydraulic Design", Acceptance Criteria 1:

"SRP Section 4.2 specifies the acceptance criteria for evaluation of fuel design limits. One of the criteria provides assurance that there be at least a 95% probability at a 95% confidence level that the hot fuel rod in the core does not experience a departure from nucleate boiling (DNB) or transition condition during normal operation or anticipated operational occurrence.

Uncertainties in the values of process parameters, core design parameters, and calculational methods used in the assessment of thermal margin should be treated with at least a 95% probability at a 95% confidence level."

An acceptable approach to meet this criterion is given as:

"For DNBR, CHFR or CPR correlations, the limiting (minimum) value of DNBR, CHFR, or CPR is to be established such that at least 99.9% of the fuel rods in the core would not be expected to experience departure from nucleate boiling or boiling transition during normal operation or anticipated operational occurrences."

A bounding statistical analysis was performed by General Electric [7] to determine the fuel cladding integrity safety limit for 8x8, 8x8R and P8x8R fuel types. The results of the analysis show that at least 99.9% of the fuel rods in the core are expected to avoid boiling transition if the MCPR is equal to or greater than the applicable value listed in Table 4.3-1.

Thus, the thermal limits will be met if

$$MCPR = ICPR\ (1+ \Delta CPR/ICPR) \geq MCPR\ limit$$

for all normal operation or anticipated operational occurrences.

4.3.2 ASME VESSEL OVERPRESSURIZATION

Reference 5, Section 5.2.2, "Overpressure Protection", Acceptance Criteria A:

"For overpressure protection, during power operation of the reactor, the relief valves shall be designed with sufficient capacity to preclude actuation of safety valves, during normal operational transients, when assuming the following conditions at the plant:

a. The reactor is operating at licensed core thermal power level.

b. All system and core parameters are at values within normal operating range that produce the highest anticipated pressure.

c. All components, instrumentation, and controls function normally.

Safety valves shall be designed with sufficient capacity to limit the pressure to less than 110% of the RCPB design pressure (as specified by the ASME Boiler and Pressure Vessel Code [15]), during the most severe abnormal operational transient and the reactor scrammed. Also, sufficient margin shall be available to account for uncertainties in the design and operation of the plant assuming:

i. The reactor is operating at a power level that will produce the most severe overpressurization transient.

ii. All system and core parameters are at values within normal operating range, including uncertainties and technical specification limits that produce the highest anticipated pressure.

iii. The reactor scram is initiated by the second safety-grade signal from the reactor protection system.

iv. The discharge flow is based on the rated capacities specified in the ASME Boiler and Pressure Vessel Code [15], for each type of valve."

Compliance with this limit requires that the reactor pressure not exceed 110% of the design pressure (1.1 * 1250 = 1375 psig) under upset conditions.

For Monticello, the most limiting upset condition, with respect to reactor pressure, is an MSIV closure transient with a failure of the MSIV position scram, followed by a flux scram and considering one failed S/R valve.

4.3.3 SYSTEM STABILITY

Reference 5, Section 4.4, "Thermal and Hydraulic Design", Acceptance Criteria 3:

"The reactor should be demonstrated to have sufficient margin to be free of undamped oscillations and other thermal-hydraulic instabilities for all conditions of steady-state operation (including part loop operation), and for anticipated operational occurrences."

Compliance with this limit is determined by performing setpoint step change analyses for the control systems; i.e., feedwater controller, pressure controller, and recirculation flow controller. The analyses are performed at the most limiting point along the power-flow operating map, typically the intersection of the natural circulation line and the 100% rod line. The reactor system shall be considered stable if the decay ratio is less than 1.0.

Note that the bundle channel stability analysis is performed separately by the fuel vendor.

4.4 EVALUATION AND APPLICATION OF UNCERTAINTIES

There are four areas of uncertainty which must be accounted for when performing licensing analyses. These are measurement uncertainties, code modeling uncertainties, input parameter uncertainties, and the uncertainties associated with use of a particular correlation. In general, these four categories overlap in their definitions. However, they can be used to describe all the areas of uncertainties.

Once the uncertainties have been defined, they are quantified against the available data to show conservatism and then combined within the NSPNAD methodology. That is to say, they are all applied in the conservative direction in order to produce conservative results.

The following sections describe the evaluation and application of the four categories of uncertainties described above to the three acceptance criteria described in Section 4.3.

4.4.1 THERMAL LIMITS

Measurement Uncertainties

The GETAB methodology [18, 19, 20] generically includes uncertainties on the initial core operating conditions (see table S.2-1 of Reference 7) in determination of the GEXL correlation safety limit. Therefore, no additional uncertainties need be applied.

Code Modeling Uncertainty

Code modeling uncertainties were quantified by comparing the calculated versus measured ΔCPR/ICPR for the Peach Bottom turbine trip tests and the Monticello turbine trip start up test (see sections 3.2.2.1 and 3.2.2.2.1 respectively). The results are summarized in Table 4.4-1. The results show that in all cases DYNODE-B overpredicts ΔCPR/ICPR by approximately 10 percent. Therefore, no additional uncertainties need be applied for the thermal hydraulic part of the model excluding the core. The core uncertainty is covered by the input parameters uncertainty.

Input Parameters Uncertainty

An uncertainty of 0.021 ΔCPR/ICPR will be used to increase transient ΔCPR to determine the limiting CPR for operations. Section 7.27 shows how this uncertainty factor was determined.

CPR Correlation Uncertainty

The GETAB methodology includes the GEXL correlation uncertainty in the determination of the safety limit. Therefore, no additional uncertainties need be applied for any case except the Fuel Loading Error transient. Reference 7 states that an additional penalty of 0.02 on ΔCPR must be applied to the misoriented bundle results to account for uncertainties associated with the ability of GEXL to predict CPR for an axially varying R-factor.

4.4.2 ASME VESSEL OVERPRESSURE

Measurement Uncertainties

The transient analyses used to determine compliance with the ASME Vessel Overpressure criteria are initiated from 1040 psia steam dome pressure. This initial operating pressure includes a 0.5 percent uncertainty (one standard deviation).

Code Modeling Uncertainty

Code modeling uncertainties were quantified by comparing the calculated versus measured steam dome pressures for the Peach Bottom turbine trip tests, the Monticello turbine trip start up test, and the Monticello MSIV closure start up test (See Section 3.2.2.1, 3.2.2.2.1 and 3.2.2.2.2 respectively). The results are summarized in Table 4.4-2. The results show that in all cases DYNODE-B overpredicts the peak steam dome pressure by approximately two percent. Therefore, no additional uncertainties need be applied.

Input Parameter Uncertainty

Since the input parameter uncertainty of 5.5 psi is approximately 60 times less than the bias in determining the ASME vessel overpressure limit which is estimated to be 310 psi, no pressure uncertainty need be taken. See section 7.27 for the determination of the 5.5 psi.

Correlation Uncertainty

No special empirical correlations are used in the calculation of vessel pressure. Therefore, this section is not applicable.

4.4.3 SYSTEM STABILITY

Measurement Uncertainties

The transient analyses used to determine compliance with the system stability criteria are initiated from an operating condition which includes a +2% uncertainty on reactor power and a -3% uncertainty on core flow. These values represent one standard deviation and are taken from Reference 16.

Code Modeling Uncertainties

Code modeling uncertainties were quantified by comparing the calculated versus measured APRM decay ratio for the Monticello feedwater controller level setpoint step, pressure regulator setpoint step, and automatic flow decrease start up tests (See Sections 3.2.2.2.6, 3.2.2.2.5, and 3.2.2.2.4, respectively). The results are summarized in Table 4.4-3. The results show that in all cases DYNODE-B conservatively overpredicts the APRM decay ratio. Therefore, no additional uncertainties need be applied.

Input Parameter Uncertainty

The input parameter uncertainty of 0.19 will be added to the decay ratio calculated by DYNODE-B to account for input parameter uncertainty. See section 7.27 for details on the calculation of this value.

Correlation Uncertainty

No special empirical correlations are used in the calculation of the decay ratio. Therefore, this section is not applicable.

Table 4.1-1

SPECTRUM OF EVENTS FOR THERMAL LIMITS ACCEPTANCE CRITERIA EVALUATION

Event	Kinetics Model to be Used for Evaluation*	Thermally Limiting or Near Limiting (Typically)
DECREASE IN REACTOR CORE COOLANT TEMPERATURE		
Loss of Feedwater Heating	POINT	X
Feedwater Controller Failure - Maximum Demand	ONE-D	X
Pressure Regulator Failure - Open	POINT	
INCREASE IN REACTOR PRESSURE		
Pressure Regulator Failure - Closed	ONE-D	
Generator Load Rejection	ONE-D	X
Turbine Trip	ONE-D	
Main Steamline Isolation Valve Closure	ONE-D	
Loss of Condenser Vacuum	ONE-D	

Table 4.1-1 (continued)

Events	Kinetics Model to be Used for Evaluations*	Thermally Limiting or Near Limiting (Typically)
Loss of AC Power Transformer	POINT	
Loss of Auxiliary Power - All Grid Connections	ONE-D	
Loss of Feedwater Flow	POINT	
DECREASE IN REACTOR COOLANT SYSTEM FLOW RATE		
Recirculation Pump Trip	POINT	
Recirculation Flow Control Failure - Decreasing Flow	POINT	
REACTIVITY AND POWER DISTRIBUTION ANOMALIES		
Abnormal Startup of Idle Recirculation Pump	POINT	
Recirculation Flow Control Failure With Increasing Flow	POINT	
Control Rod Withdrawal	POINT and NDH^{+}	
Fuel Loading Error	NDH^{+}	

Table 4.1-1 (continued)

Event	Kinetics Model to be Used for Evaluation*	Thermally Limiting or Near Limiting (Typically)
INCREASE IN REACTOR COOLANT INVENTORY		
Inadvertent HPCIS or RCICS actuation	POINT	
DECREASE IN REACTOR COOLANT INVENTORY		
Inadvertent Safety/Relief Valve Opening	POINT	

* Not all transients are reanalyzed for operating plant reload applications.

\+ The Control Rod Withdrawal and Fuel Loading Error will be done using the three dimensional nodal code NDH which is described in Reference 1.

Table 4.1-2

SPECTRUM OF EVENTS FOR ASME VESSEL
OVERPRESSURE ACCEPTANCE CRITERIA EVALUATION

Event	Kinetics Model to Be Used for Evaluation
MSIV Closure with Position Switch Scram Failure (i.e., MSIV Flux Scram)	ONE-D

Table 4.1-3

SPECTRUM OF EVENTS FOR SYSTEM STABILITY ACCEPTANCE CRITERIA EVALUATION

Event	Kinetics Model to Be Used for Evaluation
Level Controller Setpoint Step	POINT
Pressure Controller Setpoint Step	POINT
Flow Controller Setpoint Step	POINT

Table 4.1-4

DYNODE-B OPTION MODEL SELECTION FOR LICENSING APPLICATIONS

Model Option	Licensing Value
Number of Oxide Radial Nodes	5
Number of Cladding Radial Nodes	2
Number of Axial Nodes	24
Oxide Heat Capacity	Curve Fit
Gap Heat Transfer Coefficient	Constant
Cladding Surface Heat Transfer Coefficient	Thom
Critical Power Ratio*	GEXL
Main Steam Line Representation	Method of Characteristics
Steam Dome Pressure Model	Based on Riser and Dome Fluid. Liquid assumed to be subcooled if dome $\Delta P/\Delta t \geq$ 1.0 psi/sec
Carryunder	Included
Turbine Model	Included
Pressure Regulator	Detailed
Void Model	Profile Fit Non-Equilibrium Flow Quality
Kinetics	See Tables 4.1-1, 4.1-2, and 4.1-3
Delayed Neutron Groups	6
Decay Heat	1971 ANS Standard
Bypass Heating	Included

* Fuel Vendor Dependent

Table 4.1-4 (continued)

Model Option	Licensing Value
Reactor Flow	Dynamic
Relief Valve	Bank
Relief Valve Stroking	Linear
MSIV Area versus Position	Non-Linear
Stop Valve Area versus Position	Non-Linear
Control Valve Area versus Position	Non-Linear
Bypass Valve Area versus Position	Non-Linear
Feedwater Controller	Detailed Three Element
Reactor Protection System Setpoints and Delays	Included
Radial Heat Generation	Included
Reactor Vessel Temperature Distribution Model	Included
M/G Flow Controller	Detailed with 2nd order Scoop Tube Servo Model
Heat Conductors	Ignored
Direct Moderator Heating	Included
Recirculation Pump Heating	Included

Table 4.1-5

SENSITIVITY OF CPR TO VARIOUS THERMAL-HYDRAULIC PARAMETERS

Parameter	[ΔCPR / Nominal CPR] / [ΔParameter / Nominal Parameter] GE [7]	DYNODE-B
Bundle Power	-1.0	-1.01
Bundle Flow	+0.2*	+0.29
Core Inlet Subcooling	+0.1	+0.06
Core Pressure**	-0.6	-0.56
GEXL R-factor	-2.1	-2.18

NOTE: All DYNODE-B cases performed at nominal Monticello HFP conditions ± 10%.

* Value for BWR/4

** Constant Subcooling

Table 4.2-1

INITIAL CONDITIONS AND INPUT PARAMETERS FOR DYNODE-B COMPARISONS TO ODYN AND REDY RELOAD SAFETY EVALUATION OF MONTICELLO

Parameter	Licensing Value
Initial Power (% NBR)	100
Initial Steam Flow (% NBR)	100
Initial Core Flow (% NBR)	100
Initial Feedwater Flow (% NBR)	100
Initial Core Inlet Enthalpy (Btu/lbm)	524.7 [7]
Initial Steam Dome Pressure (psia)	1038 [7]
Initial S/RV Steamline Pressure (psia)	1031
Initial Turbine Throttle Pressure (psia)	990
Initial Vessel Water Level (inches)	30
Core Exposure	EOC
Power Distribution	Haling
Heat Generated in Fuel (%)	96.5
Heat Deposited in Bypass (%)	1.5
Initial Core Bypass Flow Fraction (%)	10
Gap Heat Transfer Coefficient (Btu/hr ft^2°F)	1000
Void Model Parameters	Default Values
Critical Power Ratio	See Section 4.2.3
Plant Geometry	Monticello Unique
Initial Control Rod Pattern	All Rods Out
Control Rod Motion	All Rods with Same Speed
CRD Scram Time	See Section 4.2.2
Kinetics Parameters	See Section 4.2.1
Scram Setpoints	Tech Spec [12]
Reactor Protection Logic Delay	Maximum Tech Spec [12] (50 ms)
Relief Capacity	Tech Spec [12] (7/8 valves)
Relief Valve Setpoint	Tech Spec [12] (1119.1 psig)

Table 4.2-1 (continued)

Parameter	Licensing Valve
Relief Valve Response	Tech Spec [12] (400 ms delay/150 ms stroke)
Turbine Stop Valve Closure	Fastest Specified (100 ms)
Turbine Control Valve Closure	Fastest Specified (246 ms)
MSIV Closure	Fastest Tech Spec [12] (3 sec)
Flow Control	Manual
Flow Controller Setpoints	Monticello Unique
Feedwater Controller Setpoints	Monticello Unique
Pressure Controller Setpoints	Monticello Unique

Table 4.2-2

AXIAL POWER FACTORS FOR THE HOT CHANNEL MODEL

	Node	APF	Node	APF		Node	APF
(Bottom)	1	0.47	9	1.29		17	1.15
	2	0.55	10	1.34		18	1.08
	3	0.64	11	1.38		19	1.01
	4	0.74	12	1.40		20	0.93
	5	0.85	13	1.39		21	0.84
	6	0.97	14	1.36		22	0.74
	7	1.10	15	1.30		23	0.60
	8	1.21	16	1.23	(Top)	24	0.43

Table 4.2-3

STEADY STATE CRITICAL POWER RATIO COMPARISONS

FUEL TYPE	BUNDLE POWER (MW)	BUNDLE FLOW (10^3 lbm/hr)	CPR GE	CPR DYNODE-B
8x8	5.320	99.2	1.34	1.347
8x8R	5.683	98.3	1.37	1.369

Inlet Conditions: H_{in} = 524.2 Btu/lbm
P = 1038 psia

Table 4.3-1

FUEL CLADDING INTEGRITY LIMIT MCPR FOR MONTICELLO

Fuel Type	MCPR LIMIT
Reload Core 8x8	1.06
Reload Core 8x8R	1.07
Reload Core P8x8R	1.04
Reload Core BP8x8R	1.04
Reload Core GE8x8E	1.04
Reload Core GE8x8EB	1.04

Table 4.4-1

COMPARISON OF MEASURED VERSUS CALCULATED TRANSIENT ΔCPR/ICPR

Transient Event	ΔCPR/ICPR Measured	ΔCPR/ICPR Calculated	% Difference*
Peach Bottom Turbine Trip Test TT1	0.170	0.187	+10.0
Peach Bottom Turbine Trip Test TT2	0.136	0.149	+ 9.6
Peach Bottom Turbine Trip Test TT3	0.132	0.149	+12.9
Monticello Turbine Trip Start-Up Test	0.003	0.156	+5000

* % Difference = [(Calculated - Measured)/Measured] * 100

Table 4.4-2

COMPARISON OF MEASURED VERSUS CALCULATED
MAXIMUM TRANSIENT STEAM DOME PRESSURE

Transient Event	Maximum Steam Dome Pressure (psia) Measured	Calculated	% Difference*
Monticello Turbine Trip Start-Up Test	1130	1154	+2.0
Monticello MSIV Closure Start-Up Test	1084	1109	+2.3
Peach Bottom Turbine Trip Test TT1	1031	1047	+1.6
Peach Bottom Turbine Trip Test TT2	1038	1062	+2.3
Peach Bottom Turbine Trip Test TT3	1061	1082	+2.0

* % Difference = [(Calculated - Measured)/Measured] * 100

Table 4.4-3

COMPARISON OF MEASURED VERSUS CALCULATED
TRANSIENT POWER DECAY RATIO

Transient Event	DECAY RATIO Measured	Calculated	Difference*
Monticello Feedwater Controller Setpoint Step Start-Up Test	0.0	0.0	0.0
Monticello Pressure Controller Setpoint Step Start-Up Test	0.0	0.21	+0.21
Monticello Flow Controller Setpoint Step Start-Up Test	0.25	0.89	+0.64

* Difference = Calculated - Measured

5.0 CONCLUSIONS

This report is intended to show two major conclusions:

1) DYNODE-B is capable of accurately modeling all of the transient phenomena of a Boiling Water Reactor Nuclear Steam Supply System during abnormal transient events.

2) DYNODE-B, when used in conjunction with the methodology described in Section 4, conservatively predicts the transient response of a BWR NSSS.

The first conclusion is shown in Sections 2 and 3 of this report by first describing the models used and then benchmarking those models against other licensing computer codes and against transient test data.

The second conclusion is shown in Section 4 by first describing the methodology used and then quantifying it with test data.

Based on the information presented in this report, it is concluded that the Northern States Power Nuclear Analysis Department is capable of performing BWR Transient Licensing Analyses, within the limits described herein, utilizing the DYNODE-B computer code and the methodology described in this report.

6.0 REFERENCES

1. "Monticello Nuclear Generating Plant, Qualification of Reactor Physics Methods for Application to Monticello," NSPNAD-8609, Rev. 0, September 1986.

2. Northern States Power Co, "Monticello Nuclear Generating Plant Final Safety Analysis Report," Docket 50-263, November 1968.

3. Northern States Power Co, "Monticello Nuclear Generating Plant Updated Safety Analysis Report," Docket 50-263 October 1981.

4. General Electric Co., "Supplemental Reload Licensing Submittal for Monticello Nuclear Generating Plant Reload 10 (Cycle 11)," 23A1673, January 1984.

5. U.S. Nuclear Regulatory Commission , "Standard Review Plan for the Review of Safety Analysis Reports for Nuclear Power Plants," NUREG-0800, July 1981.

6. Northern States Power Co, "DNB86098 Computer Code Users Manual," June 1986.

7. General Electric Co., "General Electric Standard Application for Reactor Fuel," NEDE-24011-P-A-7-US, August 1985.

8. R.B.Linford, "Analytical Methods of Plant Transient Evaluations for the General Electric Boiling Water Reactor," NEDO-10802, February 1973, and Amendments 10802-01 and 10802-02.

9. General Electric Co., "Qualification of the One-Dimensional Core Transient Model for Boiling Water Reactors," NEDO-24154, October 1978.

10. R.C.Kern,et.al, "Best Estimate Analysis of Peach Bottom 2 Turbine Trip Tests at End of Cycle 2," NAI 77-49, August 1977.

REFERENCES (continued)

11. "Core Design and Operating Data for Cycles 1 and 2 of Peach Bottom Unit 2," EPRI-NP-0563, June 1978.

12. Northern States Power Co., "Monticello Nuclear Generating Plant Technical Specifications," Docket 50-263, License DPR-22.

13. "Monticello Nuclear Power Station Unit No. 1 Plant Transient Design Analysis Report," NEDC-10069, July 1969.

14. General Electric Co., "Monticello Unit No. 1 Startup Test Results," NEDO-10563, April 1972.

15. ASME Boiler and Pressure Vessel Code, Section III, Article NM-7000, "Protection Against Overpressure," American Society of Mechanical Engineers

16. "Transient and Stability Tests at Peach Bottom Atomic Power Station Unit 2 at End of Cycle 2," EPRI NP-564, June 1978.

17. Northern States Power Co., "Prairie Island Nuclear Power Plant Reload Safety Evaluation Methods," NSPNAD-8102P Rev. 3, March 1985.

18. "General Electric BWR Thermal Analysis Basis (GETAB): Data, Correlation and Design Application," January 1977 (NEDE-10958-PA and NEDO-10958-A).

19. "Basis for 8x8 Retrofit Fuel Thermal Analysis Application," September 1978 (NEDE-24131).

20. Letter, R. E. Engel (GE) to D. G. Eisenhut and R. L. Tedesco (NRC), "Additional Information, 8x8R Fuel GETAB R-Factors," March 30, 1979.

21. Letter, R. H. Buchholz (GE) to P.S. Check (NRC), "Response to NRC Request for Information on ODYN Computer Model," September 5, 1980.

22. J. M. Holzer, et.al., "A Code System to Produce Point Kinetics Parameters for LWR Calculations," ANS Trans, 39, 946-7, 1981.

7.0 Response to NRC Qestions

7.1 Question 1

Does the DYNODE-B fuel rod gap heat transfer coefficient account for exposure and fuel temperature dependence and, if not, what error does this simplification introduce?

Response

The DYNODE-B model for the gap heat transfer coefficient allows for the effects of fuel temperature and exposure to be included. However, in the current methodology neither of these effects is modeled. Instead, a constant value of 1000 Btu/hr ft^2 ^oF is used, as is done in the REDY and ODYN analyses performed by General Electric (References 7.1.1 and 7.1.2). As the fuel vendor, General Electric has reported that this assumption conservatively bounds the actual predicted values of gap conductance. The error introduced by this assumption is, therefore, in the conservative direction. The DYNODE-B model for the gap heat transfer coefficient is described in Equation (10) of the DYNODE-B user's manual.

Reference 7.1.1 NEDS-20016, "Monticello Nuclear Generating Plant Second Reload License Submittal," General Electric Co., October 1973.

Reference 7.1.2 NEDE-24011-P-A, "General Electric Standard Application for Reactor Fuel, " General Electric Co., Revision 8, May 1986.

7.2 Question 2

What direct moderator heating fraction is used and is this value conservative for the transients to be analyzed (Table 4.1-1, MSIV closure, etc.)?

Response

For these benchmarks, a constant value of 0.02 is used for the direct moderator heating fraction in all transients, as was done in the corresponding ODYN and REDY analyses. This is a nominal value based on General Electric's calculations of bypass heating and non-fuel heating fractions for the reloads in question.

This value may change for future reloads. For licensing purposes, a conservatively small bounding value will be determined on the basis of fuel design, bundle and channel geometry, void fraction, and control fraction. This value will normally be provided by the fuel vendor.

7.3 Question 3

Comparisons have been presented for the DYNODE-B and the Nuclear Data Handling (NDH) System prediction of control rod worth and void reactivity. How do DYNODE-B and NDH compare with respect to Doppler reactivity? Give a more detailed explanation as to why the DYNODE-B and NDH void and Doppler reactivities are so close.

Response

A comparison of the Doppler reactivities calculated with NDH and with DYNODE-B using cycle 11 data is shown below. The base case uses a core average fuel temperature of 917.6°K. The second case imposes a 50% increase in ΔT between the fuel and the moderator.

	k_{eff}	
	NDH	DNB
ΔT_{base}	1.0199	1.0199
(150% ΔT_{base})	1.0155	1.0155
Reactivity Change =	0.0044	0.0044

These results show that DYNODE-B and NDH Doppler feedbacks are equivalent when using 1-D collapsed parameters directly from NDH. The fact that the reactivity change obtained from DYNODE-B matches exactly with the NDH value is indicative of the precision of the collapsing procedure and the compatability of the neutronic models in NDH and DYNODE-B. The comparison using the transient tables is shown in section 7.24 of this report.

7.4 Question 4

In the DYNODE-B/REDY comparisons, what REDY input was unknown and how was it determined? Was this input data adjusted to improve the DYNODE-B/REDY comparisons?

Response

The purpose of the code to code comparisons is to show that comparable results are produced by modeling identical transients, rather than by using identical input parameters. There has therefore never been a direct comparison made between the DYNODE-B and REDY inputs, nor is one necessary.

In general, only the input data published in the FSAR or USAR, or the cycle-specific parameters determined jointly by GE and NSP are known to have been used in the GE analyses. These include fuel geometry, scram and ECCS initiation setpoints, relief valve setpoints and capacities, bypass valve capacity, certain kinetics parameters, and the initial plant conditions for the transient.

The unknown input included such items as the modeling of the various controllers; main steam line geometry, friction factors, loss coefficients, and valve characteristics; scram curve and scram system delay; ECCS pump curves; RCP characteristic curves and drive motor data; reactor vessel geometric and fluid region modeling; reactor vessel pressure drop coefficients and inertias; and delayed neutron modeling.

The DYNODE-B input decks were prepared on the basis of the Monticello FSAR, USAR, reload licensing submittals, plant drawings, equipment manuals, nuclear and thermal-hydraulics textbooks, engineering manuals, correspondence between NSP and General Electric, and several industry and General Electric publications. It is believed that much of the REDY input is taken from these same sources, and therefore much of the unknown REDY input should match that used in DYNODE-B.

The DYNODE-B input was based on the best available information and was not arbitrarily adjusted in order to improve the comparisons.

7.5 Question 5

The reduction in voids in the top of the core is expected to affect the axial albedo for the upper reflector. Has this effect been accounted for and, if not, what is the effect of this simplification on the DYNODE-B predictions?

Response

The axial albedos at the top and bottom of this core are assumed to be constant during the transient. These albedos are constant and equal to the corresponding NDH values for consistency with the 3-D reference models for the particular initial conditions. The axial albedo does not significantly affect the axial power distribution (and hence reactivity) for Monticello cores, since the top and bottom six inches of the fuel are natural U. The natural U regions act as buffers, reducing the importance of the fluid/structure reflector outside the active fuel region. In addition, the void fraction at the core exit (and hence in the reflector region) does not change significantly during the important portion of the transient, i.e., the period prior to the peak neutron power. The core exit void fraction changes by 2% to 3% during this period for the Monticello Cycle 11 benchmark cases. Thus, there is no significant effect due to this modeling assumption.

7.6 Question 6

Are any codes that have not been approved by the NRC being used to provide input to DYNODE-B?

Response

No. All DYNODE-B input is prepared by hand except for those physics parameters generated according to the methods described in NSPNAD-8609.

7.7 Question 7

The recirculation loop modeling for both REDY and ODYN has been verified by comparison to recirculation pump trip tests. Has similar qualification been performed for DYNODE-B?

Response

This model has been benchmarked for the case of a single RCP trip transient using the startup test data taken on the Susquehanna Unit 1 as described in Reference 7.7.1. These qualifications demonstrate the adequacy of the model for analysis of RCP trip transients. The recirculation loop modeling in DYNODE-B has been qualified for recirculation pump trip tests for Monticello as described in Section 3.2.2.2.3 of NSPNAD-8608.

Reference 7.7.1 R. C. Kern, "Qualification of a Loss-of-Recirculation Flow Model for Jet-Pump BWR's ," Trans. Am. Nuc. Soc., 54, 241 (1987).

7.8 Question 8

What is the direction of conservatism for each input parameter, for which a conservative uncertainty allowance will be included, for the transients to be analyzed (Table 4.1-1., MSIV closure, etc.)?

Response

The input parameters for each transient will be the nominal value for the void coefficient, Doppler coefficient, control rod worth (SCRAM), and kinetic parameters. A ΔCPR/ICPR uncertainty (see section 7.27) will be added to the calculated ΔCPR/ICPR for each transient to account for the model input uncertainties. Therefore, the uncertainties will not be applied to those input parameters.

7.9 Question 9

Are the void models in DYNODE-B and NDH identical? Are the values for the void concentration parameter, C_o, and drift velocity, V_{gj}, used in the NDH calculations the same as used in DYNODE-B? If not, what is the effect of this inconsistency on the K_∞ and M^2 calculated by DYNODE-B and on the DYNODE-B results?

Response

The void models in DYNODE-B and NDH are not identical, and the values of the void concentration parameter and drift velocities are different. This inconsistency is taken into account in the method used to compute the void reactivity feedback parameters which are input to DYNODE-B in the following manner. The NDH model is perturbed from the reference (initial) condition to produce a change in the local void fractions and hence k_∞ and M^2. Normally this perturbation is introduced by changing the subcooling and maintaining all other thermal hydraulic parameters constant. The DYNODE-B model is perturbed in an identical manner to generate the corresponding local void fraction changes. The changes in k_∞ and M^2 obtained from NDH are then correlated to the changes in the DYNODE-B void fraction changes. Thus, the two models predict the same change in reactivity for the same change in the boundary thermal hydraulics conditions, so that the overall results of the two models are self-consistent. Refer to section 7.24 for additional information.

7.10 Question 10

List all significant code and modeling differences between DYNODE-B, and REDY and ODYN and provide estimates of the effect of these differences on the DYNODE-B predictions when it cannot be demonstrated that the differences provide improved modeling or more conservative results.

Response

The significant code and modeling differences between DYNODE-B and REDY and ODYN codes are discussed in Sections 3.2.1.1 and 2.3, respectively, and are summarized below.

REDY

Dynamic Void Effects:

REDY: second order sweep model
DYNODE-B: profile-fit non-equilibrium flow quality void model

The profile-fit model in DYNODE-B is an improved model.

Decay Heat:

REDY: Stehn-Clancy Correlation (1965)
DYNODE-B: 1971 ANS Correlation

The DYNODE-B correlation offers improved modeling over the REDY correlation.

Cladding Surface Heat Transfer Coefficient:

REDY: Constant value
DYNODE-B: Thom correlation

The Thom correlation accounts for the effects of changing fluid and heat flux conditions, and therefore provides improved modeling.

ODYN

Core neutronics:

ODYN: one-group diffusion theory
DYNODE-B: total fission source nodal equations

The DYNODE-B nodal formulation can be derived from the one-group equations; these models are equivalent.

Decay Heat:

ODYN: exponential decay model
DYNODE-B: 1971 ANS correlation

The 1971 ANS Standard is a more sophisticated model for decay heat calculation.

3D to 1D radial collapsing:

The collapsing procedure for DYNODE-B is more rigorous than that used for ODYN, because the 3D and 1D neutronic models are identical in NDH and DYNODE-B, providing improved modeling by ensuring self-consistency between the 3D and 1D formulations.

Steam Line:

ODYN: single-phase 1D nodal representation
DYNODE-B: 1D conservation of mass, energy, momentum, and state - Method of Characteristic (MOC) Solution

The MOC methodology is more rigorous and does not assume that the steam is isentropic. This therefore represents improved modeling.

Reactor Vessel Pressure Distribution:

ODYN: explicit calculation of pressures at reactor inlet and reactor vessel dome
DYNODE-B: explicit calculation of dome pressure; reactor pressure based on transport delay between dome and core outlet.

Because the changes in pressure in the vessel dome during an overpressurization event are larger than those in the core, the DYNODE-B method conservatively overpredicts the core pressure.

These are the only significant differences known to exist between DYNODE-B and REDY and ODYN. Unknown differences may exist, but since the effects of any such differences are included in the benchmarks, and since those benchmarks show good agreement with REDY and ODYN, any unknown differences have little effect on the overall results.

Thus, for each of the modeling differences, DYNODE-B provides either improved or more conservative modeling.

7.11 Question 11

Reference 7 of the DYNODE-B user manual recommends the mechanistic rather than the profile-fit void model for transient applications. Since DYNODE-B allows both the mechanistic and profile-fit void model, what is the basis for the selection of the profile-fit model?

Response

The profile-fit model was selected on the basis of the results described in Reference 7.11.1. The major conclusion of that work is that the profile-fit model produced larger void fraction changes during over-pressurization events and hence resulted in a more conservative result. It has since been discovered that an error existed in the Reference 7.11.1 analysis, rendering it inconclusive. Nevertheless, the model qualification presented in NSPNAD-8608 has demonstrated the adequacy of the use of the profile-fit model for transient applications for Monticello based on comparisons to test data and other licensing calculations.

Reference 7.11.1 R. C. Kern, et. al. "Qualification of an Advanced BWR Transient Model for Pressurization Transients," Trans. Am. Nuc. Soc. 39, 629 (1981).

7.12 Question 12

The DYNODE-B definition of the volumetric flow fraction, β, the concentration parameter, C_o, and the drift velocity, V_{gj}, involve arbitrary constants (viz., C_{00}, C_{01}, b_1, β_1, V_{gj1}, V_{gj2}). How are these constants determined and what uncertainty is introduced into the DYNODE-B calculations by the selection of these constants? Also, the definition of β in DYNODE-B appears to be in error.

Response

The constants used to define the void concentration parameters, the drift velocity, and β are given in Reference 7.12.1, which are the DYNODE-B code default values. The uncertainties associated with these values are included in the total model uncertainty, which the benchmarks show to be conservative. The defining equation for β in the DYNODE-B user manual is incorrect, but the coding uses the correct definition. The user's manual will be corrected to read:

$$\langle\beta\rangle = \frac{\langle x\rangle\beta_1}{\langle x\rangle+(\rho_g/\rho_1)\,(1-\langle x\rangle)} \qquad (36)$$

Reference 7.12.1 R. T. Lahey, Jr. and F. J. Moody, "The Thermal-Hydraulics of a Boiling Water Nuclear Reactor," ANS Monograph Series on Nuclear Science and Technology, 1977.

7.13 Question 13

Describe in detail the core thermal-hydraulic model used to determine the axial pressure, void, flow and enthalpy distributions. Have the resulting equations been tested for numerical stability?

DYNDOE-B assumes a constant pressure across the core. This assumption may be nonconservative because the use of nodal pressure would result in a higher relative power peaking in the top of the core than assuming constant pressure.

Response

The profile-fit non-equilibrium flow quality model used in this analysis is described in detail in section 3.3.2 of the DYNODE-B manual. The axial void distribution is determined by computing the void fractions at the ends of each axial node, and the node average void fraction is obtained by assuming a linear distribution within each node. For the first node in which voids appear, the void fraction is assumed to be linear between the point of bubble detachment and the top end of the node.

Because the pressure drop across the core is relatively small, and because in practice most of the drop occurs across the bottom core plate rather than in the active fuel region, the actual pressure variation from node to node is small enough to be of little impact in determining conditions in each node when compared to the much larger effect of such changing variables as fluid enthalpy. Therefore, in performing core calculations, the core pressure is assumed to be axially uniform.

The axial flow distribution is determined by the conservation of mass. The enthalpy distribution is determined by simultaneously solving the equations of conservation of mass and energy (refer to Eqn (15) in the DYNODE-B manual).

These equations are solved using the Runge-Kutta-Merson method as referenced in the manual. Numerical stability is ensured by choosing the input parameters such that the code selects adequately small time steps which are much less than the Courant limit.

The DYNODE-B core pressure model is conservative for the following reasons which are based on a consideration of overpressurization events.

- The initial core pressure is assumed to be the Reactor Vessel (RV) dome pressure which is less than the actual core pressure resulting in a higher initial void fraction in the core. The transient core pressure is obtained from the RV dome pressure response which is time-delayed to represent the transport delay from the dome to the core exit. The increase in the RV dome pressure is greater than or equal to the core pressure increase because of dissipation in the sonic wave as it passes from the dome to the core. This effect can be seen in the pressure responses recorded for the Peach Bottom Turbine Trip Tests.

- The core pressure increase at the core exit is then conservatively applied throughout the core by the assumption that the core pressure is axially uniform.

- This uniform increase in pressure causes a higher absolute power increase at each axial location of the core, because the reactivity addition at each axial node will be larger. The increase in absolute power with smaller relative power peaking for the uniform increase in pressure will give a higher heat flux at the top of the core than the axially varying pressure.

- Even though the relative peak in the top of the core is larger with the axially varying pressure, the influence of the scram on the absolute power in the top of the core for the case of uniform pressure will not be overestimated. The reason for this effect is that the neutron population is larger in the top of the core prior to the scram with the uniform pressure assumption.

Therefore, using the uniform increase in pressure is conservative.

7.14 Question 14

In the calculation of steam dome pressure, what uncertainty is introduced by the use of the "steam-dome pressure model" rather than the "non-equilibrium steam-dome pressure model"?

Response

The model qualifications presented in NSPNAD-8608 demonstrate that the steam-dome pressure model used in the analysis consistently produces conservative results. It is therefore unnecessary to apply uncertainties due to the choice of pressure model.

7.15 Question 15

In the static flow distribution calculation, how is the bypass flow fraction determined and does it vary during the transient?

Response

The initial bypass flow fraction is an input parameter. Its value is chosen to be identical to the value used in NDH for the core physics calculations. During initialization, DYNODE-B calculates the corresponding bypass pressure drop coefficient in order to establish the desired bypass flow fraction at initial, steady-state conditions. The bypass flow then varies during the course of the transient according to the equations of conservation of momentum.

7.16 Question 16

How are the feedwater flow, recirculation flow, power level, turbine bypass and stop valve controller lead-lag, lag and controller constants determined and do they change for each cycle?

Response

The lead, lag, and controller constants used in modeling the various controllers represented in DYNODE-B are based on references 7.16.1, 7.16.2, and 7.16.3. Other controller data is assembled from the Monticello Operations Manual, the FSAR, and correspondence between NSP and GE. This data is not cycle-specific and would normally only be altered if the controllers themselves were modified.

Reference 7.16.1 NEDC-10069, "Monticello Nuclear Power Station Plant Transient Design Analysis Report," General Electric Company, July 1969.

Reference 7.16.2 NEDO-10563, "Monticello Unit No. 1 Startup Test Results," General Electric Company, April 1972.

Reference 7.16.3 NEDO-10802, "Analyical Methods of Plant Transient Evaluations for the General Electric BWR," General Electric Company, February 1973.

7.17 Question 17

The flux, ϕ, rather than the source, $S=\nu\Sigma_f\phi$, satisfies the standard time-dependent diffusion equation. Has the additional term $\phi\partial_t(\nu\Sigma_f)$ been accounted for in the DYNODE-B source equations and, if not, what error is introduced by this approximation?

Response

The derivation of the time-dependent source equation used in DYNODE-B from the standard diffusion equation results in the left hand side (LHS) of Equation 80 of the user's manual as:

$$LHS = \frac{1}{v}\,\partial_t\,\phi$$

Multiplying the numerator and denominator by the initial value of $\nu\Sigma_f$ yields:

$$LHS = \frac{1}{v\nu\Sigma_f(0)}\,\nu\Sigma_f\,(0)\,\partial_t\phi$$

$$= \ell_0\,\partial_t\,(\nu\Sigma_f(0)\phi) \simeq \ell_0\,\partial_t S$$

Since DYNODE-B uses the initial value for ℓ and assumes it to be constant, it is necessary to explicitly omit the $\phi\partial_t(\nu\Sigma_f)$ term for consistency. This formulation introduces only a small error, since the neglected terms are relatively small for events which result in large neutron flux changes due to significant reactivity changes. In these cases, the major changes in the source are due to changes in flux rather than in $\nu\Sigma_f$.

7.18 Question 18

What is the mechanism responsible for the underprediction of the scram curves (Figure 3.1-4) and can this result in a non-conservative overprediction for other static and transient states?

Response

The results presented in section 3.1.1 of Revision 0 for the scram curve calculations were based on comparing the change in K-effective relative to the all-rods-out case. For the DYNODE-B cases, the k_∞ and M^2 axial distributions were the 1-D collapsed values as produced by NDH. Hence, these differences were attributable to the use of the collapsed 1-D parameters in the 1-D neutronic static model.

The results presented in section 3.1.1 of Revision 1 establish the fact that this difference will not result in an overprediction of the scram worth in DYNODE-B for transient states, since the methodology which is used to calculate the dynamic scram effects produces a conservative underestimate of the scram insertion for the important portion of the transient (i.e. the time prior to the occurrence of the MCPR). This underestimation is the net effect of the differences noted above and the manner in which the scram reactivity parameters are generated utilizing the data from the all-rods-out and all in but the highest worth rod fully inserted case data produced by NDH. The latter effect demonstrates that the scram rod reactivity is conservative below 88% insertion.

7.19 Question 19

How do the DYNODE-B and ODYN peak powers in the load rejection, feedwater controller failure and MSIV closure transients of Figure 3.2-93, 3.2-100 and 3.2-107, respectively, compare? Are these differences due to DYNODE-B and ODYN modeling differences and, if so, why should they not be considered as a measure of the uncertainty in performing transient analyses of Monticello reloads?

Response

The figures provided by the vendor which document the results of the ODYN analyses do not show values beyond those presented in Figures 3.2-93, -100, and -107. Thus, it is not possible to compare the peak powers between DYNODE-B and ODYN. Differences in peak power predictions are due to both modeling and input differences. Because of the extremely high slope of the power spike during these transients, the predicted peak value is highly sensitive to any changes which affect the time at which the peak occurs; thus, meaninglessly small input changes can produce large changes in peak power.

However, the peak power is of less importance than the integral under the power curve, since this latter value determines the energy deposition in the fuel and hence the heat flux and ΔCPR. Because the power spike is quite narrow, the area is relatively insensitive to the peak value, and is not unduly sensitive to minor changes. Comparisons of the heat flux curves indicate that DYNODE-B does yield reasonable agreement with ODYN for the transient heat flux response. Those differences which are attributable to void and scram reactivity parameters used in the two different models are discussed in the respective sections of this report. No additional uncertainties are required for performing transient analyses of Monticello reloads because of these differences.

7.20 Question 20

Describe how DYNODE-B is used in the calculation of the fuel misloading error and how the reactivity input is determined. How are radial redistribution effects accounted for?

Response

DYNODE-B is not used in the calculation of the fuel misloading error. This event is evaluated with the NDH and CASMO computer codes which are described in report NSPNAD-8609. For the mis-oriented or rotated bundle, CASMO will be run to determine the increase in the fuel type local peaking factor. For the mis-located bundle, NDH will be run to determine the effect on the core power distribution. There was an error on Table 4.1-1 in Revision 0 of this report stating that the fuel loading error is evaluated using point kinetics. Table 4.1-1 has been corrected in Revision 1 of this report.

7.21 Question 21

In the application of DYNODE-B to the control rod withdrawal event, what error is introduced by not including the radial flux distribution changes explicitly in the calculation? Does the non-equilibrium model include the time dependent mass and energy balance for the (1) riser and dome steam (2) riser liquid (3) dome liquid and (4) the entrapped steam. If not, what error is introduced by this approximation?

Response

The control rod withdrawal error event is analyzed with the 3-D nodal code, NDH, which calculates the effects of radial and axial flux redistribution. DYNODE-B may be used to determine the transient pressure response to this event, so that the influence of the changing pressure may be included in the NDH calculations if desired.

The non-equilibrium steam dome pressure model does include the time-dependent mass and energy balance for each of these four thermodynamic "compartments".

7.22 Question 22

Explain any differences between the Table 4.2-1 initial conditions and input parameters and the corresponding values and conditions assumed in the ODYN analyses. What effect do these differences have on the DYNODE-B predictions of ΔCPR, peak pressure and decay ratio for the transients to be analyzed?

Response

The initial conditions listed in Table 4.2-1 are those used in the DYNODE-B comparisons to ODYN and REDY; these will not necessarily be unchanged for future reload analyses. For clarification, Table 4.2-1 has been retitled in Revision 1 of this report to "Initial Conditions and Input Parameters for DYNODE-B Comparisons to ODYN and REDY Reload Safety Evaluations of Monticello."

The only known differences between these conditions and those used in the ODYN analysis are as follow:

	DYNODE-B	ODYN	Comments
Core inlet enthalpy (Btu/lbm)	524.7	524.2	Corresponds to rated steam flow. No other significant impact is expected.
Turbine Control Valve closure (msec)	246	300	The TCV closure in DYNODE-B is completed 54 msec sooner than in ODYN, making the resulting pressure spike slightly more severe.
Initial Vessel Water Level-Sensed (inches)	36.9	36.5	Table 4.2-1 of Revision 0 contained a typographical error: the initial DYNODE-B water level is 30 inches, which corresponds to a sensed level of 36.9 inches. No significant impact on the transient results due to this difference is expected.

The known differences in initial conditions are slight, and are expected to have no noticeable effect on the transient results.

7.23 Question 23

How are the uncertainties in the bundle power and relative inlet flow due to differences in the static and transient radial power and flow distributions accounted for in the determination of ΔCPR?

How is the time dependence of power and flow distribution handled? What is the uncertainty?

The peak power location will generally have a higher void content and undergo a larger increase in local power upon void collapse during an overpressurization transient. Based on the LPRM transient response during the PB-2 turbine trip tests, what is the increase in local power at these high powered locations?

Response

The uncertainties in bundle power and flow during the transient are assumed to be the same as those associated with the initial conditions, except for small radial changes during the transient. The ratio of the transient to initial CPR is expected to be uniform throughout the core, since the radial power distribution (and hence flow distribution) remains relatively unperturbed during the transient.

This can be shown by measuring the peak LPRM responses recorded during the Peach Bottom turbine trip test TT1 and then averaging the four LPRMs per string to obtain a LPRM string peak. The increase in the LPRM string response is used to represent the increase in the bundle thermal power. The MCPR is inversely proportional to the peak bundle thermal power. The mean value of the LPRM string peaks for test TT1 is 468.5% with a standard deviation of 4.3%. Assuming a normal distribution, the 95/95 uncertainty would be 10.6%. Assuming that the CPR changes inversely with the bundle power which is proportional to the change in LPRM string response, the change in ΔCPR/ICPR is .0045 for a change in the LPRM string peak power from 468.5% to 479.1%. The LPRM string with the highest initial power had a string peak change of 472.4%. This is within one standard deviation of the mean value of all the LPRM string peaks.

To ensure that a conservative ΔCPR is evaluated for each transient, a set of bundles with different initial powers and flows will be determined such that the minimum transient CPR for each of these bundles will equal the safety limit.

This set will be selected on the basis of physically realistic initial conditions which are assumed at the onset of the event. The bundle with the highest ICPR will then be used to calculate the ΔCPR for the event.

The uncertainties in the absolute bundle power and flow are taken into account in the input parameter uncertainty factor which is applied to the ΔCPR/ICPR as established from the sensitivity study evaluation in section 7.27 of this report.

7.24 Question 24

What range of operating state variables, including power level, flow, inlet subcooling, control rod pattern and exposure, were used to determine the collapsing factor (AF)? Demonstrate that this set of states is sufficient in view of the wide range of intended applications (Table 4.1-1, MSIV closure, etc.). What is the Doppler reactivity collapsing factor (AF) and how is this uncertainty accounted for?

Do the AF factors account for the change in state?

Response

The range of the operating state variables used to generate the feedback parameters are determined for each specific transient which is being analyzed and is sufficient to cover the range over which these variables change during the important portion of the event; i.e., up to the time of the minimum CPR. The manner in which the range is covered is also consistent with the manner in which the variables change during the event and cover the changes in going from the initial to the maximum perturbed states. The feedback parameters are obtained by considering the changes between the two extreme states. As an example, consider an overpressurization transient in which void collapse occurs. For this case, the void reactivity parameters are calculated using the NDH and DYNODE-B models, as described in section 7.9, by increasing the core pressure and maintaining the inlet enthalpy which effectively increases the subcooling. The core pressure change is at least as large as the value which occurs at the time of the minimum CPR. The axial collapsing factor for the void reactivity is determined for this same specific set of conditions and calculations, as follows. The base case DYNODE-B K^{∞} and M^2 distributions are identical to those obtained from the collapsed NDH results. For a perturbed case, DYNODE-B is used to establish the change in the local moderator density. This change in density is used in conjunction with the feedback tables which are used by the code to determine the changes in K^{∞} and M^2 which are then applied to the base values. DYNODE-B is then run to calculate K-eff for the base and perturbed cases and this change is compared to the K-eff change obtained from NDH. The ratio of

the DYNODE-B to NDH K-eff changes are defined as (1+AF). In the case for the void reactivity, an AF>0 is indicative that DYNODE-B is conservative and hence no additional uncertainty is required due to the collapsing process. Thus, AF is determined in an appropriate manner for each specific case and over the appropriate range for the feedback parameters. The AF factors for Doppler and scram are determined in a similar manner. If the AF factor is less than zero for Doppler and scram reactivities, DYNODE-B is conservative relative to NDH. The opposite is true for void reactivities.

The above described procedure has been used to calculate the data needed to establish AF factors for two sets of conditions, namely, the maximum perturbed state and an intermediate state, for the scram, void, and Doppler parameters. The results are shown in Table 7.24.1 in terms Δk-eff for the intermediate and maximum perturbed cases relative to the base case for both DYNODE-B and NDH.

The results reported here are based on the Cycle 13 core design, whereas section 7.3 relates to results based on the Cycle 11 core design as reported in Revision 0. This accounts for the difference in Δk-eff Doppler between the two revisions.

The results shown on Table 7.24.1 indicate the following. Since AF>0 for the void, the DYNODE-B model is conservative and hence the AF need not be considered for voids. Since AF>0 for the Doppler, the DYNODE-B model is not conservative and hence an additional uncertainty is applied to the ΔCPR/ICPR model uncertainty. The scram results indicate that AF<0 for the intermediate case and AF>0 for the maximum perturbed case. The results shown in Figure 3.1 of Revision 1 of this report indicate that AF<0 for nodes 1 through 21 which concerns the important time of the transient, so that the AF for the scram also need not be considered.

TABLE 7.24.1

Reactivity Changes for DYNODE-B and NDH

	Base Case	Intermediate Case	Maximum Perturbed Case
Scram			
Rod Position	ARO	21% Inserted	ARI
Δk (DYNODE)		-.0020	-.1688
Δk (NDH)		-.0022	-.1663
Void			
Core Average Void	.396	.378	.362
Δk (DYNODE)		.0016	.0032
Δk (NDH)		.0015	.0029
Doppler			
Core Average Fuel Temperature	801 °K	870 °K	944 °K
Δk (DYNODE)		-.0022	-.0043
Δk (NDH)		-.0021	-.0041

Note: $\Delta k = k_{eff}$ (perturbed) - k_{eff} (base)

7.25 Question 25

Describe in detail the method used to determine the DYNODE-B equivalent one-dimensional k^{∞}, M^2, g_v and albedos from the three-dimensional NDH solutions. Describe the perturbed states used in this determination in terms of core power, flow, inlet subcooling, pressure and exposure.

Demonstrate that these selected perturbed states provide an adequate representation of the transient states encountered in the events to be analyzed (Table 4.1-1, MSIV closure, etc.). How are the k^{∞}, M^2, g_v and albedos determined for the control rod insertion/withdrawal events?

The DYNODE-B neutronics parameters are represented as a function of local void fraction and fuel temperature. The void fraction dependence, for example, is determined by performing perturbation calculations with both DYNODE-B and the three-dimensional simulator program NDH. In the NSP procedure (described in response to question 9), the change in neutronics parameters observed in NDH (as a result of void changes in NDH) is correlated as a function of the void fraction calculated by DYNODE-B. Since there are substantial differences between the DYNODE-B and NDH system modeling and void calculations, this procedure introduces an additional uncertainty into the DYNODE-B calculation. What is the effect of this procedure on the DYNODE-B predictions?

Response

The method for determining the DYNODE-B equivalent one-dimensional k^{∞}, M^2, g_v and albedos from the three-dimensional NDH solutions is described in detail in Reference 7.25.1. This reference describes the technique for both the initial conditions and the feedback parameters. The method for determining the perturbed states is also described in the sections which deal with generation of the feedback parameters with the following changes:

1. Fuel Temperature
   In NDH the local reactivity changes are represented by the equation in section 2.2.2.2 of the NDH manual. The change in the NDH cases is done by changing the input value to B20 and not PR as stated in Reference 7.25.1. The effect is exactly the same.

2. Delayed Neutrons
   The BELLEROPHON program is not used as discussed in Reference 7.25.1. The delayed neutron parameters are calculated as shown in the NDH manual section 2.2.5.

3. Source to Power Ratio
   The equation to calculate the source to power ratio is shown in section 2.2.3 of the NDH manual.

Reference 7.25.1 also covers the cases in which control rods are either inserted or withdrawn.

Through comparison to measured data, NDH has been shown to calculate reactivities with a known reliability factor for given core conditions. Since void distributons cannot be measured, it is not known whether the specific void distribution calculated for those conditions is also correct. For this reason, the goal in preparing DYNODE-B input from NDH results is not to preserve the ratios of $\Delta k^{\infty}/\Delta U$ or $\Delta M^2/\Delta U$ from NDH, since these are not known to be correct, but rather to ensure that DYNODE-B reproduces the core reactivity predicted by NDH for any given statepoint. These statepoints are specified in terms of thermal-hydraulic conditions which are measured and used in the model qualification process.

Because the thermal-hydraulic models which calculate the void distribution and fuel temperature in DYNODE-B are different from those in NDH, these parameters are expected to be different between the two codes for any given statepoint. Since void reactivity effects and fuel temperature effects are modeled in DYNODE-B as changes in k^{∞} and M^2 corresponding to the changes in water density and fuel temperatures calculated by DYNODE-B, it is necessary to transform these parameters from the NDH-generated values to the corresponding DYNODE-B values in order for DYNODE-B to reproduce the core reactivity predicted by NDH for any given statepoint.

As described in Reference 7.25.1, this transformation is done by running two NDH cases at different statepoints to determine the changes in k^{∞} and M^2 for that change in statepoint, then running two DYNODE-B cases at the identical statepoints to determine the change in moderator density which DYNODE-B

associates with that statepoint change. This data is then used to construct the DYNODE-B input tables of Δk^{∞} and ΔM^2 versus ΔU. The validity of this method is demonstrated in the response to Question 24.

This methodology is identical in nature to that described in section 2.5.1.1 of Reference 7.25.2, in which the cross sections calculated by the CORE code are correlated as a function of RETRAN thermal-hydraulic parameters. This same approach is also recommended in Reference 7.25.3, where the RAMONA-3B polynomial coefficients for the cross sections are recomputed using the TRAC-BF1 hydraulic properties.

Two turbine trip without bypass transients were run to determine the effect of correlating the DYNODE-B neutronics parameters to void fractions and fuel temperatures calculated by NDH versus DYNODE-B. The first case correlated the neutron parameters to DYNODE-B void fraction and fuel temperatures. The ΔCPR/ICPR for this case is 0.157. The second case correlated the neutron parameters to NDH void fraction and fuel temperatures. The ΔCPR/ICPR for this case is 0.137.

The local void reactivity coefficient is larger in the top of the core and smaller in the bottom of the core when using the DYNODE-B void fraction versus using the NDH void fraction. Since the power shape shifts to the top of the core during this transient, using the DYNODE-B void fraction is conservative as demonstrated from these results. It is believed that correlating the neutronics parameters to the DYNODE-B void fraction and fuel temperature is correct and that there is no additional uncertainty in the model.

Reference 7.25.1 R. C. Kern, "Methods and Guidelines for Obtaining One-Dimensional Nodal Constants for DYNODE-B from Three-Dimensional Nodal Calculations," NAI 82-26, Rev. 1, May 20, 1982.

Reference 7.25.2 TVA-TR81-01-A, "BWR Transient Analysis Model Utilizing the RETRAN Program," Tennessee Valley Authority, April 7, 1983.

Reference 7.25.3 W.L.Weaver III and K.C.Wagner, "One-Dimensional Neutron Kinetics in the TRAC-BF1 Code," Proceedings Anticipated and Abnormal Transients in Nuclear Power Plants Conference, Atlanta, Georgia, April 12-15, 1987, Volume 1, p. VII-60, Section 2.3.

7.26 Question 26

The ODYN model has had difficulty in predicting core inlet flow oscillations above 5 hz. If DYNODE-B will be required to analyze oscillations above this frequency, demonstrate that DYNODE-B does not have the same difficulty.

Response

Because of the uncertainty in obtaining the test rig design and test data for jet pump flow oscillation measurements, stability analyses with DNB will be restricted to events with flow oscillations of less than 5 hz.

7.27 Question 27

The qualification data base provided to demonstrate the accuracy of the DYNODE-B code (e.g., Tables 4.4-1, 4.4-2 and 4.4-3) is insufficient in the number and quality of the comparisons to allow a reliable estimate of the code uncertainty. For example, the Peach Bottom turbine trip calculations were normalized to insure that DYNODE-B reproduced the measured peak and integrated power, and the comparison for the Monticello turbine trip startup test includes a large (-300%) DYNODE-B/measurement transient power discrepancy. A detailed code uncertainty analysis is therefore required to insure there is sufficient margin to the thermal-hydraulic design basis and the reactor coolant pressure boundary limit.

Provide a listing of the important sources of uncertainty in the DYNODE-B predictions required for the intended reload analyses. Consideration should be given to factors such as: void coefficient, controller set points, jet pump loss coefficients, scram reactivity, void model, separator model, steam line model, neutronics collapsing, etc. Estimate the 95% probability limits for these uncertainties, and determine the corresponding ΔCPR/ICPR for each uncertainly for the turbine trip without bypass transient. Determine the corresponding Δ-pressure (%) for each of these uncertainties for the MSIV closure event with position switch scram failure. Also, provide an estimate of the corresponding uncertainty in the calculated decay ratio.

Additional items concerning the DYNODE-B uncertainty analysis:

(a) What uncertainty is introduced into the DYNODE-B calculations as a result of uncertainty in the core void coefficient (defined in terms of the core-wide reactivity response to a change in core void fraction)?

(b) What uncertainty is introduced into the DYNODE-B calculations as a result of the profile-fit void model?

(c) The Monticello Cycle-13 DYNODE-B prediction of ΔCPR/ICPR is 0.1556. What is the corresponding GE prediction?

Response

Sensitivity studies using three transients were run in order to determine input parameter uncertainties. The turbine trip without bypass transient was used for the ΔCPR/ICPR uncertainty, the MSIV closure with high flux scram was used for the pressure uncertainty, and the automatic flow controller decrease transient was used for the power decay ratio uncertainty. The parameters used to perform the sensitivity studies are listed in Table 7.27-1. Any additional parameters which could affect the uncertainty were included in the sensitivity discussed below, and the results are summarized in Tables 7.27-2 through 7.27-4.

Turbine Trip Without Bypass Sensitivity Study

The turbine trip without bypass transient was established using conservative licensing basis modeling criteria for Monticello Cycle 13. The transient was run under the following initial conditions; 100% power and core flow, 100% steam flow, 1040 psia steam dome pressure, all rods out, and Haling end of hot full power depletion. The results of the sensitivity study are summarized in Table 7.27-2.

The key physics parameters of interest are the void coefficient, Doppler coefficient, and the scram reactivity. In addition, the sensitivity to the effective total delayed neutron decay fraction was also determined. The results in Table 7.27-2 show that both the void and Doppler coefficient uncertainties compare well with results from past sensitivity studies. The relative insensitivity of the scram reactivity in comparison to past analyses is due to a difference in methodology. Past analyses have adjusted the scram velocity to achieve a 10% reduction in reactivity insertion at the time of peak heat flux. In contrast, NSP's analysis reduced the total control rod bank worth by 10%. Using the procedure of reducing the scram velocity by 10%, a change in ΔCPR/ICPR of -.014 was obtained, which compares well with past results. However, the method used by NSP is both conservative and appropriate for two reasons. First, the reduction of the total control rod bank worth, instead of the scram velocity, applies the 10% uncertainty to the correct parameter. Second, NSP's model already uses a conservative scram insertion rate because the scram velocities are the slowest allowable by Technical Specification limits.

There was also a relatively small change in ΔCPR/ICPR for the effective total delayed neutron fraction sensitivity study. The delayed neutron fraction will not demonstrate a large sensitivity to the ΔCPR/ICPR until the core approaches prompt criticality. At the time of the peak k-eff in this transient, the total core reactivity was 0.56 dollars, which is not close to prompt critical.

The uncertainties in the parameters included in the recirculation system model and the steam line model of Table 7.27-2 are relatively small. The DYNODE-B code conservatively uses the steam dome pressure, rather than a core average pressure, in calculating a power response during a transient. The parameters in question have a relatively small influence over the steam dome pressure as is seen in Table 7.27-4.

There are several additional parameters which have been included in Table 7.27-2. The axial collapsing factor (AF) uncertainties for the void coefficient, Doppler coefficient, and scram reactivity are discussed in detail in section 7.24. The radial power redistribution uncertainty is discussed in detail in the response to Question 23. Although it is included in the calculation of the overall uncertainty, it is not a significant factor.

A value of 0.021 was obtained for the ΔCPR/ICPR input parameter uncertainty.

MSIV Closure With High Flux Scram Sensitivity Study

The MSIV Closure with High Flux Scram was established using conservative licensing basis modeling criteria for Monticello Cycle 13. This transient was run under the following initial conditions: 100% power and core flow, 100% steam flow, 1040 psia steam dome pressure, all rods out, and Haling end of hot full power depletion. The scram on MSIV closure is disabled. The results of the sensitivity study are summarized in Table 7.27-3.

The key parameters of interest in this transient are the void coefficient, Doppler coefficient, the scram reactivity drift velocity and core pressure drop. The results in Table 7.27-3 show that these parameters also produced the largest uncertainty in the vessel pressure, as expected.

The ΔP input parameter uncertainty of 5.5 psi is comparable to past analyses. The 5.5 psi uncertainty is small in comparison to the ASME vessel overpressure limit material bias of approximately 310 psi. Therefore, the ΔP input parameter uncertainty does not need to be taken into account in the DYNODE-B calculations.

Automatic Flow Controller Decrease Sensitivity Study

Sensitivity studies for the automatic flow controller decrease transient were performed with the Monticello Cycle 1 startup test case. The Cycle 1 case was selected because it exhibited larger power oscillations than the current cycles and would therefore be more conservative. In any sensitivity study cases in which the power oscillations produced a scram (typically on high or low vessel water level), an additional conservatism was added by disabling that scram and allowing the power oscillations to continue. The results of the sensitivity study are summarized in Table 7.27-4.

Most parameters are relatively insensitive in this transient and produce small uncertainties. The largest uncertainty is due to a +100% change in the speed controller of the motor/generator recirculation flow controller. The +100% reliability factor in the speed controller is an excessively conservative value intended only to provide a bounding analysis. When more data becomes available a determination of a more appropriate reliability factor may be made along with a new input parameter uncertainty.

A value of 0.19 was obtained for the power decay ratio input parameter uncertainty.

Additional Items Concerning the DYNODE-B Uncertainty Analysis

(a) To determine the core wide void coefficient, ΔK-eff was calculated for two DYNODE-B cases. The first case was the base case and the second case had the local reactivity coefficients changed by 10%. The ΔK-eff showed a 10.1% change for the 10% change in local reactivity values. This difference results because the power shifts to the top of the core where the larger local void coefficients exist. This change will be essentially the same for the turbine trip without bypass analysis; therefore, there is no additional uncertainty in the model.

(b) The uncertainties associated with the DYNODE-B profile-fit model for subcooled voids was assessed by comparisons with data given in References 7.27.1 and 7.27.2 over a wide range of pressure and heat flux conditions. This same data base was used in the model qualifications presented in Reference 7.27.3. The 95/95 model reliability factor for the subcooled void fraction was determined to be 0.071 (7.1%). Thus the DYNODE-B base case was changed to effectively increase the void fraction in the subcooled region by 7.1%.

(c) The following tables show a comparison between the cycle 13 transient results obtained using GE and NSP methods:

	ΔCPR/ICPR			
Transient	GE (Point)	GE (1-D)	NSP (Point)	NSP (1-D)
TT W/O BP	-	0.137	-	0.157
FWCF	-	0.130	-	0.147
LFWH	0.116	-	0.101	0.105

The ΔCPR/ICPR's do not include uncertainties except for the GE and NSP point kinetics calculation of the loss of feedwater heating.

	MCPR			
	GE (Option A)	GE (Option B)	NSP (Point)	NSP (1-D)
TT W/O BP	1.30	1.25	-	1.30
FWCF	1.29	1.24	-	1.29
LFWH	1.21	1.21	1.19	1.22

All MCPR's include uncertainties. For NSP 1-D analyses, the uncertainty is 0.021 ΔCPR/ICPR.

The limiting MCPR is 1.30 for GE option A, 1.25 for GE option B, and 1.30 for NSP. This shows that the NSP model with a .021 ΔCPR/ICPR uncertainty gives the same MCPR as GE option A.

Errors were found in the physics input to the turbine trip without bypass transient during the verification process. The correct ΔCPR/ICPR value for the turbine trip without bypass transient using NSP methods as described in this report is .1569, and not the .1556 or other draft values discussed.

The MSIV closure transient was also run for cycle 13. The GE pressure increase was 160 psi and the NSP pressure increase was 167 psi without uncertainties. The maximum reactor vessel pressures including uncertainties are 1227 psia for GE and 1245 psia for NSP.

TABLE 7.27-1

INPUT PARAMETER UNCERTAINTIES USED FOR SENSITIVITY STUDIES

Parameter	Uncertainty
I. Reactor Core Model	
1. Nuclear Model	
a. Core Average Void Coefficient	α_v ± 10%
b. Core Average Doppler Coefficient	α_d ± 25%
c. Scram Reactivity	α_s ± 10%
d. Prompt Neutron Heating	Conservative
2. Thermal Hydraulic Model	
a. Drift Flux Parameter	
i. C_o	1.0
ii. V_{gj}	±30%
b. Profile Fit Model (subcooled void)	+7.1%
3. Fuel Heat Transfer Model	
a. Pellet Heat Distribution	Conservative
b. Pellet Heat Transfer Parameters	Conservative
II. Recirculation System Model	
1. System Inertia	+200%
2. Jet Pump Losses	-20%
3. Core Pressure Drop	+1.5 psi
4. Separator (L/A)	-30%
5. Separator ΔP	Conservative
III. Steam Line Model	
1. Pressure Loss Coefficient	-20%

TABLE 7.27-2

TURBINE TRIP WITHOUT BYPASS

SENSITIVITY STUDY

	ΔCPR/ICPR	Δ (ΔCPR/ICPR)
Base Transient Case	.1569	-
I. Reactor Core Model		
1. Nuclear Model		
a. Core Average Void Coefficient, +10%	.1710	.0141
b. Core Average Doppler Coefficient, -25%	.1686	.0116
c. Scram Reactivity, -10%	.1593	.0024
d. Effective Total Delayed Neutron Fraction, -4%	.1582	.0012
2. Thermal Hydraulic Model		
a. Drift Velocity, +30%	.1520	-.0050
b. Profile Fit Model, +7.1%	.1512	-.0058
II. Recirculation System Model		
1. System Inertia, +200%	.1560	-.0010
2. Jet Pump Losses, -20%	.1570	.0000
3. Core Pressure Drop, +1.5 psi	.1568	-.0001
4. Separator L/A, -30%	.1570	.0000
III. Steam Line Model		
1. Pressure Loss Coefficient, -20%	.1575	-.0006
IV. Additional Parameters		
1. AF, Void Coefficient	-	.0000
2. AF, Doppler Coefficient	-	.0023
3. AF, Scram Reactivity	-	.0000
4. Radial Power Redistribution Uncertainty	-	.0045

ΔCPR/ICPR Input Parameter Uncertainty = .021

TABLE 7.27-3

MSIV CLOSURE WITH HIGH FLUX SCRAM

SENSITIVITY STUDY

	Maximum Vessel Pressure (psia)	ΔP (psia)
Base Transient Case	1242.9	
I. Reactor Core Model		
1. Nuclear Model		
a. Void Coefficient, +10%	1245.8	3.0
b. Doppler Coefficient, -25%	1246.5	3.6
c. Scram Reactivity, -10%	1243.4	0.6
d. Effective Total Delayed Neutron Fraction, -4%	1243.0	0.2
2. Thermal Hydraulic Model		
a. Drift Velocity, +30%	1241.1	-1.8
b. Profile Fit Model, +7.1%	1241.6	-1.3
II. Recirculation System Model		
1. System Inertia, +200%	1242.3	-0.6
2. Jet Pump Losses, -20%	1242.9	0.0
3. Core Pressure Drop, +1.5 psi	1244.3	1.5
4. Separator L/A, -30%	1242.9	0.0
III. Steam Line Model		
1. Pressure Loss Coefficient, +20%	1243.4	0.5

ΔP Input Parameter Uncertainty = 5.5 psi

TABLE 7.27-4

AUTOMATIC FLOW CONTROLLER DECREASE

SENSITIVITY STUDY

	Decay Ratio (Q)	ΔQ
Base Transient Case	0.815	-
I. Reactor Core Model		
1. Nuclear Model		
a. Void Coefficient, +10%	0.821	0.006
b. Doppler Coefficient, -25%	0.819	0.004
c. Scram Reactivity, -10%	0.815	0.000
d. Effective Total Delayed Neutron Fraction, -4%	0.819	0.004
2. Thermal Hydraulic Model		
a. Drift Velocity, +30%	0.808	-0.007
b. Profile Fit Model, +7.1%	0.813	-0.002
II. Recirculation System Model		
1. System Inertia, +200%	0.814	-0.001
2. Jet Pump Losses, -20%	0.821	0.006
3. Core Pressure Drop, +1.5 psi	0.819	0.004
4. Separator L/A, -30%	0.819	0.004
III. Steam Line Model		
1. Pressure Loss Coefficient, +20%	0.811	-0.004
IV. Additional Parameters		
1. Flow Controller Setpoint, +100%	1.000	0.185

ΔQ Input Parameter Uncertainty = .19

Reference 7.27.1 Rouhani, S.Z., "Void Measurement in the Region of Subcooled and Low-Quality Boiling," Symposium on Two-Phase Flow, University of Exetor, Devon, England, June 1965

Reference 7.27.2 Rouhani, S.Z., "Void Measurement in the Region of Subcooled and Low-Quality Boiling," Part II, AE-RTL-788, Aktiebolager Atomenergi, Studsvik, Sweden, April 1966

Reference 7.27.3 General Electric Co., NEDE-24154-P, "LTR-Qualification of ODYN," Volume 3, October 1978

7.28 Question 28

What mesh is used in the MOC representation of the steam line and does this satisfy the stability criteria? The steam line flow in Figure 3.2-96 does not exhibit the same behavior as the ODYN prediction. What is causing this difference?

Response

The mesh used in the Monticello DYNODE-B steam line MOC model varies between 22.3 and 29.4 feet. This mesh representation is stable, since the normal time step size for the steam line solution is 0.001 sec for overpressurization events and the speed of sound in steam is about 1500 ft/sec. Thus, the Courant limit is not exceeded. The steam line flow differences between DYNODE-B and ODYN as seen in Figure 3.2-96 are attributable to model differences as noted in Section 2.3.2 of NSPNAD-8608 and in the response to question 10. The volume-junction representation used in ODYN is more susceptible to instabilities relative to the MOC method, provided the latter model does not exceed the Courant limit. As noted in Figure 3.2-96, the DYNODE-B steam line flow settles to the new asymptotic value more quickly and smoothly compared to the ODYN result.

7.29 Question 29

How does the DYNODE-B decay heat precursors model compare with more recent revisions of this standard (e.g., the ANS standard of September, 1978)?

Response

For any given case, the later standard for decay heat calculations, ANSI/ANS-5.1-1979, may yield a decay heat value which is either greater or smaller than the value derived using the 1971 ANS-5.1 Draft standard, depending on the specific conditions being analyzed; it therefore cannot be said that either method is always the more conservative. However, the uncertainties associated with the 1971 methods are much larger than with the 1979 standard; as a result, when the uncertainties are applied, the 1971 methods consistently produce a more conservative prediction of decay heat. For all licensing calculations, those uncertainties are included in the DYNODE-B model, thereby ensuring a conservative decay heat calculation.

7.30 Question 30

Run the Peach Bottom licensing basis turbine trip test.

Response

As requested by the NRC, Northern States Power (NSP) has analysed the licensing basis transient (LBT). The LBT is based on a turbine trip without bypass occurring in the Peach Bottom Unit 2 reactor operating at 104.5% of rated power and 100% of rated flow at the end of cycle 2 with all rods fully withdrawn. The input used by NSP is consistent with References 7.30.1 and 7.30.2. The response predicted by NSP has been compared to both the BNL and the GE predicted response.

Model Input

The same NSSS model and kinetics data used in the Peach Bottom Unit 2 turbine trip benchmarking were used in the LBT analysis except as noted below. The initial axial power distribution was changed to match the GE curve in Figure 68 of Reference 7.30.1. The control rods were modelled as being completely withdrawn. The total scram reactivity was changed to match the value given in Reference 7.30.3.

The direct moderator heating was set to 0.02, and the power generated in the fuel was taken as 0.96 to be consistent with the GE model (Reference 7.30.1). The delayed neutron group data from Table 1 of Reference 7.30.1 was used.

The setpoints of the safety relief valves were consistent with Reference 7.30.1. The valve characteristics were assumed to be the same as those used in the Peach Bottom Unit 2 turbine trip test benchmarking. The safety valve was assumed to have 80% flow when it initially opened and was assumed to have a linear capacity between this point and full open.

Following the turbine trip signal, time delays of 0.182 seconds before stop valve motion and 0.28 seconds before control rod motion begins were used (References 7.30.4 and 7.30.2 respectively).

The initial conditions used in this analysis are given in Table 7.30.1. These values are consistent with those given in References 7.30.1 and 7.30.2. A constant fuel rod gap conductance of 1000 Btu/hr-ft^2-^{o}F was used (Reference 7.30.1, page 14).

Data Comparisons

Figure 7.30.1 shows the initial axial power, void, temperature, and heat flux distributions as well as the transient power, heat flux, temperature, void, and pressure behavior. This figure includes the revised BNL and the GE results given in Reference 7.30.1. The DYNODE-B curves shown in the portions of the figure which contain spacial axial information are drawn as straight line segments between the average values at the centers of the twelve equally spaced nodes.

The initial axial power shape between DYNODE-B, BNL and GE are essentially the same. This is to be expected, since the GE distribution was used to determine the DYNODE-B distribution. The corresponding initial heat flux and initial fuel temperature distributions calculated by DYNODE-B, BNL, and GE also compare well. The DYNODE-B initial fuel temperature distribution is between the BNL and GE predicted temperature distributions. As expected, the initial axial void distribution calculated by DYNODE-B is slightly larger than the BNL and GE values. This is because DYNODE-B conservatively uses the steam dome pressure for all thermal-hydraulic calculations as noted in section 7.13 of this report.

The rise in the core average pressure predicted by DYNODE-B compares well with the pressure rise predicted by both BNL and GE. The difference in the time at which the pressure begins to rise as predicted by DYNODE-B, GE, and BNL is probably due to the time delay for stop valve characteristics used in the different analyses. It should be noted that DYNODE-B matches the data in Figure 6-6 of Reference 7.30.4 better. The slopes of the pressure responses of all three curves are similar. Both BNL and GE predict that the pressure will level off somewhat between 0.6 and 0.7 seconds whereas DYNODE-B predicts a constant pressure rise. The leveling off of the core pressure is also seen in Reference 7.30.4. It is believed that the leveling off of the pressure is due to momentum effects within the vessel. Since DYNODE-B conservatively uses the steam dome pressure for all thermal-hydraulic calculations, it does not predict the above behavior.

The rate of change of the core average void fraction predicted by DYNODE-B also compares well with BNL and GE. The changes in void fraction relative to the initia values are very similar for all three curves.

The general trends in the core power as predicted by DYNODE-B, BNL, and GE are consistent. All three predict a decrease in power at 0.28 seconds which is due to the beginning of scram rod motion. As the positive reactivity insertion due to collapsing voids overcomes the negative reactivity insertion of the control rods, the core power begins to rise. This behavior is seen in the DYNODE-B, BNL, and GE results. The power begins rising later in the DYNODE-B analysis because, as stated earlier, the pressure rise predicted by DYNODE-B starts later. The power peaks sooner in the DYNODE-B analysis for two reasons. Since DYNODE-B starts with a higher void fraction, the positive reactivity insertion caused by collapsing voids is higher in DYNODE-B. Thus the power rise predicted by DYNODE-B is steeper than BNL or GE. The second reason has to do with the leveling off of the core pressure discussed above. When the pressure levels off, the collapsing of voids also levels off. Since the positive reactivity insertion is due to the collapsing of voids, the power rise also levels off. This is seen in the BNL analysis near 0.65 seconds and is somewhat seen in the GE analysis near 0.75 seconds. Both of the above phenomena result in a conservative predicted power response by DYNODE-B.

The area under the power curve is similar for both the DYNODE-B and GE analysis. This is seen in the core average heat flux response. The general behavior of the DYNODE-B and the GE predicted heat flux response is the same. Both start to fall as scram rods are inserted and both peak near 1.1 seconds into the transient with similar magnitudes.

The average fuel temperature response predicted in the GE analysis was not available, therefore only the DYNODE-B and BNL responses are compared. Both predicted a small initial drop in the fuel temperature due to the power reduction caused by the scram and a subsequent rise corresponding with the rise in core power. Since DYNODE-B predicts a peak in core power earlier than BNL, the temperature rises sooner in DYNODE-B than in BNL. The changes in the fuel temperatures relative to the initial values are very similar.

The axial heat flux profiles at 0.8 seconds and 1.2 seconds are also given in Figure 7.30.1. The heat flux distribution predicted by DYNODE-B are spatially similar to both the GE and the BNL predicted distributions.

TABLE 7.30.1

INITIAL CONDITIONS FOR LICENSING BASIS TRANSIENT

Parameter	Value
Core Thermal Power (MWt)	3441.0
Total Core Flow (million lbs/hr)	101.0
Bypass Flow (%)	10.0
Turbine Steam Flow (lbm/sec)	3672.8
Core Inlet Enthalpy (BUT/lbm)	521.4
Lower Plenum Pressure (psia)	1070.0
Upper Plenum Pressure (psia)	1046.0
Steam Dome Pressure (psia)	1035.0
Turbine Inlet Pressure (psia)	984.4
Control Rods Position	All Rods Out
Total Steam Line Length (ft)	400.0
Total Delay Before Rod Movement (sec)	0.28
Constant Fuel Gap Conductance (BTU/(hr-sq ft-deg F)	1000.0
Relief valves set to operate at the following pressures:	
4 valves: 1090.8 psia open; 1070.8 psia close	
4 valves: 1100.9 psia open; 1080.9 psia close	
3 valves: 1111.0 psia open; 1091.0 psia close	
Safety valves set to operate at the following pressures:	
2 valves: 1242.0 psia open; 1222.0 psia close	

LICENSING BASIS TRANSIENT

Figure 7.30.1

DYNODE-B

BNL - - -

GE ____

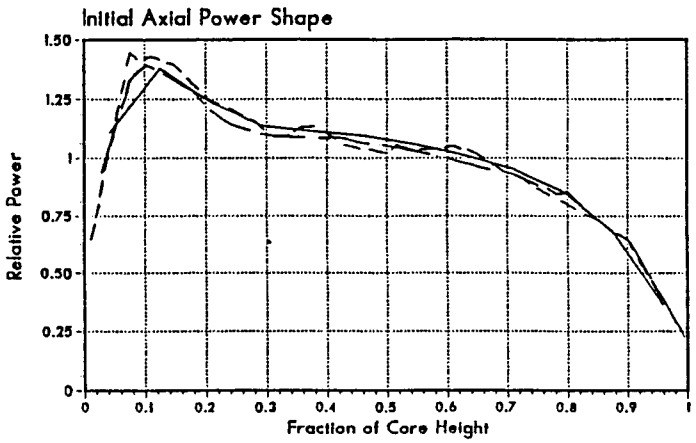

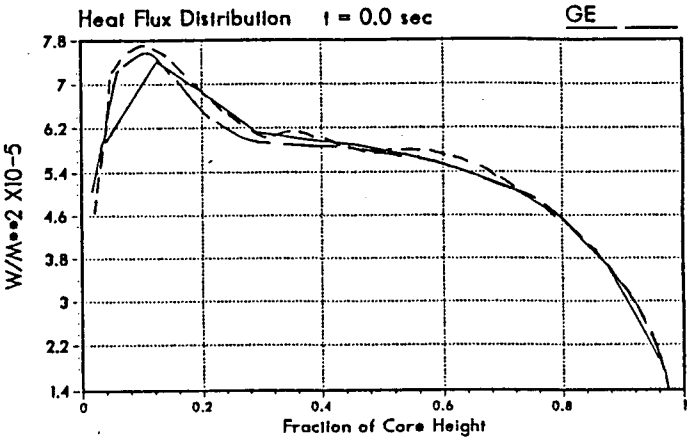

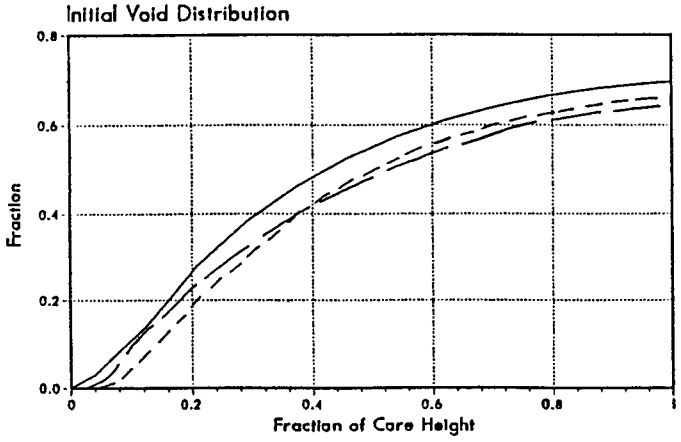

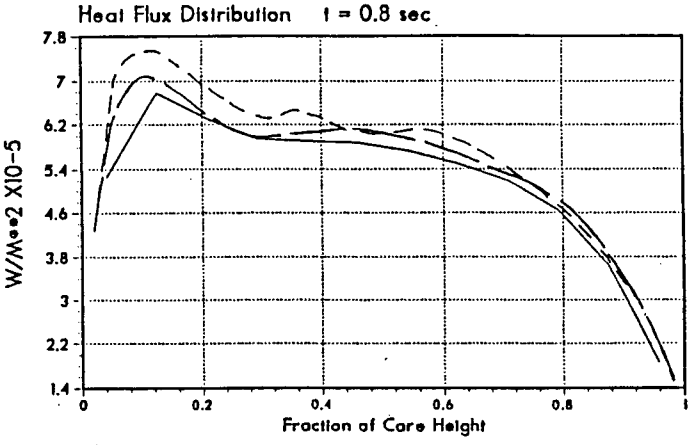

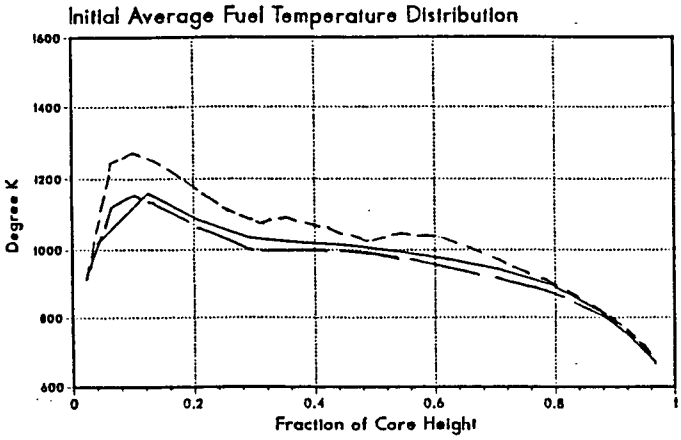

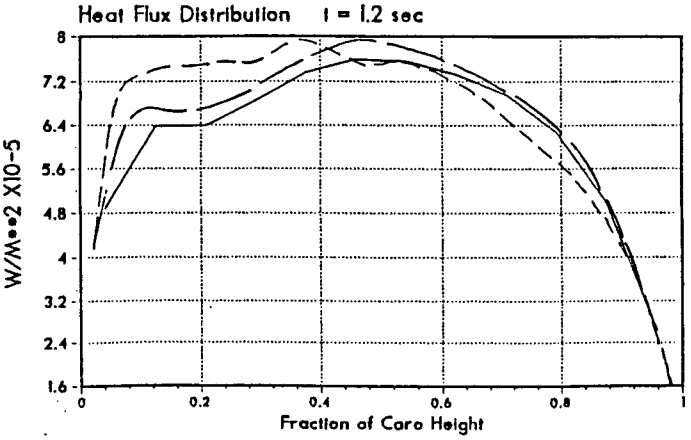

LICENSING BASIS TRANSIENT

Figure 7.30.1 - Continued

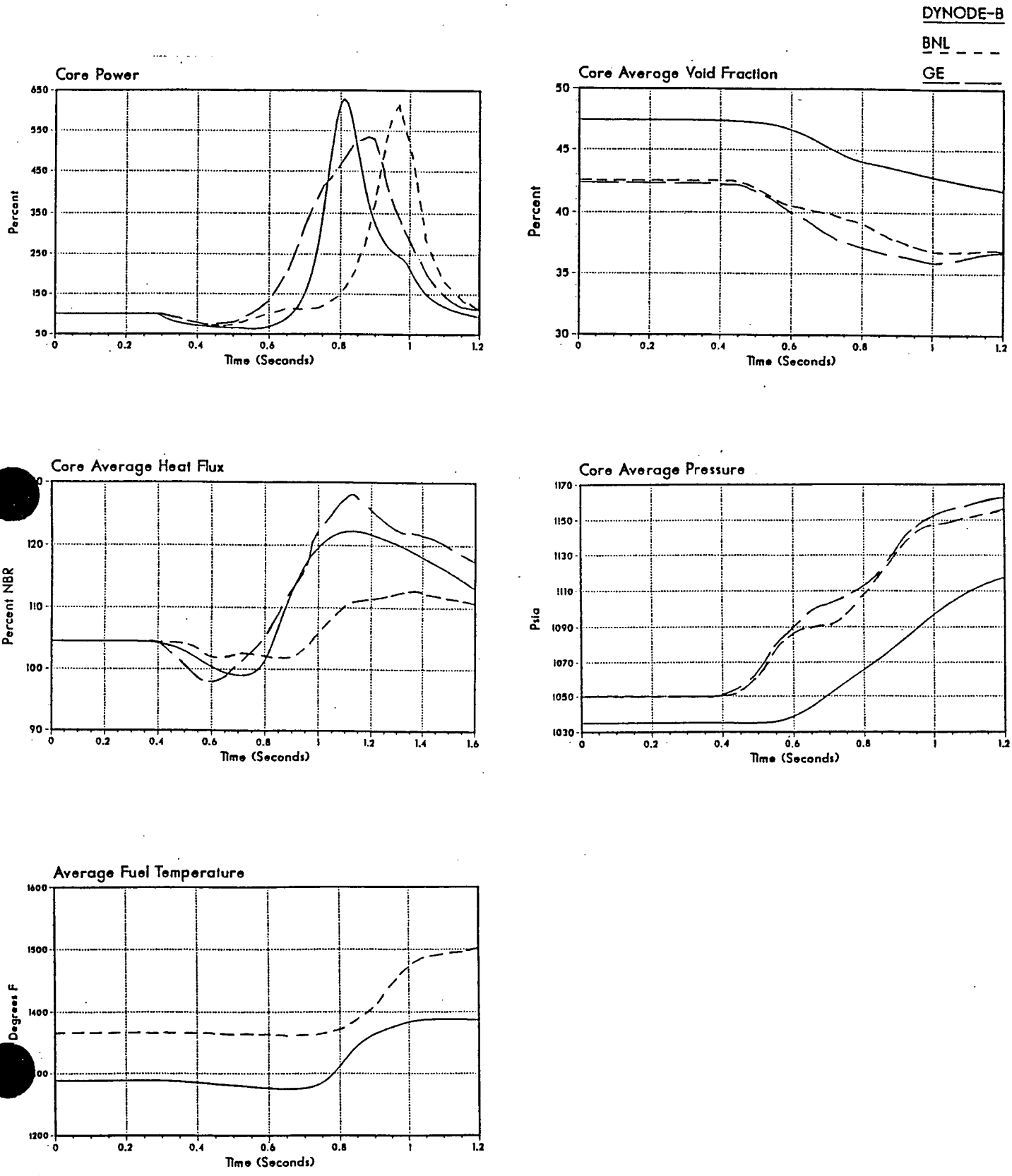

References

7.30.1 BNL-NUREG-26684, "Analysis of Licensing Basis Transients for a BWR/4," M.S.Lu, et.al., September 1979.

7.30.2 Table I and II transmitted to NSP from NRC during the 12/4/87 meeting in Bethesda MD.

7.30.3 NAI Internal Memo from U.C.Lee to R.C.Kern, "Summary of Physics Constants Input for Safety Test," July 22, 1977.

7.30.4 EPRI NP-564, "Transient and Stability Tests at Peach Bottom Atomic Power Station Unit 2 at End of Cycle 2," June 1978.